



HAL
open science

Human infection with zoonotic simian foamy retroviruses (SFVs): characterization of epitopic regions recognized by neutralizing antibodies in infected humans

Lasse Toftdal Dynesen

► To cite this version:

Lasse Toftdal Dynesen. Human infection with zoonotic simian foamy retroviruses (SFVs): characterization of epitopic regions recognized by neutralizing antibodies in infected humans. Adaptive immunology. Université Paris Cité, 2022. English. NNT: . tel-04121362

HAL Id: tel-04121362

<https://theses.hal.science/tel-04121362>

Submitted on 7 Jun 2023

HAL is a multi-disciplinary open access archive for the deposit and dissemination of scientific research documents, whether they are published or not. The documents may come from teaching and research institutions in France or abroad, or from public or private research centers.

L'archive ouverte pluridisciplinaire **HAL**, est destinée au dépôt et à la diffusion de documents scientifiques de niveau recherche, publiés ou non, émanant des établissements d'enseignement et de recherche français ou étrangers, des laboratoires publics ou privés.

THÈSE DE DOCTORAT

Université Paris Cité

École Doctorale Bio Sorbonne Paris Cité (ED562)
Unité Épidémiologie et Physiopathologie des Virus Oncogènes
CNRS UMR 3569 – Département de Virologie, Institut Pasteur, Paris, France

Human infection with zoonotic simian foamy retroviruses (SFVs)

—

Characterization of epitopic regions recognized by neutralizing antibodies in infected humans

Lasse Toftdal DYNESEN

Thèse de Doctorat en Infectiologie

Dirigée par Florence BUSEYNE

Présentée et soutenue publiquement à Paris, le 2 décembre 2022

Devant un jury composé de:

Sylvie VAN DER WERF, PU	Université Paris Cité	Présidente du jury
Arnaud MORIS, DR	Université Paris-Saclay	Rapporteur
Martine BRAIBANT, MCU-HDR	Université de Tours	Rapportrice
Alessia ZAMBORLINI, PU	Université Paris-Saclay	Examinatrice
Ahidjo AYOUBA, DR	Université de Montpellier	Examinateur
Florence BUSEYNE, DR	Institut Pasteur	Directrice de thèse
Antoine GESSAIN, DR	Institut Pasteur	Membre invité

PREFACE

The study presented in this PhD thesis was conducted under supervision of Dr. Florence Buseyne in the ‘*Immunité des Infections Rétrovirales Humaines*’ group part of the ‘*Epidémiologie et Physiopathologie des Virus Oncogènes*’ (EPVO) unit headed by Professor Antoine Gessain in Department of Virology at the Institut Pasteur, Paris, France.

This PhD project was funded by a three-year running grant from the Pasteur-Paris-University (PPU) Doctoral Program, a 12-month 4th year thesis grant from Fondation pour la Recherche Médicale (FRM) with supplementary funding from ANR IBEID and internal ‘bourses de soudure’ from the Department of Virology in agreement with the Institut Pasteur, Université Paris Cité and École Doctorale Bio Sorbonne Paris Cité, Paris, France. In addition, a travel grant was awarded from the Danish Pasteur Society and personal supportive grants were obtained from Augustinus Fonden, Knud-Højgaards Fond and Viet-Jacobsen Fonden.

Illustrations were created with PyMOL and BioRender.com under institutional licenses.

Lasse Toftdal DYNESEN

October 2022

ACKNOWLEDGEMENTS

I sincerely thank my PhD advisor Dr. Florence Buseyne for giving me the opportunity to be part of her group. I am forever grateful for the scientific guidance and support during the past +4yrs. It allowed me to stay curious and importantly – become a better scientist.

I would like to send a special thank you to all jury members who agreed to evaluate my work and be part of my PhD Thesis dissertation: Prof. Sylvie Van Der Werf, Dr. Arnaud Moris, Dr. Martine Braibant, Prof. Alessia Zamborlini and Dr. Ahidjo Ayouba.

A big thank you to Prof. Antoine Gessain and all members of the EPVO unit for the support and for providing a brilliant and professional environment for scientific growth. I want to thank Dr. Philippe Afonso for the many important discussions during my PhD and interests in my work. Thank you to Olivier Cassar for many great moments and all sorts of administrative support, especially when arriving as a foreigner in Paris. Big thank you to Dr. Youna Coquin and Thomas Montange for sharing office and for your vital contributions to my manuscript. I am grateful for your help and company during the many hours spend together in the P2+. Also, thank you to fellow and former PhD students in the lab for creating a lively, fun and open space: Dr. Jim Zoladek, Dr. Jill-Lea Ramassamy and (soon to be Dr.) Sophie Desgraupes. Thank you to Prof. Pierre-Emmanuel Ceccaldi, Dr. Aurore Vidy-Roche, Patricia Jeannin, Jeanne Pascard, Jocelyne Creff and Isma Ziani as well as former EPVO members Dr. Mathilde Coutaudier, Ingrid Fert, Dr. Claudia Filippone and Dr. Mathieu Hubert for help, support and all the good moments in the lab.

A very special thank you to my #TeamFoamy collaborators Dr. Ignacio Fernandez, Dr. Marija Backovic and Prof. Félix Rey. Their contributions and support in my project are beyond words. I am so grateful for all their structural and biochemical expertise and inputs including countless discussions on experimental settings and trouble-shootings. Thank you for helping me bring this project to the next level. It has been an absolute privilege to work with all of you!

I would like to thank the PPU for giving me this opportunity to come and pursue my PhD at Institut Pasteur. This program made a big difference for me and I am grateful for all the support, network and friendships I have made through the PPU. Thank you to Dr. Susanna Celli, Dr. Nathalie Pardigon, Katri Vuollet and everybody involved. Also thank you to all my fellow PhD students from the PPU Trefouël Class for many great moments, both scientifically and socially despite the COVID pandemic.

Acknowledgements

Thank you to my Thesis Advisory Committee members Dr. Hugo Mouquet, Dr. Andrés Alcover and Dr. Arnaud Moris. I appreciate the many great inputs and suggestions during the first three years of my PhD.

Thank you to all colleagues at the 4th floor of LWOFF building in the Schwartz, Charneau and Di Nunzio labs for the nice atmosphere and interesting scientific discussions over the years.

Thank you to all my friends in Paris within and outside Pasteur for the many memories and for making Paris my second home: Theis, Astrid, Michelle, Kevin, Marija, Julie, Claudia, Val, Viviana, Viola, Fabiana, Mara, Lena, Gaëlle, Nathan, Lu, Min, Michael, Chloe, Carys, Crispin, Kyle and Pierre.

Thank you to the experts at the cytometry platform at Pasteur for their expertise and help, in particular Pierre-Henri Commere for help with single-cell sorting experiments.

Thank you to the FRM and the Department of Virology at Institut Pasteur for funding to extend my PhD with 15 months.

Lastly, thank you to my family and friends in Denmark for their endless support during the years when I have been away and missing out on important gatherings. You mean the world to me and I am so grateful to have you all in my life. Tak!

RÉSUMÉ

Titre: *Infection humaine par des rétrovirus foamy simiens (VFS) zoonotiques - Caractérisation des régions épitopiques reconnues par les anticorps neutralisants chez les personnes infectées*

Les virus foamy simiens (VFS) sont des rétrovirus de type complexe anciens et très répandus. Ils ont évolué conjointement avec leur espèce hôte pendant des millions d'années. Ces virus peuvent être transmis à l'homme, principalement par des morsures, entraînant l'établissement d'une infection persistante. Malgré la transmission zoonotique fréquente des VFS des PNH aux humains en Afrique centrale et en Asie, aucune pathologie sévère ou transmission interhumaine des VFS n'a encore été décrite. Mon laboratoire a émis l'hypothèse que le système immunitaire contrôle efficacement la réplication virale chez les humains infectés par des zoonoses. Mes collègues ont démontré que des anticorps neutralisants (AcNs) sont présents à des titres élevés chez les chasseurs d'Afrique centrale infectés par des souches de VFS de gorille et de chimpanzé. Deux génotypes viraux circulent parmi les primates non humains (PNHs) et les hommes infectés par le VFS. Une région variante au sein du domaine de surface (SU) de la glycoprotéine d'enveloppe virale (Env), appelée SUvar, constitue la base des deux génotypes. Le domaine de liaison au récepteur (RBD, pour receptor binding domain) chevauche la région SUvar. Ces anticorps neutralisants ciblent strictement la région SUvar de l'Env du VFS.

Mon objectif était de caractériser les épitopes reconnus par les AcN situés dans la région SUvar de l'Env du VFS. Pour cartographier les épitopes AcN au sein de la SUvar, j'ai réalisé des tests de neutralisation en présence de protéines SU recombinantes agissant comme compétiteurs de l'enveloppe des particules virales pour la liaison aux AcN. J'ai utilisé des échantillons de plasma provenant de chasseurs d'Afrique centrale infectés par le VFS du gorille et des vecteurs viraux foamy exprimant l'Env du VFS de l'un ou l'autre des deux génotypes. J'ai généré des protéines SU mutantes en supprimant systématiquement des sites de glycosylation, en insérant des sites de glycosylation pour modifier des épitopes et en échangeant des domaines entre les deux génotypes.

J'ai montré que les épitopes neutralisants ont une localisation spécifique au génotype. Grâce à une collaboration avec le laboratoire du professeur Félix Rey qui a résolu une structure d'un RBD du VFS du gorille, j'ai pu montrer que la plupart des AcNs spécifiques du VFS ciblent des épitopes situés à l'apex de Env, en particulier trois boucles mobiles situées à l'interface entre les protomères. Des vecteurs dont l'enveloppe est délétée pour chacune de ces boucles se fixent aux cellules mais sont non infectieux, ce qui suggère que les AcNs ciblent des épitopes ayant une importance fonctionnelle. De plus, nous avons trouvé un deuxième épitope majeur dans la partie inférieure du RBD ciblé par les AcNs provenant d'individus infectés par l'un des deux génotypes. Cette région est impliquée dans la fixation aux cellules. Mes résultats suggèrent que les AcNs spécifiques du VFS pourraient bloquer l'entrée du virus, soit en inhibant l'interaction entre Env et la surface de la cellule soit en empêchant le changement de conformation de Env permettant la fusion des membranes virale et cellulaire. Mes données confirment que les AcNs pourraient contribuer à contrôler la réplication virale et la transmission interhumaine des VFS.

Mots clés: Virus foamy simien, Rétrovirus, Zoonose, Anticorps neutralisants, Épitopes

ABSTRACT

Simian foamy viruses (SFVs) are ancient and wide-spread complex-type retroviruses that have co-evolved with their non-human primate (NHP) species for millions of years. These viruses can be transmitted to humans, primarily through bites, leading to the establishment of a life-long persistent infection. Despite frequent zoonotic transmission of SFVs from NHPs to humans in Central Africa and Asia, no overt pathology or human-to-human transmission of SFVs have been reported yet. My host laboratory hypothesized that the immune system efficiently controls viral replication in zoonotically infected humans. They demonstrated that neutralizing antibodies (nAbs) are present at high titers in Central African hunters infected with gorilla and chimpanzee SFV strains. My colleagues showed that two viral genotypes are circulating among SFV-infected NHPs and humans. A variant region within the surface domain (SU) of the viral envelope glycoprotein (Env), termed SUvar, forms basis of the two genotypes. The receptor binding domain (RBD) overlaps the SUvar region. The nAbs strictly target the SUvar region on the SFV Env.

I aimed to characterize nAb epitopes located within the SUvar region of SFV Env. To map nAb epitopes within SUvar, I performed neutralization assays in presence of recombinant SU proteins that compete with Env at the surface of viral particles for nAb binding. I used plasma samples from Central African hunters infected with gorilla SFVs and foamy viral vectors expressing SFV Env from each of the two genotypes. I generated mutant SU proteins by systematically deleting glycosylation sites, inserting glycans to disrupt epitopes and by swapping residues between the two genotypes.

I have described that nAb epitopes have a genotype-specific location. Through collaborative work with the laboratory of Prof. Félix Rey who solved the crystal structure of a gorilla SFV RBD, I have discovered that most SFV-specific nAbs target epitopes located at the apex of Env, in particular three mobile loops located at the interface between protomers. Vectors with deleted loops were produced and bound to cells but were non-infectious, suggesting that nAbs target epitopes with functional importance. In addition, we found a second major epitope in the bottom part of the RBD targeted by nAbs from individuals infected by one of the two genotypes. This region is involved in binding to cells. My results suggest that SFV-specific nAbs could block viral entry either by preventing Env binding to the cell surface or by preventing conformational changes of the Env trimer and fusion of viral and cellular membranes. Collectively, my data support the role of nAbs in the control of viral replication and human-to-human transmission.

Key words: Simian foamy virus, Retrovirus, Zoonosis, Neutralizing antibodies, Epitopes

RÉSUMÉ SUBSTANTIEL EN FRANÇAIS

Le travail de cette thèse de doctorat est présenté sous la forme de deux publications. Le premier manuscrit décrit la structure du domaine de liaison au récepteur (RBD pour récepteur binding domain) de la glycoprotéine d'enveloppe (Env) du virus foamy simien (VFS), tandis que le deuxième manuscrit représente le travail principal de ma thèse sur les épitopes des anticorps neutralisants (AcNs). Ces deux articles sont le résultat d'un travail collaboratif. Par conséquent, je présenterai les deux manuscrits et soulignerai ma contribution précise à ces travaux, y compris une explication plus détaillée des expériences que j'ai réalisées.

Manuscrit I: Nouvelle structure d'un RBD de VFS

Nous avons collaboré avec le laboratoire du Prof. Félix Rey qui est un expert en virologie structurale et en particulier des mécanismes de fusion des glycoprotéines virales. Ce travail a été réalisé par Dr. Ignacio Fernandez et dirigé par Dr. Marija Backovic, respectivement chercheur post-doctoral et chercheuse permanente. L'objectif était d'obtenir une structure de l'Env du VFS, de mieux comprendre les mécanismes de fusion de l'Env du VFS et l'utilisation potentielle des récepteurs. En outre, ces connaissances ont aidé et aideront à caractériser les épitopes des AcNs, et à comprendre leurs mécanismes d'action. De plus, comme les virus foamy (VF) sont des virus extrêmement anciens qui ont évolué conjointement avec leurs hôtes pendant des millions d'années, ces connaissances structurelles pourraient donner de nouvelles indications sur l'évolution des VF et leur relation avec les orthorétrovirus.

Environ 18 mois après le lancement de ce projet, nos collaborateurs ont réussi à résoudre une structure cristalline aux rayons X à une résolution de 2.6Å d'un RBD de la souche zoonotique BAK74 (GII-K74) du génotype II du gorille, isolée dans notre laboratoire à partir de cellules mononuclées du sang périphérique (PBMCs) provenant d'un chasseur d'Afrique centrale infecté accidentellement. La structure présente une forme sans précédent et ne présente donc aucune similitude avec les RBD d'autres rétrovirus tels que le virus de la leucémie murine (MLV), le virus leucémogène félin (FeLV) et le virus de l'immunodéficience humaine de type 1 (VIH-1). La nouvelle structure du RBD a une forme de haricot avec un domaine supérieur et inférieur.

Une précédente structure de cryo-microscopie électronique (EM) à basse résolution des particules virales d'une souche de génotype I du chimpanzé (CI-PFV) a révélé que l'Env formait des structures (Effantin et al., 2016). La nouvelle structure RBD GII-K74 du VFS s'est bien adaptée à la structure du trimère de l'Env du CI-PFV, ce qui confirme que le RBD se situe dans

la partie supérieure du trimère de l'Env du VFS. Cela confirme également que leur structure RBD est repliée dans la conformation proche de celle observée sur les particules virales.

Ma première contribution a été de valider que le RBD adopte une forme native. J'ai réalisé des tests de neutralisation dans lesquels le RBD soluble recombinant et l'Env exprimée à la surface des particules virales sont en compétition pour se lier à des AcNs présents dans des échantillons de plasma de personnes infectées par des souches homologues de VFS de gorille. La liaison des AcNs au RBD entraîne une augmentation de l'infection par rapport aux particules virales incubées avec un échantillon de plasma en présence de la protéine d'Env d'un virus non apparenté. La protéine RBD a été produite dans des cellules d'insecte S2 ou des cellules de mammifère Expi293F qui produisent des protéines présentant des types distincts de glycosylation de surface. Les deux protéines ont été diluées en série et incubées avec du plasma de donneurs infectés par le VFS avant l'ajout de vecteurs viraux foamy (VFFs). Une augmentation de l'infectivité a été observée pour les deux protéines RBD de manière dose-dépendante. Ces résultats confirment que les protéines RBD adoptent une conformation reconnue par les AcNs.

Le VFS utilise l'héparane sulfate (HS) comme un facteur d'attachement pour l'entrée virale dans les cellules sensibles. Afin de rechercher un site potentiel de liaison à l'héparane (HBS) sur l'Env du VFS, nos collaborateurs ont déterminé le potentiel électrostatique de surface du RBD et ont utilisé la modélisation d'une molécule d'HS sur la surface accessible au solvant pour identifier un HBS potentiel. Leurs prédictions ont mis en évidence quatre résidus (K342, R343, R356 et R369) présentant un nombre élevé de contacts avec le HS modélisé dans une zone chargée positivement du domaine inférieur du RBD. Ces résidus ont été mutés par paires (K342/R343 et R356/R369) en alanine dans les protéines ectodomaines trimériques. J'ai mis en place un test de liaison cellulaire basé sur la cytométrie en flux pour mesurer l'impact des mutations sur la liaison aux HS. La liaison de l'ectodomaine sauvage (WT) dépend des niveaux d'expression de l'HS sur les cellules sensibles, étant plus élevé sur les cellules HT1080 que sur les cellules BHK-21. Les ectodomaines mutants se lient environ dix fois moins sur les deux lignées cellulaires que l'ectodomaine sauvage GII-K74. J'ai ensuite traité les cellules HT1080 avec de l'héparinase III pour éliminer les HS. La liaison de l'ectodomaine aux cellules traitées a été réduite pour l'ectodomaine WT alors qu'elle n'a pas été affectée pour les homologues mutants. Ces résultats confirment que les résidus identifiés K342, R343, R356 et R369 interviennent dans la liaison de l'Env du VFS à l'HS exprimé sur les cellules.

La structure de RBD nous permet de comprendre ses sous-domaines fonctionnels. Les deux sous-domaines essentiels à la liaison forment le sous-domaine inférieur et une partie du domaine supérieur. Le HBS est en effet situé dans le domaine inférieur. Le sous-domaine qui peut être supprimé sans affecter la liaison de l'Env aux cellules (appelé RBD de jonction, RBDj) est situé dans le domaine supérieur. La prédiction computationnelle AlphaFold 2.0 (AF) du RBD GII-K74 a révélé une structure très similaire à la structure du RBD obtenue expérimentalement. La comparaison des structures de RBD prédites par AF à partir des VFs distincts confirme que le RBD se replie dans un "centre commun" (CC) conservé entre les différents VFs. En revanche, les régions extérieures, y compris certaines boucles très flexibles au sommet du RBD, présentent une grande divergence de repliement, y compris entre des génotypes VFSs distincts. Les boucles forment des contacts entre les protomères RBD lorsqu'elles sont superposées dans la carte cryo-EM du trimère CI-PFV. Ainsi, notre hypothèse est que ces boucles mobiles stabilisent le trimère Env dans une conformation de pré-fusion. Collectivement, nos données soutiennent que le domaine supérieur du RBD de VFS est impliqué dans la stabilisation du trimère tandis que le domaine inférieur est impliqué dans la liaison aux HS.

Manuscrit II: Caractérisation des épitopes des AcNs

Dans la partie principale de mon projet de doctorat, j'ai étudié la localisation et les caractéristiques des épitopes ciblés par les AcNs dans des échantillons de plasma provenant de chasseurs d'Afrique centrale infectés par les virus zoonotiques du gorille. Il a été démontré précédemment que ces AcNs ciblent la région variable du domaine SU de l'Env du VFS (SUvar), qui recouvre la majeure partie du RBD et définit deux génotypes du VFS. Avant mon arrivée, une étudiante de M2 a réalisé une cartographie des épitopes linéaires en utilisant des peptides couvrant les régions épitopiques de SUvar prédites *in silico*. Comme peu de réactivités ont été observées envers ces peptides linéaires dans le test enzyme-linked immunosorbent assay (ELISA), j'ai opté pour la cartographie des épitopes conformationnels dans notre recherche d'épitopes AcNs spécifiques au génotype.

J'ai cartographié les épitopes conformationnels en utilisant des protéines recombinantes comme concurrentes de l'Env exprimée par des vecteurs viraux pour la liaison aux AcNs dans les tests de neutralisation. J'ai d'abord utilisé les données publiées sur le sous-domaine de liaison Env et les sites de glycosylation définis par des tests fonctionnels. Ensuite, je me suis concentré sur les séquences spécifiques des génotypes et sur les prédictions *in silico* d'épitopes B linéaires.

Lorsque la structure du RBD GII-K74 est devenue disponible, je l'ai utilisée pour la conception rationnelle de nouvelles mutations sur les protéines du domaine SU. J'ai d'abord testé plusieurs constructions pour l'expression dans des cellules de mammifères et d'insectes à partir de souches de VFS de gorilles zoonotiques des deux génotypes, GI-D468 et GII-K74, et de la souche CI-PFV adaptée en laboratoire. Ces constructions comprenaient des domaines RBD et SU monomères, des protéines immunoadhésines dimères composées du domaine SU fusionné au Fc de mIgG2a (SU-Ig) et des ectodomains trimériques. Parmi ces constructions, les protéines chimériques SU-Ig étaient les seules à présenter un niveau d'expression protéique adéquat pour deux génotypes distincts. Pour ces raisons, j'ai utilisé les SU-Ig pour l'étude de cartographie des épitopes. J'ai mis en place la production, la purification et la validation des protéines SU-Ig homologues GII-K74 et hétérologues CI-PFV pour la cartographie des épitopes AcNs spécifiques de GII et GI, respectivement. Les protéines ont été utilisées comme concurrentes dans des tests de neutralisation. J'ai confirmé que ces protéines bloquent les AcNs plasmatiques d'une manière spécifique au génotype et dose-dépendante sans affecter l'entrée des vecteurs viraux. Ces protéines ont été titrées à plusieurs reprises contre un panel d'échantillons de plasmas provenant de donneurs infectés par le VFS, dilués à leur IC₉₀ respectif. Cette dilution a été choisie pour permettre la saturation des AcNs par les protéines recombinantes. Deux paramètres ont été définis pour caractériser la capacité de la protéine à bloquer les AcNs; l'IC₅₀ comme mesure de leur affinité et le % d'inhibition maximale (MaxI) qui correspond à la fraction d'AcNs inhibée. Des mutations ont ensuite été introduites dans ces protéines SU-Ig pour cartographier les épitopes des AcNs dans les tests de neutralisation en comparant les valeurs de la IC₅₀ et du MaxI (%) des mutants à celles du WT. L'introduction de mutations a généralement donné l'un des quatre résultats suivants: I) aucun impact et une activité identique à celle de la protéine WT, II) une affinité plus faible des AcNs pour la protéine mutante, comme en témoigne une IC₅₀ plus élevée par rapport à la WT, III) un plateau MaxI plus bas, ce qui signifie qu'une fraction des AcNs n'est plus bloquée par la protéine mutante, ou IV) les deux.

J'ai d'abord étudié le rôle de la glycosylation dans les épitopes des AcNs et j'ai observé que les glycanes de type complexe et à haute teneur en mannose n'influençaient pas le blocage des AcNs dans notre test. En revanche, la déglycosylation a eu un effet notable et a diminué de manière significative l'affinité des protéines SU-Ig pour la liaison aux AcNs plasmatiques de six des huit donneurs testés. Ces résultats suggèrent que certains épitopes peuvent être composés d'un glycanes. Pour identifier le glycanes impliqué dans cette reconnaissance, j'ai supprimé six des sept sites de glycosylation individuels au sein de la SUvar sur la protéine SU-

Ig homologue GII-K74, tandis que le glycan conservé N8 a été ignoré car il est essentiel à l'expression de la protéine. Parmi tous les mutants, la délétion du glycan N7' a eu l'effet le plus fort et a entraîné une perte significative de l'activité de blocage de l'AcN pour cinq des sept donneurs infectés par GII testés. Ce glycan est situé au CC du RBD dans le domaine inférieur et à proximité immédiate du glycan N8 conservé. L'élimination du glycan N10, qui a un emplacement spécifique au génotype, n'a pas affecté le blocage des AcNs pour tous les échantillons de plasma testés.

J'ai également cherché à savoir si les AcNs reconnaîtraient le nouveau site de liaison de l'héparane sulfate que nous avons cartographié sur le domaine inférieur du RBD (manuscrit I). Cependant, les protéines portant les quatre mutations HBS ont conservé une activité égale à celle du WT pour trois des quatre donneurs infectés par le GII testés. Nous concluons donc que le HBS n'est pas une cible dominante des AcNs.

Ensuite, nous avons examiné le rôle des domaines fonctionnels. Ainsi, nous avons généré des protéines SU-Ig mutantes RBDj des deux génotypes et testé leur capacité à inhiber les AcNs. L'élimination du RBDj a complètement aboli l'activité bloquante de la protéine SU pour sept des huit donneurs, ce qui suggère que les principaux épitopes AcNs sont situés dans cette région. Nous avons ensuite généré un échange de SU-Ig GII avec un sous-domaine GI-RBDj qui a bloqué les AcNs plasmatiques de quatre donneurs infectés par GI. Ces résultats confirment que le sous-domaine RBDj est une cible dominante des AcNs chez les humains infectés par les souches de génotype I du gorille.

Sur la structure 3D, le RBDj se situe à l'apex du RBD et du trimère. De plus, nous avons observé que cette région comporte les quatre boucles supposées être impliquées dans la stabilisation du trimère. Parmi ces boucles (L1-4), L1 semble enfouie dans le trimère et probablement non accessible pour les AcNs. Ainsi, pour mieux définir les épitopes dans cette région, nous avons conçu des protéines SU-Ig avec des mutations au niveau des boucles pour les deux génotypes. Les trois boucles sommitales restantes (L2; aa 278-293, L3; aa 410-433 et L4; aa 442-458) ont été supprimées individuellement. Les nouveaux mutants de boucle ont démontré un ciblage spécifique du génotype par les AcNs. Les AcNs spécifiques de GI ciblent principalement la région L3 (CI-PFV L3; aa 411-436), tandis que les AcNs spécifiques de GII ont une réponse plus large et ciblent les trois boucles. Pour confirmer les résultats pour GI, nous avons généré un mutant avec un échange GII-L3 dans le squelette SU-Ig du CI-PFV et nous avons confirmé que ce mutant perdait sa capacité à bloquer les AcNs de six échantillons de plasma spécifiques de GI testés. Ensuite, une chercheuse post-doctorale, Dr. Youna Coquin, a produit des VVFs

avec des délétions du RBDj et des boucles correspondant à celles conçues sur les protéines SU-Ig. Elle a démontré que ces mutants se liaient aux cellules sensibles au VFS mais n'étaient pas infectieux. Ces données confirment que les AcNs ciblent des épitopes sur le sommet du RBD qui sont fonctionnellement importants pour l'entrée virale.

Avant que nos collaborateurs ne résolvent la structure du RBD, j'ai utilisé des outils de prédiction *in silico* pour concevoir sept mutations en insérant des glycanes pour la rupture d'épitope sur le squelette SU-Ig GII-K74. Parmi celles-ci, plusieurs mutations étaient situées à l'intérieur ou à proximité des boucles d'apex, et certaines d'entre elles ont confirmé nos résultats selon lesquels ces boucles contiennent des épitopes. Certaines mutations ont également été confirmées dans le squelette CI-PFV pour la cartographie des AcNs plasmatiques spécifiques de GI. De manière intéressante, j'ai découvert un épitope spécifique de GII situé dans une région en boucle (aa 345-353) sur le domaine inférieur du RBD. Les insertions de glycanes dans cette boucle ont fortement aboli le blocage des anticorps plasmatiques spécifiques de GII mais pas de GI. Des mutations supplémentaires à l'intérieur et à proximité de cette boucle, y compris des échanges chimériques, ont confirmé que cette région était une cible dominante des anticorps spécifiques provenant d'humains infectés par des souches de VFS de génotype II du gorille.

Collectivement, nos deux manuscrits et le rapport précédent nous ont permis de proposer un nouveau modèle avec attribution de rôles fonctionnels à certaines caractéristiques structurales du RBD du VFS. Nous proposons que le domaine supérieur du RBD et les boucles d'apex soient impliqués dans les interactions protomères-protomères et potentiellement dans la stabilisation du trimère Env. En revanche, le domaine inférieur du RBD contient un HBS est potentiellement impliqué dans la liaison à d'autres molécules réceptrices encore à identifier. Mon étude sur les AcNs a permis d'identifier des épitopes sur les deux domaines du RBD et sur le CC du RBD. Plus précisément, j'ai identifié des cibles spécifiques du génotype dans les régions du RBD supérieur, tandis qu'un épitope strictement spécifique du GII a été défini à la base inférieure du RBD.

TABLE OF CONTENTS

PREFACE	i
ACKNOWLEDGEMENTS	ii
RÉSUMÉ	iv
ABSTRACT	v
RÉSUMÉ SUBSTANTIEL EN FRANÇAIS.....	vi
Manuscrit I: Nouvelle structure d'un RBD de VFS	vi
Manuscrit II: Caractérisation des épitopes des AcNs	viii
TABLE OF FIGURES	1
LIST OF TABLES	3
LIST OF ABBREVIATIONS.....	4
CHAPTER I.....	6
1 INTRODUCTION.....	7
1.1 Genetic and molecular characterization of foamy viruses	10
1.1.1 Phylogeny of retroviruses	11
1.1.2 FV evolution	12
1.1.3 FV virions, genome, protein synthesis and replication cycle.....	14
1.1.3.1 FV virions and genomic organization	14
1.1.3.2 Synthesis of FV proteins	17
1.1.3.3 FV replication cycle	18
1.1.4 Functional and structural characterization of SFV Env	24
1.1.4.1 Env primary sequence, receptor binding domain and 3D structure	25
1.1.4.2 Env glycosylation	27
1.1.4.3 Env-dependent FV particle budding and subviral particle release	27
1.1.4.4 Env-induced superinfection resistance	28
1.1.5 Genetic variability and recombination of SFVs	30
1.1.5.1 Genetic stability of FVs	30
1.1.5.2 FV diversity and recombination.....	30
1.1.5.3 Env diversity of SFV strains infecting humans and Apes in Central Africa	31
1.2 Epidemiology and zoonotic transmission of SFVs	35
1.2.1 SFV prevalence and transmission in and between NHPs	35
1.2.1.1 African continent – OWMs and Apes	36
1.2.1.2 South and Southeast Asia – OWMs and Apes	37
1.2.1.3 Central and South America – NWMs	38

Table of Contents

1.2.2 SFV in vivo tropism and pathology in NHPs.....	39
1.2.3 Zoonotic SFV infections	40
1.2.3.1 Zoonotic cases in West and Central Africa	42
1.2.3.2 Zoonotic cases in South and Southeast Asia	43
1.2.3.3 Zoonotic cases of NWM SFV.....	44
1.2.4 Pathology and clinical signs associated with SFV-infection in humans	44
1.2.4.1 In vivo tropism of SFVs in humans	45
1.3 Immune responses to FVs	48
1.3.1 Overview of immune responses to retroviruses.....	48
1.3.1.1 Innate sensing	48
1.3.1.2 Restriction factors	49
1.3.1.3 Cellular effectors of innate immunity.....	49
1.3.1.4 Interactions between innate and adaptive immunity.....	50
1.3.1.5 Adaptive immunities	50
1.3.1.5.1 T lymphocytes.....	51
1.3.1.5.2 B lymphocytes.....	52
1.3.1.6 Role of nAbs during viral infections	55
1.3.2 Innate immunity to FVs.....	56
1.3.2.1 Innate sensing of FVs	57
1.3.2.2 FVs are susceptible to IFNs	57
1.3.2.3 FV restriction by well-characterized host factors	58
1.3.2.4 FV restriction by novel intrinsic host factors	60
1.3.2.5 FV restriction by miRNAs	63
1.3.3 Antibody responses to FVs.....	63
1.3.3.1 FV serology and diagnostics	64
1.3.3.1.1 FV serotypes	64
1.3.3.1.2 Studies of Central-African hunters	65
1.3.3.1.3 Mapping of linear epitopes on Env	67
1.3.3.1.4 FV-specific nAbs and cell-to-cell transmission	68
1.3.4 nAb epitopes on Env from other retroviruses	69
1.3.4.1 MLV.....	69
1.3.4.1.1 Env capture among MLVs – tropism and recognition by nAbs	71
1.3.4.2 HTLV.....	72
1.3.4.3 HIV	74
CHAPTER II	78
2 PHD THESIS AIMS AND HYPOTHESIS.....	79
CHAPTER III.....	80
3 PRESENTATION OF PUBLICATIONS	81

3.1 Manuscript I: Novel structure of an SFV RBD.....	81
3.2 Manuscript II: Characterization of nAb epitopes	83
CHAPTER IV	86
4 MANUSCRIPT I.....	87
4.1 Abstract	87
4.2 Introduction	88
4.3 Results.....	90
4.3.1 The X-ray structure of the SFV RBD reveals a novel fold	90
4.3.2 The sugar attached to the strictly conserved 8 th N-glycosylation site plays a structural role	93
4.3.3 The RBD fold is predicted to be conserved within the Spumaretrovirinae subfamily	95
4.3.4 Fitting of the RBD atomic model into Env cryo-EM density map reveals the trimeric RBD arrangement	96
4.3.5 Positively charged residues in the lower subdomain form a heparan sulfate binding site	98
4.4 Discussion	103
4.5 Materials and Methods	107
4.5.1 Expression construct design (SFV RBD and ectodomains for HS binding studies).....	107
4.5.2 Recombinant SFV RBD and ectodomain production and purification	107
4.5.3 Crystallization	109
4.5.4 X-ray diffraction data collection and SFV RBD structure determination.....	109
4.5.5 Cells, viral sequences and production of foamy virus viral vectors.....	110
4.5.6 Prediction of RBD heparan-binding site and mutant design	112
4.5.7 Env interactions with heparan sulfate assayed by binding to heparin-sepharose.....	112
4.5.8 Env interactions with heparan sulfate on cells (in vitro): Env protein binding assay	112
4.5.9 Heparan sulfate removal and detection	113
4.5.10 FVVs binding assay	113
4.5.11 Statistics	113
4.5.12 Data availability	114
4.6 Acknowledgements	114
4.7 Author contributions.....	114
4.8 Competing interests.....	114
CHAPTER V	115
5 MANUSCRIPT II.....	116
5.1 Abstract	116
5.2 Introduction	117
5.3 Results.....	119
5.3.1 Infrequent binding of plasma antibodies to linear epitopes located on the SUvar domain	119
5.3.2 SFV SU protein competes with the virus for binding to nAbs	121
5.3.3 Certain nAbs target glyco-epitopes	124

Table of Contents

5.3.4 SFV-specific nAbs target loops at the RBD apex	127
5.3.5 SFV-specific nAbs target the base of the SUvar region	129
5.3.6 GI and GII-specific nAbs target different epitopes.....	131
5.3.7 Human plasma samples contain nAbs targeting a variable number of epitopic regions.....	133
5.3.8 Functional studies	134
5.3.8.1 Protein binding to susceptible cells.....	134
5.3.8.2 The epitopic regions targeted by nAbs are involved in viral infectivity	135
5.3.9 Three-dimensional map of epitopic regions.....	136
5.4 Discussion	138
5.5 Materials and Methods	142
5.5.1 Human plasma samples.....	142
5.5.2 Viral strains, amino-acid numbering, and Env domain nomenclature.....	142
5.5.3 Cells.....	142
5.5.4 Peptides.....	143
5.5.5 ELISA	143
5.5.6 Plasmids	144
5.5.7 Protein expression and purification	145
5.5.8 Western-blot	146
5.5.9 Foamy viral vectors (FVVs)	146
5.5.10 Neutralization assays	147
5.5.11 SFV Env binding to cells	148
5.5.12 Analysis of FVVs carrying mutated Env	148
5.5.13 Statistical analysis	150
5.6 Acknowledgements	151
5.7 Funding.....	151
5.8 Authors contribution.....	151
CHAPTER VI.....	152
6 DISCUSSION AND PERSPECTIVES	153
6.1 Achievements on nAb epitopes.....	153
6.1.1 SFV nAb epitopes are conformational.....	153
6.1.2 Localization of nAb epitopes on RBD and possible mode of actions	153
6.1.3 Limitations of current data and opportunities to address them in future studies	159
6.1.4 Epitope comparison to nAbs targeting orthoretroviruses.....	161
6.2 Achievements regarding the two genotypes	161
6.2.1 Discovery of genotype-specific epitopes	161
6.2.2 Genotype-specific determinants of binding	162
6.2.3 A similar global fold of RBD among distinct FVs	162
6.2.4 Genotype-specific ELISA assay and tools to identify co-infected individuals	163
6.3 Next step on epitope mapping.....	164

Table of Contents

6.4 Env mutations useful for selecting Env-specific B cells.....	164
6.5 Next step on SFV Env structure	165
6.6 Next step on SFV receptor	166
6.6.1 HBS	166
6.7 Next step on antiviral role of antibodies	166
CHAPTER VII	168
7 CONCLUSIONS	169
CHAPTER VIII.....	170
8 LIST OF REFERENCES	171
CHAPTER IX.....	196
9 APPENDICES	197
9.1 Supplementary Tables - Manuscript I.....	197
9.2 Supplementary Figures - Manuscript I	201
9.3 Supplementary Tables – Manuscript II.....	214
9.4 Supplementary Figures - Manuscript II.....	220

TABLE OF FIGURES

Figure I-1 – Different stages of emerging zoonotic viral agents	9
Figure I-2 – Electron microscopy pictures of HFV derived from tissue cultures of a Kenyan patient	10
Figure I-3 – Phylogenetic tree of retroviruses belonging to the Retroviridae family	11
Figure I-4 – Phylogenetic relationship of simian members in the Spumaretrovirinae subfamily	13
Figure I-5 – Evolution of FV co-speciation within vertebrate hosts	14
Figure I-6 – Structural organization of FV particle	15
Figure I-7 – Genomic organization of PFV and its viral transcripts	16
Figure I-8 – Schematic and electron microscopy representation of PFV replication cycle	23
Figure I-9 – Primary sequence and 3D structure of trimeric PFV Env	26
Figure I-10 – Schematic overview of PFV Env gp130	28
Figure I-11 – Schematic overview of superinfection resistance	29
Figure I-12 – Phylogenetic analysis of SFV strains based on the conserved and variable region of env	32
Figure I-13 – Recombination analysis of fifty-four SFV env sequences	33
Figure I-14 – Schematic overview of SUvar region within PFV SU gp80	34
Figure I-15 – A view of the global distribution of NHPs	36
Figure I-16 – Global distribution of zoonotic SFV-infections reported to date	41
Figure I-17 – SFV in vivo tropism in Central African hunters	46
Figure I-18 – Pyramidal scheme of zoonotic SFV transmission and potential immune control	47
Figure I-19 – Schematic structural overview of human Ig molecules and subclasses	54
Figure I-20 – Overview of dynamics during germinal center reaction and B cell fates	55
Figure I-21 – Neutralization profiles of donors infected with zoonotic SFV strains from two genotypes	67
Figure I-22 – Organization of distinct retroviral Envs	69
Figure I-23 – Fr-MLV SU gp70 sequence and RBD structure	71
Figure I-24 – HTLV-1 SU gp46 sequence and location of nAb epitopes	73
Figure I-25 – Structure of HIV-1 Env pre-fusion trimer and location of major classes of bnAb epitopes ..	76
Figure IV-1 – Overview of the novel fold adopted by the SFV RBD	91
Figure IV-2 – SFV secondary structure topology diagram	93
Figure IV-3 – The oligosaccharide linked to N390 plays a structural role in the RBD	94
Figure IV-4 – The RBDs form a trimeric assembly at the apex of the full-length Env	97
Figure IV-5 – Prediction of HS binding residues and design of the variants impaired in binding	99
Figure IV-6 – The SFV RBD residues K342, R343, R356 and R369 mediate Env binding to HS	101
Figure V-1 – SFV Env	119
Figure V-2 – Only a small proportion of plasma samples bind to peptides covering the SUvar domain ...	121
Figure V-3 – The SFV SU block nAbs without affecting viral entry	123
Figure V-4 – SFV-specific nAbs recognize glycans on SUvar	126
Figure V-5 – Most SFV-specific nAbs recognize the RBDj domain	128
Figure V-6 – Epitope disruption by glycan insertion revealed additional sites recognized by nAbs	130
Figure V-7 – GI and GII-specific nAbs target different epitopes	132

Table of Figures

Figure V-8 – Most samples contain nAbs that recognize several epitopic regions on SUvar	133
Figure V-9 – nAbs target epitopic regions involved in SU binding to susceptible cells or required for viral infectivity	135
Figure V-10 – Schematic summary of current knowledge on SFV Env	137
Figure VI-1 – Summary of discovered genotype-specific epitopic regions	154
Figure S.IV-1 – The fold of the FV RBD is maintained by hydrophobic and polar interactions	201
Figure S.IV-2 – Mobile loops decorate the apex of the RBD	202
Figure S.IV-3 – Comparison of glycosylated vs deglycosylated RBD structures	203
Figure S.IV-4 – Comparison of the SFV RBD fold with that of the RBD of Orthoretroviruses	204
Figure S.IV-5 – Sequence conservation of FV Env	206
Figure S.IV-6 – Intramolecular contacts between N8 sugar and RBD	207
Figure S.IV-7 – Functional features of FV RBD mapped onto the structure	208
Figure S.IV-8 – AlphaFold models of FV RBDs	208
Figure S.IV-9 – FV RBD common core excludes a large portion of the upper subdomain	209
Figure S.IV-10 – The inter-protomer RBD contacts formed by the upper domain loops show poor sequence conservation	210
Figure S.IV-11 – Recombinant RBD variants remain monomeric in solution	210
Figure S.IV-12 – Flow cytometry gating strategy	211
Figure S.IV-13 – Effect of mutations on FVV release and infectious titer	212
Figure S.IV-14 – Structural basis for RBDjoin region being dispensable for binding to cells	213
Figure S.V-1 – CI-PFV, GI-D468, and GII-K74 Env sequence alignment	221
Figure S.V-2 – Recombinant SFV Env oligomerization and mammalian-specific glycolysation do not affect the capacity to inhibit GII-specific nAbs	222
Figure S.V-3 – Western-blot analysis of WT SU proteins used in the study	223
Figure S.V-4 – Purity of immunoadhesins used in the study assessed by Coomassie blue gel staining	224
Figure S.V-5 – Plasma antibodies do not bind to peptides covering the loops located at the apex of the RBD and targeted by nAbs	225
Figure S.V-6 – The ^{GII351glyc} immunoadhesin is unable to block nAbs – exclusion of a nonspecific effect of protein aggregation	226
Figure S.V-7 – Sequences from gorilla SFV strains circulating in Central Africa are conserved in the epitopic regions targeted by nAbs	227
Figure S.V-8 – Recombinant immunoadhesins bind to susceptible cells	228
Figure S.V-9 – Env proteins deleted of RBDj, L2, L3 or L4 sequences are expressed in transfected cells	229

LIST OF TABLES

Table I-1 – Properties of FV in comparison to orthoretroviruses and hepadnaviruses	18
Table I-2 – In vitro cell tropism of replicative or vector-based PFV and HS expression	20
Table I-3 – Details on zoonotic SFV-infections documented to date	41
Table I-4 – In vivo SFV cell tropism in infected NHPs and humans	45
Table I-5 – Summary of PFV restriction by intrinsic host factors	62
Table I-6 – List of historical SFV serotypes	65
Table S.IV-1 – X-ray crystallography data collection and refinement statistics	197
Table S.IV-2 – Secondary structure content in GII RBD	198
Table S.IV-3 – Intramolecular interactions within GII RBD	199
Table S.V-1 – Plasma samples used for the ELISA assays	214
Table S.V-2 – Synthetic peptides used to search for linear epitopes	215
Table S.V-3 – SFV Env proteins produced for the study	216
Table S.V-4 – Plasma samples used for the neutralization study	218
Table S.V-5 – Methods used to predict epitopic regions and to design the mutant SU proteins	219

LIST OF ABBREVIATIONS

aa	Amino acid	ER	Endoplasmic reticulum
Ab	Antibody	ERV	Endogenous retrovirus
ADCC	Ab-dependent cellular cytotoxicity	ET	Electron tomography
ADCP	Ab-dependent cellular phagocytosis	Fab	Antigen-binding fragment
AF	AlphaFold	FBS	Fetal bovine serum
AGM	African green monkey	Fc	Crystallizable fragment
AID	Activation-induced cytidine deaminase	FcR	Fc receptor
AIDS	Acquired immunodeficiency syndrome	FDC	Follicular dendritic cell
APC	Antigen presenting cell	FeLV	Feline leukemia virus
APOBEC	Apolipoprotein B editing complex	FFV	Feline foamy virus
ART	Antiretroviral therapy	FP	Fusion peptide
ATL	Adult T-cell leukemia/lymphoma	FV	Foamy virus
BCR	B cell receptor	FVV	Foamy viral vector
Bet	Between <i>env</i> and <i>tas</i>	Gag	Group-specific antigen
BFV	Bovine foamy virus	GC	Germinal center
BHK	Baby hamster kidney	GI	Gorilla genotype I
bnAb	Broadly neutralizing antibody	GII	Gorilla genotype II
C	Constant	GLUT	Glucose transporter
C-ter	C-terminus	H	Heavy chain
CAT	Cationic aa transporter	HBS	Heparan binding site
CC	Common core	HBV	Hepatitis B virus
CI	Chimpanzee genotype I	HEK	Human embryonic kidney
CoV	Corona virus	HFV	Human foamy virus
CPE	Cytopathic effect	HIV	Human immunodeficiency virus
CRM	Chromosomal maintenance	HS	Heparan sulfate
CTD	C-ter domain	HSPG	Heparan sulfate proteoglycan
CTE	Constitutive transport element	HTLV	Human T-cell leukemia virus
CTL	Cytotoxic T lymphocyte	IC	Inhibitory concentration
CyD	Cytoplasmic domain	IFITM	Interferon-induced transmembrane
D	Diversity	IFN	Interferon
DC	Dendritic cell	Ig	Immunoglobulin
DRC	Democratic Republic of Congo	IL	Interleukin
ds	Double stranded	ILC	Innate lymphoid cell
DS	Disulfide bonds	IN	Integrase
EFV	Equine foamy virus	IP	Internal promotor
ELISA	Enzyme-linked immunosorbent assay	ISG	Interferon stimulated gene
EM	Electron microscopy	IU	Infectious unit
Env	Envelope glycoprotein	J	Joining

List of Abbreviations

JAK	Janus kinase	pLDDT	Predicted local distance difference test
KIR	Killer Ig-like receptor	PML	Promyelocytic leukemia
L	Light chain	PMNL	Polymorphonuclear leucocytes
LP	Leader peptide	PNGS	Potential N-glycosylation site
LTR	Long terminal repeat	Pol	Polymerase
MA	Matrix	PR	Protease
mAb	Monoclonal antibody	PRR	Pattern-recognition receptor
MaxI	Maximum inhibition	PRRH	Proline rich hinge region
MBC	Memory B cell	PSFV	Prosimian foamy virus
MFI	Mean fluorescence intensity	RBD	Receptor binding domain
MHC	Major histocompatibility complex	RBDj	Joining RBD subdomain
miRNA	Micro RNA	RH	RNAse H
MLV	Murine leukemia virus	rmsd	Root mean square deviation
MOV10	Moloney leukemia virus 10-like	RT	Reverse transcriptase
MPER	Membrane-proximal external region	SAMHD	Sterile alpha motif and HD domain
mRNA	Messenger RNA	SARS	Severe acute respiratory syndrome
MSD	Membrane spanning domain	SERINC	Serine incorporator
MTD	Membrane targeting domain	SFV	Simian foamy virus
MTOC	Microtubule organizing center	SGK	Serum/glucocorticoid regulated kinase
Mx	Myxovirus resistance	SHM	Somatic hypermutation
N-ter	N-terminus	SIV	Simian immunodeficiency virus
nAb	Neutralizing antibody	SLFN	Schlafen
NAG	N-acetyl glucosamine	SP	Signal peptide
NEAA	Non-essential aa	ss	Single stranded
NES	Nuclear export sequence	STLV	Simian T-cell leukemia virus
NHP	Non-human primate	SU	Surface domain
NK	Natural killer	SUcon	Constant region of SU
NLS	Nuclear localization signal	SUvar	Variable region of SU
NRP	Neuropilin	Tas	Trans-activator of spumavirus
NTD	N-ter domain	T_{FH}	Follicular T helper
NWM	New-World monkey	Th	T helper
OASL	Oligoadenylate synthase-like	TLR	Toll-like receptor
ORF	Open reading frame	TM	Transmembrane
OWM	Old-World monkey	TM-score	Template modelling score
PAMP	Pathogen-associated molecular pattern	TNF	Tumor necrosis factor
PBMC	Peripheral blood mononuclear cell	TRIM	Tripartite-motif
pDC	Plasmacytoid dendritic cell	Ub	Ubiquitin
PFV	Prototype foamy virus	V	Variable
PHF	PHD finger domain protein	VR	Variable region
PIC	Preintegration complex	WT	Wild-type

CHAPTER I

INTRODUCTION

1 | INTRODUCTION

The emergence of pathogenic infectious agents in the human population is often the result of a transmission from an animal reservoir, a so-called zoonosis (Jones et al., 2008; Taylor et al., 2001). Pathogenic zoonotic viruses have led to numerous outbreaks with major impacts on human society during the past century (Jones et al., 2008; Morens et al., 2008). Of notice are the 1918 and 2009 avian/swine flu pandemics (Garten et al., 2009; Potter, 2001) as well as the ongoing severe acute respiratory syndrome corona virus 2 (SARS-CoV-2) pandemic (Wu et al., 2020; Zhou et al., 2020). Besides pandemics, outbreaks of reemerging viruses are frequent: important examples include Ebola viruses (Malvy et al., 2019), hantaviruses (Martínez et al., 2020) and vector born arboviruses such as Zika, Dengue and Chikungunya (Marston et al., 2014). The introduction of zoonotic viruses is influenced by factors like live animal markets, rapid urbanization and ongoing climate changes (Bloom et al., 2017; Daszak et al., 2000). Indeed, recent model simulations predict that hotspots for viral sharing and cross-species transmissions will expand and increase in regions with high biodiversity and dense human populations as global warming continues in the coming 50 years (Carlson et al., 2022). The likelihood of infectious organisms to emerge in humans is influenced by both the organism species and presence of geographical overlap between their animal hosts and humans (Davies and Pedersen, 2008).

In line with this, the continuing rise of human density in rural forest areas including deforestation and non-human primate (NHP) bushmeat marked sales have likely favored retrovirus cross-species transmissions from simian reservoirs to humans in Central Africa (Locatelli and Peeters, 2012), and led to the emergence of human immunodeficiency virus (HIV) in the 1980s (Rua and Gessain, 2015; Sharp and Hahn, 2011).

A broad range of Old-World monkeys (OWMs) and Apes are natural hosts of several retroviruses including the simian immunodeficiency virus (SIV) and simian T-cell leukemia virus (STLV) (Locatelli and Peeters, 2012). Today, more than 40 different SIVs have been discovered in African OWMs and Apes while more than 30 NHP species across Africa and Asia have been shown to naturally carry STLVs. A complex transmission pattern of SIVs from smaller monkeys including the *Cercopithecus* species to certain chimpanzee subspecies – and from chimpanzees to a subspecies of gorillas have influenced the emergence of the human immunodeficiency virus type 1 (HIV-1) (Peeters and Delaporte, 2012; Sharp and Hahn, 2011). Indeed, a single cross-species transmission of SIVcpz from chimpanzees (*Pan troglodytes*

troglydytes) in Southeastern Cameroon gave rise to the HIV-1 group M epidemic, while an additional SIVcpz transmission in South-central Cameroon led to the HIV-1 group N strains infecting a more limited number of individuals (Keele et al., 2006; Sharp and Hahn, 2011). The endemic HIV-1 group O and P strains have been shown related to SIVgor from Western lowland gorillas (*Gorilla gorilla*) (D'Arc et al., 2015; Plantier et al., 2009). This gorilla subspecies likely acquired its SIV-infection from chimpanzees about 100-200 years ago (Takehisa et al., 2009). The SIVcpz transmission event which led to the HIV-1 group M pandemic was estimated to have occurred in Kinshasa in the Democratic Republic of Congo (DRC) in the 1920s (Faria et al., 2014). Concurrently, the less pathogenic and distally related HIV-2 resulted from nine independent transmission events of SIVsmm from sooty mangabey monkeys (*Cercocebus atys*) in West Africa (Ayoub et al., 2013; Chen et al., 1996; Hirsch et al., 1989). These transmissions gave rise to endemic HIV-2 group A and B strains infecting approx. 1-2 million people in West Africa, and seven 'dead-end' infections (group C to I) each described only in one or two individuals to date (Visseaux et al., 2016). Another human retrovirus with oncogenic features was isolated from a patient with cutaneous T-cell lymphoma, today known as human T-cell leukemia virus type 1 (HTLV-1) (Poiesz et al., 1980). HTLV-1 is highly endemic in areas of Japan, sub-Saharan Africa, the South Americas, the Caribbean and among Aboriginal groups of Australia. An estimated 5-10 million people are carriers of HTLV-1 and although most cases remain asymptomatic, approximately 5% are associated with severe disease like adult T-cell leukemia/lymphoma (ATL) (Gessain and Cassar, 2012). Epidemiology and molecular virology studies on the simian counterpart to HTLV-1 (STLV-1) suggest that cross-species transmission of STLV-1 to humans occurred approximately 27,300 years ago in Africa (Jegado et al., 2019; Peeters and Delaporte, 2012). Importantly, zoonotic transmissions of SIVsmm and STLV-1 are still ongoing today in populations exposed to NHPs (Ayoub et al., 2013; Filippone et al., 2015; Kazanji et al., 2015; Wolfe et al., 2005).

The foamy viruses (FVs, also named spumaviruses) constitute the third family of complex retroviruses found widespread among many animal species including both OWMs, Apes and New-World monkeys (NWMs). My host laboratory has described that bites from NHPs constitute the major route of zoonotic transmission of simian FVs (SFVs) into humans (Betsem et al., 2011; Calattini et al., 2007). Human SFV-infection leads to the establishment of a lifelong persistent infection without reported severe pathogenicity or human-to-human transmission. The course of animal pathogens to emerge and cause disease in the human population can be explained by five stages (Wolfe et al., 2007). SFVs represent a stage 2 pathogen. This stage

describes a zoonotic spill-over from an animal reservoir into a human without subsequent human-to-human transmission. Most SFV-infected humans reported direct contact with NHPs and are therefore the first human host of these zoonotic viruses. In contrast, HTLV-1 and HIV-1 group M represent stage 4 and 5 pathogens, respectively (Fig. I-1). Stage 4 delineate several cycles of animal-to-human and/or human-to-human transmissions while stage 5 transmissions are driven solely by a human reservoir.

With this in mind, FVs constitute a good model to study one key step of emergence of a simian retrovirus: its persistence in the primary human host and the restriction of its transmission to other human hosts. The work of this PhD thesis has been focusing on the humoral immune responses directed against zoonotic SFVs with use of plasma samples from SFV-infected Central African inhabitants from Cameroon bitten by gorillas during hunting activities. Neutralizing antibodies from individuals were tested against viral derived vectors and proteins whose sequence are identical to the SFV strains they are infected with.

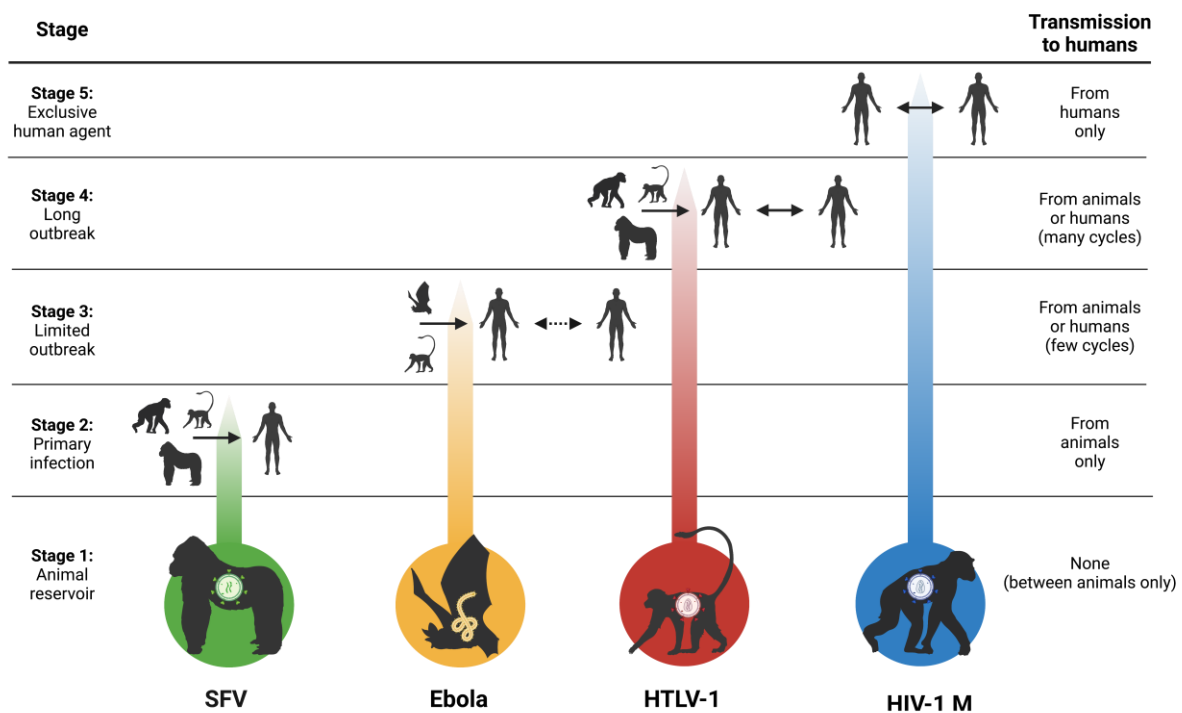


Figure I-1 – Different stages of emerging zoonotic viral agents

Examples of different stages of infection/spill-over (left column) by four major zoonotic viruses in accordance to the reservoir mediating transmission to humans (right column). **Stage 2 agents:** characterized by human acquisition from direct contact with animal reservoir and no human-human transmission, exemplified by SFV transmission from NHP reservoirs. **Stage 3 agents:** characterized by human cases acquired from animal reservoirs leading to smaller human outbreaks with limited human-human transmission, exemplified by Ebola virus from bat and NHP reservoirs. **Stage 4 agents:** described by longer endemic outbreaks with human-human transmission as main route, although animal-human transmissions still occur as exemplified by HTLV-1 originating from NHP reservoirs. **Stage 5 agents:** characterized by the establishment of a long epidemic outbreak with exclusive human-

human transmission, as seen for HIV-1 group M originating from a single spill-over from a chimpanzee reservoir. *Figure created with BioRender.com and adapted from (Wolfe et al., 2007).*

1.1 Genetic and molecular characterization of foamy viruses

FVs were discovered by coincidence in 1954 by Enders and Peebles who observed cytopathic effects (CPEs) in rhesus monkey kidney cell culture (Enders and Peebles, 1954). In the following years several strains of SFVs were isolated from tissue cultures of rhesus and cynomolgus macaques as well as from baboons and red grass monkeys (Clarke et al., 1969; Johnston, 1961; Rustigian et al., 1955). Then in 1971, Achong and colleagues isolated a similar virus (Fig. I-2) from a nasopharyngeal carcinoma biopsy of a patient from Kenya causing CPEs in human cells (Achong et al., 1971). The virus was initially termed human foamy virus (HFV) and subsequent serological characterizations of HFV showed high similarities to strains isolated from chimpanzees (Brown et al., 1978; Nemo et al., 1978). Isolation of the HFV strain initially led to speculations on naturally circulating HFVs. However, a comprehensive study with appropriate testing (serology and PCR) failed to detect HFV in samples from 223 patients and did not find antibodies in any of >2600 human sera samples from suspected high-risk areas (Meiering and Linial, 2001; Schweizer et al., 1995). Sequencing of HFV demonstrated this strain to be closely related to a chimpanzee SFV strain (Herchenroder et al., 1994). A later study found the *integrase* (IN) and *group-specific antigen* (gag) sequences of HFV to be 96% identical at the nucleotide level with SFV strains isolated from the chimpanzee subspecies *Pan troglodydes schweinfurthii* (SFVpsc), suggesting the Kenyan HFV isolate to represent a unique case of zoonotic spill-over from NHPs (Switzer et al., 2004). Today, HFV is referred to as prototype foamy virus (PFV) which is the most commonly studied laboratory adapted strain.

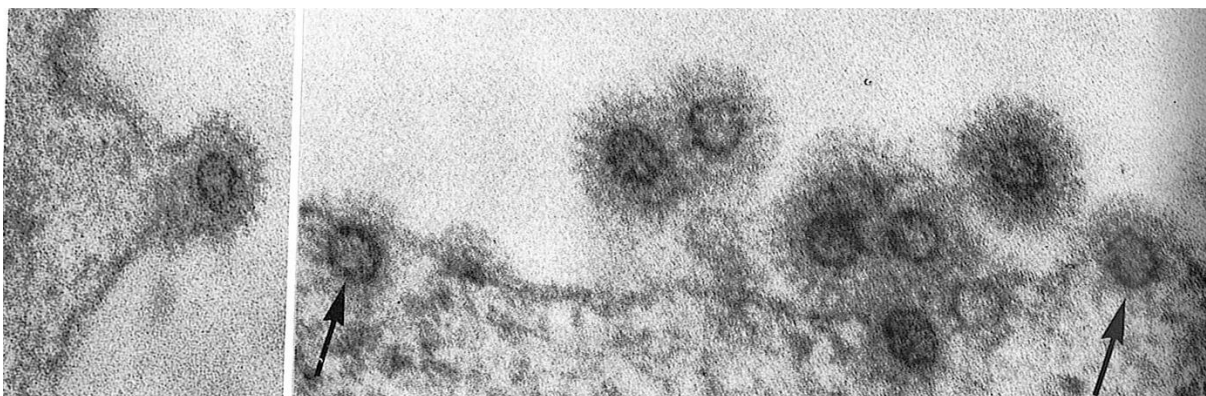


Figure I-2 – Electron microscopy pictures of HFV derived from tissue cultures of a Kenyan patient

Left: Mature viral particle budding from cell surface plasma membrane (x137,500). **Right:** Mature and immature (arrows) viral particles budding from cell surface plasma membrane (x180,000). Authors acquired the pictures by a Phillips EM 300 electron microscope. *Figure from (Achong et al., 1971).*

1.1.1 Phylogeny of retroviruses

Retroviruses are single stranded (ss) RNA viruses named after their characteristic enzyme, the reverse transcriptase that transcribes their ssRNA genome into double stranded (ds) DNA. The *Retroviridae* family consists of both exogenous and endogenous retroviruses (ERVs) (Fig. I-3). The exogenous retroviruses are divided into seven distinct genera (*Alpha-*, *Beta-*, *Delta-*, *Epsilon-* and *Gamma retrovirus*, *Lenti-* and *Spumavirus*) which are separated into two subfamilies; the *Orthoretrovirinae* and *Spumaretrovirinae*. The FVs constitute a single genus of the *Spumaretrovirinae* subfamily. This taxonomy reflects that FVs are basal and distinct from other exogenous retroviruses due to their unusual style of replication which share properties with that of hepatitis B virus (HBV) from the *Hepadnaviridae* family (Rethwilm, 1996). The exogenous retroviruses are also classified as either simple or complex type based on the absence or presence of viral accessory genes. Three genus of complex type retroviruses are found among several vertebrate animal species, including primates and humans: *Lentivirus* which comprise the SIV/HIV, *Deltaretrovirus* which comprise the STLV/HTLV and *Spumavirus*.

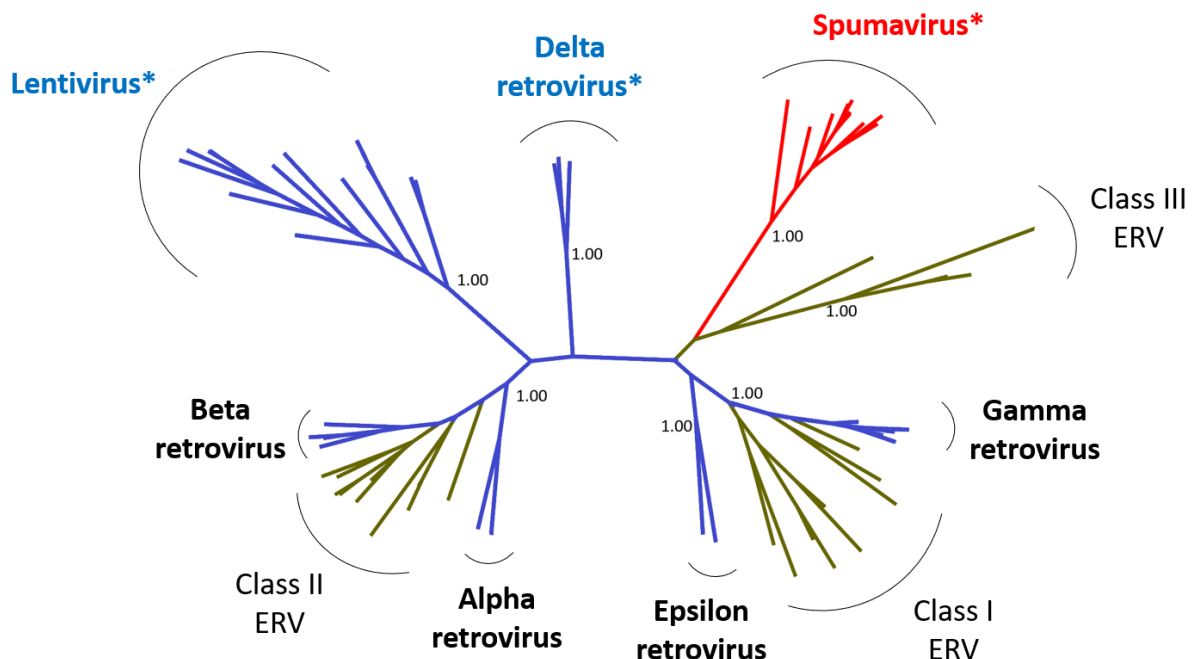


Figure I-3 – Phylogenetic tree of retroviruses belonging to the *Retroviridae* family

Phylogenetic tree of exogenous and endogenous members from the *Retroviridae* family based on the conserved sequence of *pol*. Genera belonging to the *Orthoretrovirinae* and *Spumaretrovirinae* subfamilies are shown in blue and red, respectively. The three classes of ERVs are shown in olive. Complex type retroviruses are highlighted with a star by the name of genus in order to distinguish these from simple type retroviruses. Posterior probabilities shown near selected nodes. Figure adapted from (Han and Worobey, 2012a).

1.1.2 FV evolution

The exogenous family of *Spumavirus* is divided into five distinct genera; *Simiispumavirus* (SFVs), *Prosimiispumavirus* (prosimian FVs, PSFVs), *Felispumavirus* (feline FVs, FFV), *Bovispumavirus* (bovine FVs, BFVs) and *Equispumavirus* (equine FVs, EFVs) (Khan et al., 2018). Exogeneous FVs are found naturally in many mammals counting cats and pumas (Kechejian et al., 2019; Riggs et al., 1969), cattle and bisons (Amborski et al., 1987; Malmquist et al., 1969), horses (Tobaly-Tapiero et al., 2000), sheeps (Flanagan, 1992), bats (Wu et al., 2012), prosimians (Katzourakis et al., 2014) and notably in a broad range of NHP species (Fig. I-4). These include both Asian and African OWMs and Apes (Hussain et al., 2003) as well as NWMs in the South Americas (Gherzi et al., 2015; Muniz et al., 2015; Muniz et al., 2013), and SFVs have been shown to co-speciate with their NHP hosts for 30 million years (Switzer et al., 2005).

To reflect on FV evolution, the nomenclature of FVs use the virus host name and “foamy virus” in three letter capitals (i.e. FFV for feline FV, SFV for simian FV) followed by a three-letter lowercase of the latin host species name. The three-letter lowercase comprises the first letter of the host genus followed by the first two letters of the species/subspecies. Isolate-identifying information are added after an underscore such as the host from which it was isolated, for instance “hu” for human or isolate name (Khan et al., 2018). As an example, the HFV/PFV strain which was the first human isolate later demonstrated to be a zoonotic chimpanzee (*Pan troglodytes schweinfurthii*) SFV strain also termed HSRV clone 13 is designated SFVpsc_huHSRV.13 and the zoonotic gorilla (*Gorilla gorilla*) SFV strain BAK74 isolated from an accidentally infected African hunter is designated SFVggo_huBAK74 (Khan et al., 2018; Rua et al., 2012a).

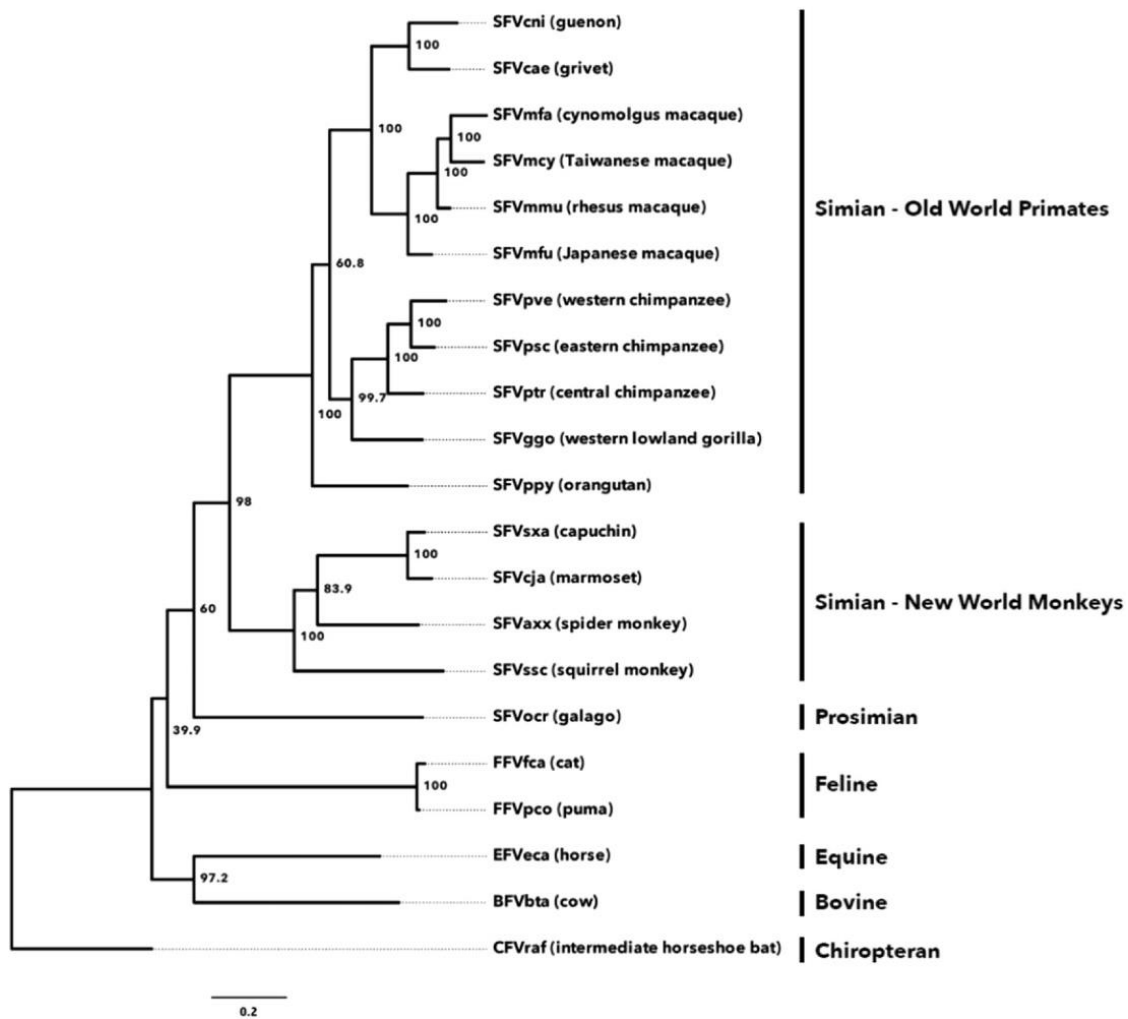


Figure I-4 – Phylogenetic relationship of simian members in the *Spumaretrovirinae* subfamily

Phylogenetic tree of *pol* and *env* sequences from 21 diverse mammalian FV hosts including 15 distinct species of NWMs, OWMs and Apes. Names of viral species mentioned at branch tips with three-letter lower case code of subspecies and name of common mammalian host species in brackets. Figure from (Khan et al., 2018).

Interestingly, the polymerase (*pol*) gene from the human ERV type L has been shown related to *pol* from FVs (Cordonnier et al., 1995). Indeed, FV-like sequences have been discovered as ERVs in a diverse group of animal species including zebra- and platyfish (Llorens et al., 2009; Scharl et al., 2013), the ancient marine fish coelacanth (Han and Worobey, 2012a), sloths (Katzourakis et al., 2009), reptiles (Aiewsakun et al., 2019b), the prosimian aye-aye (Han and Worobey, 2012b), as well as birds and snakes (Aiewsakun, 2020) suggesting an extremely ancient FV evolution for more than 450 million years (Fig. I-5) (Aiewsakun and Katzourakis, 2017). These studies on the macroevolutionary history of FVs have shown that all major vertebrate groups have been hosts of FVs in the past and that long-term co-speciation histories exist. FVs likely originated in the ocean half a billion years ago before co-diversifying with early vertebrate hosts into fish. Amphibian and reptile FVs radiated to dry land during this process (Aiewsakun, 2020). Moreover, the results on endogenous FVs suggest that cross-group

transmissions have appeared from reptiles once or maybe twice, likely from iguanas, lizards or snakes (Toxicofera group), which ultimately gave rise to mammalian and avian FV lineages (Fig. I-5) (Aiewsakun, 2020).

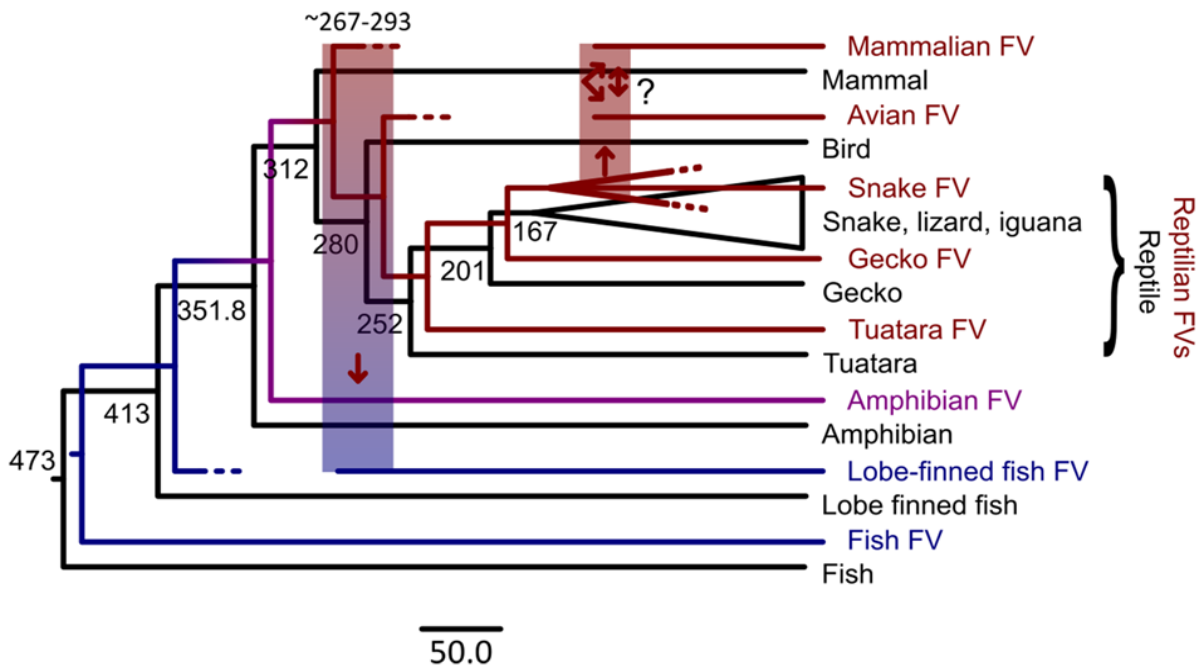


Figure I-5 – Evolution of FV co-speciation within vertebrate hosts

FV phylogeny in colored lines and host phylogeny in black lines. Colors represent aquatic, amphibian and terrestrial FVs in blue, purple and red colors, respectively. Dotted lines represent extinct or yet to be discovered FV lineages. Cross-clade transmissions are depicted as thick vertical transparent bars demonstrating direction of transmission by arrows. Certain transmission routes are unclear (?) to this date due to limited data. Host evolutionary timescale and scalebar are in units of million years. *Figure from (Aiewsakun, 2020).*

1.1.3 FV virions, genome, protein synthesis and replication cycle

Most of the knowledge on FV has been obtained with use of the PFV strain (SFVpsc_huHSRV.13) and a viral vector model system based on PFV (Heinkelein et al., 2002; Trobridge et al., 2002), and reviewed by (Lindemann and Rethwilm, 2011). Unless specified, literature presented refers to this strain.

1.1.3.1 FV virions and genomic organization

FV virions are enveloped spherical structures at a size of 100-140nm with characteristic long spikes (~14nm) on their surface when observed by electron microscopy (EM) (Fig. I-2) (Delelis et al., 2004; Effantin et al., 2016). FVs contain two copies of positive sense ssRNA genomes contained inside a protein capsid (Fig. I-6). In the infected cell, a late retrotranscription generates particles with dsDNA. The genome of PFV is approx. 13kb and follows the classical complex retrovirus organization with canonical structural genes *gag*, *pol* and envelope

glycoprotein (*env*) flanked by 5' and 3' long terminal repeats (LTRs). These genes encode for structural protein Gag, the viral enzymes protease (PR), reverse transcriptase (RT), RNase H (RH) and IN as well as the Env. Env is cleaved into three subunits; leader peptide (LP), surface domain (SU) and transmembrane domain (TM) (Lindemann and Rethwilm, 2011).

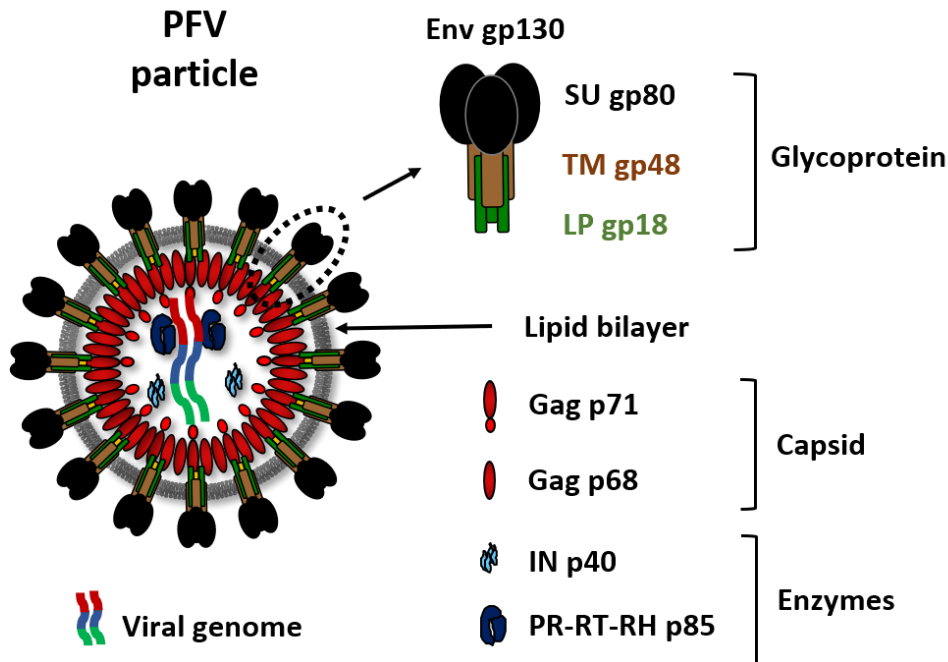


Figure I-6 – Structural organization of FV particle

Structure of PFV virion with enlargement of Env gp130 and its three subdomains LP gp18, SU gp80 and TM gp48. Other viral components including Gag p71/p68, IN p40, PR-RT-RH p85 and the viral genome highlighted below. Figure adapted from (Lindemann and Rethwilm, 2011).

The genome of FVs contains two open reading frames (ORFs) in the 3' part of the genome, *tas* and *bet*, which encode for two accessory proteins, Tas and Bet. The 5' LTR harbors the typical retroviral promoter in its U3 region and an unusual internal promoter (IP) located in *env* upstream of *tas*. The low basal activity of the IP leads to Tas expression that activates transcription at the IP, resulting in a positive feedback loop. Transcription of structural FV genes is strictly dependent on Tas since the promoter in 5' LTR U3 region is practically inactive (Keller et al., 1991; Löchelt et al., 1994; Löchelt et al., 1993; Löchelt et al., 1995). The only known function of Bet is to inhibit the restriction factor from the APOBEC3 family, as described in further detail in section 1.3 (Löchelt et al., 2005; Russell et al., 2005).

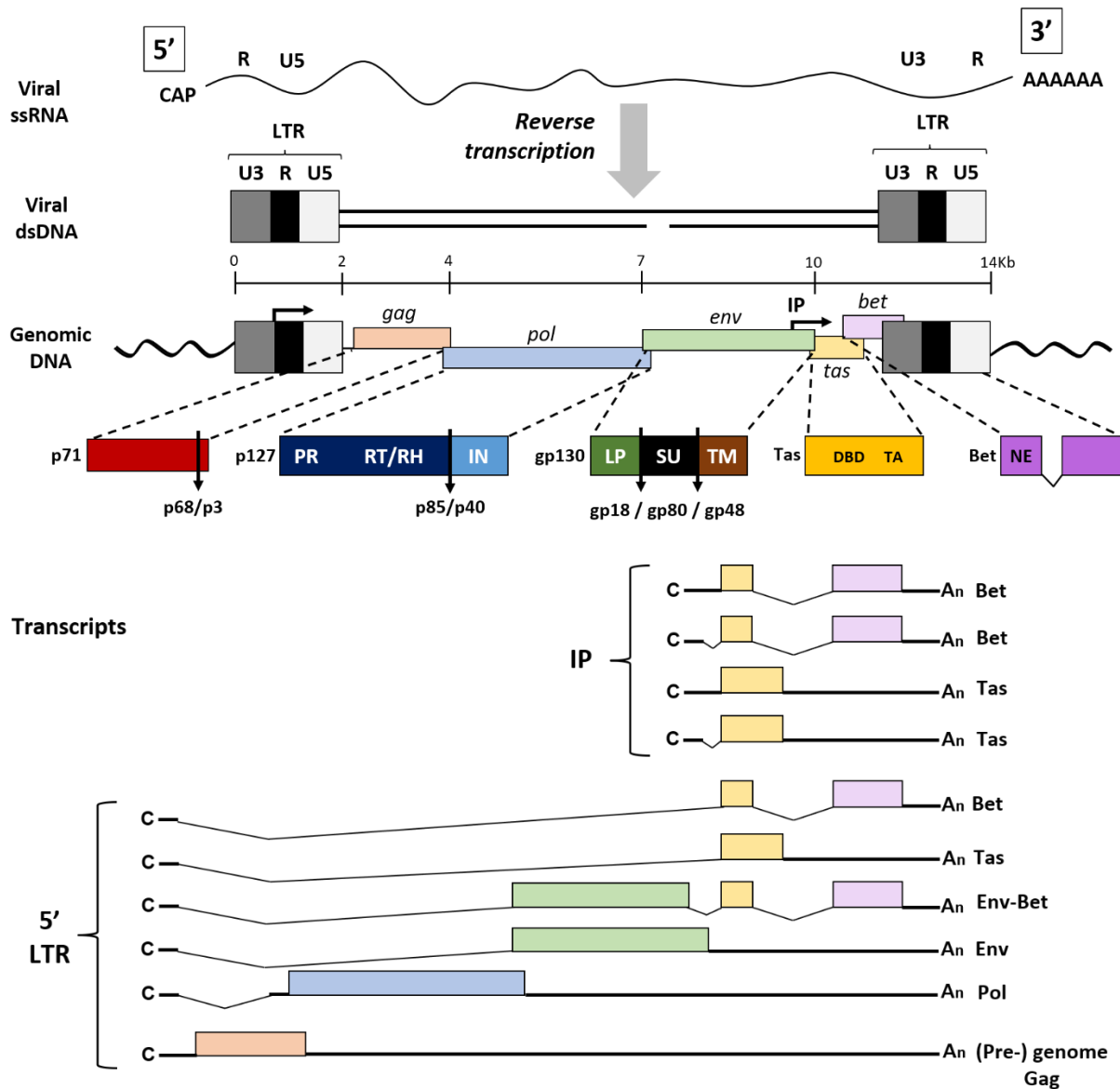


Figure I-7 – Genomic organization of PFV and its viral transcripts

Top: The viral RNA genome harbors a cap at its 5' end and a polyadenylation tail at its 3'. The viral ssRNA is reverse transcribed into viral dsDNA. The LTR includes a U3, R and U5 region shown in dark grey, black and light grey boxes, respectively. Provirus is generated by integration of the viral dsDNA into the host genome. The FV genome includes two promoters; a classical retroviral promoter in the U3 region of the 5' LTR and an unusual IP in *env* shown by black curved arrows. The viral genes *gag*, *pol*, *env*, *tas* and *bet* are shown in faded orange, blue, green, yellow and purple boxes, respectively encoding polyproteins shown below in dark shades. The protein Gag p71 is cleaved at its C-ter yielding p68 and p3 products shown in red. The protein Pol p127 containing the viral enzymes PR, RT, RH and IN is cleaved between RT and IN yielding PR-RT-RH p85 and IN p40 shown in dark and light blue, respectively. The surface Env gp130 is cleaved twice yielding LP gp18, SU gp80 and TM gp48 subunits shown in dark green, black and brown. The accessory proteins Tas and Bet are illustrated by dark yellow and purple boxes. Proteins cleavage sites shown by black vertical arrows. **Bottom:** Spliced and full-length primary transcripts derived from the IP or 5' LTR promoters are shown below polyproteins with ORFs colored accordingly. The cap and polyA tail are represented by C and An symbols, respectively. *Figure adapted from (Delelis et al., 2004; Hamann and Lindemann, 2016; Pollard and Malim, 1998).*

1.1.3.2 Synthesis of FV proteins

The Gag precursor protein p71 of approximately 71kDa is encoded by a full-length viral RNA which undergoes a rather limited processing: FV Gag is cleaved just once near its C-terminus (C-ter) yielding two subunits (p3/p68) of which the larger product p68 joins the p71 precursor to form the viral capsid (Fig. I-7, top) (Flügel and Pfrepper, 2003). The smaller cleavage product p3 has yet to be demonstrated present in budding virions and its role is currently less clear. This unusual and restricted cleavage of Gag is of great importance as cleavage mutants fail to yield infectious viruses, although lack of cleavage does not affect viral particle expression (Enssle et al., 1997). Thus, the FV Gag is unique and does not include the typical matrix (MA), capsid (CA) and nucleocapsid (NC) products observed in orthoretroviruses (Lindemann and Rethwilm, 2011).

FV Pol is translated as an independent precursor p127 protein from a separate messenger RNA (mRNA). FV pol cleaves itself into two separate enzymatic subunits: p85 with PR, RT and RH activities and a smaller p40 product with IN activity (Fig. I-7, top) (Cartellieri et al., 2005; Lee et al., 2013). Both of these subunits have been described to localize in the nucleus of PFV-infected cells (Imrich et al., 2000). Inactivation of the PR results in non-infectious viral particles still able to bud and enter target cells (Baldwin and Linial, 1998; Lehmann-Che et al., 2005). An active IN is required for FV replication (Enssle et al., 1999). The 3D structure of the p40 IN subunit in complex with its viral and target DNA substrates (nucleoprotein complex termed intasome) was the first full-length retroviral IN to be solved and shows the viral DNA strands located in the cleft between two IN dimers and target DNA below (Maertens et al., 2010). Studies also demonstrated PFV susceptible to the clinically approved HIV-1 IN inhibitors elvitegravir and raltegravir (Hare et al., 2010b). The structure of PFV intasome complexed to HIV-1 IN inhibitors revealed their mode of action as strand-transfer inhibitors that function by displacement of the viral DNA ends from the active sites in the intasome (Hare et al., 2010a). Overall, the synthesis of Pol independently of Gag and the regulation of protease activity are unusual compared to orthoretroviruses.

The FV Env is translated as a full-length precursor gp130 protein. The LP targets Env gp130 for the secretory pathway in the rough endoplasmic reticulum (ER) (Lindemann et al., 2001; Lindemann and Rethwilm, 2011). The gp130 is proteolytically processed into its three cleavage products LP gp18, SU gp80 and TM gp48 (Fig. I-7, top) during transfer to the cell surface membrane (Geiselhart et al., 2004). All FVs contain optimal furin cleavage site consensus motifs (R-x-x-R) between the three subunits. The cleavage between SU gp80 and TM gp48

have been shown of particular importance for viral infectivity, while LP gp18/SU gp80 cleavage is less essential (Bansal et al., 2000; Duda et al., 2004).

1.1.3.3 FV replication cycle

The general retroviral replication cycle comprises the following sequential steps:

- 1) Attachment of the virus to its surface expressed receptor on target cell
- 2) Entry of the virus into the cytoplasm and release of capsid
- 3) Decapsidation and reverse transcription of viral ssRNA into dsDNA
- 4) Transport of the viral dsDNA into the nucleus and integration into the host-cell chromosomes (creation of provirus)
- 5) Transcription of proviral genome by host-cell RNA polymerase II into genomic RNA (replication) and mRNA for synthesis of viral proteins
- 6) Virus assembly in cytoplasm
- 7) Maturation process including budding and egress of new mature viral particles from host-cell

These steps are also followed by FVs, however some differ from orthoretroviruses including steps that resemble more of what is observed for HBV such as the late RT step giving rise to budding particles containing dsDNA (Table I-1) (Yu et al., 1996).

Table I-1 – Properties of FV in comparison to orthoretroviruses and hepadnaviruses

Properties	<i>Orthoretroviridae</i>	<i>Spumaretroviridae</i>	<i>Hepadnaviridae</i>
Viral genome	RNA	RNA/DNA	DNA
Reverse transcription stage	Early	Early/Late	Late
Synthesis of <i>pol</i> transcript independently of <i>gag</i>	No	Yes	Yes
Integration step	Yes	Yes	Rarely
Particle budding site	Plasma membrane	Intracellular membrane, ER or Golgi	Intracellular membrane, ER

Step 1 – Attachment: Heparan sulfate (HS) has been demonstrated as an attachment-factor for FV entry (Nasimuzzaman and Persons, 2012; Plochmann et al., 2012). FVs have an extremely broad cell tropism *in vitro* explained by the ability of PFV to infect virtually all cell lines tested with exception of a few derived from human and zebrafish origin (Table I-2) (Mergia et al., 1996; Stirnagel et al., 2010). Interestingly, studies on FV entry found that cells with low HS

expression, including the two cell lines resistant to FV-infection, still exhibited surface binding by Env which might indicate that FVs may require additional co-factors for efficient viral entry (Nasimuzzaman and Persons, 2012; Stirnagel et al., 2010). This ability of FVs to enter a broad range of cell types provides a useful tool for delivery of therapeutic genes by foamy viral vectors (FVVs) (Hill et al., 1999). Of note, the use of FVVs as an *in vivo* hematopoietic stem cell (HSC) therapy has been applied to several monogenetic pre-clinical animal models, most notably the model of canine X-linked severe immunodeficiency (SCID-X1) in dogs (Burtner et al., 2014; Trobridge et al., 2012). Such studies have highlighted the safety of *in vivo* FVV therapy and these vectors was shown as efficient as lentiviral vectors in long-term transduction of blood CD34⁺ cells in the canine model (Rajawat et al., 2019; Trobridge et al., 2009). More recently, FVVs have been optimized and used for delivery of gene editing tools such as CRISPR/Cas9 which is an interesting alternative strategy and highlights the many possibilities of FVVs in gene therapy (Lindel et al., 2019).

Step 2 – Entry/fusion: The broad cell tropism suggests that FVs utilize one or more ubiquitously expressed cell surface receptor(s) for entry into its target cells, which is still unknown. The fusion process by which viral and cellular membrane merge is Env and pH-dependent, with a preference of acidic pH of 5.5 for most FVs, except PFV (Picard-Maureau et al., 2003). A recent study demonstrated fusion of PFV to occur at both the plasma membrane as well as from endosomes while a macaque SFV strain only was found to fuse from endosomes (Dupont et al., 2020). A novel intermediate fusion step was observed in which capsids and Env were still tethered despite separated by up to 400nm before complete separation (Dupont et al., 2020).

Step 3 – Decapsidation: In the cytosol, released capsids bind dynein motor protein complexes and accumulate by the microtubule organizing center (MTOC) (Fig. I-8) (Petit et al., 2003; Saïb et al., 1997; Yu et al., 2006). Capsid uncoating is protease and cell cycle-dependent (Lehmann-Che et al., 2005; Patton et al., 2004). Consequently, FVs do not infect non-proliferating cells resembling gamma retroviruses but differing from lentiviruses (Bieniasz et al., 1995b).

Table I-2 – *In vitro* cell tropism of replicative or vector-based PFV and HS expression

Cell line	Species	Tissue	Sensitivity to PFV infection	Cell surface level HS-expression	References
Mammalian					
293/293T	Human	Embryonic kidney epithelium	++	++	(Hill et al., 1999; Nasimuzzaman and Persons, 2012)
A549	Human	Lung epithelium	++	++	(Nasimuzzaman and Persons, 2012)
BHK-21	Hamster	Kidney fibroblasts	+++	++	Reference cell line
CHO-K1	Hamster	Cervix/ovary epithelium	+++	+++	(Hill et al., 1999; Nasimuzzaman and Persons, 2012;
COS-7	AGM	Kidney fibroblast-like	+++	+++	Plochmann et al., 2012)
CRFK-LL	Cat	Kidney epithelium	+++	+++	(Plochmann et al., 2012)
G1E-ER4	Mouse	Pro-erythroblasts	-	ND	(Stirnagel et al., 2010)
HEL	Human	Lung fibroblasts	++++	ND	(Hill et al., 1999)
Hep G2	Human	Liver epithelium-like	+++	++	(Plochmann et al., 2012)
hMSC-Tert	Human	Bone marrow mesen-chymal stem cells	++++	+++	(Plochmann et al., 2012)
HT1080	Human	Fibrosarcoma epithelium	++++	+++++	Reference cell line
HT29	Human	Colorectal epithelium	+	ND	(Hill et al., 1999)
Indian Muntjac	Deer	Skin fibroblasts	++++	ND	(Hill et al., 1999)
Jurkat	Human	T lymphocyte	++	++	(Nasimuzzaman and Persons, 2012; Stirnagel et al., 2010)
K562	Human	Myeloid bone marrow	++	++	(Nasimuzzaman and Persons, 2012)
LMtk	Mouse	Fibroblasts	++++	ND	(Hill et al., 1999)
Mouse L	Mouse	Subcutaneous, adipose, areolar fibroblasts	+++	+++	(Stirnagel et al., 2010)
MPK	Minipig	Kidney fibroblasts	++	ND	(Hill et al., 1999)
MRC-5	Human	Lung fibroblasts	++++	+++	(Plochmann et al., 2012)
Mv.1.Lu	Mink	Lung fibroblasts	++	ND	(Hill et al., 1999)
NIH-3T3	Mouse	Embryonic fibroblasts	+++	+++	(Hill et al., 1999; Nasimuzzaman and Persons, 2012)

Introduction

Cell line	Species	Tissue	Sensitivity to PFV infection	Cell surface level HS-expression	References
Mammalian					
PAE	Pig	Aorta epithelium	+++	ND	(Hill et al., 1999)
PK15	Pig	Kidney epithelium	+	ND	(Hill et al., 1999)
Raji	Human	B lymphocyte	-	- (+)	(Nasimuzzaman and Persons, 2012), This Thesis, EPVO
Ramos	Human	B lymphocyte	-	-	(Nasimuzzaman and Persons, 2012)
Rat-1	Rat	Rat fibroblasts	++	ND	(Hill et al., 1999)
RD	Human	Rhabdo-myosarcoma	+++	ND	(Hill et al., 1999)
SK-N-SH	Human	Brain epithelium	+++	+++	(Plochmann et al., 2012)
Sog9	Mouse	Subcutaneous, adipose, areolar fibroblasts	++	-	(Stirnagel et al., 2010)
Sp1K	Dolphin	Kidney epithelium	+++	ND	(Hill et al., 1999)
St Iowa	Swine	Testis fibroblasts	+	ND	(Hill et al., 1999)
Vero	AGM	Kidney epithelium	+++	+++	(Nasimuzzaman and Persons, 2012)
WOP	Mouse	Embryonic fibroblasts	++++	ND	(Hill et al., 1999)
Avian					
CBGQ	Goose	Fibroblasts	++++	ND	(Hill et al., 1999)
QT6	Quail	Fibroblasts	+++	ND	(Hill et al., 1999)
Reptilian					
IgH-2	Iguana	Heart epithelium	++	ND	(Hill et al., 1999)
Fish					
Pac2	Zebrafish	Embryonic fibroblasts	-	ND	(Stirnagel et al., 2010)

Cell surface HS-expression level according to (Nasimuzzaman and Persons, 2012; Plochmann et al., 2012; Stirnagel et al., 2010), ND; not determined. *Table adapted from (Hill et al., 1999).*

Step 4 – Nuclear entrance: *In vitro*, the FV genome persists in infected cells undergoing cell cycle-arrest while no integration is observed (Lo et al., 2010; Trobridge and Russell, 2004). The preintegration complex (PIC) comprises IN and viral DNA. The nuclear localization signal (NLS) from IN allows the translocation of PIC into the nucleus. The viral Gag protein also harbors an NLS within the second of three Gly-Arg (GR) rich boxes located in the C-ter (Schliephake and Rethwilm, 1994). Once nuclear entrance occurs, Gag enhances proviral integration by tethering to host-cell chromatin through an evolutionary conserved arginine residue inside the GR2 box (Paris et al., 2018; Tobaly-Tapiero et al., 2008), as well as nuclear RNA export through a nuclear export sequence (NES) in the N-ter of Gag (Lesbats et al., 2017; Renault et al., 2011).

Step 5 – Transcription and nuclear export: An unusual feature of FVs is that each gene is encoded by at least one separate transcript derived from either the U3-promotor or the IP. These transcripts are spliced into more than 15 different mRNAs. However, the genomic pre-RNA genome which span the complete coding region is the transcript preferentially encapsidated into the budding particles, reviewed by (Bodem, 2011). The fully spliced viral mRNAs are believed to exit the nucleus by the same pathway as cellular mRNAs. In contrast to other complex-type retroviruses, FV do not express a regulatory protein to export intron-containing transcripts. Instead, FVs relies on the RNA-binding host protein nuclear export machinery for final export of full-length transcripts (Bodem et al., 2011). One of such machineries is host-cell exportin 1 also termed chromosomal maintenance 1 (CRM1) superfamily of karyopherin soluble nuclear transport factors also used by other retroviruses, reviewed by (Cullen, 2003). Indeed, CRM1 was shown essential for the nuclear export of FV full-length transcripts. However, this study demonstrated that the viral RNA binds a cellular protein named HuR, and that HuR generates a complex with other cellular proteins including CRM1 that facilitates nuclear export (Bodem et al., 2011). In addition, viral RNA export has also been proposed to rely on the leucine-rich NES of Gag which is recognized by CRM1 as well (Renault et al., 2011).

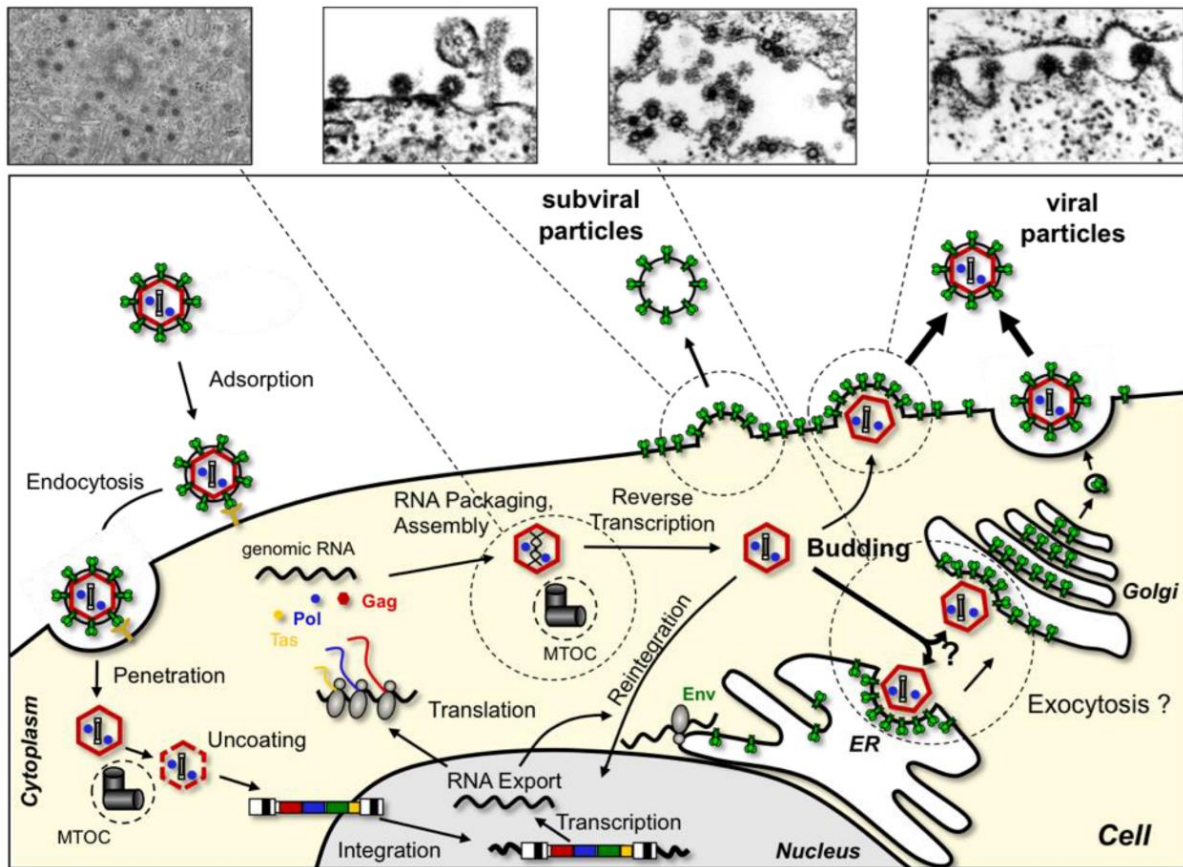


Figure I-8 – Schematic and electron microscopy representation of PFV replication cycle

The PFV virion binds to a ubiquitously expressed surface molecule(s) on a host target cell. Post fusion of viral and cellular membranes, the viral capsid migrates to the MTOC. Uncoating of the capsid releases the viral genome. The viral ssRNA genome is transcribed into dsDNA by RT and translocated into the nucleus. The viral genome is integrated into the host chromosomes by IN. Host-cell machinery transcribes the viral genome and differentially spliced viral RNAs are exported out of the nucleus. Pol, Gag and Tas transcripts are translated into protein by the ribosome in the cytosol while Env is translated by ER. Capsids containing viral RNA are formed at the MTOC and a late RT event may occur after capsid assembly and before budding resulting in capsids containing viral dsDNA. The majority of capsids migrate to the ER and Golgi where they fuse with intracellular membranes containing Env. Mature viral particles bud from intracellular compartments depending on Env and are most likely released from the cell through exocytosis. Some capsids acquire Env by the plasma membrane and small amounts of capsid-less SVPs are also released from the cell surface. *Figure from (Lindemann and Rethwilm, 2011).*

Step 6 – Protein synthesis and viral assembly: Upon export of mRNA from the nucleus, viral protein translation takes place in the cytoplasm with the exception of Env in the rough ER (see section 1.1.3.2). The precise capsid assembly in the cytoplasm is driven by Gag and the formation of capsids are observed near centrosomes (Lindemann et al., 2021). Although not essential for formation of capsids, Pol encapsidation and PR-mediated processing of Gag precursor is required for closed capsid structures (Baldwin and Linial, 1998; Fischer et al., 1998). Moreover, Gag interaction with viral nucleic acids through cis-acting sequence (CAS) elements in the viral RNA genome (located in the C-ter GR-rich domain of Gag) is also essential for formation of normal shaped capsids. Similarly, Pol also engages CAS elements important

for its encapsidation into the capsid (Hamann and Lindemann, 2016; Hamann et al., 2014). The precise sequence and location of these events are not entirely defined (Lindemann et al., 2021). One important feature of FV replication is that reverse transcription of the packaged RNA genome occurs after capsid assembly (Fig. I-8) but before particle release resulting in FV particles containing full-length proviral DNA (up to 10-20% of total). This proviral DNA has been shown to contribute substantially to viral infectivity (Moebes et al., 1997; Yu et al., 1999) and DNA extracted from cell-free PFV particles are directly infectious upon transfection (Yu et al., 1996). Later studies showed that early *in vitro* treatment of cells with the zidovudine (AZT) RT inhibitor completely abolished PFV replication, proviral integration and DNA synthesis at a low multiplicity of infection (MOI) (Delelis et al., 2003; Zamborlini et al., 2010). These results suggest a requirement of an early RT event for FV replication, at least under low MOI conditions with limited presence of infectious viral DNA from incoming virions (Zamborlini et al., 2010).

Step 7 – Budding: Finally, release of mature viral particles from FV-infected cells is strictly Env-dependent in opposition to other retroviruses for which budding is Gag-dependent. Budding of FV virions predominantly occur intracellularly at ER or Golgi rather than by the plasma membrane (Fig. I-8). The mature virions are most likely exported by exocytosis and contain Env incorporated into a host-cell derived lipid bilayer surrounding the viral capsid and genome (Baldwin and Linal, 1998; Effantin et al., 2016; Fischer et al., 1998). Budding of capsid free virus-like particles (VLPs), so-called subviral particles (SVPs) from the plasma membrane (Fig. I-8) also occur to a lesser extent (Stange et al., 2008), as discussed in section 1.1.4.3. Also discussed in this section, the Env LP gp18 directly interacts with the viral capsid which is essential for viral particle budding. The precise timing of this capsid interaction with Env during the Env maturation process is unclear, but may be enhanced by proteolytic cleavage of the Env precursor by furin (Lindemann et al., 2021).

1.1.4 Functional and structural characterization of SFV Env

As the main topic of this thesis is SFV-specific antiviral antibodies directed against Env, the function and structure of Env will be explained in detail. Retroviral Envs are type-I class TM proteins composed of an extracellular SU domain and a transmembrane TM domain. This class of fusogens presents a post-fusion structure that forms a trimer with prominent central α -helical coiled-coils (Rey and Lok, 2018). The Envs are synthesized as precursors which are co-translationally imported into the ER leading to a maturation process involving Env folding, oligomerization and attachment of surface glycans. Following these steps, the Env precursors

from orthoretroviruses are transported to the trans golgi network where furin or furin-like proteases cleave the SU and TM subunits apart. While FV Env share many of these events, some aspects differ from orthoretroviruses beyond their unusual organization with LP-SU-TM subunits as described above (Jones et al., 2011; Lindemann et al., 2001; Lindemann and Rethwilm, 2011).

1.1.4.1 *Env primary sequence, receptor binding domain and 3D structure*

The PFV Env is a 130kDa precursor glycoprotein of 989 amino acids (aa). Its three subunits the N-ter LP, central SU and C-ter TM are 126, 446 and 417 aa long, respectively. The LP and TM subunits mediate membrane anchorage while the SU subunit contain the receptor binding domain (RBD). FV Env folds as a heterotrimeric spike protein which further assembles mostly in hexagonal arrangements or lattices in clusters on the surface of virions as shown by cryo-electron tomography (Fig. I-9, bottom) (Effantin et al., 2016). These trimers are distanced $\sim 110\text{\AA}$ from each other in the hexagonal assembly with additional interactions between Env trimers observed $\sim 45\text{\AA}$ above the membrane level (Effantin et al., 2016).

The LP contains an intracellular tail also termed the cytoplasmic domain (CyD) upstream of a hydrophobic aa sequence named the H domain. This H domain is located within the LP and is 22 aa long (aa 68-90). The TM also contains a CyD located in the C-ter downstream of the predicted and evolutionary conserved membrane spanning domain (MSD) (Fig. I-9, top) (Lindemann et al., 2001; Pietschmann et al., 2000; Sun et al., 2012). Both hydrophobic regions (H domain and MSD) are predicted to fold in α -helices. Such helices were visualized by cryo-EM of the trimeric folded PFV Env in its pre-fusion state (Fig. I-9, middle). Interestingly, the helices cluster in a hexagonal close proximity with outer and inner helices buried in the membrane.

The TM gp48 subunit mediate the fusion step with the target cell membrane using an α -helix fusion peptide (FP) located in the N-ter of TM (Sun et al., 2012; Wang et al., 2016b). Three central helices were observed by cryo-EM below the upper part of the trimer (Fig. I-9, middle). These FPs appear shielded by the central SU domains which was hypothesized to fold primarily as the upper part of the trimer (Effantin et al., 2016).

PFV Env gp130

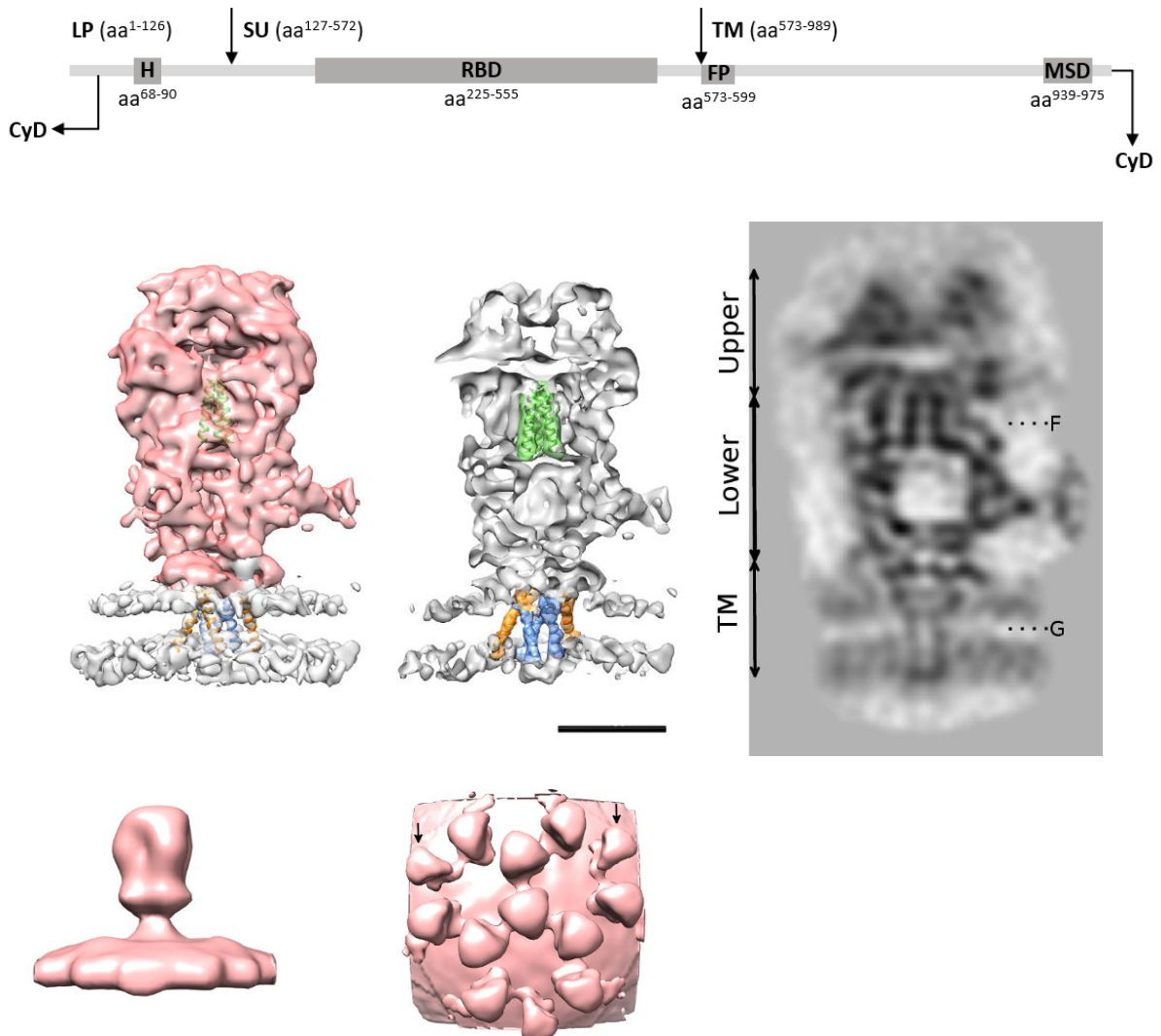


Figure I-9 – Primary sequence and 3D structure of trimeric PFV Env

Top: Schematic of PFV Env gp130 primary sequence with C-ter LP gp18, central SU gp80 and N-ter TM gp48 subunits in light grey. PFV aa numbering and cleavage site (arrows) location indicated on top of sequence. Essential domains of each subunit shown by dark grey boxes with specific aa location below. **Middle:** Cryo-EM 3D sideview full (left), cut (center) and grey density map (right) reconstruction of a single PFV WT Env trimer (iNAB mutant deficient in Gag-RNA binding) at resolution of approximately 9Å (EMD:4011). Extracellular domain presented in salmon (left) and grey (center). The three central TM gp48 FP helices are presented in green. The LP gp18 and TM gp48 helices spanning the membrane are colored orange (outer helices) and blue (inner helices) but cannot be attributed due to insufficient resolution. Scalebar present 50Å. **Bottom:** Subtomogram averaging of WT PFV Env (left). Hexagonal assembly of PFV Env from WT particles at 32Å resolution (right) (EMD:4006). *Figure adapted from (Effantin et al., 2016; Lambert et al., 2018).*

The SU domain is exclusively extracellular and contains the RBD (Fig. I-9, top). The RBD of PFV has been characterized by flow cytometry cell-binding assays with use of recombinant Env (Duda et al., 2006; Herchenroder et al., 1999). By mutating progressively shorter domains of the PFV SU, Duda et al. demonstrated the RBD to be a discontinues region spanning from

aa 225-555 with a non-essential joining RBD (RBDjoin) at aa position 397-483 (Fig. I-10) (Duda et al., 2006). Of notice, previous binding studies of recombinant fusion Env proteins suggested PFV to interact with two receptors of different affinity (Herchenroder et al., 1999). PFV Env also harbors 24 cysteine residues spanning all three subunits which potentially form disulfide bonds important for folding (Fig. I-10). Cell-binding assays using wild-type (WT) and mutant recombinant Env revealed essential roles of cysteines located within the C-ter of the SU domain as well as a glycosylation site within the RBD (Duda et al., 2006).

1.1.4.2 *Env glycosylation*

SU primarily contains complex type glycans while the LP and TM present attachment of high mannose or hybrid type glycans (Luftenegger et al., 2005). The primary FV Env sequence usually harbors between 14 and 16 potential N-glycosylation sites (PNGS) and glycans contribute by about 50% of its molecular weight (Sun et al. 2012). This level of glycosylation intermediates between the highly glycosylated HIV Env (median of 25 PNGS per monomeric SU gp120 subunit) and murine leukemia virus (MLV) Env (less than 10 PNGS) (Luftenegger et al., 2005). Sequence alignments of Env from different FVs reveal certain N-glycosylation sites to be highly conserved across species-specific FVs. For PFV, two PNGS are located at the LP, ten at the SU and three at the TM (Fig. I-10). A study demonstrated 14 out of 15 sites to be in use, for which the only PNGS not attached by a glycan was the very first located on the CyD of LP. Three evolutionary conserved glycans have been shown of particular importance for Env expression and intracellular transport; glycan number 8 located at N₃₉₁ in the SU domain and glycans 13 and 15 located at N₇₈₂ and N₈₃₃ in the TM domain (Fig. I-10) (Duda et al., 2006; Luftenegger et al., 2005).

1.1.4.3 *Env-dependent FV particle budding and subviral particle release*

Egress and intracellular transport of FV particles are highly dependent on Env in contrast to orthoretroviruses able to release VLPs in absence of Env. The FV budding relies on the evolutionary conserved W-x-x-W motif located in the N-ter region of the LP subunit (Fig. I-10). This motif interacts with Gag during budding (Fischer et al., 1998). The capsid region interacting with the N-ter of LP is located in the N-ter of Gag as observed in crystal structures of N-ter Gag (aa 1-179) complexed to LP N-ter peptides (aa 1-20) (Goldstone et al., 2013; Reh et al., 2013; Wilk et al., 2001). Similar LP-Gag interaction occurs in FFV (Geiselhart et al., 2003).

either extracellular Env binding to the entry receptor at the surface of infected cells or Env binding to the receptor intracellularly. Both scenarios lead to masking and/or downregulation of receptor expression on the cell surface (Nethe et al., 2005). FV Env-transduced cells stably expressing PFV Env on their surface are less susceptible to infection than non-transduced cells (Berg et al., 2003; Herchenroder et al., 1999; Hill et al., 1999). SIR depends upon the CyD and/or MSD domains from the TM. Artificial anchoring of the Env by substituting the MSD with a phosphoinositol signal sequence could restore SIR and cell surface expression (Berg et al., 2003). Secreted SFV SU does not mediate SIR. This contrasts with the inhibition of MLV-infection by monomeric SU (Battini et al., 1995). Expression of PFV Env was also able to induce SIR against PFV vectors pseudotyped with heterologous Env from SFV, FFV, BFV and EFV strains, suggesting that at least one host molecule is used for entry by FVs infecting different mammalian species (Berg et al., 2003). SIR was also observed against strains from different genotypes that will be defined in section 1.1.5 (Hill et al., 1999). This lack of resistance to infection mediated by soluble recombinant Env is a key property, which allowed the epitope mapping strategy possible (section 5, Manuscript II).

Superinfection resistance (SIR)

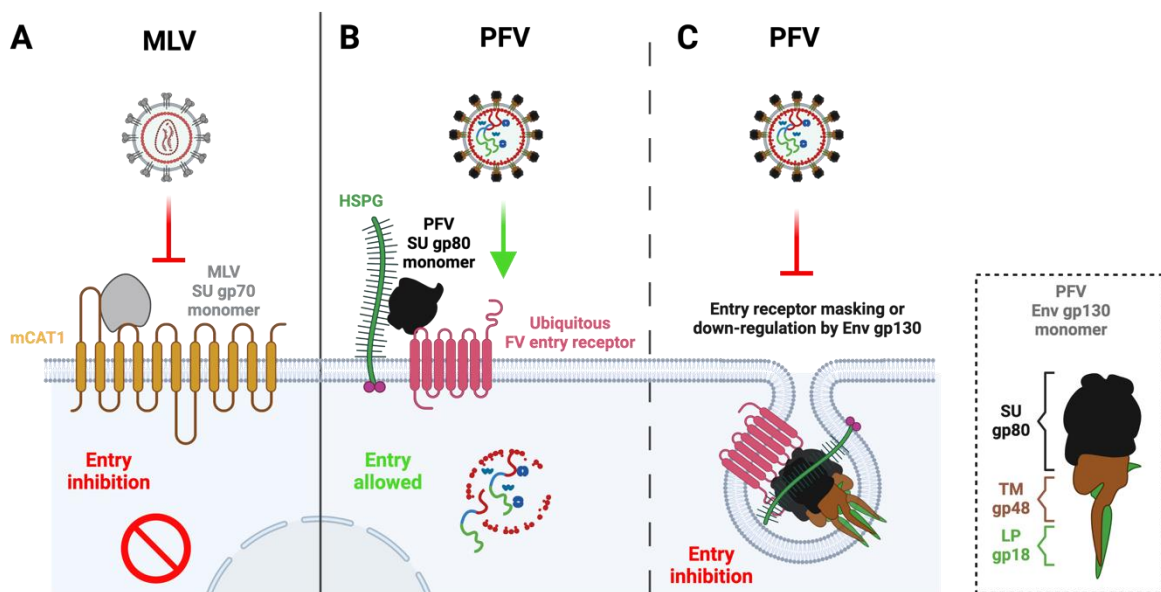


Figure I-11 – Schematic overview of superinfection resistance

Comparison of superinfection resistance (SIR) scenarios for MLV and PFV. **A:** Cellular entry of MLV is inhibited by soluble MLV SU gp70 monomer (grey subunit) bound to the MLV entry receptor mouse cationic aa transporter 1 (mCAT1) shown in yellow. **B:** Cellular entry of PFV is allowed in presence of soluble PFV SU gp80 monomer (black subunit), despite SU gp80 binding to cell surface expressed heparan sulfate proteoglycan (HSPG) attachment factor (shown in green) and a currently unknown but assumedly ubiquitously expressed FV-specific entry receptor (shown in pink). **C:** Cellular entry of PFV is inhibited by cell-surface expressed Env gp130 on PFV-

infected cells and on cells stably expressing Env gp130 at their surface through Env-mediated entry receptor masking or down-regulation mechanisms. *Figure created with BioRender.com.*

1.1.5 Genetic variability and recombination of SFVs

Despite the fact that FVs contain an RNA phase in their replication cycle, their genomes are very stable *in vivo*. The mutational error rate of PFV in cell cultures has been shown in the range of 1.7×10^{-4} to 1.1×10^{-5} substitutions per nucleotide per replication cycle (Boyer et al., 2007; Gärtner et al., 2009). For comparison, the average mutation rate of HIV-1 and influenza A viruses is 6.3 and 2.5×10^{-5} , respectively (Sanjuán and Domingo-Calap, 2016). The genetic stability of SFVs is also evident from their historical evolution characterized by ancient co-speciation with their species-specific NHP and by evidence of cross-species transmission events (Muniz et al., 2015; Rethwilm and Bodem, 2013; Switzer et al., 2005).

1.1.5.1 Genetic stability of FVs

FV evolution was studied in co-housed African green monkeys (AGMs) (*Cercopithecus aethiops*) imported from Kenya harboring SFV_{agm}. Viral clones obtained during a 13-year period from one of these monkeys and an animal caretaker from the facility who accidentally acquired a SFV_{agm}-infection, had between 99.5 and 100% aa identity (Schweizer et al., 1997). This remarkable stability of FVs in a single host and their slow genetic drift during evolution could potentially be explained by two scenarios: a low replication rate of FVs *in vivo* or a very high-fidelity FV RT. Indeed, viral replication (i.e., presence of SFV RNA) is primarily restricted to the oral cavity and mucosa in NHPs while proviral DNA can be detected in the majority of tissues indicative of a largely latent infection, discussed further in section 1.2 (Falcone et al., 1999a; Murray et al., 2008). The PFV RT has an *in vitro* error rate similar to the one of HIV-1 RT. PFV RT does however not seem to focus errors at specific hotspots *in vitro* as for HIV-1 RT but produces more insertions and deletions overall (Boyer et al., 2007). Interestingly, a study reported that all PFV nucleotide mutations observed *in vitro* was of guanosine to adenosine (G to A) suggesting *in vitro* activity of the apolipoprotein B editing complex 3 (APOBEC3) family of proteins (Gärtner et al., 2009). These mutations were reduced by 50% when co-expressing recombinant Bet protein supporting its antagonistic role, discussed further in section 1.3 (Gärtner et al., 2009).

1.1.5.2 FV diversity and recombination

A central genetic alteration giving rise to viral diversity is recombination. Genetic recombination can occur when two distinct but related viruses infect the same cell, also termed

homologous recombination. Frequent SFV recombination events occurred *in vitro* with use of the PFV vector system (Gärtner et al., 2009). Phylogenetic analyses of *pol* gene have been conducted on tissue samples from chimpanzees living in the Taï National Park in Côte d'Ivoire and fecal samples collected from four chimpanzee subspecies living at 25 sites spread over equatorial Africa. They revealed intra- and interspecies transmission by SFV strains between chimpanzees and from African *Colobus* and *Cercopithecus* monkeys to Apes. In fact, since chimpanzees often prey on smaller monkeys the occurrence of such SFV superinfections could give rise to new recombinant SFVs (Blasse et al., 2013; Leendertz et al., 2008; Liu et al., 2008). Indeed, recombination have been observed in Bangladesh using *gag* sequences from rhesus macaque monkeys showing that SFVmmu (*Macaca mulatta*) strains cluster according to geographical sampling (Feeroz et al., 2013). Further evidence supports that deforestation and NHP translocation, as observed by nomadic people travelling with performance monkeys, are influencing SFV transmission and diversity in this region (Feeroz et al., 2013).

SFV *env* is overall more conserved than *gag* across NHP species, which is the opposite of simian lentiviruses presenting greater variabilities in *env* leading to immune response escape mutations (Rethwilm and Bodem, 2013). Despite this, significant divergence within SFV *env* have also been observed. The first observation is based on the 19 co-housed AGMs. Their *env* sequences clustered into four SFVagm subtypes showing >95% sequence similarity within clusters but 3 to 25% aa divergence between clusters (Schweizer et al., 1999).

Following full-length sequencing of SFV_{mcy} from Taiwanese Formosan Rock macaques (*Macaca cyclopis*), it was observed that one of two isolated SFV_{mcy} strains presented a greater SU aa similarity to SFV_{agm} compared to SU from the other SFV_{mcy}. The researchers proposed that recombination occurred between SFV strains and suggested that recombination hotspots may be present in the SU region (Galvin et al., 2013). Similar hotspots had previously been observed within the SU domain of Env from SFV_{agm} (Schweizer et al., 1999) and FFV strains (Winkler et al., 1998). FFV sequences clustered into two subgroups presenting less than 60% identity in SU between each other, while identity was >97% found within each group (Winkler et al., 1998).

1.1.5.3 *Env diversity of SFV strains infecting humans and Apes in Central Africa*

My research unit has contributed extensively to the discovery and prevalence of new zoonotic SFV strains through epidemiological studies in humans living in rural areas of Cameroon and Gabon (Betsem et al., 2011; Calattini et al., 2011; Calattini et al., 2007; Mouinga-Ondémé et

al., 2012). Five primary zoonotic SFV strains have been isolated by coculture of peripheral blood mononuclear cells (PBMCs) from infected Central African hunters with BHK-21 cells which are highly susceptible to SFVs. Two strains belonged to the gorilla SFV species, two to the chimpanzee species and one to the Cercopithecus species (Rua et al., 2012a). Molecular characterization of these SFV strains demonstrated high degree of genetic conservation between zoonotic and NHP sequences. Natural SFV polymorphisms in *gag*, *tas*, *bet* and the U3 region of the LTR were observed (Rua et al., 2012a). The *env* gene was the most variable one. Therefore, *env* DNA was amplified from blood samples of 40 individuals infected with chimpanzee or gorilla SFVs and from wild caught NHPs living in surrounding rural areas of the study population. Phylogenetic alignment of the obtained sequences revealed presence of a variant region within the central region of SU whose sequence do not segregate according to host species, in contrast to the flanking parts of the *env* gene. Recombination was the most probable origin of these two variants, but one parental strain was unidentified (Fig. I-12) (Richard et al., 2015).

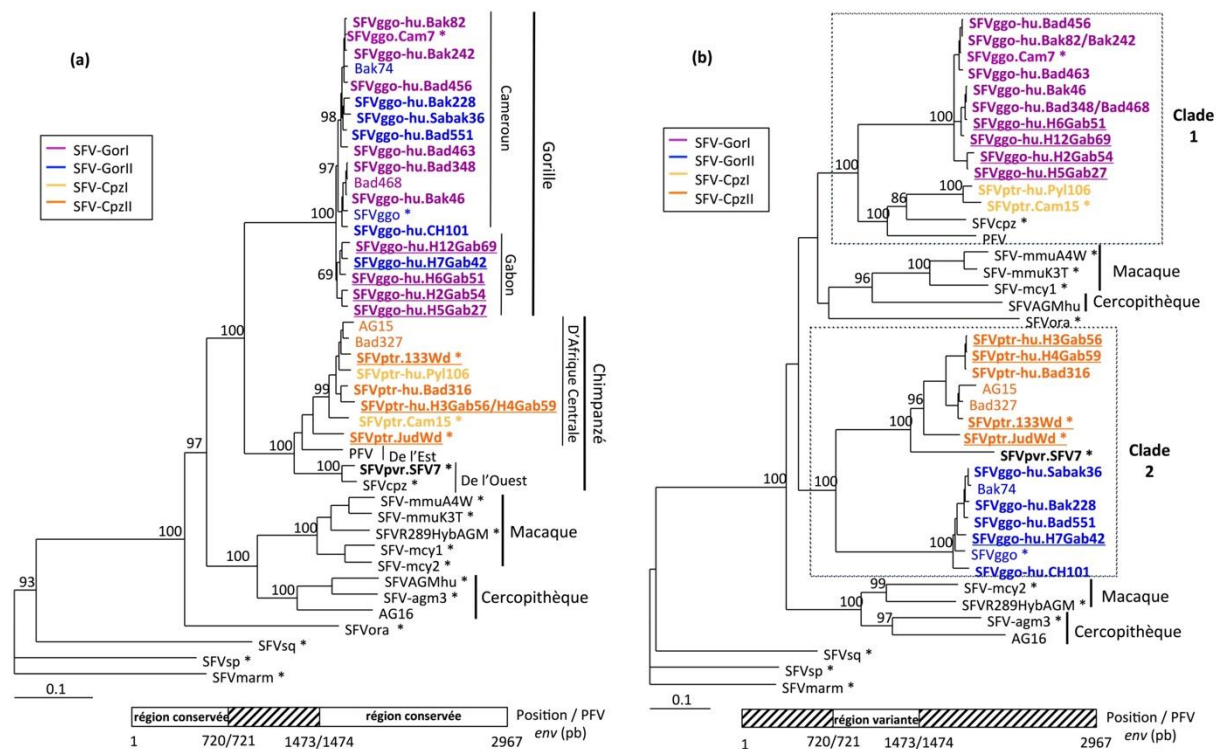


Figure I-12 – Phylogenetic analysis of SFV strains based on the conserved and variable region of *env*

Phylogenetic alignment of SFV *env* sequences from NHPs and zoonotically infected humans based on the conserved (a) or variant (b) region of *env* located within the SU gp80 domain. SFVggo sequences shown in purple or blue and SFVcpz sequences shown in yellow or orange, respectively. Alignments based on the variable region demonstrate the presence of two SFV clades or genotypes circulating among gorillas and chimpanzees in Central Africa. *Figure from (Richard et al., 2015).*

The two SFVcpz/ggo genotypes were characterized by *env* recombination hotspots located within SU as previously reported for SFVmcv/agm and FFV. More recent studies have also determined two SU genotypes circulating among mandrills (*Mandrillus sphinx*, SFVmsp) from Cameroon and Gabon (Aiewsakun et al., 2019a). In that study the authors predicted the SU based genotypes circulating among NHPs to have originated approximately 30 million years ago during the diversification of OWMs and Apes (Fig. I-13) (Aiewsakun et al., 2019a).

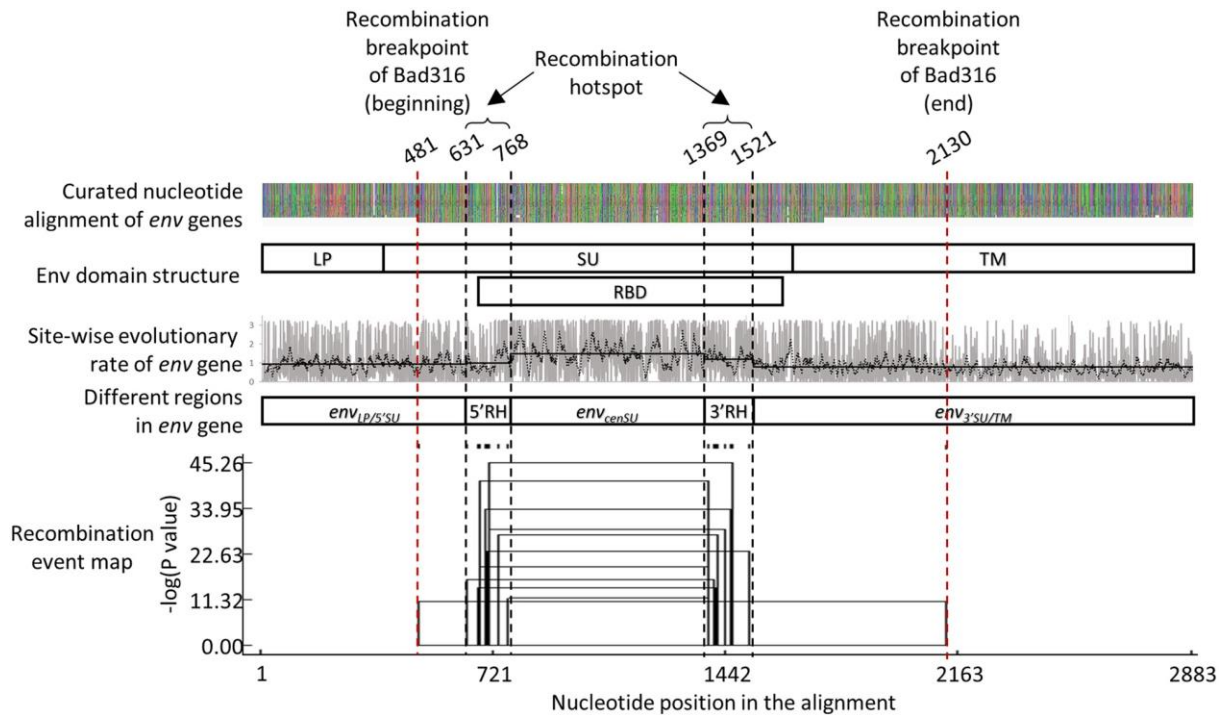


Figure I-13 – Recombination analysis of fifty-four SFV *env* sequences

Recombination event map based on *env* sequences from fifty-four SFV strains (forty-seven full-length). Two recombination hotspots were discovered between nucleotide 631/768 and 1369/1521, respectively. Site-wise evolutionary rate shown according to Env. SFV strain Bad316 was predicted to have a recombination site outside the predicted recombination hotspot that defines SUvar. *Figure from (Aiewsakun et al., 2019a).*

A more recent study took advantage of the species-specific SFV co-speciation with NHPs to address evolution of Japanese macaques (*Macaca fuscata*) (Hashimoto-Gotoh et al., 2020). This study showed that the conserved region of *env* presented remarkable high correlation with phylogenetic trees of NHP evolution based on host genome sequences and further confirmed the presence of a variable region within SU among the new SFVmfu isolates (Hashimoto-Gotoh et al., 2020).

The studies on Cameroonian and Gabonese zoonotic SFVggo strains (Richard et al., 2015) provide evidence for SFV strain clustering according to geographical location, which goes in line with observations from previous studies on macaque SFVs in Bangladesh (Feeroz et al., 2013) and mandrill SFVs in Gabon (Mouinga-Ondeme et al., 2010). Moreover, these mandrill

SFVmsp strains from Gabon cluster according to location in the North and South which is separated by the Ogooué river with the two SU variants occurring in both populations (Aiewsakun et al., 2019a). These results further strengthen that phylogenetically distinct clades display host co-divergence and separation patterns based on geography.

After these genetic studies, we referred to the divergent SU region as SU variant (SUvar). The remainder of the SU domain spanning the N-ter and C-ter region is very conserved (SUcon) as for the LP and TM domains (Fig. I-14). In addition to forming two phylogenetically distinct *env* clades or potential genotypes, the SUvar region also overlaps the bipartite RBD which could explain neutralization profiles of different serotypes (see section 1.3.3). Finally, following work from our unit provided strong evidence that the SUvar region is targeted by nAbs from the majority of SFV-infected African hunters confirming the match between SFV genotype and serotype (Lambert et al., 2018). This important study by Lambert et al. serves as basis for the work of this thesis aiming to further characterize the zoonotic SFV-specific nAb epitopes located within SUvar, explained in depth in section 1.3.

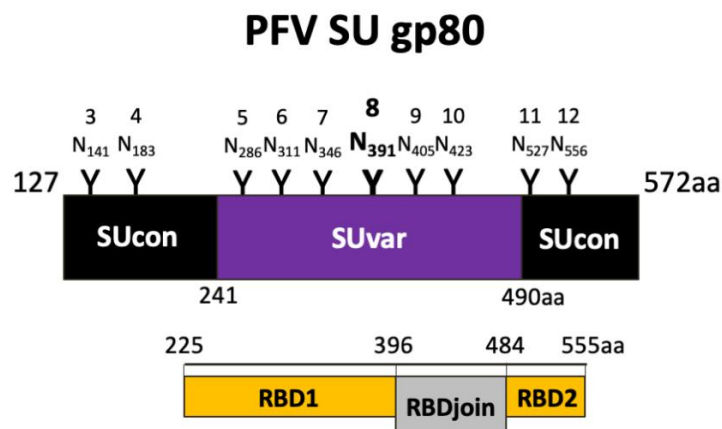


Figure I-14 – Schematic overview of SUvar region within PFV SU gp80

The sequence of SU gp80 protein with SUcon and SUvar regions shown in black and purple, respectively. Numbering and location of N-linked glycans highlighted according to PFV Env aa sequence. The SU domain harbors the bipartite RBD composed of RBD1 and -2 domains in orange separated by the non-essential RBDjoin domain in grey as shown below the SU domain box. The 249aa long SUvar region overlaps the majority of the RBD. *Figure adapted from (Duda et al., 2006; Richard et al., 2015).*

1.2 Epidemiology and zoonotic transmission of SFVs

Since the discovery of FVs in the 1950s, epidemiological surveys have been performed across continents. This section will focus on what is currently known on zoonotic SFV transmissions to humans with emphasis on prevalence in NHPs, transmission modes and risk factors. Then, I will describe investigations on the *in vivo* tropism and pathology. In addition to SFVs, non-primate FVs are also abundant in their respective hosts (cats, cows, and horses). Although understudied in comparison to SFVs, human transmissions of FFV and EFV have not been reported, while some rare BFV antibody positive human cases have been documented, reviewed by (Kehl et al., 2013). The epidemiological review of these FVs is beyond the scope of this thesis, but the following studies have addressed the prevalence of FFV (Ledesma-Feliciano et al., 2019; Winkler et al., 1999), BFV (Okamoto et al., 2020; Romen et al., 2007) and EFV (Kirisawa et al., 2019) and reviewed by (Pinto-Santini et al., 2017).

1.2.1 SFV prevalence and transmission in and between NHPs

Primates are distributed over a large global area spanning Central and South America, nearly all parts of Africa, Southwest parts of the Middle East and most regions of South and Southeast Asia (Fig. I-15). The frequency of SFV has been investigated in specimens from Apes, OWMs, and NWMs. The first SFV strains were successfully isolated from several NHP species (Gajdusek et al., 1969; Hooks et al., 1972; Johnston, 1961; Rogers et al., 1967; Rustigian et al., 1955; Stiles et al., 1964) showing that SFV is widespread and that prevalence rates in adult NHPs are as high as up to 100% in some cases (Jones-Engel et al., 2007). Today, the methods used for detection are PCR and/or serology. Most SFV prevalence studies have used blood and tissue samples (Leendertz et al., 2010). Novel sampling techniques allowed the study of wild animals with non-invasive methods such as feces or urine (Liu et al., 2008), discarded plants eaten by NHPs (Smiley Evans et al., 2016) and ropes hidden inside distributed food sources (Smiley Evans et al., 2015).

SFV prevalence across different NHP species has been shown to increase with age and captivity, which could be due to a horizontal transmission route through aggressive behavior in elder and sexually mature monkeys as well as forced contacts between monkeys in captivity compared to in nature resulting in bites and wounds facilitating SFV transmission (Calattini et al., 2006b; Feeroz et al., 2013; Ghersi et al., 2015) and reviewed by (Meiering and Linial, 2001). The following synthesis will report results grouped by geographical areas and by living conditions (wild, semi-free ranged or captivity) that influence SFV transmission. When studied,

the association of age with SFV prevalence reported is described in the following paragraph on transmission modes summarized.

Global distribution of wild NHPs

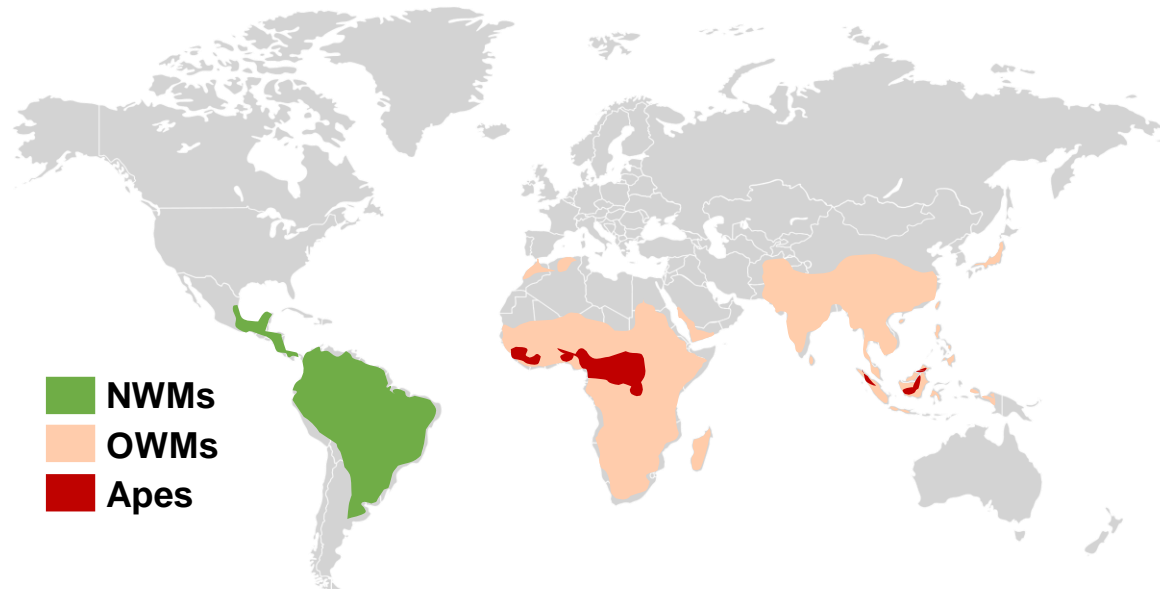


Figure I-15 – A view of the global distribution of NHPs

World map highlighting regions across 90 countries that are hosts for native species of primates spanning Latin America, Africa, the Middle East and Asia. SFV is endemic in primates from all regions including Madagascar. Regions hosting NWMs, OWMs and Apes are highlighted in green, pale orange and dark red, respectively. *Figure created with BioRender.com and adapted from (Santos et al., 2019).*

1.2.1.1 African continent – OWMs and Apes

Captive: Early studies in the US and Germany investigated the SFV prevalence in baboon and AGM breeding colonies which was above 95% in both cases (Blewett et al., 2000; Schweizer et al., 1999). Larger screening on >350 sera samples obtained from various NHP species held in captivity, including 43 different species of OWMs and Apes, described SFV prevalence of 68% across all species tested (Hussain et al., 2003).

Semi-free ranged: In the context of semi-free ranged NHPs, SFV prevalence was found to be 83% in Mandrill colonies in Gabon by our lab (Mouinga-Ondeme et al., 2010) and 44% in baboons (*Papio Anubis*) from Uganda (Smiley Evans et al., 2015).

Wild: Studies in wild living and wild caught NHPs from Africa also described high SFV prevalence. Our lab has demonstrated a wide distribution of SFV in mandrills, drills, chimpanzees and lowland gorillas (*Gorilla gorilla gorilla*) housed in zoos and sanctuaries in Cameroon and Gabon (Calattini et al., 2006a; Calattini et al., 2004; Mouinga-Ondeme et al.,

2010). In contrast, SFV was not detected in wild living populations of mountain gorillas (*Gorilla beringei beringei*) in the rain forest spanning the border of Rwanda, Uganda and DRC using a non-invasive sampling method of discarded plants. SFV was readily detected in sympatric golden monkeys (*Cercopithecus mitis kandti*) from same region using the same sampling method, excluding this non-invasive technique as reason for lack of detection in mountain gorillas (Smiley Evans et al., 2016). In a survey using fecal samples (n=724) from wild chimpanzees collected at 25 field sites over equatorial Africa, Liu et al. demonstrated that SFVcpz is wide-spread across the four chimpanzee (*Pan troglodytes*) subspecies (*P.t. verus*, *vellerosus*, *troglodytes* and *schweinfurthii*) (Liu et al., 2008). SFV was documented at all sites and the prevalence ranged from 44-100%. This non-invasive method has previously been used for detection of SIV-infection and SFV-SIV coinfections have been described (Keele et al., 2006; Santiago et al., 2005). Interestingly, the prevalence of SFV (86%) was shown to exceed that of SIV (82%) and STLV-1 (50%) in a wild population of red colobus monkeys (*Piliocolobus badius badius*) in Côte d'Ivoire Tai National Park (n=54) (Leendertz et al., 2010). The study on wild chimpanzee populations supports horizontal transmission as the primary route because infection was not detected in young animals (Liu et al., 2008). Another study documented frequent mother-offspring transmissions in a colony of wild chimpanzees, in which mother-infant pairs were identified (*P. t. verus*) (Blasse et al., 2013). In addition to vertical transmission, cases of superinfections were described supporting a continuous acquisition of diverse SFV strains throughout life via the horizontal route in Apes (Blasse et al., 2013). Thus, chimpanzees are the only NHP species for which vertical transmission has been described. The proportion of primary infections due to vertical transmission is however controversial. Importantly, cross-species transmission of SFV happens in-between NHPs in the wild, likely through aggressive contacts (Leendertz et al., 2008; Liu et al., 2008).

1.2.1.2 South and Southeast Asia – OWMs and Apes

Captive: In a captive but free-breeding colony of *Macaca tonkeana* housed at a primatology center in Strasbourg, France, SFV was detected in up to 89.5% of adult animals (Calattini et al., 2006b). In Bangladesh, SFV prevalence was 79% in performance macaques from nomadic people (Bedey) travelling with their monkeys (n=38) (Feeroz et al., 2013) and 52.9% among urban performance *M. fascicularis* monkeys in Indonesia (n=20) (Schillaci et al., 2005). In captive Orangutans (*Pongo pygmaeus*) hosted in zoos in London and Zurich, the seroprevalence was 100% among tested animals (n=14) and replicative virus was isolated from two of the Apes (McClure et al., 1994).

No evidence for vertical transmission of SFV was observed in the breeding colony of *M. tonkeana* in Strasbourg (Calattini et al., 2006b) and most SFV-infected mother-offspring pairs were infected with distinct strains. Moreover, SFV seropositivity was extremely rare in young macaques as described in animals before their sexual maturity (Jones-Engel et al., 2007).

Semi-free ranged: SFV prevalence was 39% in a rhesus macaque (*Macaca mulatta*) population (n=74) living semi-free ranged in a zoo in Yunnan, China (Huang et al., 2012).

Wild: Macaques represent the most studied species of NHPs to date, as these monkeys live in close contact with humans across Asia, Northern Africa and Gibraltar (Fig. I-15). The total SFV prevalence rate was 92% (n=118) in adult free ranging Asian monkeys spanning five macaque taxa; *M. mulatta*, *fascicularis*, *assamensis*, *nemestrina* and *arctoides* sampled in Thailand and Singapore (Jones-Engel et al., 2007). All animals above three years old were infected. SFV was also detected in 38/39 (97.4%) rhesus macaques living in and around temples in Nepal (Jones-Engel et al., 2006). This contrasted a later study which found SFV in only 18% of free ranging *M. mulatta* in Nepal (Smiley Evans et al., 2015). In Bangladesh, SFV prevalence was 94.4% in free ranging macaques (n=126) (Feeroz et al., 2013), 88% in adult *M. sylvanus* macaques (n=79) in Gibraltar (Engel et al., 2008), 98% among free living Indian rhesus macaques (n=35) (Nandi et al., 2021) and 56.5% in long-tailed *M. fascicularis* (n=649) across Thailand (Kaewchot et al., 2022).

1.2.1.3 Central and South America – NWMs

Lastly, SFVs has also been shown to have a wide distribution in neotropical monkeys inhabiting the Latin Americas – in contrast to SIVs and STLVs which do not circulate in NWMs and are exclusively found in Asian and/or African NHP species (Santos et al., 2019). Ghersi et al. demonstrated SFV in 11/15 genera from captive and wild-caught NWMs in the US and Peru reaching prevalence of 45.2% and 37.5%, respectively (Ghersi et al., 2015). Those data expanded results from previous reports from Brazil (Muniz et al., 2015; Muniz et al., 2013). The SFV prevalence in that study ranged from 0-100% in distinct NWM species, although sampling numbers were low for some groups. Moreover, seropositivity was observed in NWMs held at a rescue center (18.9%) and illegal trade markets (42.9%) in Peru (Ghersi et al., 2015). Phylogenic trees of the sequenced strains also showed strong co-speciation of SFV with their NWM host, as known for OWMs, and provided evidence for cross-species transmission during evolution, even across genera (Ghersi et al., 2015).

1.2.2 SFV *in vivo* tropism and pathology in NHPs

SFV has been shown by many groups to latently infect most tissues *in vivo* in naturally infected NHPs, supporting the broad *in vitro* tropism observed. One of the first studies detected SFV DNA in all samples of a broad range of tissues from AGMs naturally infected with SFV_{agm} (n=4) (Falcone et al., 1999a). Samples included tissue from less commonly tested sites such as bone marrow, brain, testes, prostate and uterus. SFV RNA was only detected in one monkey in the oral mucosa (Falcone et al., 1999a). Following this study, Murray et al. were the first to confirm that the primary site of viral replication and presence of viral RNA *in vivo* locates to the oral cavity by *in situ* hybridization – more specifically to a small cell niche of superficial epithelial cells (Murray et al., 2008). These results were proposed to explain why SFV-infection is largely non-pathogenic in NHPs, since these epithelial cells are short-lived and shed into the saliva. The data also explains the efficient transmission of SFV between monkeys and support bites as a major horizontal route of infection. Moreover, a later study on rhesus macaques in Bangladesh (n=61) demonstrated a strong correlation between viral strains obtained from blood cells and buccal mucosal samples, suggesting that the actively transcribing – and likely transmitting viruses in the oral mucosa – are also those integrated throughout the body (Soliven et al., 2013).

In blood from infected NHPs, SFV DNA was detectable in T cell, B cell, monocytes and polymorphonuclear leucocytes (PMNL) from chimpanzees (n=4) and AGMs (n=9) (Table I-4) (von Laer et al., 1996). *In vitro*, PFV-infection induce CPEs in chronically HTLV-1 and HIV-1 infected T cell lines (Mikovits et al., 1996). However, no transactivation of the PFV LTR by HTLV-1 Tax or vice versa was observed (Keller et al., 1991; Mikovits et al., 1996). This is in contradiction with most recent data showing that HTLV-1 Tax transactivate the PFV LTR *in vitro* (Alais et al., 2018). In line with this, SFV-STLV-1 dual-infected baboons had significantly higher proviral DNA loads in their PBMCs compared to SFV mono-infected animals (Alais et al., 2018).

To date, SFV-infection has not been directly associated with overt pathology in naturally infected NHPs. However, one study demonstrated acceleration in progression towards AIDS-like disease and death in experimentally SIV-infected rhesus macaques with chronic SFV-infection compared to SFV negative animals (Choudhary et al., 2013). In SFV mono and SFV-SIV co-infected animals, the presence of SFV RNA was tested across several tissues; buccal epithelium, pharyngeal epithelium, tongue, tonsils, lung, small intestine, mesenteric lymph node, parotid salivary glands, colon and blood (PBMCs). SFV viral transcripts were abundant

in lung, tongue, tonsils, buccal and pharyngeal epithelium in both groups, however SFV viral RNA was also found in the small intestine and lymph nodes of SIV co-infected animals suggesting an expansion of tissue tropism (Murray et al., 2006). These results emphasize the importance of understanding SFV-SIV or SFV-HIV co-infections in humans which has been reported (Switzer et al., 2008; Switzer et al., 2016) and reviewed by (Murray and Linial, 2019).

1.2.3 Zoonotic SFV infections

The prevalence of SFV in the human population has been investigated in 23 principal studies to date. Taking into account all published and reviewed data (Gessain et al., 2013; Pinto-Santini et al., 2017) including recent reports (Halbrook et al., 2021; Muniz et al., 2017; Switzer et al., 2016), a total of 251 cases of humans with serologic evidence of SFV infection (i.e., a Gag doublet on Western blot, WB) have been reported since the isolation of PFV from a Kenyan individual in 1971 (Fig. I-16) (Achong et al., 1971). Among these, 123 cases were confirmed by virus detection, either its isolation or viral DNA amplification by PCR or viral culture isolation (Table I-4). An additional six cases were diagnosed by PCR in absence of serological confirmation, yielding a total of 129 reported zoonotic SFV cases. SFV acquisition occurred in natural or occupational settings. Natural settings include NHP hunting, handling of bushmeat, keeping monkeys as pets or through other contacts including at religious sites or temples in Asia. Occupational settings include zookeepers and animal care takers infected in a work context, with most cases reported in North America (Heneine et al., 1998; Schweizer et al., 1997) and a single case of accidental laboratory infection reported in Germany (von Laer et al., 1996).

Zoonotic SFV transmission to humans

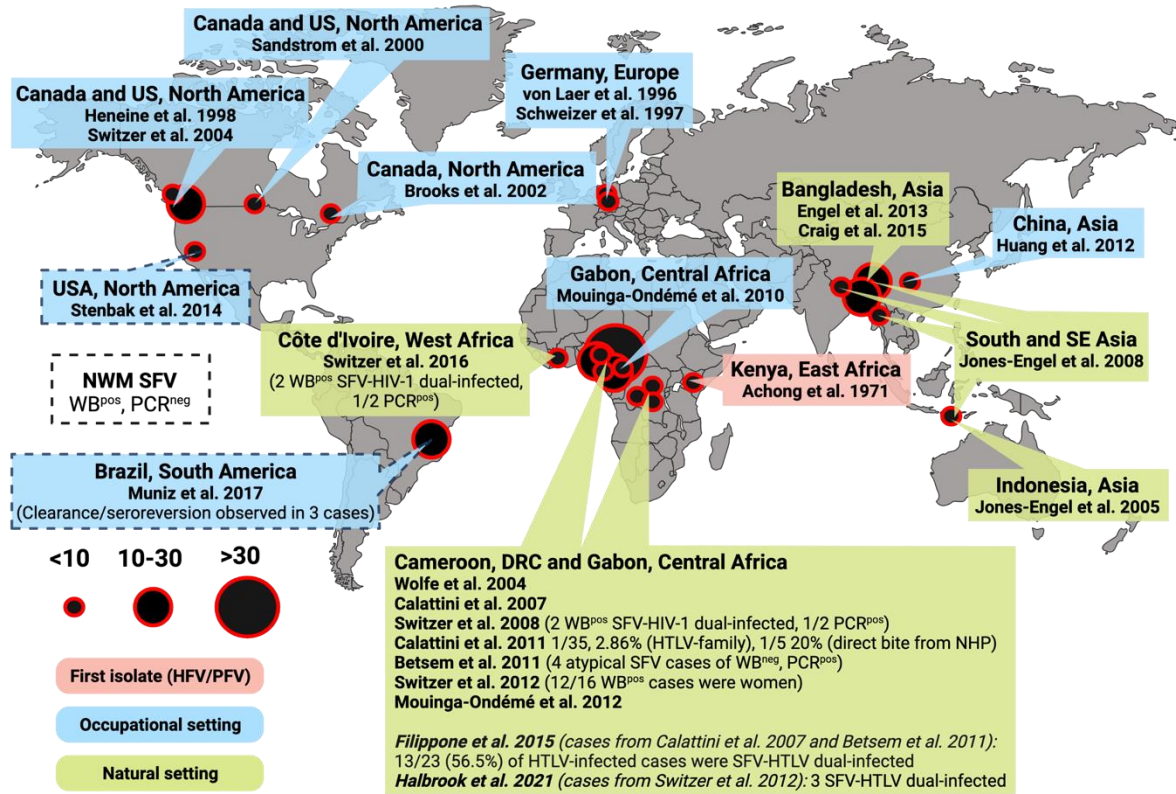


Figure I-16 – Global distribution of zoonotic SFV-infections reported to date

World map highlighting documented zoonotic SFV-infections in humans, through occupational (blue) or natural settings (green). The first isolated strain (HFV/PFV) highlighted in red. Circular symbols placed at approximate location of reported SFV-cases shown in size according to number of cases reported for the region. Name of country and region entitled in boxes and details of studies conduction in the region shown below according to infection setting. Relevant additional information for individual studies such as retroviral co-infections or proportion of cases in subdivided groups are shown in parenthesis. Studies with no PCR documented human cases (NWM SFV) highlighted in dashed boxes. Total number of reported cases in respective settings according to testing method or retroviral co-infection for respective studies are detailed in Table I-3 below. *Figure created with BioRender.com.*

Table I-3 – Details on zoonotic SFV-infections documented to date

Location	Setting	No. (Study cases)	WB ^{pos} (%)	PCR ^{pos} (%)	Reference
<i>Europe</i>					
Germany	Occupational	2 (Primate center and lab worker)	ND (50) 1 (50)	2 (100)	(von Laer et al., 1996) (Schweizer et al., 1997)
<i>North America</i>					
Canada, US	Occupational	231 (Research centers)	4 (1.8)	4 (1.8)	(Heneine et al., 1998)
Canada, US	Occupational	133 (Zoo workers)	4 (3)	ND	(Sandstrom et al., 2000)
Canada	Occupational	46 (Primate centers)	2 (4.3)	1 (2.2)	(Brooks et al., 2002)
Canada, US	Occupational	187 (Research and zoos)	10 (5.3)	9 (4.8)	(Switzer et al., 2004)
US	Occupational	116 (Primatologist)	8 (6.9)	0 (0)	(Stenbak et al., 2014)
<i>South America</i>					
Brazil	Occupational	56 (Research and zoos)	10 (17.8)	0	(Muniz et al., 2017)

Introduction

<i>Africa</i>					
Kenya	First isolate	1 (HFV/PFV)	ND	1 (Culture)	(Achong et al., 1971)
Cameroon	Natural	1099 (NHP contact)	10 (0.91)	3 (0.27)	(Wolfe et al., 2004)
Cameroon	Natural	1164 (Gen. population)	21 (1.8)	4 (0.34)	(Calattini et al., 2007)
Cameroon, DRC	Natural	85/102 (NHP contact)	10 (9.8)	9 (8.8)	
		139 (Sex workers)	1 (0.72)	0 (0)	(Switzer et al., 2008)
		41 (STD patients)	0 (0)	0 (0)	
Gabon	Occupational	179 (Blood donors)	1 (0.56)	1 (0.56)	
		20 (Primate center)	2 (10)	2 (10)	(Mouinga-Ondeme et al., 2010)
Cameroon	Natural	35 (HTLV-3 case family)	5 (14.3)	1 (2.9)	(Calattini et al., 2011)
Cameroon	Natural	1321 (Gen. population)	26 (2)	2 (0.2)	(Betsem et al., 2011)
		198 (NHP contact)	53 (26.7)	41 (20.7)	[4/41 WB^{neg}]
Gabon	Natural	78 (NHP contact)	19 (24.4)	15 (19.2)	(Mouinga-Ondémé et al., 2012)
DRC	Natural	3846 (Rural population)	16 (0.34)	3 (0.08)	(Switzer et al., 2012)
Côte d'Ivoire	Natural	1529 (Sick patients, pregnant women and TB patients)	3 (0.20)	1 (0.07)	(Switzer et al., 2016)
<i>Asia</i>					
Indonesia	Natural	82 (Temple workers)	1 (1.2)	1 (1.2)	(Jones-Engel et al., 2005)
Bangladesh, Indonesia, Nepal, Thailand	Natural	305 (Total)	8 (2.6)	3 (0.98)	(Jones-Engel et al., 2008)
		234 (Temple workers)			
		21 (Pet owners)			
		23 (Bushmeat hunters)			
		8 (Zoo workers)			
China	Occupational	19 (Villagers)			
		12 (Zoo workers)	ND	2 (16.7)	(Huang et al., 2012)
Bangladesh	Natural	209 (Villagers)	18 (8.1)	11 (5)	(Engel et al., 2013)
		13 (Bedey nomads)	0 (0)	0 (0)	
Bangladesh	Natural	269 (Villagers)	17 (6.4)	12 (4.5)	(Craig et al., 2015)
		45 (Bedey nomads)	1 (2.2)	0 (0)	
<i>Sum of cases</i>					
Global	Occupational	803	41 (5.1)	20 (2.5)	WB^{pos} only: n=21
Global	Natural	10655	210 (2.0)	108 (1.0)	WB^{pos} only: n=106
Global	Total	11456	251 (2.2)	128 (1.1)	WB^{pos} or PCR^{pos}: n=129 [WB^{neg}/ND, PCR^{pos}: n=6]
<i>Retroviral co-infections</i>					
Cameroon	SFV-HTLV	16	13	13 (100)	(Filippone et al., 2015)
DRC			3	3 (100)	(Halbrook et al., 2021)
Cameroon, DRC	SFV-HIV	4	2	1 (50)	(Switzer et al., 2008;
Côte d'Ivoire			2	1 (50)	Switzer et al., 2016)

PFV strain isolated from cell culture was included as a PCR^{pos} case. ND; not determined, Gen.; general, STD; sexually transmitted disease, TB; Tuberculosis. Setting colors according to *Figure I-16. Table adapted from (Pinto-Santini et al., 2017).*

1.2.3.1 Zoonotic cases in West and Central Africa

Our lab has performed surveys on humans exposed to NHPs and their body fluids over the past two decades in Central Africa in collaborations with the *Centre Pasteur du Cameroun* in Yaoundé, Cameroon and *Centre International de Recherche Médicale de Franceville* in Gabon. These tested individuals belonged to tribes of Pygmies and Bantus and were living in rural

settlements of rainforest regions in southern Cameroon. Individuals were screened by WB; samples with positive or indeterminate serology were then tested by two PCR assays, amplifying the LTR and IN region. PCR assays were carried out for all individuals who reported contact with NHPs, leading to the identification of four individuals who tested negative in WB. In total, 74 individuals tested positive in at least one PCR assay. In these studies, only individuals with a positive PCR were considered as infected (Betsem et al., 2011; Calattini et al., 2011; Calattini et al., 2007; Mouinga-Ondeme et al., 2010; Mouinga-Ondémé et al., 2012). The majority of the individuals reported bites by NHPs during hunting activities and were infected with SFV strains derived from gorillas and chimpanzees. Infection by SFV from monkeys was less frequent (Mouinga-Ondeme and Kazanji, 2013). Our lab has also shown that a severe bite from an NHP is strongly associated with acquisition of SFV (Filippone et al., 2015). In that study, 56.5% (13/23) of SFV-infected individuals were co-infected with STLV-1/HTLV-1, which could have been acquired at the same time as their SFV-infection (Fig. I-16, Table I-3) (Filippone et al., 2015).

Moreover, five studies have searched for SFV-infection by testing Biobanks constituted for HIV or Monkeypox surveys in urban or rural areas of Cameroon, Côte d'Ivoire and DRC (Halbrook et al., 2021; Switzer et al., 2008; Switzer et al., 2012; Switzer et al., 2016; Wolfe et al., 2004). Seroprevalence ranged from 0.2 - 0.91%. These studies also reported four cases of SFV-HIV-1 (2/4 PCR confirmed) (Switzer et al., 2008; Switzer et al., 2016) and three cases of SFV-HTLV-1 dual-infection (3/3 PCR confirmed) (Halbrook et al., 2021). Interestingly, the SFV-infected population living in rural areas from DRC is distinct from the one described in Gabon and Cameroon: most were women (12/16) who had contact with NHPs or their body fluids, but none reported wounds (Switzer et al., 2012).

1.2.3.2 Zoonotic cases in South and Southeast Asia

Human SFV-infection was reported in four epidemiological surveys in South and Southeast Asia (Craig et al., 2015; Engel et al., 2013; Jones-Engel et al., 2005; Jones-Engel et al., 2008). Nine SFV WB^{POS} cases including four PCR confirmed were found among temple workers in close contact with macaque monkeys living around these religious buildings in Bali and Nepal (Jones-Engel et al., 2005; Jones-Engel et al., 2008). Similarly, an SFV_{mac} frequency of up to 5% was shown in villagers from Bangladesh (Engel et al., 2013). In contrast, SFV could not be confirmed in seminomadic people (n=45) from an ethnic group called Bedey who own performance monkeys in Bangladesh and generally have extensive exposure to macaques (Craig et al., 2015). The resistance mechanism to SFV infection, if any, has not been elucidated.

One study built a model using these data and predicted that SFV_{mac} would be transmitted to approximately six individuals out of every 1000 visitors at religious temples in Bali, Indonesia (Engel et al., 2006).

1.2.3.3 Zoonotic cases of NWM SFV

Human SFV-infections from NWMs has also been reported, primarily in zookeepers and people working in primate research centers (Muniz et al., 2017; Stenbak et al., 2014). Interestingly, these cases were based on serological evidence only and could not be confirmed by PCR. Moreover, one report demonstrated potential sero-reversion in three cases over a 2-3 year period (Muniz et al., 2017). Thus, human NWM SFV infection may be cleared or fully silenced. Those results suggest that the persistence and/or replication levels in humans depends on the relatedness of the SFV host species with humans, with more frequent persistence of SFV from Apes and OWM compared to NWM SFVs.

Taking into account the number of people exposed to NHPs in many places of the world, the absence of SFV screening policies – except in research studies described above – it is highly probable that a large number of people are living with an undiagnosed SFV-infection. Furthermore, SFV cross-species transmissions are currently ongoing worldwide.

Despite >100 individual zoonotic SFV cases documented, there is yet to be reported any human-to-human transmission of SFV. Indeed, several of the abovementioned studies investigated SFV sero-reactivity in close relatives of zoonotic and accidentally SFV-infected cases (Betsem et al., 2011; Boneva et al., 2007; Heneine et al., 1998; Schweizer et al., 1997; Switzer et al., 2012). Only one sample from a relative had a WB^{pos} SFV test, which was confirmed PCR^{neg} supporting a general lack of secondary SFV-transmission (Betsem et al., 2011). In line with this, no evidence of SFV transmission was found in four recipients of transfused blood from an accidentally infected donor (Boneva et al., 2002).

1.2.4 Pathology and clinical signs associated with SFV-infection in humans

Our lab has performed the first thorough case-control matched studies on clinical signs, blood tests and immune status of Cameroonian hunters infected with zoonotic gorilla SFVs (Buseyne et al., 2018; Gessain et al., 2019). Only healthy individuals were included and the frequency of clinical signs did not differ between infected cases and controls. Levels from some hematological and biochemical parameters differed between cases and controls. The most pronounced difference was the lower level of hemoglobin in SFV-infected cases. Mild to moderate anemia was observed in 58% of cases and 17% of controls matched for age and

ethnicity. Urea, creatinine, protein and lactate dehydrogenase were higher than in controls (Buseyne et al., 2018). In regards to plasma biomarkers and blood-cell phenotypes, gorilla SFV-infected cases had higher levels of soluble scavenger receptor CD163 in the plasma and higher levels of CD4⁺ T cells expressing programmed death receptor 1 (PD-1) compared to matched controls. Cases had a significantly higher percentage of CD8⁺ T cells, while other immune cells such as B cells, natural killer (NK) cells and CD4⁺ T cells were unchanged (Gessain et al., 2019). Thus, chronic asymptomatic SFV-infection is associated with T cell differentiation as well as monocyte activation, and reduced hemoglobin levels.

In addition to work from our lab, one early study reported on clinical and hematological status of nine accidentally SFV-infected cases (Boneva et al., 2007). Clinical laboratory testing was normal or as expected according to co-morbidities such as diabetes. On the other hand, hematological abnormalities were observed for three individuals which included one case with low eosinophil count, one case with thrombocytopenia and one case with mild thrombocytopenia and NK-cell lymphocytosis above upper limit at three independent time points (Boneva et al., 2007). No symptoms related to the clinical status were reported.

1.2.4.1 *In vivo tropism of SFVs in humans*

Three studies investigated the *in vivo* SFV tropism using PBMC samples from SFV-infected humans (Boneva et al., 2007; Rua et al., 2014; von Laer et al., 1996). Our lab detected SFV DNA in PBMC-derived blood cells from SFVggo-infected Central African hunters – primarily in T and B cells, while rarely in CD14⁺ and CD56⁺ monocytes and NK cells (Table I-4 and Fig. I-17) (Rua et al., 2014).

Table I-4 – *In vivo* SFV cell tropism in infected NHPs and humans

	Infesting virus (#donors)	CD4+ T cells	CD8+ T cells	CD19+ B cells	CD14+ monocytes	Other cell types	References
NHP	SFVagm (9)	1/3	9/9	5/9*	2/7	PMNL: 1/7	(von Laer et al., 1996)
	SFVcpz (4)	3/4	4/4	3/4*	1/4	PMNL: 3/4	
Human	SFVagm (1)	0/2	2/2	0/2	0/2	CD56+	(von Laer et al., 1996)
	PFV (1)					NK cells: 0/2	
	SFVgor (11)	9/11	10/11	7/11	2/11	CD56+ NK cells: 1/11	(Rua et al., 2014)

*Non-T lymphocytes (CD4-CD8-).

In accidentally infected humans (n=7) working at zoos and primate centers, SFV DNA was detected by PCR in 19/19 PBMCs samples, 2/5 urine and 1/1 semen samples taken over a 5-year period (Boneva et al., 2007). One study readily detected SFV in CD8⁺ T cells from two SFV-infected humans but failed to detect in other cell populations. In contrast, SFV was detected in T cells, B cells, NK cells and PMNLs in naturally infected NHPs (n=13) from the same study (von Laer et al., 1996).

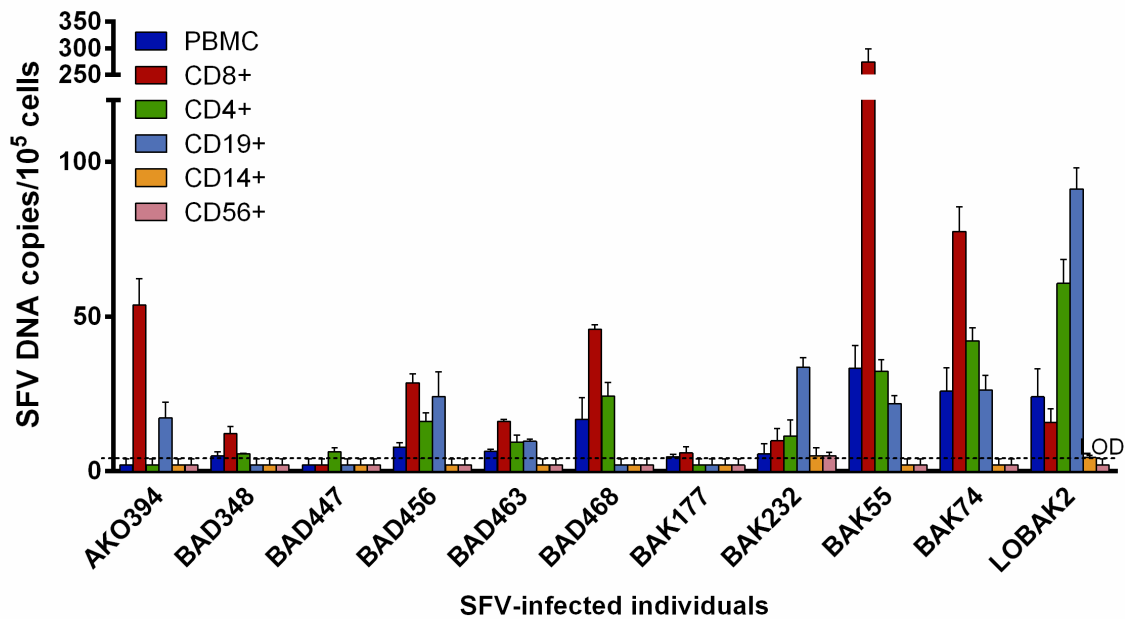


Figure I-17 – SFV *in vivo* tropism in Central African hunters

SFV DNA copies in PBMC populations isolated from Central African hunters (n=11) infected with SFV_{ggo} strains. SFV DNA loads below the limit of detection (LOD) arbitrarily set as two SFV DNA copies/10⁵ cells equal to half the LOD. Figure from (Rua et al., 2014).

Since SFV replicates in the oral cavity of infected NHPs, saliva samples were examined in humans. SFV DNA was detected in saliva and throat swabs from accidentally infected zoo keepers and African hunters, although at lower levels compared to PBMCs (Boneva et al., 2007; Huang et al., 2012; Rua et al., 2013). All these studies focused on SFV DNA, indicative of a latent infection. In contrast, viral RNA has not been detectable in human samples tested so far, suggestive of primarily latent infection and potential immune control in SFV-infected humans (Rua et al., 2013).

In vitro, PFV was shown to infect primary human CD4⁺ T lymphocytes, monocytes and brain-derived microglial cells, but poorly infected primary CD8⁺ T cells (Mikovits et al., 1996). Moreover, whereas strong cytopathic characteristics were observed for most cell lines and primary cells productively infected *in vitro*, monocyte-derived macrophages did not show

cytopathology upon PFV-infection (Mikovits et al., 1996). Lack of productive *in vitro* PFV-infection of CD8⁺ T lymphocytes contrast with the detection of SFV DNA in CD8⁺ T cells from Cameroonian hunters and occupationally infected humans, including one human case who acquired PFV itself from a lab (Fig. I-17) (Rua et al., 2014; von Laer et al., 1996).

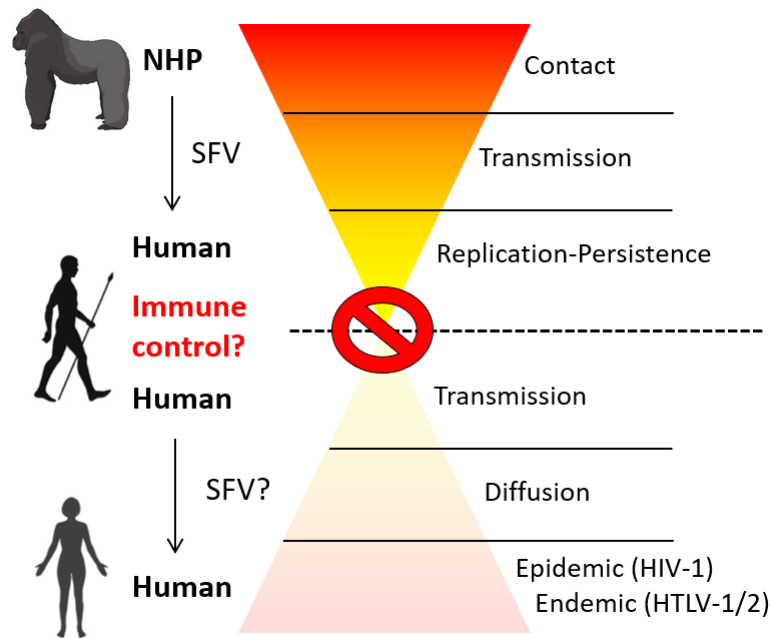


Figure I-18 – Pyramidal scheme of zoonotic SFV transmission and potential immune control

Schematic illustration of zoonotic SFV transmission from NHPs to humans. SFV efficiently cross the species-barrier to humans leading to a replication-competent and life-long persisting infection. Immune control may prevent human-to-human transmissions and subsequent diffusion of SFV into the human population which is in stark contrast to the epidemic and endemic HIV-1 and HTLV-1/2. *Figure adapted from (Gessain et al., 2013).*

The findings discussed above indicate limited pathology associated with zoonotic SFV infections. Based on the current knowledge addressed so far, we propose the following model for SFV transmission and its subsequent diffusion into the human population (Fig. I-18, from top to bottom): SFV is frequently transmitted to humans in close contact with NHPs, leading to a persistent and replication competent life-long infection. In zoonotically infected humans, SFV does not cause disease and is not transmitted to close relatives suggesting that the virus is under a potential immune control from the host. This immune control is preventing the further transmission and subsequent diffusion of SFV into the human population on a larger scale. This scenario is in strong contrast to SIVs and STLVs which efficiently generated epidemic (HIV-1) and endemic (HTLV-1/2) outbreaks in the human population from related simian reservoirs (Gessain et al., 2013).

1.3 Immune responses to FVs

The immune response against retroviruses is characterized by both innate as well as adaptive immunity including cell-mediated and humoral responses. The innate immune response constitutes the first line of defense against a foreign pathogen while the adaptive immune response is raised later, is antigen specific and persists over time (Sáez-Cirión and Manel, 2018). In this final introduction section, an overview of immunity to retroviruses will be given in line with what is known for FVs including a detailed description on nAbs and epitopes.

1.3.1 Overview of immune responses to retroviruses

The first innate defense mechanisms against viruses are constitutively expressed host restriction factors that interfere with the different steps of viral replication. Sensors of innate immunity recognize viral components and/or damage associated with infection and induce the production of IFN. IFNs belong to three families defined by their respective cell surface receptor. The type I IFN family comprises many IFN- α subtypes and IFN- β . The type II IFN family comprises IFN- γ only, and the type III IFN family comprises three subtypes of IFN- λ . Upon binding to their respective cell surface receptor complex, all IFNs initiate signaling pathway cascades involving janus kinase (JAK) and signal transducer and activator of transcription (STAT) proteins leading to induction of IFN-stimulated genes (ISGs) encoding for many of the restrictions factors that mediate the early innate defense (Platanias, 2005).

1.3.1.1 Innate sensing

The early innate immune response relies on the recognition of pathogen-associated molecular patterns (PAMPs) by a limited number of universal germ-line encoded receptors termed pattern-recognition receptors (PRRs) (Yan and Chen, 2012). PRRs include Toll-like receptors (TLRs), nucleotide oligomerization and binding domain-like receptors (NLRs) and retinoic acid-inducible gene I-like receptors (RLRs). The TLRs are expressed on several innate immune cell types like dendritic cells (DCs), macrophages, NK cells, $\gamma\delta$ T cells, granulocyte-like mast cells, neutrophils and eosinophils. The TLR family comprises 10 members which differ from one another by ligand specificities and gene expression upon activation. TLR3, -7, -8 and -9 are exclusively located intracellularly in endosomes and are specialized in sensing foreign nucleic acids. These TLRs are the primary receptors to recognize viral PAMPs. TLR9 senses viral DNA while TLR7/8 and -3 recognize ssRNA and dsRNA, respectively (Diebold et al., 2004; Pang and Iwasaki, 2012). TLR2 and -4 are expressed extracellularly on the cell surface membrane of innate immune cells and recognize PAMPs unique to microbes not produced by

the host such as viral proteins (Barbalat et al., 2009). Engagement of PRRs leads to the production of interferons, cytokines and proinflammatory molecules, activation of complement cascades and activation of cellular immunity facilitating the induction of apoptosis.

1.3.1.2 Restriction factors

Upon sensing of viral PAMPs by PRRs and/or production of IFNs, a broad variety of intrinsic host factors are induced, some with antiviral functions. Among these, some of the best characterized restriction factors shown to target multiple viruses include; Tetherin, APOBEC3 family, TRIM5 α of the tripartite-motif (TRIM) family, sterile alpha motif and HD domain 1 (SAMHD1), myxovirus resistance (Mx) proteins, the family of serine incorporator (SERINC) proteins and the IFN-induced transmembrane (IFITM) family members (Colomer-Lluch et al., 2018; Yan and Chen, 2012). These host factors interfere with different parts of the viral replication cycle including both early and late steps. Examples of early steps include inhibition of cytosolic entry and fusion (IFITMs, SERINC), block of viral capsid uncoating (TRIM5 α) and inhibition of RT and/or transcription (APOBEC3s, SAMHD1). Examples of late step interference include inhibition of nuclear accumulation/integration (MxB) and blocking the release of budding viral particles (Tetherin) (Colomer-Lluch et al., 2018). Moreover, many viruses including retroviruses evolved mechanisms to counteract these cellular host factors through adaptation of their accessory proteins (Kirchhoff, 2010).

1.3.1.3 Cellular effectors of innate immunity

The cellular component of the innate immunity is composed of a wide range of cells. Some of the most crucial cell types include granulocytes such as neutrophils and mast cells, monocytes – the precursor of DCs and macrophages which constitute antigen presenting cells (APCs) and innate lymphoid cells (ILCs) which include NK cells among other subtypes of ILCs. As described above, these cellular effectors of the innate immune response are important for the sensing of PAMPs through binding to the cellular PRRs and subsequent induction of antiviral restriction factors and IFNs (Rich and Chaplin, 2019). The main driver of type I IFN production is a subtype of DCs termed plasmacytoid DCs (pDCs) which are highly activated during viral infections (Malleret et al., 2008). The innate immune cells also harbor additional functions of great importance including killing and phagocytosis of infected or damaged cells. Neutrophils, monocytes and macrophages are the primary cells with such phagocytic functions (Rich and Chaplin, 2019).

ILCs such as NK cells are innate lymphoid cells that do not express diverse, rearranged and clonally distributed antigen-specific receptors as seen for T and B lymphocytes. Instead, they

express their germ-line encoded PRRs. In addition, NK cells express killer Ig-like receptors (KIRs) that can recognize major histocompatibility complex (MHC) class I molecules and peptides presented by non-classical HLA-E. These KIRs are categorized into inhibiting and activating receptors based on the signal cascades induced by the immunoreceptor tyrosine-based inhibitory and activating motifs (ITIMS and ITAMs, respectively) located at their cytoplasmic tails, reviewed by (Saunders et al., 2015).

1.3.1.4 Interactions between innate and adaptive immunity

Beyond serving as an early defense against evading pathogens, innate immune cells provide a link between the innate and adaptive immunity. APCs like DCs and macrophages can release stimulatory cytokines and through their MHC class I and II molecules present processed foreign peptides to cytotoxic T lymphocytes (CTLs) and T helper (Th) cells, respectively. Upon stimulation, NK cells and other ILCs are characterized by the production of different stimulatory cytokines including IFN- γ and tumor necrosis factor (TNF) (Rich and Chaplin, 2019). Moreover, NK cells, monocytes and neutrophils express a variety of crystallizable fragment (Fc) receptors (FcRs), including Fc γ Rs able to bind the Fc portion of IgGs with distinct affinity. This interaction can occur on free as well as cell-bound antigens coated by plasma IgG antibodies, leading to degranulation and release of molecules like perforin and granzyme B by NK cells (Bruhns and Jonsson, 2015). In the case of cell-bound or cell-expressed antigens (such as on an infected cell), the release of these cytotoxic molecules facilitates cytolytic destruction and elimination of the target cell in a process termed antibody-dependent cellular cytotoxicity (ADCC). For monocytes and neutrophils, this Fc γ R-antibody-antigen complex can mediate antibody-dependent cellular phagocytosis (ADCP) while the fixation of complement on antibody-bound antigen can facilitate antibody-mediated complement activation to destroy target cells, reviewed by (Lu et al., 2018). In a similar fashion, monocytes and macrophages also express complement receptors recognizing complement factor C3b opsonized on cell-free or cell-expressed antigens. This interaction also mediates phagocytosis of the foreign antigens and infected cells (Rich and Chaplin, 2019).

1.3.1.5 Adaptive immunities

The adaptive immune response is acquired during acute infection, is highly specific for antigens, and memory cells and effector molecules persist after clearance of infection to provide protection against subsequent challenge by the same pathogens. The adaptive immune cells are CD4⁺ and CD8⁺ T lymphocytes and B lymphocytes.

1.3.1.5.1 *T lymphocytes*

T cells principally recognize peptide-MHC complexes presented by APCs instead of the antigen in its native conformation, although some T cell subpopulations like $\gamma\delta$ T cells bind to diverse but intact non-peptide antigens including proteins, glycolipids as well as other small molecules. This recognition is mediated by the T cell receptor (TCR) which is composed of variable (V) and constant (C) Ig domains forming a heterodimer of α - and β -chain or a γ - and δ -chain, respectively. TCR signaling transduction is dependent on TCR association with multimeric CD3 complex. The diversity of TCRs is generated by genetic recombination of the V domain of the TCR, by rearrangement of gene segments designated V and J (joining) for α - and γ -chains, and gene segments V, D (diversity) and J for β - and δ -chains. This TCR-peptide/MHC interaction and following secondary co-stimulatory interactions leads to proliferation and differentiation of the naïve T cell into distinct effector T cell subsets (Rich and Chaplin, 2019). For CD4⁺ Th cells, subsets are defined on the basis of secretion of cytokines. The three major Th cell subsets are Th1, Th2 and Th17 cells. Th1 cells predominantly secrete IL-2 and IFN- γ that exclusively promote the cytotoxic effector functions of CD8⁺ CTLs and NK cells capable of killing viral infected cells. Th2 cells secrete primarily IL-4 and -13 which facilitate induction of humoral immunity by activation of B cells producing antibodies. Th17 cells produce IL-17 and play an important role in the exacerbation and induction of autoimmunity as well as in host defense against various pathogens. Another T cell subpopulation serving a crucial role in the regulation of T cell-dependent B cell responses are the T follicular helper (T_{FH}) cells. T_{FH} cells are essential for promoting the survival, proliferation, Ig isotype class switching, affinity maturation and B cell differentiation in the germinal center (GC) (Rich and Chaplin, 2019).

The role of CD8⁺ CTLs is similar to that of NK cells. They mediate cytolytic lysis of infected cells by secretion of perforin which creates pores in the target cell membrane and granzymes that can passively diffuse into the cytosol for induction of apoptosis through caspase-cascades (Fevrier et al., 2011). Moreover, the activity of CTLs is enhanced by IFN- γ . The importance of CD8⁺ T cells during retroviral infections is well highlighted by studies demonstrating that early, persistent and specific CTL responses during primary HIV-1 infection significantly correlate with plasma viral loads and CD4⁺ T cell counts (Streeck et al., 2009). Of notice, currently no data exist on SFV antigen-specific T cell responses in infected humans or NHPs which remains a high priority for future work on immune control of zoonotic SFV-infections.

1.3.1.5.2 *B lymphocytes*

The B cell receptor (BCR) consists of four Ig chains; two identical heavy (H) and two identical light (L) chains. The light chain exists as two isotypes; kappa (κ) and lambda (λ). These heavy and light chains have two or more domains, each consisting of two sandwiched β -pleated sheets linked by a disulfide bond. As for the TCR, these domains are grouped as either constant or variable. The chain contains one N-ter variable domain and a varying number of C-ter constant domains. In addition, the chains form two functional domains separated by a hinge region. These functional domains include an antigen-binding fragment (Fab) and the Fc region. The Fab is formed by the entire light chain (V_L+C_L) and the V_H and C_{H1} domains of the heavy chain. The Fc region is composed of a varying number of C_H domains and is linked to the plasma membrane in the BCR due to alternative splicing of the Ig transcript at its 3' end (Rich and Chaplin, 2019). On secreted antibodies, the Fc region can bind to cellular sensors that deploy host-mediated effector functions as described above (Fig. I-19). The BCR also engages noncovalently with heterodimeric complexes $Ig\alpha:Ig\beta$ ($CD79\alpha:CD79\beta$) essential for signal transduction. In contrast to the TCR, the BCR is able to bind virtually any foreign molecules in their native folds. The binding interface is mediated by the V_L/V_H domains and are formed by three hypervariable loop regions termed complementarity-determining regions (CDRs) interspaced between four stable framework (FR) sequences in both V domains (Rich and Chaplin, 2019).

B cells arise from the bone marrow and transit as immature B cells with functional BCRs to the peripheral blood. From there, further development into mature naïve B cells occurs through more selection processes in the spleen. The great variety of the Ig gene can be attributed to recombination of the V(D)J germline Ig sequences, just as for the TCR. However, in contrast to the TCR, further diversity of the BCR is generated through affinity maturation and somatic hypermutations (SHMs) in the variable domains of the Ig gene upon antigen-exposure leading to an extraordinary diversity. This BCR affinity maturation process occurs in GCs where naïve B cells with unmutated low-affinity V(D)J germline sequences migrate in and out of GCs in search for antigens trapped and displayed by follicular DCs (FDCs) in the light zone of the GC (Fig. I-20) (Victora and Nussenzweig, 2022). SHMs are induced by the enzyme activation-induced cytidine deaminase (AID) and happens when naïve B cell clones enter in the GC dark zone. During the GC-reaction, SHM-acquired clones will re-transit into the light zone of the GC where an antigen affinity-based selection occurs ultimately giving rise to affinity-matured B cell clones (Mesin et al., 2016; Victora et al., 2010). In this process, co-engagements with

T_{FH} cells are highly important for the support of B cell antibody generation as mentioned in section 1.3.1.5.1 (Fig. I-20) (Crotty, 2019). The B cell fate upon first time encounter with a pathogen is crucial for establishment of long-term immunity and a single naïve B cell is in fact capable of generating all types of B cell progenies including GC B cells, plasma cells and memory B cells (MBCs). Several factors are influencing the fate of the B cells within the GC including BCR affinity towards antigens and self. A deeper description of these processes is beyond the scope of this thesis but have been studied and reviewed elsewhere (Sabouri et al., 2014; Viant et al., 2020; Victora and Nussenzweig, 2022).

Upon activation through engagement of the BCR with an antigen, B cells first produce low affinity IgM. The affinity-maturated B cells can differentiate into several subsets including short-lived Ab-secreting plasma cells and long-lived MBCs (Moir and Fauci, 2017). These MBC subsets can express five different subclasses of Igs based on the C_H domains: IgM, IgD, IgG, IgA and IgE, respectively (Fig. I-19) (Lu et al., 2018). Class-switching from IgM to IgG or IgA usually happens within the first week post-infection, and is maintained further.

In response to a reinfection or booster vaccination, preexisting pathogen-experienced plasma cells act as a constitutive first line of reactive defense rapidly producing antibodies capable of neutralizing the reinvading pathogen. On the other hand, sentinel tissue resident MBCs found in mucosae and other strategic locations provide second line of reactive humoral immunity. The MBCs are capable of further affinity maturation by reentering the GC, reviewed by (Inoue et al., 2018). The long-term protective immunity however seems to depend on both the MBC and plasma cell pools as shown by a comprehensive study which found highly stable levels and long half-lives of circulating serum antibodies without frequent correlation between these and peripheral blood MBCs (Amanna et al., 2007).

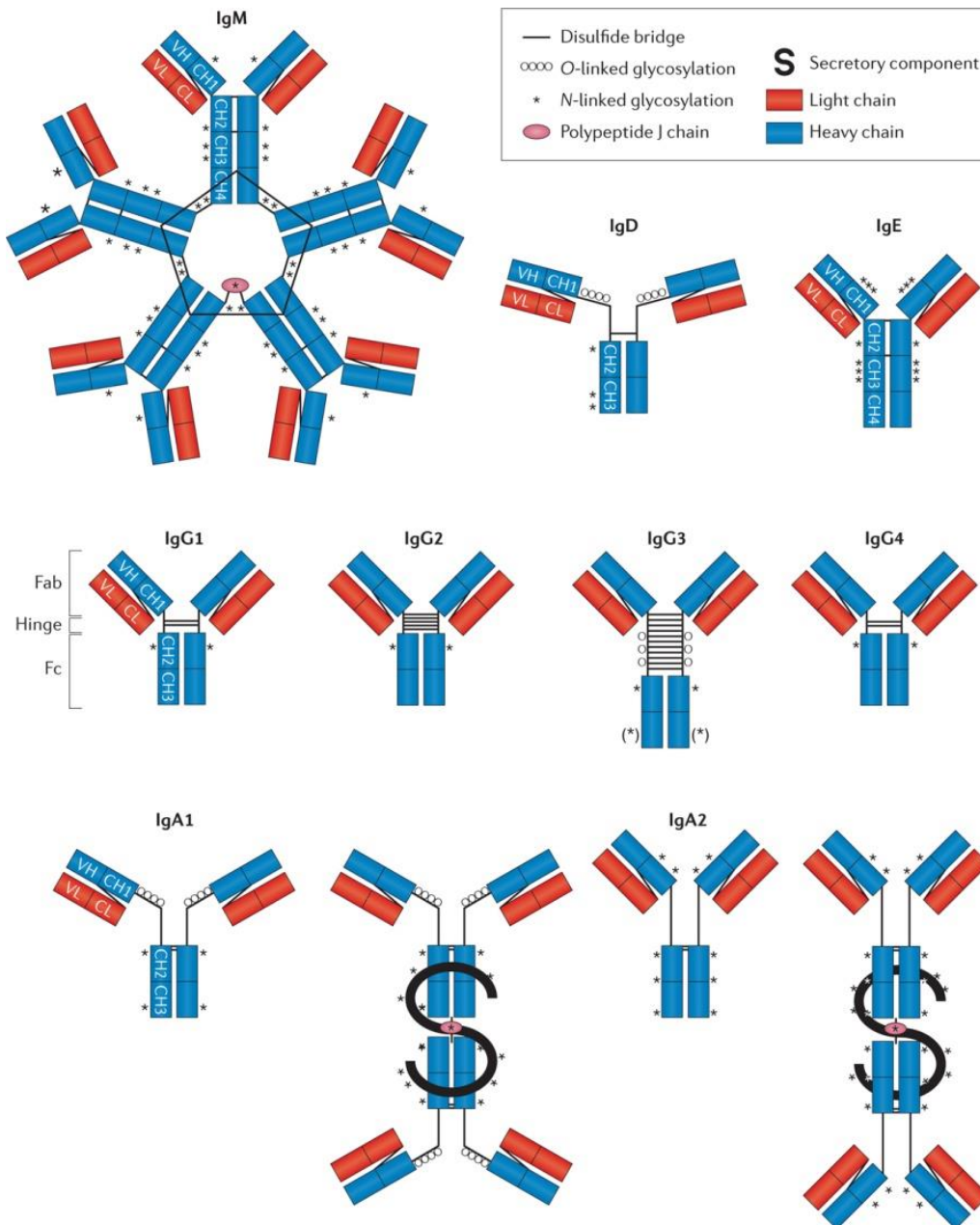


Figure I-19 – Schematic structural overview of human Ig molecules and subclasses

Human Ig molecules consist of two functional domains linked by a hinge region. The Fab binds the antigen while the Fc region bind sensors which deploy host-mediated effector functions. All Igs are composed of four chains; two identical heavy chains (blue) and two identical light chains (red). These chains are further subdivided into variable (V_H/V_L) and constant (C_H/C_L) domains. Ig light chains also exist as κ and λ types. The human Ig molecules exist as five subclasses: IgM, IgD, IgE, IgG and IgA including four IgG (IgG1-4) and two IgA (IgA1-2) isotypes. These molecules either form monomers, dimers or multimers depending on subclass and isotype for which multimers are linked through disulfide bonds. Dimeric IgA further contains a secretory component (or J chain). Fab and Fc binding to antigen and receptors are highly affected by features like hinge length and flexibility, glycosylation sites and disulfide bonds. *Figure from (Lu et al., 2018).*

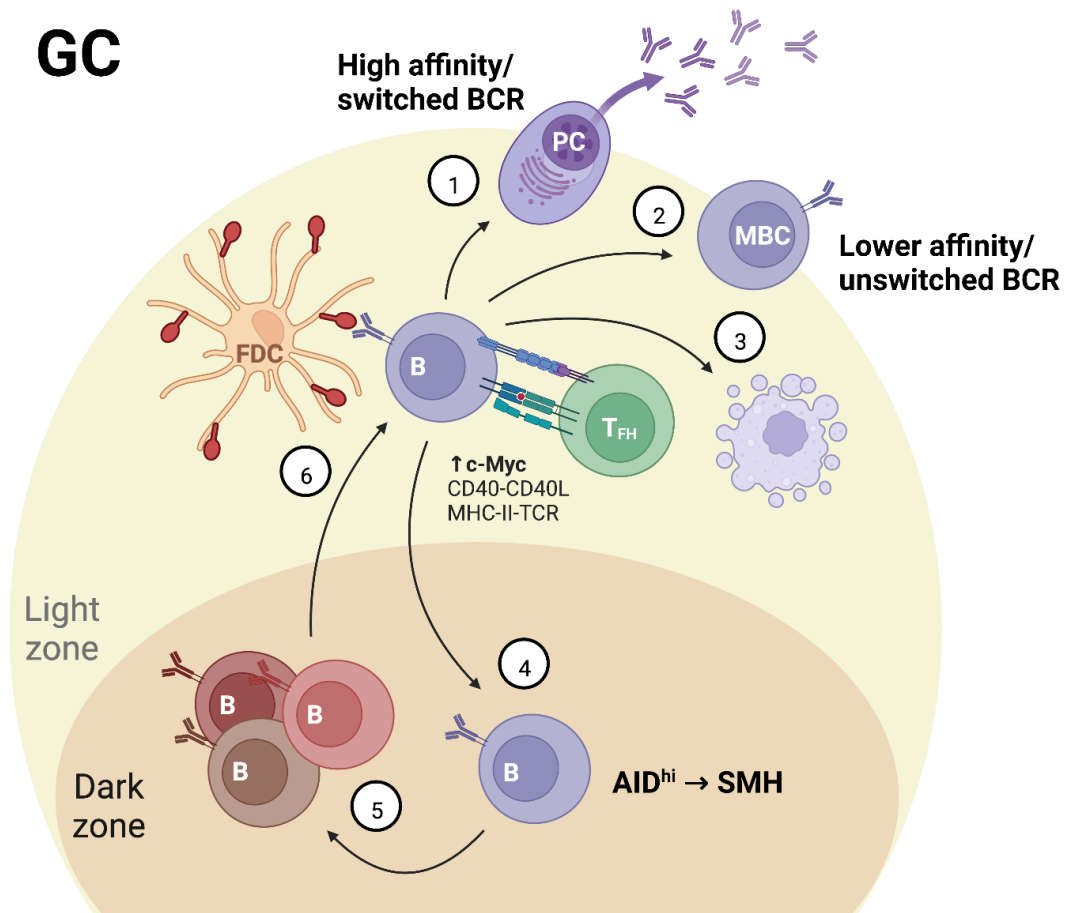


Figure I-20 – Overview of dynamics during germinal center reaction and B cell fates

Schematic of fates taken by a GC B cell. In the dark zone of the GC, a B cell acquires SMHs through AID which yield B cell clones with higher BCR affinity for cognate antigen. In the light zone of the GC, the B cell will test its BCR affinity to foreign antigen presented by an FDC while also engage with T_{FH} cells through CD40-CD40L and MHC-II-TCR complexes. In case of high affinity of the BCR to the presented antigen and strong B cell-T_{FH} interaction (1), the B cell can leave the GC as a plasma cell (PC) which undergoes Ig-class switching and produce large amounts of soluble antibodies. In case of lower BCR affinity to the antigen and weaker B cell-T_{FH} interaction (2), the B cell can leave the GC as an MBC with an unswitched BCR. In case of inadequate BCR antigen affinity or high self-reactivity, the B cell can either die through apoptosis (3) or recycle into the dark zone of the GC for additional SMHs (4). The AID-mediated SHMs may give rise to B cell clones with increased BCR antigen affinity (5), which is tested by reentering the light zone and engage with antigen presented by FDCs once again (6). *Figure created with BioRender.com and adapted from (Mesin et al., 2016).*

1.3.1.6 Role of nAbs during viral infections

The humoral antiviral response relies on antigen-specific antibodies. One of their major functions is to bind and ‘neutralize’ invading pathogens. These nAbs mainly interfere with early steps of the viral replication cycle by blocking viral particles from entry into host cells (Murin et al., 2019). A second role of nAbs is the elimination of infected cells, mediated by cellular effectors as described in section 1.3.1.4. The importance of nAbs in antiviral immunity is demonstrated by prophylactic vaccines against major viral pathogens which induce antibodies able to neutralize virus or interfere with their spread in the organism (Plotkin, 2010). Another

example includes maternal antibodies transferred to neonates during pregnancy and through breast-feeding which protect the infant against infections during the first months of life, reviewed by (Hansda et al., 2022). Moreover, passively administered viral antigen-specific polyclonal Igs are able to hinder infections in occasions of no prior immunity or in absence or lack of efficacious vaccines. Such plasma therapies have been well established for prevention of rabies virus infection in particular (Cabasso et al., 1971; Rupprecht and Gibbons, 2004), and have been successfully used against hepatitis A virus (Stapleton, 1992) and varicella zoster/human herpes virus type 3 infections (Sauerbrei, 2016).

Importantly, nAbs not only prevent infection but can also be used as treatment of established infection as it has been demonstrated in response to HIV-1 (Barin and Braibant, 2019). Immunotherapy by passively administered broadly neutralizing antibodies (bnAbs) can suppress viremia in HIV-1 infected humanized mice and SHIV-infected NHPs (Barouch et al., 2013; Gautam et al., 2018; Klein et al., 2013; Moldt et al., 2012; Shingai et al., 2013). Moreover, such anti-HIV-1 bnAbs have been and are currently being tested as immunotherapy or as prophylaxis in humans. Although passive infusion of individual bnAbs in most cases have led to mAb-resistant viruses, a combination of two potent bnAbs was able to suppress viremia and delay viral rebound in HIV-1 infected individuals undergoing analytical ART interruption (Bar-On et al., 2018; Mendoza et al., 2018) and reviewed by (Barin and Braibant, 2019; Caskey, 2020; Gruell and Schommers, 2022). Although larger studies are required, a recent study reported evidence for a decrease in size of intact proviral reservoirs in HIV-infected individuals treated with such bnAb combinations (Gaebler et al., 2022). Thus, nAbs play essential roles in the control of established viral infections and in prevention of their transmission to new hosts. For this reason, my host laboratory initiated a research program on antibodies raised by humans infected with zoonotic SFVs.

1.3.2 Innate immunity to FVs

Although the *in vivo* role of innate immunity during FV-infection has not been studied in depth to date, it is likely that the innate immune response restricts FV replication within infected hosts. Indeed, culture system studies have shown significant restriction of FVs by both novel and well-characterized intrinsic antiviral restriction factors, reviewed by (Berka et al., 2013). Two recent studies have also reported on the direct sensing of SFVs by primary hematopoietic and myeloid cells (Bergez et al., 2019; Rua et al., 2012b). Moreover, early and recent studies have shown that SFVs are sensitive to IFNs (Bahr et al., 2016; Falcone et al., 1999b; Rhodes-Feuillette et al., 1987).

1.3.2.1 Innate sensing of FVs

Type I IFNs are produced in particular by infected cells in response to sensing of PAMPs by PRRs and these cytokines can limit the spread of virus to neighboring cells by induction of antiviral ISGs. However, early *in vitro* culture system experiments with different serotypes of SFV showed that the majority of tested strains did not induce type I IFN production in non-hematopoietic cell lines of human, simian and murine origin (Rhodes-Feuillette et al., 1987; Sabile et al., 1996).

My lab showed sensing of PFV and primary zoonotic SFV strains by primary human mononuclear cells (Rua et al., 2012b). PBMCs were activated by both SFV cell-free particles and SFV-infected BHK-21 cells. Among PBMCs, the pDCs were the main type I IFN-producing cells (Rua et al., 2012b). The sensing and production of type I IFNs was dependent on expression of FV Env and independent of RT activity (Rua et al., 2012b). Inhibition of vesicular acidification and use of an endosomal TLR antagonist significantly decreased IFN induction in response to SFV particles and infected cells. Similarly, silencing of TLR7 in a pDC-like cell line significantly decreased IFN release in response to sensing of SFV, indicative of TLR7 to be the main innate PRR activated upon SFV entry in pDCs (Rua et al., 2012b). More recently, monocyte derived macrophages and monocyte derived DCs were shown to sense full-length replication-competent PFV (Bergez et al., 2019). Knock-out of molecules involved in signaling pathways showed that the cyclic GMP-AMP synthase (cGAS) and STING were the principal sensors in this cell type by detection of reverse transcribed SFV DNA present in incoming viral particles. A fusion-defective mutant virus furthermore failed to induce ISG-expression indicative of cytoplasmic presence to be important for myeloid sensing of PFV. Integration deficient or accessory Tas/Bet protein mutant viruses were all sensed (Bergez et al., 2019).

1.3.2.2 FVs are susceptible to IFNs

The addition of recombinant human IFN- α , - β or - γ to SFV-infected cells significantly decreased the CPEs on the culture indicative of antiviral activities (Rhodes-Feuillette et al., 1990; Rhodes-Feuillette et al., 1987; Sabile et al., 1996). IFN- γ produced by mitogen activated human primary blood leukocytes was shown to inhibit the replication of a SFVagm strain (SFVcae_huKa) (Falcone et al., 1999b), and more recently, IFN- β was demonstrated to inhibit the early steps of FV infection (Bahr et al., 2016). In line with these studies, my lab has shown that blocking molecules involved in IFN signaling pathways such as JAK1/2 increased the replication of zoonotic primary SFVgor strains isolated from infected African hunters

(Couteaudier et al., 2019). Interestingly, FV capsid proteins primarily contain arginine as basic residues instead of lysines that are found in high numbers compared to arginine in capsid proteins from other retroviruses. Reversion of these arginines to lysines in PFV Gag showed limited impact on replication of PFV infectious molecular clones. Conversely, Arg-to-Lys reversion increased the susceptibility to IFN- α treatment for the PFV mutant clones compared to WT suggesting capsid-dependent restriction by an unknown host factor (Matthes et al., 2011).

1.3.2.3 FV restriction by well-characterized host factors

Tetherin is an IFN-inducible transmembrane restriction factor that also acts as a ligand for the immunoglobulin-like transcript 7 (ILT7) receptor expressed on pDCs (Cao et al., 2009). Tetherin is known to block the release of viral particles from a broad range of viruses including retro- and filoviruses in infected cells (Jouvenet et al., 2009). The mechanism of action likely involves the C-ter glycosyl phosphatidylinositol membrane anchor of Tetherin inserted into the viral membrane, while its N-ter domain is anchored in the cell membrane. Tethered viral particles are then internalized and degraded in endosomes, reviewed by (Colomer-Lluch et al., 2018). For PFV, virion release is strongly inhibited by the human, simian, bovine and canine Tetherin and this inhibition was shown dependent on the membrane anchor and on Tetherin dimerization (Jouvenet et al., 2009; Xu et al., 2011).

The E3 ubiquitin ligase TRIM5 α also function as a retroviral restriction factor, in addition to its role as an PRR specific for retroviral capsids and regulation of innate immune signaling (Pertel et al., 2011). PFV and SFVmac were observed sensitive to TRIM5 α from NWMs, but resistant to TRIM5 α from OWMs and Apes. FFV was restricted by TRIM5 α from Apes whereas TRIM5 α from OWMs did not restrict any of the three FV isolates (Yap et al., 2008). NWM SFVs are inhibited by TRIM5 α from related NWM species but are not affected by their own species-specific TRIM5 α potentially reflecting FV evolution and adaptation of host TRIM5 α (Pacheco et al., 2010). Structural studies support that TRIM5 α restricts FVs through interaction of its B30.2 domain with viral Gag C-ter domain, as shown for orthoretroviruses (Goldstone et al., 2013).

FVs have been shown resistant to the human Mx proteins (Bahr et al., 2016; Regad et al., 2001). This is in contrast to the demonstrated inhibition of influenza A virus pol activity by MxA and the late-step capsid-dependent inhibition of HIV by Mx2 (Goujon et al., 2013; Kane et al., 2013; Mänz et al., 2013). The restrictive function of SAMHD1 works by limiting the intracellular

pool of dNTPs (Colomer-Lluch et al., 2018). An ISG library screen did not find restriction of PFV by human SAMHD1, in agreement with a functional study (Gramberg et al., 2013; Kane et al., 2016). However, the screen detected modest restriction of early PFV replication by the simian SAMHD1 (Kane et al., 2016). The SERINC proteins have been shown to harbor antiviral activity against HIV-1 and the accessory protein Nef can counteract SERINC2 – with the exception of the human paralog SERINC2 (Colomer-Lluch et al., 2018; Ramdas et al., 2021). On the contrary, FVs are resistant to SERINC2. Interestingly, SERINC2 from the ancient coelacanth was able to restrict HIV-1 but not FV. Overexpression of FV Env rescued HIV-1 infectivity, suggesting Env to counteract SERINC2. These results elucidate a long evolutionary relationship between SERINC2 and retroviruses (Ramdas et al., 2021). While IFITMs has not been shown to restrict PFV, a study demonstrated inhibition of FFV in a late step of replication by human IFITM1, -2 and -3, although time-dependent as restriction was diminished at later time points (Kim and Shin, 2020).

A class of well-studied restriction factors is the APOBEC3 proteins. These are incorporated into virions where they deaminate cytosine residues of the viral DNA into uracil (C-to-U) leading to degradation of the viral genome. In addition, human APOBEC3F and -3G interfere with reverse transcription of HIV. The majority of U-containing viral genomes are enzymatically degraded or integrated with numerous G-to-A substitutions, reviewed by (Jaguva Vasudevan et al., 2021). In regards to FVs, human, simian and murine APOBEC3G induces G-to-A editing of the FV genome and acts as inhibitor of FV infectivity *in vitro* (Delebecque et al., 2006; Löchelt et al., 2005; Russell et al., 2005). Moreover, it was shown that human APOBEC3F and -3G as well as the three feline APOBECs interact directly with FV Bet and some with Gag (Chareza et al., 2012; Russell et al., 2005). Indeed, with one exception, most studies found that the accessory protein Bet antagonize APOBEC3 proteins and prevents their incorporation into viral particles including PFV (Delebecque et al., 2006; Russell et al., 2005) and FFV (Chareza et al., 2012; Lukic et al., 2013; Löchelt et al., 2005). PFV Bet also inhibits human APOBEC3B, -3C and -3G activity with Bet forming a complex that prevents APOBEC3 dimers and APOBEC3 degradation, which is in contrast to Vif from SIV and HIV-2 that also restrict APOBEC3s (Jaguva Vasudevan et al., 2013; Perkovic et al., 2009; Zhang et al., 2021). The *in vivo* activity of APOBEC3s on SFV has also been addressed in a few studies. Notably, G-to-A substitutions have been found in SFV genomes recovered from humans infected with gorilla SFVs (Rua et al., 2013). However, contribution of APOBEC3 proteins to the induction of these hypermutations were either too rare to represent actual *in vivo* hypermutations

(Delebecque et al., 2006), or may alternatively reflect the expansion of a few number of edited clones (Rua et al., 2013). The latter is likely since all the G-to-A mutations in distinct clones were observed at the very same position of the genome (Rua et al., 2013). A computational analysis reported a higher frequency APOBEC3 mutated macaque SFV genomes in human blood cells from infected donors than in blood and buccal cells from naturally infected macaques in Bangladesh (Matsen et al., 2014). These genetic studies of zoonotic SFV strains are the only evidence that host restriction factors may control SFV replication *in vivo*. Moreover, their interpretation is complex due to the lack of comparison between gorilla and human samples (Delebecque et al., 2006; Rua et al., 2013). The clonal expansion of edited genomes observed by Rua et al. was not taken into account in the comparison between macaque and human samples (Matsen et al., 2014). Finally, the counterselection of hypermutated defective genomes may lead to an underestimation of APOBEC3 action in the three studies (Delebecque et al., 2006; Matsen et al., 2014; Rua et al., 2013).

1.3.2.4 *FV restriction by novel intrinsic host factors*

A macaque and human ISG screen of early and late steps of viral replication identified several restriction factors that target mostly the production of PFV in HT1080 cells (Kane et al., 2016). The only few hits with a modest reduction of PFV-infectivity in the incoming screen was the human serine/threonine protein kinase PAK3 and macaque PHD finger domain protein 11 (PHF11). The production screen however found a list of candidate host factors with stronger impact on viral replication. The human ISGs included APOBEC3G, the oligoadenylate synthase-like (OASL) protein, the free fatty acid receptor 2 (FFAR2) and the human RNA helicase Moloney leukemia virus 10-like (MOV10) protein as the most significant hits. The macaque-specific ISG hits included APOBEC3B/G/F, Schlafen (SLFN) family member 12 (SLFN12), decysin-1 disintegrin and metalloprotease-like protein (ADAMDEC1), OASL, mixed lineage kinase domain-like protein (MLKL) and tumor necrosis factor superfamily member 10 (TNFSF10) (Kane et al., 2016).

Surprisingly, the screen identified restriction of late events of PFV replication by the MOV10 although silencing its expression had no effect on PFV replication in a previous report (Yu et al., 2011). A recent follow-up study described that macaque and human PHF11 (discovered as a modest antiviral factor in the incoming ISG screen) restrict several spumaviruses by specifically targeting the IP – preventing its basal transcription, Tas expression and thus viral replication (Kane et al., 2020). Moreover, after the discovery of SLFN12 protein as a modest productive restriction factor in the ISG screen (Kane et al., 2016), another group demonstrated

that its related family member SLFN11 from human, cattle and AGMs are potent inhibitors of PFV replication (Guo et al., 2021). Inhibition of viral protein expression was rescued by gene codon optimization. Moreover, the ATPase and helicase activities of SLFN11 was required for PFV restriction (Guo et al., 2021).

A series of other host factors restrict PFV as demonstrated through *in vitro* overexpression and knock-down experiments. Several of these target Tas including the promyelocytic leukemia (PML) protein (Regad et al., 2001), N-Myc interactor (Nmi) (Hu et al., 2014), the p53-induced RING-H2 (Pirh-2) protein (Dong et al., 2015) and serum/glucocorticoid regulated kinase 1 (SGK1) (Zhang et al., 2022). These factors interact with Tas either in the nucleus or in the cytoplasm (Hu et al., 2014; Regad et al., 2001). They prevent LTR and IP transactivation or target Tas for proteasomal degradation and reduce viral transcription. SGK1 was also found to reduce stability of Gag (Zhang et al., 2022). Of notice, PML was identified as an inhibitor of PFV gene expression by complexing to Tas and preventing its binding to viral DNA (Regad et al., 2001). However, a later study demonstrated that endogenous PML was not involved in FV latency questioning its role as a FV restriction factor (Meiering and Linial, 2003). Lastly, PFV replication was shown inhibited by a novel host factor TBC1D16 which belongs to the Rab GTPase-activating protein of the TBC domain-containing protein family. Overexpression inhibited transcription and expression of Tas and Gag, while silencing enhanced PFV replication (Yan et al., 2021). A summary of host proteins determined as antiviral restriction factors against PFV is shown in Table I-5.

Table I-5 – Summary of PFV restriction by intrinsic host factors

Host factor	Restriction	Host	Inter-action	Stage of viral life cycle	Counter-action	References
<i>Early steps</i>						
PAK3	Yes	Human	ND	Early step	-	(Kane et al., 2016)
SAMHD1	Yes	Macaque	ND	Early step	-	(Kane et al., 2016)
<i>Late steps</i>						
ADAMDEC1	Yes	Macaque	ND	Late step	-	(Kane et al., 2016)
APOBEC3	Yes	Feline	RT+Gag	RT	Bet	(Chareza et al., 2012; Lukic et al., 2013; Löchelt et al., 2005)
APOBEC3B	Yes	Murine	RT	RT	-	(Russell et al., 2005)
		Human	RT	RT	Bet	(Delebecque et al., 2006)
		Macaque	ND	Late step	-	(Kane et al., 2016)
APOBEC3C	Yes	Human	RT	RT	Bet	(Russell et al., 2005)
APOBEC3G	Yes	Human	RT+Gag	RT	Bet	(Delebecque et al., 2006; Russell et al., 2005)
		Murine	RT	RT	-	
		Simian	RT	RT	-	
APOBEC3F	Yes	Macaque	ND	Late step	-	(Kane et al., 2016)
		Macaque	ND	Late step	-	(Kane et al., 2016)
		Human	RT	RT	-	(Delebecque et al., 2006; Russell et al., 2005)
FFAR2	Yes	Human	ND	Late step	-	(Kane et al., 2016)
MLKL	Yes	Macaque	ND	Late step	-	(Kane et al., 2016)
MOV10	Yes*	Human	ND	Late step	-	(Kane et al., 2016; Yu et al., 2011)
Nmi	Yes	Human	Tas	Transcription	-	(Hu et al., 2014)
OASL	Yes	Human	ND	Late step	-	(Kane et al., 2016)
	Yes	Macaque	ND	Late step	-	(Kane et al., 2016)
PHF11	Yes	Human	IP	Transcription	-	(Kane et al., 2020; Kane et al., 2016)
	Yes	Human	Tas	Transcription	-	(Dong et al., 2015)
PML	Yes	Human	Tas	Transcription	-	(Meiering and Linial, 2003; Regad et al., 2001)
SGK1	Yes	Human	Tas + Gag	Transcription/ Gag stability	-	(Zhang et al., 2022)
SLFN11	Yes	Human				(Guo et al., 2021)
	Yes	Bovine				
	Yes	AGM				
SLFN12	Yes	Human	ND	Late step	-	(Kane et al., 2016)
TBC1D16	Yes	Human	ND	Transcription	-	(Yan et al., 2021)
Tetherin	Yes	Human	Env	Virion release	-	(Jouvenet et al., 2009; Xu et al., 2011)
TNFSF10	Yes	Macaque	ND	Late step	-	(Kane et al., 2016)
TRIM5α	Yes	NWMs	Gag	Capsid assembly	-	(Yap et al., 2008)
<i>Resistant</i>						
APOBEC1	No	Human	-	-	-	(Delebecque et al., 2006)
	No	Murine	-	-	-	
APOBEC2	No	Human	-	-	-	(Delebecque et al., 2006)
	No	Murine	-	-	-	
APOBEC3A	No	Human	-	-	-	(Russell et al., 2005)

MxA	No	Human	-	-	-	(Regad et al., 2001)
Mx2	No	Human	-	-	-	(Bahr et al., 2016)
SAMHD1	No	Human	-	-	-	(Gramberg et al., 2013; Kane et al., 2016)
SERINC2	No	Human	-	-	Env	(Ramdas et al., 2021)
	No	Coelacanth	-	-	Env	
TRIM5α	No	Human	-	-	-	(Yap et al., 2008)
	No	Apes	-	-	-	
	No	OWMs	-	-	-	

*Contradictory results. ND; Not determined.

1.3.2.5 FV restriction by miRNAs

MicroRNAs (miRNAs) are small regulatory RNAs that can bind to complementary mRNAs and inhibit their translation and subsequent expression. A wide range of tissue-specific cellular miRNAs are expressed in cells. Some viruses are also encoding their own miRNAs, including SFVagm that encodes two miRNAs which can regulate the innate immune response and harbor functional similarity to certain host miRNAs (Kincaid et al., 2014). Although rare, some viruses directly rely on miRNAs for their replication such as hepatitis C virus, reviewed by (Cullen, 2013). The inhibition of viruses by cellular miRNAs is rare in mammalian cells, despite frequent viral RNA silencing in plants and insects. In fact, it appears that viral inhibition by endogenous cellular miRNAs is avoided for most viruses through evolution (Bogerd et al., 2014). Despite this, a few studies have reported that miRNAs can restrict viral gene expression and replication in human cells. One example of this is PFV. The human cellular miRNA-32 was shown to inhibit translation of PFV *in vitro* and it was subsequently shown that Tas acts as a counter silencing suppressor protein, similarly to RNA silencing by plant and insect virus produced suppressor proteins (Lecellier et al., 2005).

1.3.3 Antibody responses to FVs

The humoral immune response to FV has initially been used for the diagnosis of infected animals and humans. In addition, the susceptibility of viral strains to neutralizing antibodies was used until the 90's to classify FVs into serotypes. Regarding their function, SFV-specific antibodies were shown to protect against infection in one NHP model, and their neutralizing activity has been studied in cats and in humans only. My host laboratory characterized the nAbs and viral strains from the same SFV-infected hunters and established the link between the early described serotypes and recently described *env* genotypes. FVs are transmitted as cell-free particles and as cell-associated viruses, and antibodies blocked only the first mode of

transmission. The antiviral role of non-neutralizing antibodies (ADCC, ADCP, complement dependent cytotoxicity, inhibition of viral budding) has not been studied to date.

1.3.3.1 *FV serology and diagnostics*

Serological studies have been performed with a range of distinct FV strains and sera from naturally infected NHPs, cats, cattle and accidentally infected humans. Sera from NHPs react against Gag and Bet proteins, and Gag doublet bands on immunoblots has become a common tool for diagnostic purposes (Hahn et al., 1994). In contrast, no response to Env is detected, even in the largest study based on samples from 16 humans and 129 NHPs representing 32 African and Asian species who were diagnosed as infected by PCR (Hussain et al., 2003). However, Env glycoproteins were present in radiolabeled PFV-infected cell lysates immunoprecipitated with sera from infected humans and NHPs (Netzer et al., 1990). Thus, most epitopes on Env are likely conformational. Similarly, BFV and FFV-specific sera mostly bind to Gag and Bet in enzyme-linked immunosorbent assay (ELISA) and western blot assays using infected cell lysates as source of antigen (Alke et al., 2000; Romen et al., 2007; Romen et al., 2006). Interestingly, a recombinant FFV TM protein was recognized in ELISA assay by sera from infected cats and immunized animals and binding to TM and Gag antigens was concordant (Mühle et al., 2011).

The presence of mucosal and systemic antibodies against SFV was investigated using plasma, urine and saliva samples from persistently SFV-infected humans and chimpanzees (Cummins et al., 2005). IgA responses against both Gag and Bet proteins were undetectable despite strong IgG reactivity in western blot (Cummins et al., 2005). No data are available on the presence of Env-specific antibodies in saliva of infected animals or humans and their role in SFV transmission.

1.3.3.1.1 *FV serotypes*

SFV strains were initially characterized by their susceptibility to neutralization (serotyping) which showed the segregation of SFV according to their host species and the existence of two serogroups among strains isolated from the same species (Hooks and Gibbs, 1975; O'Brien et al., 1972). For example, the first macaque SFV isolate (SFVmcy_FV21) was designated SFV type 1 (Rustigian et al., 1955), while a second macaque isolate (SFVmcy_FV34) belongs to a distinct serogroup and was designated SFV type 2 (Johnston, 1961). In total, 11 serotypes have been defined and seven of these eleven isolates has been full-length sequenced (see Table I-6).

Cross-neutralization of isolates from distinct NHP species by the same reference sera was observed (Hooks and Gibbs, 1975). For example, the first gorilla SFV strain was neutralized by sera raised against chimpanzee SFV (Bieniasz et al., 1995a). Overall, the early serologic studies have demonstrated the induction of strong nAb responses in SFV-infected hosts. Furthermore, serum-mediated neutralization by chimpanzee sera could be inhibited by competition with recombinant Env fusion proteins, and immune sera blocked Env from binding to cells (Herchenroder et al., 1999). Those findings gave first indications that Env is targeted by nAbs and that some neutralizing epitopes interfere with Env binding to susceptible cells.

Table I-6 – List of historical SFV serotypes

Serotype	NHP species	Group	Isolate	Accession Number	Reference
SFV-1	<i>Macaca cyclopsis</i> ,	OWM	SFVmcy_FV21	NC_010819	(Rustigian et al., 1955)
SFV-2	<i>Macaca cyclopsis</i>	OWM	SFVmcy_FV34 ^a	KF026286.1	(Johnston, 1961)
SFV-3	<i>Chlorocebus aethiops</i>	OWM	SFVcae_FV2014	MF582544	(Stiles et al., 1964)
	<i>Macaca mulatta</i>	OWM	SFVmmu_FV397		
SFV-4	<i>Saimiri sciureus</i>	NWM	SFVssc_1224	GU356394	(Johnston, 1971)
SFV-5	<i>Otolemur crassicaudatus</i>	Pro-simian	SFVocr_1557	KM233624	(Johnston, 1971)
SFV-6	<i>Pan troglodytes verus</i>	Ape	SFVpve_Pan1		(Rogers et al., 1967)
SFV-7	<i>Pan troglodytes verus</i>	Ape	SFVpve_Pan2		(Rogers et al., 1967)
SFV-8	<i>Ateles</i> species	NWM	SFVaxx_Hooks40	EU010385	(Hooks et al., 1973)
SFV-9	<i>Cebus</i> species	NWM			(Hooks and Gibbs, 1975)
SFV-10	<i>Papio cynocephalus</i>	OWM	SFVpcy	AF049083	(Rhodes-Feuillet et al., 1979)
SFV-11	<i>Pongo pygmaeus pygmaeus</i>	Ape	SFVppy_Bella	AJ544579	(McClure et al., 1994)

^aPartial sequence

1.3.3.1.2 Studies of Central-African hunters

My host laboratory identified more than 70 Cameroonian and Gabonese individuals infected with SFV (Betsem et al., 2011; Calattini et al., 2011; Calattini et al., 2007; Mouinga-Ondémé et al., 2012). Viral strains were of gorilla, chimpanzee and Cercopithecus origin. They aimed

to test the hypothesis that adaptive immune responses participate to the control of zoonotic SFV strains in infected humans and restrict their transmission to other human hosts. They initiated a research program to assess whether SFV-specific antibodies are present in infected individuals and to characterize their mode of action. The first step was to search for neutralizing antibodies, focusing on individuals infected by a gorilla or a chimpanzee SFV. Viral strains were those isolated from infected hunters (Rua et al., 2012a). More specifically two gorilla SFVs belonging to genotypes I and II, and a chimpanzee genotype II SFV strain. As no zoonotic chimpanzee genotype I strain was isolated, the laboratory-adapted PFV strain was used. An indicator cell line expressing the β -galactosidase gene under the control of one gorilla LTR promoter (GFAB) was constructed and used to perform microneutralization assays (i.e., in P96-well plates) (Lambert et al., 2016). Interestingly, the indicator GFAB cell line detects strains of both gorilla and chimpanzee origin.

Plasma samples from the majority of gorilla SFV infected individuals neutralized at least one SFVgor strain (40/44, 91%) (Fig. I-21A). Neutralizing titers ranged from 1:10 to 1:14,724 (Lambert et al., 2018). The strains neutralized usually belonged to the same genotype as infecting SFV strains previously determined by the sequence of PCR-amplified *env* (Richard et al., 2015) (Fig. I-21B). However, cross-neutralization of strains from both genotypes was frequent (36%). The infecting strains were characterized by an *env* genotype-specific PCR, expected to be more sensitive than the first molecular study. Eight individuals (20%) were co-infected with strains from two distinct genotypes, and all but one neutralized both genotypes. Seven other samples from single-infected donors neutralized two strains, suggesting either cross-neutralization of both genotypes or that one genotype was undetectable by PCR (Fig. I-21A) (Lambert et al., 2018).

The second part of this work was the demonstration that nAbs target exclusively the genotype-specific SUvar domain. FVVs were originally developed with Env, Gag and Pol from the PFV strain. These FVVs were pseudotyped with gorilla Env from each genotype and with chimeric Env in which the SUvar from both gorilla strains was swapped. Plasma antibody neutralization of the chimeric vectors demonstrated that nAbs strictly target the SUvar region (Lambert et al., 2018). Of note, plasma samples from individuals infected with a gorilla SFV cross-neutralized chimpanzee SFV from matched genotype and vice versa (Fig. I-21C and D).

Two genotypes based on SUvar were also described for FFV-isolates with a correlation between genotype and serum neutralization similar to the one observed for SFV (Phung et al., 2001; Phung et al., 2005; Winkler et al., 1998; Zemba et al., 2000).

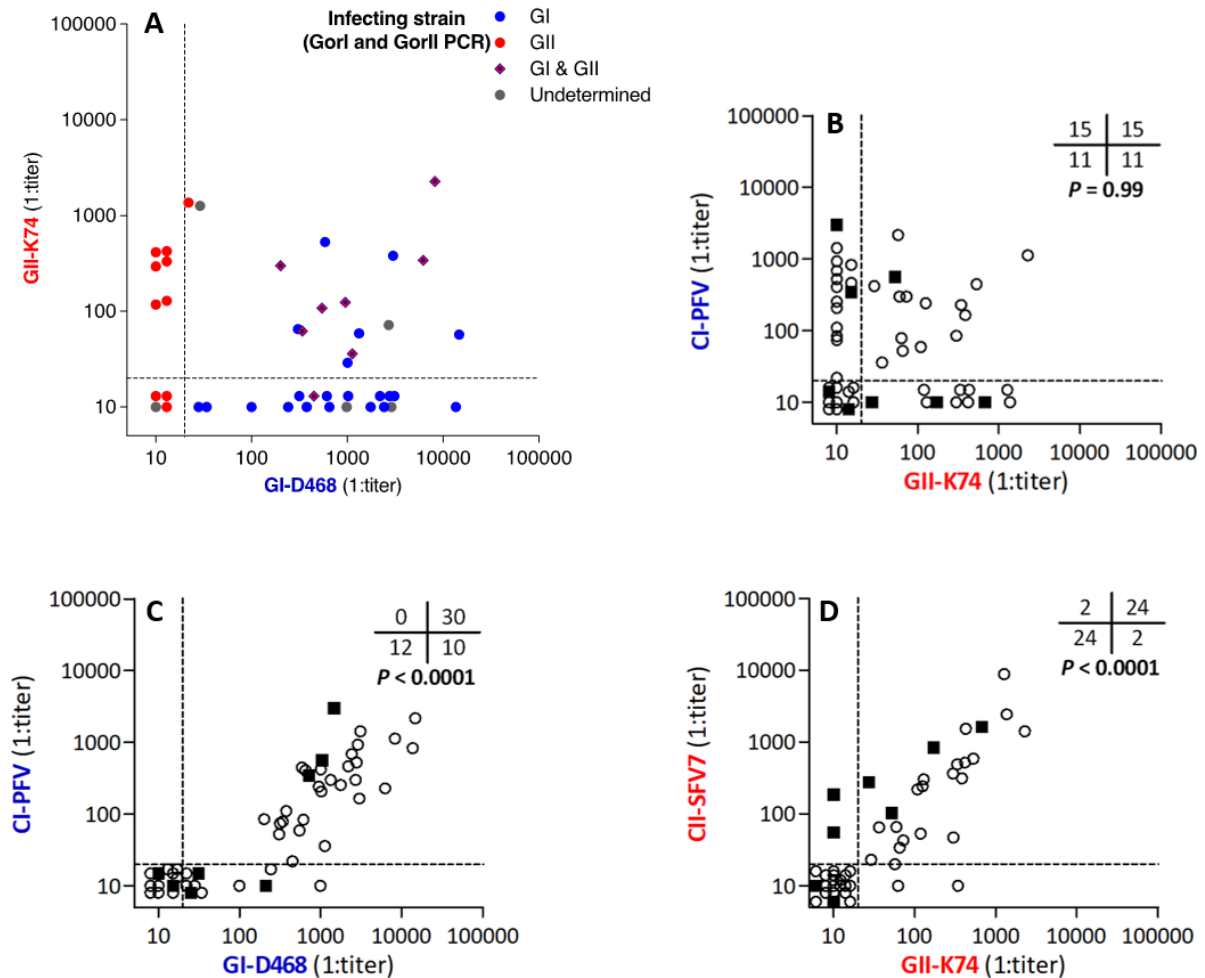


Figure I-21 – Neutralization profiles of donors infected with zoonotic SFV strains from two genotypes

A: Plasma neutralization titers against replicative GI-D468 and GII-K74 strains with symbols for each donor according to genotype of infection determined through SUvar specific PCRs. Detection threshold (1:20) set at the dashed lines. **B-D:** Neutralization titers of plasma nAbs from zoonotic SFVcpz/gor-infected African hunters (n=52) against replicative CI-PFV, CII-SFV7, GI-D468 and GII-K74 strains. Open circles and filled squares represent SFVgor- and SFVcpz-infected donors, respectively. Detection threshold (1:20) set at the dashed lines. Tables indicate number of donors with measurable nAb activity against the four strains and statistical significance according to Fischer's exact test. *Figure adapted from (Lambert et al., 2018).*

1.3.3.1.3 Mapping of linear epitopes on Env

Two studies searched for linear epitopes on Env using synthetic peptides. Through use of FFV Env gp130 peptide microarrays and samples from infected cats, pumas and immunized rats, four immunodominant clusters were identified: two in LP and two in TM (after the fusion peptide and the membrane-proximal external region (MPER)) (Mühle et al., 2017). My host laboratory used a library of 169 PFV peptides covering the Env ectodomain in an ELISA assay with 36 plasma samples from SFV-infected African hunters (Lambert et al., 2019). A single immunodominant linear B cell epitope was found in the LP mapped down to residues at position 98-108; this epitope is also present on FFV Env (residues 92-119 peptide) (Mühle et al., 2017).

Sera from an infected cat that neutralized the FUV strain representative of one of the two FFV genotypes bind to a peptide spanning residues 441-463 within the SUvar domain from FFV SU. The authors hypothesized that these residues could represent a genotype-specific nAb epitopic region (Mühle et al., 2017). A former master student from my laboratory found that a homologous peptide was recognized by plasma samples from SFV-infected hunters. However, the recognition was not genotype-specific: the peptide with genotype I sequence was recognized by plasma from an individual infected with a genotype II strain (see Manuscript II and Discussion and Perspectives section 6.1.2, Chapter V and VI, respectively (Dynesen et al., 2022, submitted)).

These two studies (Lambert et al., 2019; Mühle et al., 2017) showed that some linear antigenic sites are shared by FV from different species. Peptides from the TM were recognized by cat sera only; such may reflect different immunogenicity of the TM in felines and in humans or the use of different techniques and peptides. As mentioned, most epitopes targeted by Env-specific antibodies are conformational.

1.3.3.1.4 *FV-specific nAbs and cell-to-cell transmission*

SFVs use both cell-free and cell-associated routes to spread in cell cultures (Couteaudier et al., 2022; Heinkelein et al., 2003; Hooks and Gibbs, 1975). Some EFV and BFV isolates are strictly cell-associated without release of infectious cell-free viral particles into the culture supernatants (Bao et al., 2015; Kirisawa et al., 2019; Materniak-Kornas et al., 2019). For BFV, the transmission route depends on both cell-type and adaptations in Gag and the C-ter of Env (Bao et al., 2020; Zhang et al., 2019).

Two studies addressed the capacity of antibodies to block SFV cell-to-cell transmission. The first one assessed the role of plasma antibodies in prevention of SFV transmission through blood cell transfusion in rhesus macaques. Transfusion of blood from an SFV-infected donor macaque into a non-infected recipient donor led to infection when the plasma was removed but not when whole blood was transferred. Thus, this study shows the importance of antibodies in protection against SFV-cell associated transmission (Khan and Kumar, 2006; Williams and Khan, 2010). The second study by my host laboratory showed that plasma from SFV-infected humans do not block cell-associated transmission of SFV *in vitro*, despite inhibiting the entry of cell-free virus (Couteaudier et al., 2022). They showed plasma antibodies bound to Env expressed at the surface of infected cells opening the possibility that antibodies mediate cell destruction through

the recruitment of complement or innate immune cells with cytotoxic or phagocytic functionalities. Such functions of SFV-specific antibodies have not been studied so far.

1.3.4 nAb epitopes on Env from other retroviruses

As nAbs and their epitopes represent the main topic of this PhD thesis, I will present a brief literature review on retroviral Envs and their recognition by nAbs focusing on three retroviruses; MLV, HTLV-1 and HIV-1. As discussed in section 1.1.4, retroviral Envs are type-I class transmembrane molecules composed of two subunits: the extracellular SU domain typically harboring the RBD and the TM domain which is involved in fusion of the viral and cellular membranes (Fig. I-22) (Rey and Lok, 2018). The signal peptide (SP) of most retroviruses is cleaved off during translation, although FVs are an exception for this as the LP gp18 remains associated with SU and TM. SU/TM heterodimers form trimers at the surface of the virus particle.

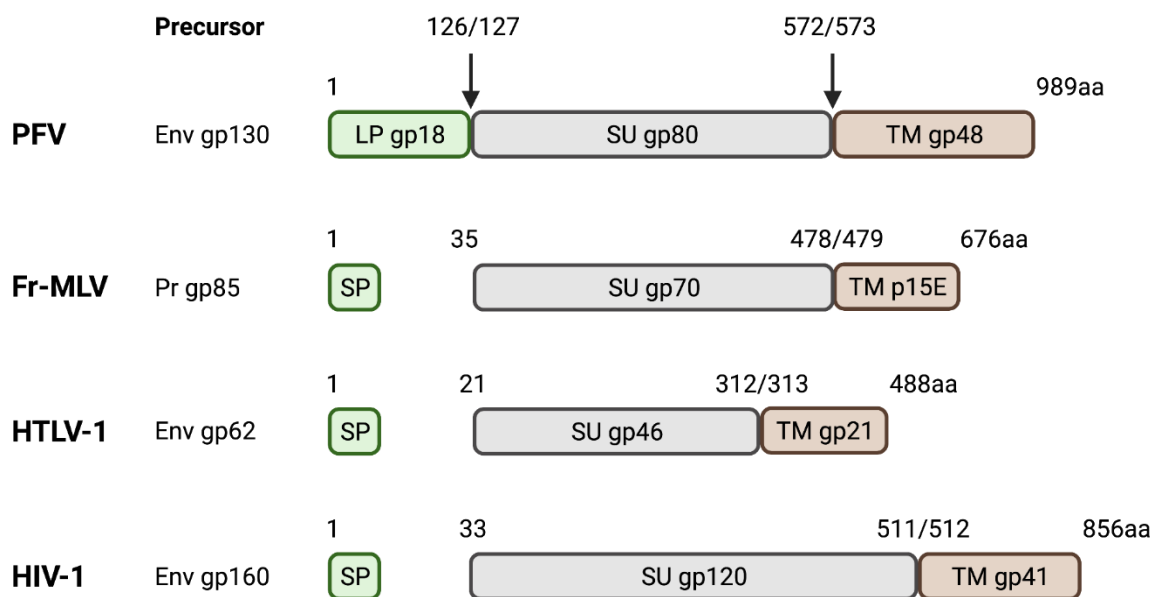


Figure I-22 – Organization of distinct retroviral Envs

Env precursors shown for four retroviruses; PFV Env, Friend MLV (Fr-MLV), HTLV-1 and HIV-1. SP, SU and TM subunits are shown in green, grey and brown, respectively. LP gp18 of FVs is cleaved by a furin-like protease and remained associated with SU and TM. Sequence numbering correspond to proteins with the following accession numbers; PFV #P14351, Fr-MLV isolate FB29 #P26804, HTLV-1 Japanese subtype A strain ATK-1 #P03381 and HIV-1 group M subtype B strain HXB2 #P04578. Figure created in BioRender.

1.3.4.1 MLV

MLVs are simple-type retroviruses belonging to the gammaretrovirus genus. They were discovered in the 1950s as the causative oncogenic agent of leukemia in inbred laboratory mice. MLVs exist both as endogenous and exogenous viruses, reviewed by (Kozak, 2014).

Three classes of MLVs are defined based on their tropism. Ecotropic strains have a strictly murine cell tropism, such as Moloney and Friend MLVs (Fr-MLV) isolates. Xenotropic strains infect cells of non-murine origin. Amphotropic/polytropic strains infect both murine and non-murine cells (Sitbon et al., 2001). The use of different receptor molecules explains the MLV tropisms and all MLV receptors belong to the superfamily of transporters for which the cationic aa-transporter mCAT-1 is used by ecotropic MLVs (Albritton et al., 1989).

The SU gp70 can be divided into three subunits; an N-ter domain (NTD), a C-ter domain (CTD) and a central proline rich hinge region (PRRH) acting as a hinge between the two. This PRRH has been shown to mediate conformational changes necessary for fusion (Lavillette et al., 1998; Lavillette et al., 2002), while the CTD forms an important disulfide bridge with the TM to generate SU/TM heterodimers (Opstelten et al., 1998). The NTD harbors the RBD and contains discontinuous variable regions (VR) termed VRA, -B and C which determine MLV tropism (Fig. I-23, top panel) (Battini et al., 1995; Battini et al., 1992). A crystal structure showed that the Fr-MLV RBD (SU aa 1-236) is composed of an Ig-like core of anti-parallel β -sheets (Fig. I-23, bottom panel) and a helical subdomain sited on the top of the core (Fass et al., 1997). The latter comprises VRA and -B folded in close proximity and VRC folded as a loop in a distinct region (Fig. I-23, bottom panel). In 2003, the RBD structure of another gammaretrovirus, the feline leukemia virus (FeLV) was solved (Barnett et al., 2003). Its structural organization is similar to the one of Fr-MLV RBD with the divergence of the variable regions, consistent with the distinct tropism of these two gammaretroviruses.

Upon infection or immunization, the majority of nAbs target the VRs within the RBD and interfere with SU-mCAT-1 interaction (Burkhart et al., 2003). Residues S84, D86 and W102 within VRA of Fr-MLV SU were shown to be important for its interaction with mCAT-1 (Davey et al., 1999). Non-neutralizing antibodies bind SU at similar affinities as nAbs, however they rarely recognize the RBD but frequently target the PRRH and CTD (Burkhart et al., 2003). Interestingly, some broadly cross or pan-neutralizing mAbs (83A25 and 573) that target the PRRH and CTD show loss of interaction to linearized SU suggestive of conformational-dependent recognition (Evans et al., 2014; Evans et al., 1990). The mode of action for such mAbs was suggested to involve inhibition of viral fusion or conformational changes needed for fusion since they do not prevent SU-mCAT-1 interaction (Burkhart et al., 2003).

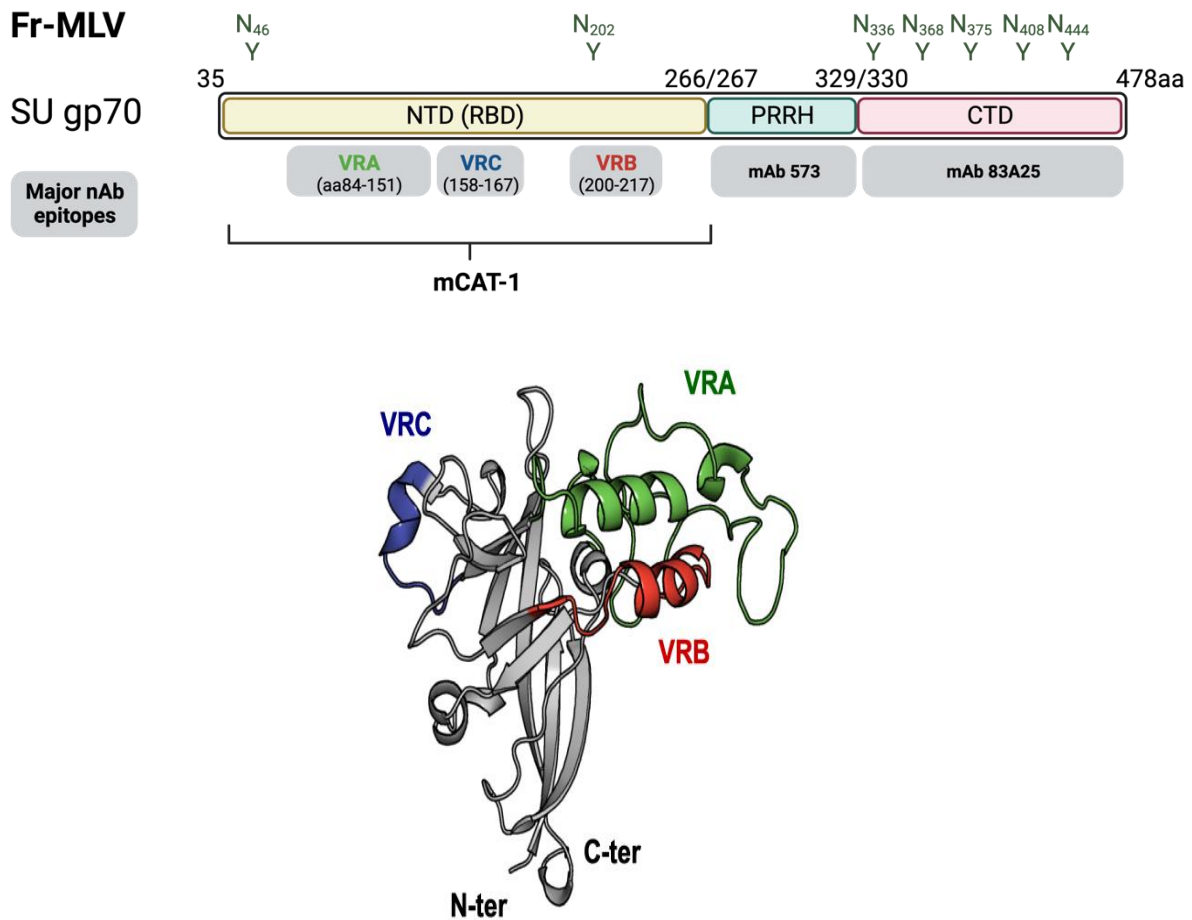


Figure I-23 – Fr-MLV SU gp70 sequence and RBD structure

Top: Schematic representation of Fr-MLV SU gp70 sequence (Env aa 35-478). Subdomains within the SU are highlighted in distinct colored boxes. The NTD comprising the RBD is shown in yellow, PRRH shown in green and CTD shown in red. Glycosylation sites (Y) and their aa position shown on top of SU subdomains. Variable regions targeted by nAbs shown in grey boxes below the SU bar, and colored according to VR-location on Fr-MLV RBD structure (bottom panel). The mCAT-1 receptor binding region shown below SU bar. Sequence numbering (aa) according to Fr-MLV isolate FB29 (accession number #P26804). **Bottom:** Monomeric RBD structure (PDB:1AOL) of Fr-MLV isolate 57 (accession number #P03390) at 2.0Å resolution. Fr-MLV structure with VRA (green), VRB (red) and VRC (blue) domains highlighted. *Figures created in BioRender and PyMOL.*

1.3.4.1.1 Env capture among MLVs – tropism and recognition by nAbs

In the 70s and 80s, studies demonstrated that polytropic MLVs arise in mice by recombination of exogenous ecotropic strains with endogenous retroviral envelope genes, and that these novel recombinants have wider tropism and greater virulence (Elder et al., 1977; Evans and Cloyd, 1985; Ruscetti et al., 1981; Stoye and Coffin, 1987). Later it was shown that specific sites of recombination occur at hotspots within the SU domain, in fact confined to a region of high homology between the exogenous and endogenous sequences (Alamgir et al., 2005). Importantly, recombined endogenous *env* sequences impact SU recognition by nAbs in mice (Tumas et al., 1993) and some of these endogenous *env* sequences were distributed or classified

into two distinct serotypes (Lavignon et al., 1994). In addition to recombination, transfer and spread of intact non-recombined endogenous viruses has also been demonstrated to occur through pseudotyping of endogenous strains by an ecotropic virus (Evans et al., 2009).

1.3.4.2 HTLV

The Env from the delta retrovirus HTLV-1 possess many similarities to Env from gammaretroviruses such as MLV. The precursor Env gp62 from HTLV-1 is composed of SU gp46 and TM gp21. Sequence alignments of MLV and HTLV-1/2 Env present an unusually high homology in several regions across both SU and TM suggestive of ancestral origins and potential MLV *env* capture by HTLV (Kim et al., 2004; Kim et al., 2000). HTLV-1 SU and MLV SU share the NTD-PRRH-CTD organization and the location of the RBD in the NTD (Fig. I-24 and I-23, top panel). No structure of HTLV Env has been solved to this date. The predicted structure from another deltaretrovirus, the bovine leukemia virus (BLV) resembles the one from Fr-MLV (Johnston et al., 2002).

Two main receptors have been determined for HTLV-1; Neuropilin 1 (NRP-1) (Ghez et al., 2006) and the main glucose transporter type 1 (GLUT-1) (Jin et al., 2006; Manel et al., 2003). The residues 90-98 and 106+114 are essential for binding of HTLV-1 SU to NRP-1 and GLUT-1, respectively. SU can directly interact with GLUT-1 and NRP-1 as a tripartite complex, reviewed by (Jones et al., 2011). GLUT-1 is involved in cell-to-cell transmission or fusion. However, it is expressed at low level on primary HTLV-1 targets (cord blood and activated CD4⁺ T lymphocytes) raising concern on its role as primary binding receptor (Takenouchi et al., 2007). In addition to NRP-1 and GLUT-1, HTLV-1 uses heparan sulfate proteoglycans (HSPGs) as a third receptor and SU binding to NRP-1 depends on conformational changes induced by HSPG binding (Jones et al., 2005; Piñon et al., 2003). HTLV-1 SU bound to HSPG mimics the pro-angiogenic factor VEGF-165, the natural ligand for NRP-1 (Lambert et al., 2009). The binding site of HSPG on HTLV-1 SU was mapped to the CTD. Interestingly, CD4⁺ T cells express higher HSPG levels than CD8⁺ T cells, while CD8⁺ T cells express higher GLUT-1 levels than their CD4⁺ counterpart potentially explaining the target cell preference by different receptor usage of HTLV-1 and -2 (Jones et al., 2006).

As HTLV is highly cell-associated, the classical neutralization assays have been adapted using vesicular stomatitis virus (VSV) pseudotyped with Env from HTLV or of syncytia formation upon co-culture of HTLV-infected donor cells with uninfected cells. Plasma nAbs were detected in HTLV-1-infected individuals with limiting cross-neutralization of HTLV-2

(Clapham et al., 1984; Hoshino et al., 1983; Nagy et al., 1983). Plasma-mediated cross-neutralization of HTLV-1 Cosmopolitan and Melanesian strains was however observed, supporting that nAbs target conserved epitopes (Benson et al., 1994). The role of nAbs was addressed *in vivo*; the plasma from HTLV-1 infected humans can protect rabbits against cell-associated HTLV-1 infection (Kataoka et al., 1990; Miyoshi et al., 1992). In a humanized mouse model, a neutralizing mAb could block cell-to-cell transmission while infusion of non-neutralizing mAbs reduced but did not prevent transmission (Saito et al., 2014). Studies on pregnant women with HTLV-1 has provided evidence that the maternally transferred HTLV-1 specific nAbs can protect against mother-to-child transmission (Iwahara et al., 1993; Takahashi et al., 1991) and reviewed by (Percher et al., 2016). The protection of newborns against breastmilk-transmitted HTLV-1 through passive transfer of plasma nAbs or neutralizing mAbs to the mother was shown in rabbits and rats (Fujii et al., 2016; Sawada et al., 1991).

To map the nAb targets, plasma from HTLV-1-infected humans were tested in syncytium formation inhibition alone or in competition with overlapping linear peptides spanning both SU and TM. Two peptides spanning aa 53-75 in NTD and 287-311 in CTD, blocked the neutralizing activity (Desgranges et al., 1994). Another common linear nAb epitope is located in the PRRH region (aa 175-215) (Fig. I-24) (Baba et al., 1993; Blanchard et al., 1999). Immunization of rabbits and mice with synthetic peptides spanning such nAb epitopic regions did not induce plasma nAbs (Grange et al., 1998). In line with this, the majority of plasma antibodies from HTLV-1 infected humans must target conformational epitopes since a strong loss of reactivity to denaturated antigens was observed in ELISA compared to native antigens (Hadlock et al., 1999). Indeed, human monoclonal nAbs targeting conformational epitopes on SU have been described (Hadlock et al., 1997; Hadlock et al., 2002).

HTLV-1

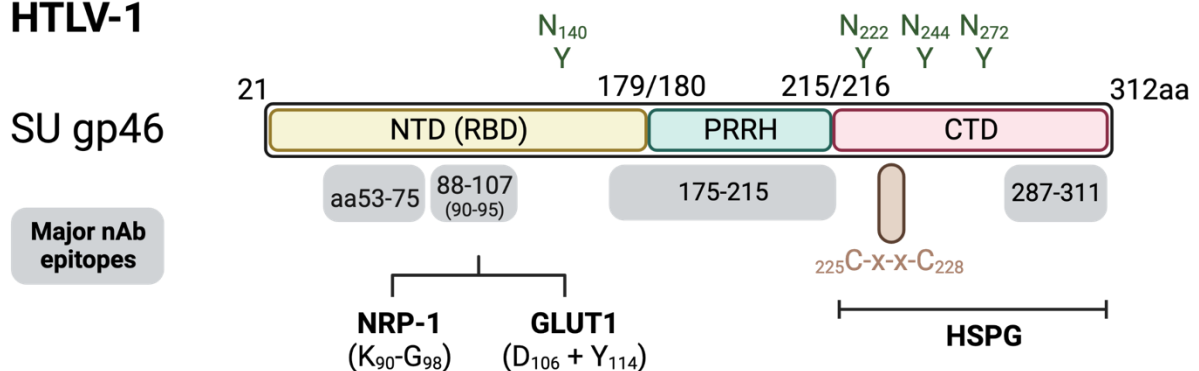


Figure I-24 – HTLV-1 SU gp46 sequence and location of nAb epitopes

Schematic representation of HTLV-1 SU gp46 sequence (Env aa 21-312). Subdomains within the SU are highlighted in distinct colored boxes. The NTD comprising the RBD is shown in yellow, PRRH shown in green

and CTD shown in red. Glycosylation sites (Y) and their aa position shown on top of SU subdomains. Regions targeted by nAbs shown in grey boxes below the SU bar. Residues involved in binding to receptors NRP-1, GLUT1 and HSPG shown below SU bar. *Figure created in BioRender.*

1.3.4.3 HIV

The HIV-1 precursor Env gp160 is composed of an extracellular SU gp120 domain responsible for binding to the CD4 receptor and CCR5/CXCR4 co-receptors and a TM gp41 subunit that contains the viral fusion machinery. The SU gp120 is composed of an inner and outer domain (Fig. I-25, panel A) (Chan et al., 1997; Kwong et al., 1998; Weissenhorn et al., 1997). A key feature of the HIV-1 Env is its extensive glycosylation which can be up to 90 N-linked glycans on a trimer depending on strain (Fig. I-25, panel B), shielding its protein surface from exposure to nAbs, reviewed by (Seabright et al., 2019; Wagh et al., 2020). This dense layer of glycans is flexible and heterogenous in its composition of sugar subunits across the Env and varies between strains (Stewart-Jones et al., 2016).

HIV-specific nAbs are usually elicited a few weeks post-infection. The early response is directed against strain-specific regions including the variable loops V1-4 (Bar et al., 2012), and is usually narrow (Piantadosi et al., 2007). These autologous nAbs drives the emergence of escape variants which induce novel nAbs and an arms-race between the humoral response and the highly mutating virus is established. Moreover, comparison of the sensitivity of historical and more contemporary HIV-1 strains to neutralization by sera from infected donors support that circulating HIV-1 strains have undergone evolutionary changes over the course of the pandemic resulting in enhanced resistance to nAbs at a population level (Bouvin-Pley et al., 2013; Bunnik et al., 2010). Nonetheless, bnAbs able to cross-neutralize several heterologous strains occur in approx. 20% of HIV-1 infected donors after several years of infection (Kwong and Mascola, 2012).

During the past two decades, monoclonal HIV-1 specific bnAbs have been isolated and cloned from such HIV-1 infected donors. The anti-HIV bnAbs target an array of different epitopes, mostly conformational (McCoy, 2018). Env is a highly metastable protein which adopts multiple closed, intermediate and open states. The nAb epitopes are influenced by these conformations (Kwong et al., 2002; Munro et al., 2014). Moreover, bnAbs have discrete modes of neutralization mechanisms beyond inhibition of gp120-CD4 and co-receptor binding including prevention of Env transition between different states, fusion inhibition and destabilization or disassembly of the Env trimer, reviewed by (Parker Miller et al., 2021). High-resolution 3D-structures of the HIV Env complexed to the respective bnAb Fabs has given a detailed map of the epitopes targeted. These can be categorized at seven epitopic regions for

which six are located on pre-fusion Env; CD4-binding site, V1V2 loops, V3 glycan, the silent face, the fusion peptide and SU/TM subunit interface (Fig. I-25, panel C) (Chuang et al., 2019). The seventh class of bnAbs recognize the MPER, reviewed by (Caillat et al., 2020). Most classes of bnAb epitopes are partially or entirely dependent on surface glycans (Wagh et al., 2020). Key characteristics of each site and bnAb mechanisms of action are given:

V1V2: This epitope locates to the apex of the Env trimer and loops in this region undergo significant conformational changes upon Env-CD4 engagement. The class of bnAbs recognizing these loops often target quaternary epitopes and function by stabilizing the Env trimer, thus preventing changes in trimer states, reviewed by (Pancera et al., 2017).

Glycan-V3: This site is located next to the V1V2 site and is usually composed of high-mannose type glycans (also termed the mannose-patch) (Pritchard et al., 2015b). Epitopes of this site are mainly composed of high-mannose type glycans but complex-type have also been reported for one bnAb (Mouquet et al., 2012). Deleting or shifting glycans at this site can lead to neutralization resistance (Pritchard et al., 2015a). The bnAbs targeting this epitope are usually interfering with Env binding to its co-receptor or prevention of conformational changes necessary for this interaction (Parker Miller et al., 2021).

CD4-binding site: bnAbs targeting the conserved CD4-binding site are some of the most potent discovered so far which function by preventing the Env-CD4 binding. This site is located in a cavity and is one of the few sites that does not require bnAb interaction with glycans despite it being highly shielded by glycosylation in a pre-fusion trimer state. Removal of glycans surrounding this site highly influence the nAb-response generated by Env-trimer immunogens in animals (Zhou et al., 2017). Some of the bnAbs targeting this site function by mimicking the CD4 interaction with Env (Parker Miller et al., 2021).

Silent face: bnAbs targeting this site were discovered more recently and completed the Env surface coverage (Zhou et al., 2018). This centered region is highly glycosylated and the antibodies make extensive contact to these. Although less structural information exists for bnAbs recognizing this site, their mode of action likely involves inhibition of conformational changes needed for cell entry and complete receptor binding, reviewed by (Parker Miller et al., 2021).

Fusion peptide: The fusion peptide at the N-ter of gp41 locates to the lower part of the Env trimer. The bnAbs recognizing this peptide function by blocking fusion through stabilization of the Env in a pre-fusion trimer ‘closed state’ and prevention of transition to post-fusion ‘open

state'. The bnAbs targeting this conserved sequence can also engage in glycan interactions, reviewed by (Caillat et al., 2020).

Subunit interface: This site locates between the gp120 and gp41 Env subunits but bnAbs have also been found to target the interface between two gp41 subunits. The mechanism of action for this class of bnAbs often involves Env trimer disassembly or decay (Dubrovskaya et al., 2019; Lee et al., 2015).

MPER: This conserved site is targeted by highly potent bnAbs that interfere with membrane fusion. However, their epitope is usually only accessible after Env receptor binding and thus neutralization efficacy is generally lower for cell-to-cell transmission (Caillat et al., 2020). Epitopes on this site are often composed of both Env and membrane components due to its proximal location just above the viral membrane (Lee et al., 2016). Poly- and autoreactivity of these antibodies are therefore more frequent.

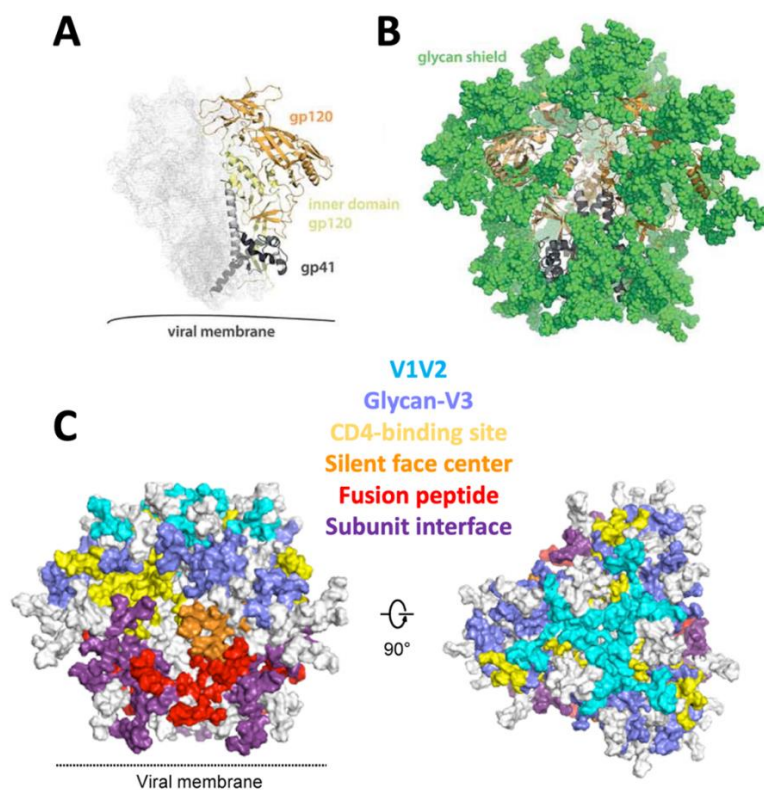


Figure I-25 – Structure of HIV-1 Env pre-fusion trimer and location of major classes of bnAb epitopes

A: Structure of HIV-1 Env ectodomain (gp140) trimer in ‘closed’ pre-fusion conformation (PDB:4TVP) from strain BG505 (accession number #DQ208458) with SOSIP-mutations and bound by bnAbs PGT122 and 35O22 (not shown) at 3.1Å resolution. One gp140 protomer shown in ribbon with gp120 outer and inner domains and gp41 highlighted in orange, pale yellow and dark grey, respectively. **B:** Glycan shield on HIV-1 Env trimer. Modelled N-linked glycans colored in green. **C:** Surface representation of pre-fusion closed Env trimer in side view (left) and top view (right) with highlight of six bnAb classes shown in distinct colors; V1V2, glycan-V3, CD4-binding site, silent face center, fusion peptide and subunit interface. MPER class of bnAbs not shown. *Figures adapted from (Chuang et al., 2019; Slieden and Sanders, 2016).*

In summary, this final section highlights common and distinct features between SFV-specific nAbs and nAbs targeting other retroviruses. Key characteristics include:

- SFV-specific nAbs solely target the RBD, while other regions are recognized on Env from MLV, HTLV and HIV
- SFV share a modular *env* gene structure with MLV, resulting from recombination and with variants encoding for the RBD and nAb epitopes
- SFV-specific nAbs target conserved sequences (within each genotype) similar to nAbs specific for HTLV-1, but in sharp contrast to nAbs against HIV-1

In addition, besides HIV, retroviral envelopes and their recognition by nAbs are poorly described. In this respect, SFV Env has no sequence homology with other retroviral Envs. My PhD project on SFV-specific antibodies has been initiated to understand the immune control of this zoonotic virus, but my work may also provide fundamental knowledge on structural basis for retrovirus inhibition by nAbs.

CHAPTER II

PHD THESIS AIMS AND HYPOTHESIS

2 | PHD THESIS AIMS AND HYPOTHESIS

SFV generates a persistent life-long infection in humans without associated pathology. Furthermore, no human-to-human transmissions has been documented to date suggesting natural immune control of viral replication *in vivo*. A better understanding of the nAbs raised against SFV upon infection, their epitopes and mechanisms of action may provide information to whether these contribute to viral control and protection against viral transmission to partners and close relatives.

We hypothesize that the immune system of zoonotically SFV-infected individuals supports the efficient control of viral replication and prevents the viral emergence of these retroviruses in the human population. The work conducted during this PhD aimed to characterize the sites on viral envelope recognized by nAbs from Central African hunters infected with zoonotic SFV strains.

Thus, my PhD thesis had the following aims:

- I. Characterize epitopes within the genotype-specific SUvar region of the SFV Env targeted by nAbs through use of polyclonal plasma samples from zoonotic gorilla SFV-infected Central African hunters
- II. Contribute to the collaborative work aiming to solve 3D-structures of the SFV Env by performing the functional study of recombinant Env-derived proteins to complete the biochemical and structural approaches

CHAPTER III

PRESENTATION OF PUBLICATIONS

3 | PRESENTATION OF PUBLICATIONS

The work of this PhD thesis is presented as two publications. The first manuscript describes the structure of the RBD from SFV Env, while the second manuscript represents the major work of my PhD on nAb epitopes. These two papers were the results of a collaborative effort. Accordingly, I will introduce the manuscripts and highlight my precise contribution to this work including a more detailed explanation of the experiments I performed.

3.1 Manuscript I: Novel structure of an SFV RBD

We engaged in a collaboration with the lab of Prof. Félix Rey who is an expert in structural virology and in particular on the fusion mechanisms of viral glycoproteins. This work was led by Dr. Ignacio Fernandez and Dr. Marija Backovic, Post-doctoral researcher and permanent scientist in the Rey unit, respectively. The aim was to obtain a structure of the Env from SFV and gain insights into the fusion mechanisms of SFV Env and potential receptor usage. In addition, this knowledge has and will aid the characterization of nAb epitopes including their mechanisms of action. Moreover, as FVs are extremely ancient viruses and have co-evolved with their hosts for millions of years, such structural knowledge could potentially give new insights to FV evolution and its relationship with orthoretroviruses.

About 18 months after initiation of this project, our collaborators succeeded in solving a high-resolution (2.6Å) X-ray crystal structure of an RBD from the zoonotic gorilla genotype II strain BAK74 (GII-K74), a strain isolated in our lab using PBMCs derived from an accidentally infected Central African hunter. The structure shows a novel fold with no precedents, and thus does not show similarity to the RBDs from other retroviruses (MLV, FeLV and HIV-1). The novel RBD structure has a bean-like shape with an upper and lower domain.

A previous low-resolution cryo-EM structure by German researchers on viral particles of the chimpanzee genotype I strain PFV (CI-PFV) found the Env to form trimeric structures on the surface (Effantin et al., 2016). The novel SFV GII-K74 RBD structure fitted well into the low-resolution cryo-EM map of CI-PFV Env, supporting that the RBD locates at the upper part of the SFV Env trimer. This also supports that their RBD structure is folded in the correct conformation seen on viral particles.

My first contribution was to validate that the RBD adopts a native fold. I performed neutralization assays in which the recombinant soluble RBD and Env expressed at the surface of viral particles compete for binding to nAbs present in plasma samples of individuals infected

with homologous gorilla SFV strains. Binding of nAbs to the RBD results in increased infection when compared to viral particles incubated with plasma sample in presence of unrelated recombinant protein. The RBD protein was produced in S2 insect cells or mammalian Expi293F cells which give rise to proteins with distinct types of surface glycosylation. Both proteins were serially diluted and incubated with plasma from SFV-infected donors before addition of FVVs. An increase in infectivity was observed for both RBD proteins in a dose-dependent manner. These results confirm that the RBD proteins adopt a conformation recognized by nAbs raised in the context of a natural infection.

SFV uses HS as an attachment factor for viral entry into susceptible cells. To search for a potential heparan binding site (HBS) on the SFV Env, our collaborators determined the electrostatic surface potential of the RBD and used structural docking/modelling of an HS molecule to the solvent accessible surface for identification of a potential HBS. Their predictions highlighted four residues (K342, R343, R356 and R369) with a high number of contacts with the modelled HS within a positively charged area of the lower domain of the RBD. These residues were mutated in pairs (K342/R343 and R356/R369) to alanine in trimeric ectodomain proteins. I set up a flow cytometry-based cell binding assay to measure the impact of mutations on binding to HS. Binding of WT ectodomain depended on the HS expression levels on susceptible cells, being higher on HT1080 than BHK-21 cells. Mutant ectodomains bound about ten-fold less on both cell lines compared to the parental GII-K74 ectodomain. I then treated HT1080 cells with heparinase III to remove HS. Ectodomain binding to treated cells was lowered for the WT ectodomain while unaffected for mutant counterparts. These results confirm that the identified residues K342, R343, R356 and R369 are mediating SFV Env binding to HS expressed on cells.

The RBD structure allows us to understand its functional subdomains. The two subdomains essential for binding form the lower subdomain and part of the upper domain. The HS is indeed located in the lower domain. The subdomain which can be removed without affecting Env binding to cells (called joining RBD, RBD_j) is located on the upper domain. AlphaFold 2.0 (AF) computational prediction of the GII-K74 RBD revealed a structure highly similar to the experimentally obtained RBD structure. Comparison of AF-predicted RBD structures from distinct FVs support that the RBD folds into a ‘common core’ (CC) conserved in overall fold between different FVs. In contrast, outer regions including some highly flexible loops at the apex of the RBD show high divergence in fold, even between distinct SFV genotypes. The loops form contacts between RBD protomers when superimposed into the CI-PFV trimer cryo-

EM map. Thus, our hypothesis is that these mobile loops stabilize the Env trimer in a pre-fusion conformation. Collectively, our data support that the upper domain of the SFV RBD is involved in trimer stabilization while the lower domain is involved in binding to HS.

3.2 Manuscript II: Characterization of nAb epitopes

In the main part of my PhD project, I have investigated the location and characteristics of epitopes targeted by nAbs in plasma samples from Central African hunters infected with zoonotic gorilla SFVs. These nAbs were previously shown to target the variable region, SUvar, which overlaps most of the RBD and defines the two SFV genotypes. Before my arrival, a master student performed linear epitope mapping using peptides spanning *in silico* predicted epitopic regions of SUvar. As few reactivities were observed towards these linear peptides in ELISA, I went towards conformational epitope mapping in our search for genotype-specific nAb epitopes.

I mapped the conformational epitopes using recombinant proteins as competitors to Env expressed by viral vectors for binding to nAbs in neutralization assays. I firstly used the published data on the functionally defined Env binding subdomain and glycosylation sites. Then, I focused on the genotype-specific sequences and linear *in silico* B-cell epitope predictions. When the X-ray crystal structure of the GII-K74 RBD became available, I used it for the rational design of novel mutations on SU domain proteins. I first tested several constructs for expression in mammalian and insect cells based on zoonotic gorilla SFV strains from the two genotypes, GI-D468 and GII-K74, and the laboratory adapted CI-PFV strain. These constructs included monomeric RBD and SU domains, dimeric immunoadhesin proteins composed of SU domain fused to Fc of mIgG2a (SU-Ig) and trimeric ectodomains. Among these, the only construct with adequate protein expression level for two distinct genotypes were the chimeric SU-Ig proteins. For those reasons, I used SU-Igs for the epitope mapping study. I set up the production, purification and validation of homologous GII-K74 and heterologous CI-PFV SU-Ig proteins for mapping of GII- and GI-specific nAb epitopes, respectively. The proteins were used as competitors in neutralization assays. I confirmed that these proteins block plasma nAbs in a genotype-specific and dose-dependent manner without affecting the entry of Env-pseudotyped viral vectors. These proteins were repeatedly titrated against a panel of plasma samples from SFV-infected donors diluted to their respective IC₉₀. This dilution was chosen to allow the saturation of nAb by recombinant proteins. Two parameters were defined to characterize the capacity of protein to block nAbs; IC₅₀ as a measure of their affinity and %

maximum inhibition (MaxI) which corresponds to the fraction of nAbs inhibited. Mutations were then introduced to these SU-Ig proteins to map nAb epitopes in neutralization assays by comparison of mutant IC_{50} and MaxI (%) values to that of WT. Introduction of mutations generally demonstrated one of four outcomes; I) no impact and activity same as for WT, II) lower affinity of nAbs to mutant protein as seen by a higher IC_{50} compared to WT, III) a lower MaxI plateau meaning a fraction of nAbs were no longer blocked by the mutant protein, or IV) both.

I firstly investigated the role of glycosylation in nAb epitopes and observed that complex and high-mannose type glycans did not influence the block of nAbs in our assay. In contrast, deglycosylation had a noticeable effect and significantly decreased the affinity of SU-Ig proteins for binding to plasma nAbs from six of eight donors tested. These results suggested that some epitopes may be composed of a glycan. To identify which glycan is involved in this recognition, I deleted six out of seven individual glycosylation sites within SUvar on the homologous GII-K74 SU-Ig protein, while the conserved glycan N8 was skipped as it is essential for protein expression. Among all mutants, deletion of glycan N7' had the strongest effect and resulted in significant loss of nAb blocking activity for five of seven GII-infected donors tested. This glycan is located at the CC of the RBD in the lower domain and in close proximity to the conserved glycan N8. Removal of glycan N10 which has a genotype-specific location did not affect block of nAbs for any plasma samples tested.

I also investigated if nAbs would recognize the novel heparan sulfate binding site that we mapped on the lower domain of the RBD in our collaborator's manuscript. However, proteins harboring the four HBS mutations retained activity equal to the WT for three of four GII-infected donors tested. Thus, we conclude that the HBS is not a dominant nAb target.

Next, we looked into the role of functional domains. Thus, we generated RBDj mutant SU-Ig proteins from both genotypes and tested their capacity to inhibit nAbs. Removal of RBDj completely abolished the blocking activity of the SU protein for seven of eight donors, suggesting that the major nAb epitopes are located within this region. We then generated a swap of GII SU-Ig with a GI-RBDj subdomain that blocked plasma nAbs from four GI-infected donors. These results confirm that the RBDj subdomain is a dominant target of nAbs in humans infected with gorilla genotype I strains.

On the 3D-structure, RBDj locates at the very apex of the RBD and of the trimer. Moreover, we observed that this region harbors the four loops hypothesized to be involved in trimer

stabilization. Among these loops (L1-4), L1 appear buried within the trimer and likely not accessible for nAbs. Thus, to further define epitopes within this region we designed SU-Ig proteins with loop mutations for both genotypes. The remaining three apex loops (L2; aa 278-293, L3; aa 410-433 and L4; aa 442-458) were individually deleted. The novel loop mutants demonstrated a genotype-specific targeting by nAbs. GI-specific nAbs mostly target the L3 region (CI-PFV L3; aa 411-436), while GII-specific nAbs had a wider response and target all three loops. To confirm the findings for GI, we generated a mutant with GII-L3 swap into the CI-PFV SU-Ig backbone and confirmed that this mutant lost its ability to block nAbs from six GI-specific plasma samples tested. Next, a Post-doctoral researcher, Dr. Youna Coquin, produced FVVs with RBDj and loop deletions matching those designed on SU-Ig proteins. She demonstrated that these mutants bound to SFV-susceptible cells but were not infectious. These data support that nAbs target epitopes on the apex of the RBD that are functionally important for viral entry.

Before our collaborators solved the RBD structure, I used *in silico* prediction tools to design seven mutations by inserting glycans for epitope disruption on the GII SU-Ig backbone. Among these, several mutations were located within or nearby the apex loops, and some of these confirmed our findings that these loops contain epitopes. Some mutations were also confirmed in the CI-PFV backbone for mapping of GI-specific plasma nAbs. Interestingly, I discovered a GII-specific epitope located in a loop (aa 345-353) region on the lower domain of the RBD. Glycan inserts to this loop strongly abolished block of GII- but not GI-specific plasma nAbs. Additional mutations within and nearby this loop including chimeric swaps confirmed this region to be a dominant target of nAbs from humans infected with genotype II gorilla SFV strains.

Collectively, our two manuscripts and previous report allowed us to propose a new model with attribution of functional roles to certain structural features of the SFV RBD. We propose that the upper domain of the RBD and apex loops are involved in protomer-protomer interactions and potentially Env trimer stabilization. In contrast, the lower domain of the RBD contains a putative HBS and is potentially involved in binding to other receptor molecules yet to be identified. My study on nAbs identified epitopes on both domains of the RBD and on the CC of the RBD. More precisely, I identified genotype-specific targets in regions of the upper RBD, while a strictly GII-specific epitope was defined at the lower base of the RBD.

CHAPTER IV

MANUSCRIPT I

4 | MANUSCRIPT I

The crystal structure of a simian foamy virus receptor-binding domain provides clues about entry into host cells

Ignacio Fernández¹, Lasse Toftdal Dynesen², Youna Coquin², Riccardo Pederzoli¹, Delphine Brun¹, Ahmed Haouz³, Antoine Gessain², Felix A. Rey¹, Florence Buseyne² and Marija Backovic^{1*}

¹Institut Pasteur, Université Paris Cité, CNRS UMR3569, Unité de Virologie Structurale, 75015 Paris, France.

²Institut Pasteur, Université Paris Cité, CNRS UMR3569, Unité d'Epidémiologie et Physiopathologie des Virus Oncogènes, 75015 Paris, France.

³Institut Pasteur, Université Paris Cité, Plateforme de cristallographie-C2RT, CNRS UMR 3528, 75015 Paris, France.

*Corresponding author: Marija Backovic, marija@pasteur.fr

4.1 Abstract

The surface envelope glycoprotein (Env) of all retroviruses mediates virus binding to cells and fusion of the viral and cellular membranes. A structure-function relationship for the HIV Env, which belongs to the Orthoretrovirus subfamily, has been well established. Structural information is however largely missing for the Env of Foamy viruses (FVs), the second retroviral subfamily. FV Envs lack sequence similarity with their HIV counterpart. We present the X-ray structure of the receptor binding domain (RBD) of a simian FV Env at 2.6 Å resolution, revealing two subdomains and an unprecedented fold. We have generated a model for the organization of the RBDs within the trimeric Env which indicates that the upper subdomain is important for stabilization of the full-length Env, and have demonstrated that residues K342, R343, R359 and R369 in the lower subdomain play key roles in the interaction of the RBD and viral particles with heparan sulfate.

4.2 Introduction

Spumaretroviruses, also known as foamy viruses (FVs) are ancient retroviruses that have co-evolved with vertebrate hosts for over 400 million years (Aiewsakun and Katzourakis, 2017; Rethwilm and Bodem, 2013). FVs are prevalent in nonhuman primates, which can transmit them to humans, most often through bites (Pinto-Santini et al., 2017). Unlike their better-studied *Orthoretrovirinae* relatives (HIV being the most notable member) FVs have extremely slowly mutating genomes and do not induce severe pathologies despite integrating into the host genome and establishing lifelong persistent infections (Buseyne et al., 2018; Ledesma-Feliciano et al., 2019). These features, along with broad tropism and host range (Meiering and Linial, 2001), make FVs attractive vector candidates for gene therapy (Rajawat et al., 2019).

Viral fusion proteins drive membrane fusion by undergoing a conformational change, which can be triggered by acidification in an endosomal compartment and / or binding to a specific cellular receptor (Harrison, 2015; White and Whittaker, 2016). FVs enter cells by endocytosis, with fusion of the viral and cellular membranes occurring in the endosomal compartment in a pH-sensitive manner, leading to capsid release into the cytosol (Picard-Maureau et al., 2003). The exception is the prototype FV (PFV) which can also fuse at the plasma membrane (Dupont et al., 2020). The FV fusion protein, the envelope glycoprotein (Env), exhibits the organization of a class I fusogen (Rey and Lok, 2018), which are synthesized as single-chain precursors and fold into trimers, within which protomers are subsequently cleaved in secretory Golgi compartments. FV Env is cleaved twice by cellular furin during maturation, giving rise to 3 fragments: the leader peptide (LP), the surface (SU) subunit, which has the receptor binding domain (RBD), and the transmembrane subunit (TM), which harbors the fusion machinery. The structural information available for FV Env is limited to cryo-electron tomography (ET) of viral particles and a 9 Å cryo-electron microscopy (EM) reconstruction of PFV Env (Effantin et al., 2016), which revealed LP-SU-TM trimers arranged in interlocked hexagonal assemblies (Effantin et al., 2016; Wilk et al., 2000), with an architecture that is different to that of HIV Env trimers (Pancera et al., 2014).

Heparan sulfate (HS) is as an attachment factor for PFV and feline FV (Nasimuzzaman and Persons, 2012; Plochmann et al., 2012) but the requirements for a surface or intracellular receptor, which would trigger membrane fusion by FV Env, remain unclear. The search for a receptor has been complicated by the FV binding to HS, which is ubiquitously expressed on

cells, masking potential candidates. A bipartite RBD, consisting of two discontinuous regions of the polypeptide chain, was identified within the FV SU by screening a panel of recombinant SU truncations for binding to cells (Duda et al., 2006). FV Env is heavily glycosylated, with at least 13 predicted N-linked glycosylation sites. Mutational analysis has revealed that three of these N-sites are essential for the PFV infectivity – two located in the TM subunit, and one in the RBD. The latter site, referred to as the glycosylation site 8 or N8 (Luftenegger et al., 2005) is conserved across the FV subfamily, and has been suggested to play a direct role in binding to a receptor (Duda et al., 2006) (to distinguish the nomenclature of the predicted N-linked glycosylation sites (N1 to N15) from the single letter symbol for asparagine residues (N), the former will be underlined throughout the text). The remaining molecular determinants of the RBD interaction with host cells remain elusive, largely due to a lack of structural information, which has precluded rational approaches to mutagenesis and functional analyses. A high-resolution structure of the FV RBD, structural information regarding the RBDs organization within the Env trimer and how the RBDs contribute to the Env activation are not available. In this manuscript we present the first X-ray structure of the RBD from a zoonotic gorilla simian FV at 2.6 Å resolution, which reveals an entirely novel fold. We propose a model for the RBD assembly in the trimeric Env and report the identification of residues involved in HS binding, with functional and evolutionary implications discussed.

4.3 Results

4.3.1 The X-ray structure of the SFV RBD reveals a novel fold

Recombinant RBDs from several simian FV (SFV) strains were tested for production in *Drosophila* S2 insect cells, and only the RBD from gorilla SFV (strain SFVggo_huBAK74 (Khan et al., 2018), genotype II; abbreviated as ‘GII’ herein) was both expressed in the quantities required for structural studies and also crystallized. The RBD was expected to be heavily glycosylated due to 8 predicted N-glycosylation sites (Fig. IV-1). To increase the chances of generating well-diffracting crystals, a fraction of the purified protein was enzymatically deglycosylated (RBD^D). Crystals were obtained for the RBD^D as well as for the untreated protein (RBD^G). The RBD^D diffracted better (2.6 Å) than RBD^G and the structural analyses presented below were carried out using the RBD^D structure, unless otherwise noted. The data collection and structure determination statistics for both crystal forms are summarized in Table S.IV-1.

The SFV RBD folds into two subdomains, each with $\alpha+\beta$ topology, which we refer to as ‘lower’ (residues 218-245, 311-369 and 491-524) and ‘upper’ subdomains (residues 246-310 and 370-490) in reference to their positioning with respect to the viral membrane (Effantin et al., 2016) (see below). The overall RBD fold approximates a ~65 Å long bean-shape, with the upper subdomain on the wider side (~45 Å diameter), and the N- and C-termini on the opposite, narrower side (~20 Å diameter) (Fig. IV-1B). The lower subdomain is comprised of a three-helical bundle ($\alpha 1$, $\alpha 7$, $\alpha 8$) that packs against an anti-parallel, twisted four-stranded β -sheet ($\beta 14$ - $\beta 1$ - $\beta 5$ - $\beta 15$) and against helix $\alpha 2$ (residues 333-346), which lays perpendicularly on the side of the bundle. Within the helical bundle and the β -sheet, the regions proximal to the N- and C- termini are tied together, and each structure is reinforced by disulfide bonds (DS) DS1 (C228-C503) and DS2 (C235-C318), respectively. Seventy- and 130-residue long segments, forming most of the upper subdomain, are inserted between $\beta 1$ and $\beta 5$, and between $\eta 4$ and $\beta 14$ of the lower subdomain, respectively (Fig. IV-2). The polypeptide chain extends upwards and back twice, finally yielding the outer strands of the β -sheet ($\beta 14$ and $\beta 15$). These secondary structural elements in the lower subdomain contain a prominent hydrophobic core that extends into the upper subdomain, which has lower secondary structure content (Table S.IV-2) and is stabilized by several networks of polar interactions (Fig. S.IV-1, Table S.IV-3). Four notable protrusions, designated loops 1 to 4 (L1-L4) emanate from the upper domain:

loop 1 (L1, residues 253-270, connecting $\beta 2$ and $\eta 1$), loop 2 (L2, residues 276-281, connecting $\eta 1$ and $\beta 3$), loop 3 (L3, residues 414-436, connecting $\alpha 6$ and $\beta 9$) and loop 4 (L4, residues 446-453, connecting $\beta 10$ and $\beta 11$). The loops L3 and L4 are particularly mobile in our structures as indicated by high B-factors ($> 105 \text{ \AA}^2$) for their $C\alpha$ atoms (Fig. S.IV-2). Electron density was observed for 7 out of the 8 predicted N-glycosylation sites (Fig. IV-1C), allowing the modelling of at least one N-acetyl glucosamine (NAG) at each site (Fig. IV-2, Fig. S.IV-3).

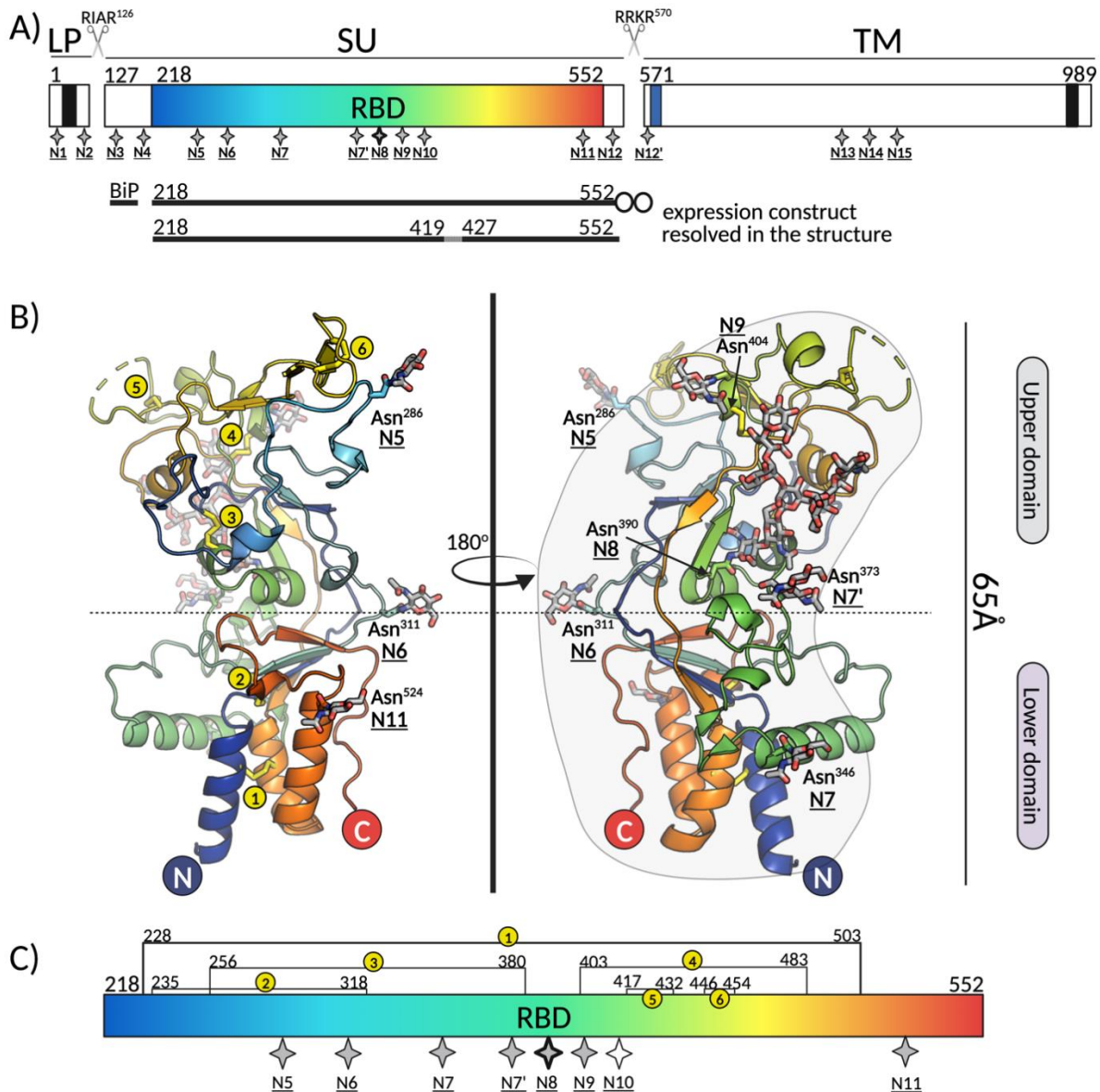


Figure IV-1 – Overview of the novel fold adopted by the SFV RBD

Schematic representation of SFV Env protein organization indicating the three constituent chains: leader peptide (LP), surface subunit (SU), and transmembrane subunit (TM). The transmembrane domains anchoring the LP and TM in the membrane are represented as black boxes; the receptor binding domain (RBD) within SU is highlighted in blue-red spectrum; the fusion peptide at the N-terminus of the TM is shown in blue. The furin sites between the LP and SU (RIAR¹²⁶), and SU and TM (RRKR⁵⁷⁰) are indicated with scissors symbols. The expression construct

contained the exogenous BiP signal at the N-terminus, residues 218 to 552 of the SFV gorilla GII Env and a double strep tag at the C-terminus (shown as two circles). The region comprising residues 420-426 is drawn as a dashed line because it was not seen in the electron density map. The 17 putative N-glycosylation sites for gorilla SFV Env are indicated with star symbols and labels N1 to N15, following the previously established nomenclature (Luftenegger et al., 2005). **B**) The X-ray structure of the RBD^D is shown in ribbon model colored from N- to C-terminus in blue to red spectrum, respectively. The dashed line indicates the separation between the upper and lower subdomains. The N-glycosylation sites are indicated with N, and the sugars as well as the asparagine side chains carrying them are displayed as sticks. **C**) The schematic representation of the RBD. The potential N-glycosylation sites are indicated with star symbols. The sites with sugars built in the RBD^D structure are shown as grey stars, and the site N10 (Asp⁴¹¹) that showed no electron density for the carbohydrate in neither RBD^D nor RBD^G is labeled with empty star symbol. The site N8 (Asn³⁹⁰) that contains the long, partially buried sugar is highlighted with a thicker border. The locations of six disulfides are indicated with yellow circles and numbers 1-6. The figure was created with PyMOL (DeLano, 2002) and BioRender.com.

Searching the PDB databank with the DALI algorithm (Holm, 2020) and the RBD and its substructures did not yield any meaningful results. Comparative analyses with the available structures of the RBDs from Orthoretroviruses (Fig. S.IV-4) did not reveal structural similarity, either at the level of the secondary structure topology or the three-dimensional fold. Therefore, the SFV RBD represents, to the best of our knowledge, an unprecedented fold.

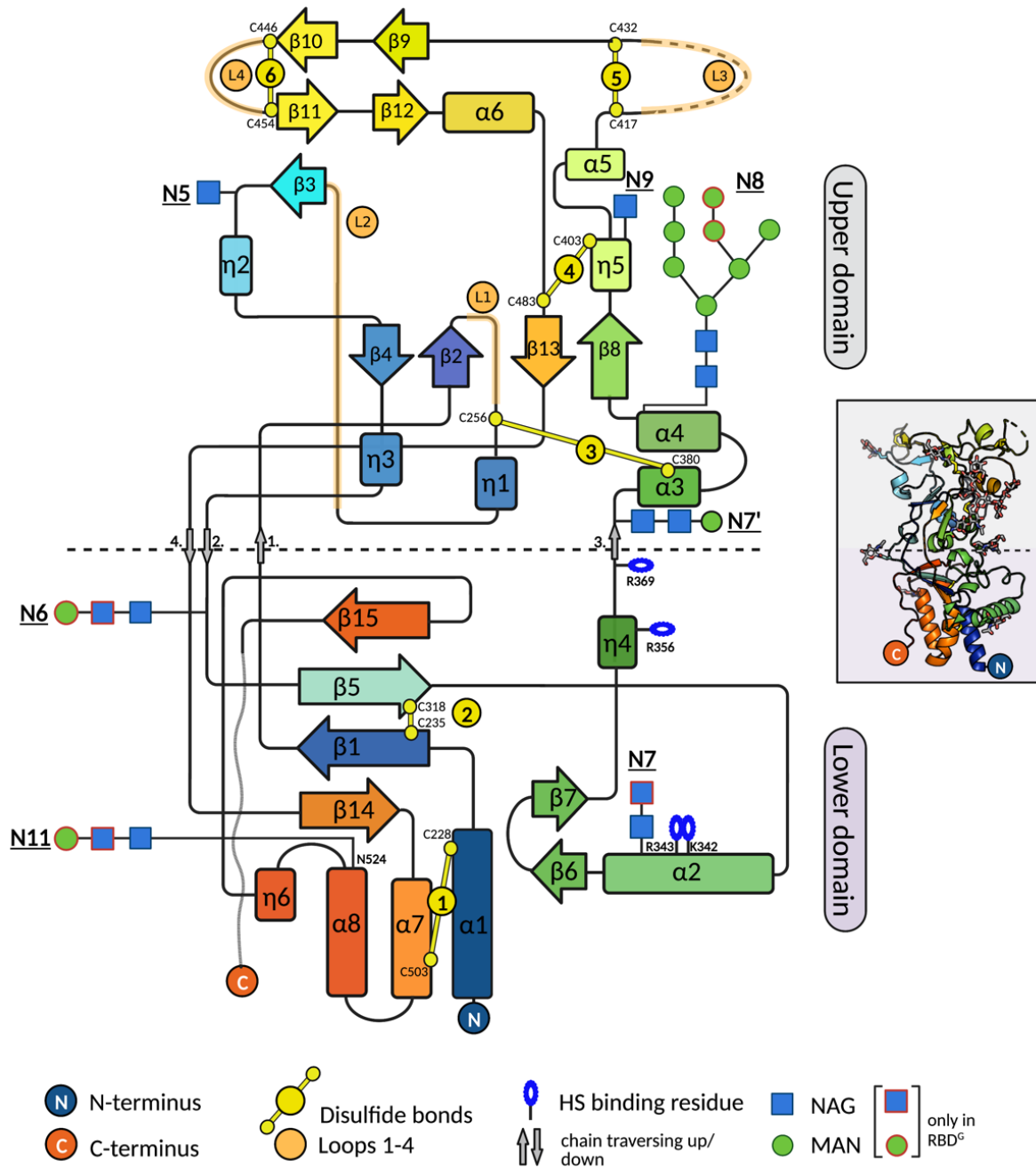


Figure IV-2 – SFV secondary structure topology diagram

The horizontal dashed line designates the boundary between the lower and upper subdomains. The NAG and MAN units built only into the RBD^G (and not RBD^D) structure are indicated with red frames. The figure was created with BioRender.com.

4.3.2 The sugar attached to the strictly conserved 8th N-glycosylation site plays a structural role

There were no major differences between the X-ray structures of RBD^D and RBD^G (their superposition yielded a root mean square deviation (rmsd) below 1Å (Fig. S.IV-3B)), except for the different number of sugar units that we could built into the electron density maps (Fig.

S.IV-3A). A prominent feature of the upper subdomain is the eighth N-linked sugar (N8) attached to the $\alpha 4$ helix residue N390. The N390 and the first two NAG residues are buried in the RBD rendering the Endo-H/D cleavage site inaccessible (Fig. IV-3B), which allowed building of 10 sugars in the RBD^G and 8 in the deglycosylated protein crystals (Fig. IV-2, Fig. IV-3A). The N8 glycan emerges from a cavity that has N390 at its base and extends upwards, remaining in contact with the protein and preserving the same conformation in both crystal forms.

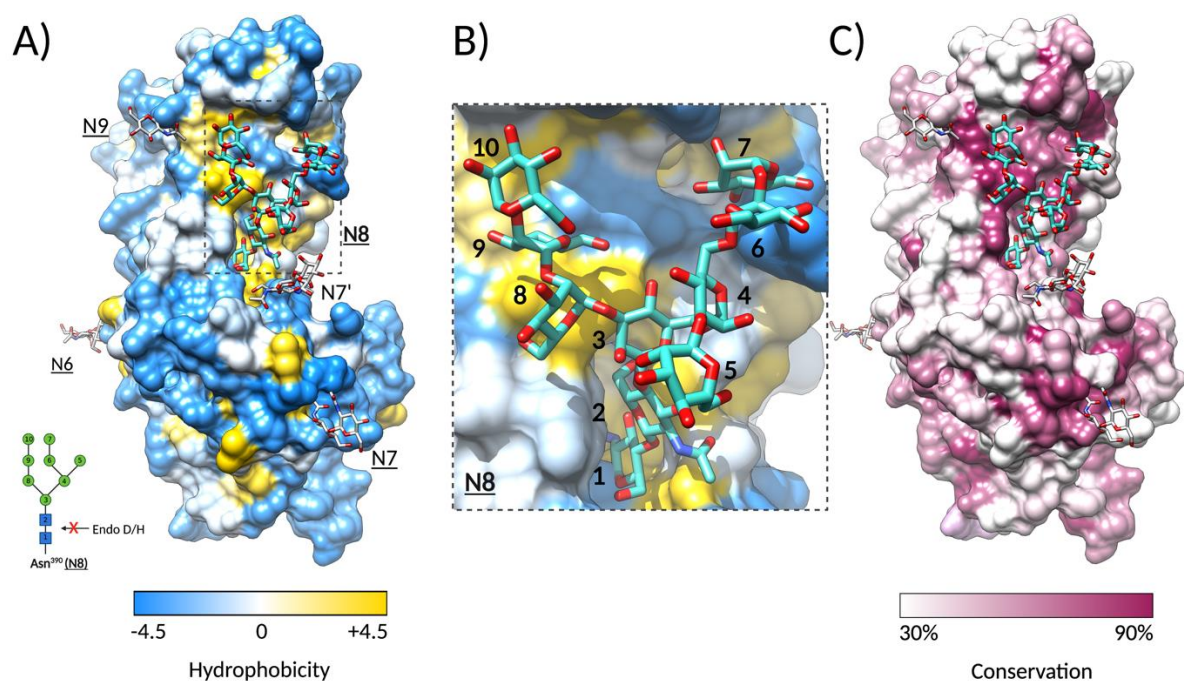


Figure IV-3 – The oligosaccharide linked to N390 plays a structural role in the RBD

A) Molecular surface representation of the SFV RBD^G colored by residue hydrophobicity. Hydrophobicity for each residue was calculated according to the Kyte and Doolittle scale (Kyte and Doolittle, 1982) in Chimera (Pettersen et al., 2004), with the gradient color key indicating the lowest hydrophobicity in blue, to the highest hydrophobicity in yellow. The sugars at sites N6, N7, N7', and N9 are displayed as white sticks, and the sugar attached to N8 as cyan sticks. The inset shows the bond cleaved by glycosydases Endo D/H, which is protected in N8. **B)** The N8 sugar attached to Asn³⁹⁰ covers a hydrophobic region. Zoom into the region within the dashed-line rectangle in panel A). The NAG and MAN residues are labeled with numbers that match the N-oligosaccharide drawn in panel A. **C)** The hydrophobic patch covered by N8 is well conserved. The SFV RBD surface is rendered by residue conservation in Chimera (Pettersen et al., 2004), according to the % of the identical residues in the 11 FV Env sequences (alignment shown in Fig. S.IV-5). Residues conserved in less than 30% and more than 90% of sequences are colored in white and purple, respectively, and residues in between with a white-purple gradient, as indicated on the color key below the surface representation.

Structural analyses revealed that the glycan establishes extensive van der Waal contacts with the residues underneath (buried surface area of 803 Å²) and forms hydrogen bonds with main chain atoms from Y394 and I484 and the side chain of E361 (Fig. S.IV-6). The oligosaccharide covers a well-conserved and hydrophobic surface (Fig. IV-3C) and thus maintains the RBD fold

and prevents aggregation, consistent with the reported misfolding and low levels of the secreted immunoadhesin carrying the RBD with a mutation in the N8 site (Duda et al., 2006). The N8 is the only N-glycosylation site in the SU that is strictly conserved across the FV subfamily (Fig. S.IV-5), and the hydrophobic patch residues laying beneath it are conserved as well (Fig. IV-3C). Thus, N8 likely plays an important structural role in all FV RBDs.

4.3.3 The RBD fold is predicted to be conserved within the Spumaretrovirinae subfamily

To investigate potential conformational differences between RBDs from different species, we used AlphaFold (AF) (Jumper et al., 2021) software to predict the RBD structures from members of each of the 5 FV genera, some of which exist as two genotypes due to the modular nature of FV Env (Aiewsakun et al., 2019a). Within each FV Env, a ~250-residue long region within the RBD, termed the variable or 'SU^{var}' region, defines two co-circulating genotypes, I and II, which have been found in gorillas (Richard et al., 2015), chimpanzees (Lambert et al., 2018) and mandrills (Aiewsakun et al., 2019a), among others. The SU^{var} regions share less than 70% identity (Fig. S.IV-5), while the rest of Env residues are highly conserved (>95% sequence identity). The SU^{var} is located within the upper subdomain and encompasses loops L1-L4 (residues 282-487 in GII RBD; Fig. S.IV-7).

All the generated models have high confidence metrics (Fig. S.IV-8) and display a conserved fold in agreement with a sequence identity >30%. Significant deviations were found only in the loops within the SU^{var}. The Template Modelling score (TM-score), which is, unlike rmsd, a length-independent measure of structural similarity (Zhang and Skolnick, 2004) has the average value of 0.891 for the 11 compared structures. The AF model of the GII RBD and our experimentally determined structure of the same strain superimpose with a TM-score of 0.96 and rmsd of 1.5 Å for 320 out of 328 C α atoms aligned, confirming the high accuracy of the AF model. A 'common core' (CC), which includes the ensemble of residues with C α rmsd values smaller than 4Å for all the pairwise superpositions, was calculated by the mTM-align webserver (Dong et al., 2018a). The CC of the FV RBD contains 239 out of 308 aligned residues (Fig. S.IV-9), with most CC residues belonging to the secondary structure elements forming the lower subdomain. The loops in the upper subdomain are largely not a part of the CC (Fig. S.IV-9).

4.3.4 Fitting of the RBD atomic model into Env cryo-EM density map reveals the trimeric RBD arrangement

To investigate the RBD arrangement within trimeric Env, we fitted the RBD atomic model into the 9Å cryo-EM map reported for trimeric PFV, (a chimpanzee genotype I FV) Env expressed on foamy viral vector (FVV) particles (Effantin et al., 2016). The fitting was justified by the high structural conservation between gorilla and chimpanzee RBDs, indicated by a TM-score of 0.88 for the superposition of the GII RBD structure and the predicted PFV RBD model (Fig. S.IV-8).

The RBD fitting was performed with the fit-in-map function in Chimera suite (Pettersen et al., 2004). The correlation coefficient of 0.96 strongly suggests that the recombinantly expressed RBD represents its biologically relevant conformation as observed at the surface of virus particles. The three RBDs are arranged around a central cavity at the apex (membrane-distal region) of Env (Fig. IV-4A). The analyses of the macromolecular surfaces of the trimeric RBD model, carried out in PDBePISA (Krissinel and Henrick, 2007), revealed a limited inter-protomer interface (<10% of the entire RBD solvent accessible surface) established solely by loops L1, L3 and L4 that form a ring-like structure at the RBD apex, leaving most of the RBD exposed (Fig. IV-4B). The three L1 loops engage in homotypic interactions at the center of the RBD, forming an inner ring, while each L3 loop contacts the L4 of a neighboring protomer, further stabilizing the interface. The sequences of the interacting loops are poorly conserved within the FV subfamily (Fig. S.IV-10). The seven N-linked glycans that we could resolve in the RBD structure are all fully solvent-exposed (Fig. IV-4C). The RBD N- and C- termini point towards the membrane, indicating that the lower half of the Env density is occupied by the TM subunit and the remaining SU residues, as previously suggested (Effantin et al., 2016).

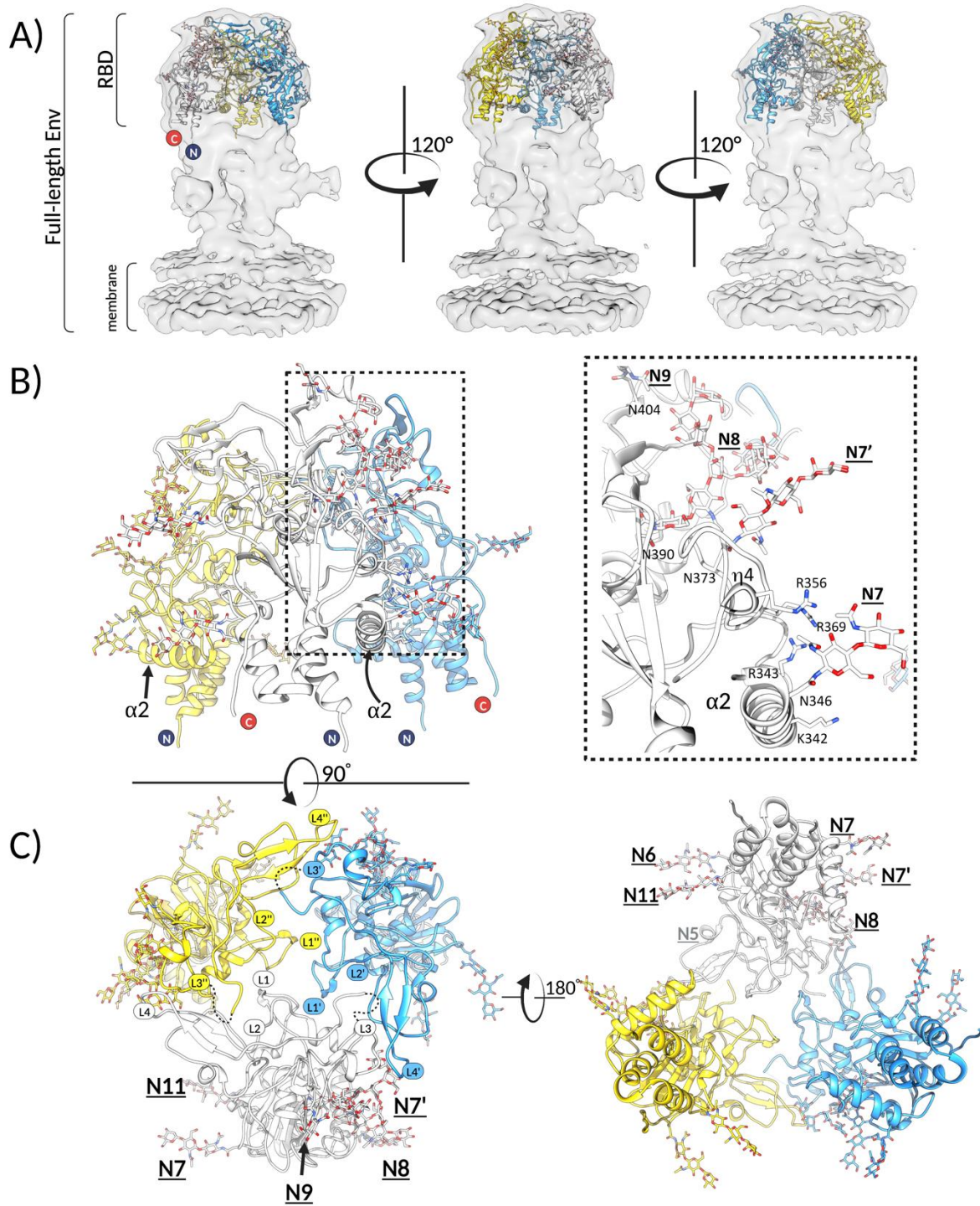


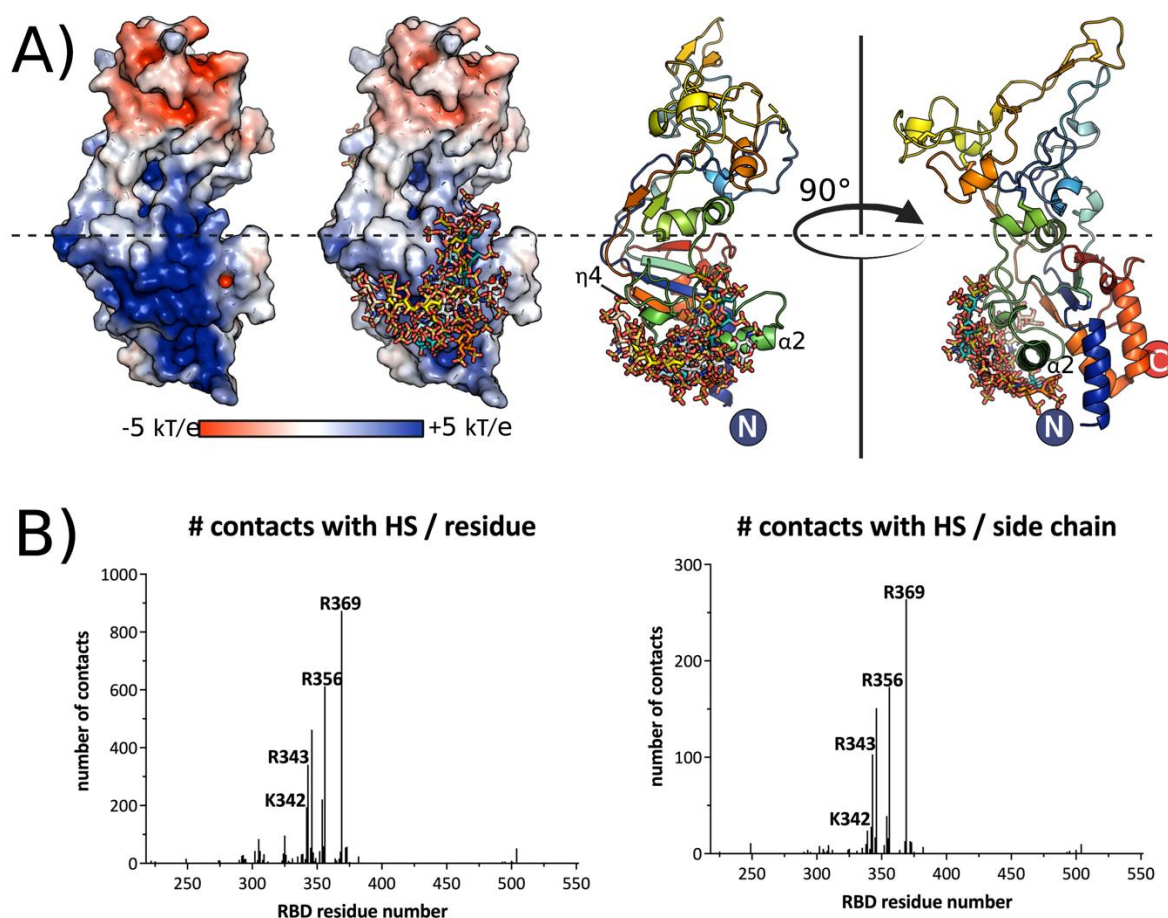
Figure IV-4 – The RBDs form a trimeric assembly at the apex of the full-length Env

A) Three SFV RBD protomers were fitted in the 9Å cryo-EM map (EMBD: 4013) obtained by cryo-EM 3D reconstruction of the full-length PFV Env expressed on viral vector particles (Effantin et al., 2016). The map is shown in light grey surface, and RBDs in cartoon mode, with each protomer colored differently (yellow, white, light blue). **B)** The three RBDs fitted as explained in panel A) are shown to illustrate that the $\alpha 2$ and $\eta 4$ helices, which carry the HS binding residues (K342, R343, R359, R369), as well as the N-linked glycosylations (N6, N7, N7', N8, N9 and N11) point outward and are solvent accessible. The boxed region on the left panel is magnified for clarity on the right panel (only one protomer, colored in white, is represented for clarity purposes). **C)** The views at the trimeric RBD arrangement from the top i.e. looking at the membrane (left) and bottom i.e. looking from

the membrane (right) are shown. The RBDs form interprotomer contacts via the L1-L4 in the upper domain. The loops belonging to each protomer are designated as L, L' and L''. Images in all three panels were generated in Chimera (Pettersen et al., 2004).

4.3.5 Positively charged residues in the lower subdomain form a heparan sulfate binding site

To locate potential HS binding regions with RBD, we investigated electrostatic potential surface distribution and identified a large, continuous region in the lower subdomain with strong positive potential (Fig. IV-5A). We next analyzed the RBD structure with the ClusPro server that predicts putative HS binding sites on protein surfaces (Kozakov et al., 2017). K342 and R343 in $\alpha 2$ helix, R359 in the preceding $\eta 4$ helix and R369 in an extended chain region were among the residues that had the highest number of contacts with HS models that were docked onto the surface (Fig. IV-5B, IV-5C). The four residues also mapped within the positively-charged region in the lower subdomain.



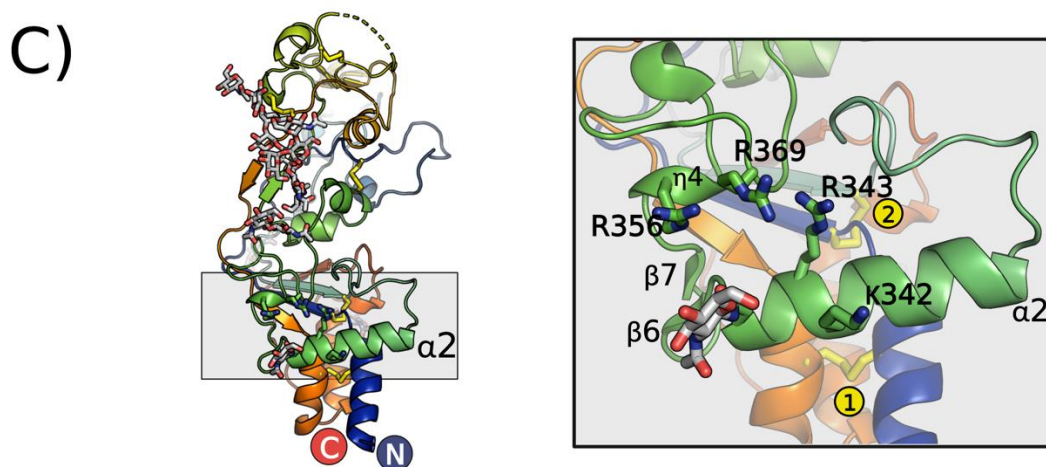


Figure IV-5 – Prediction of HS binding residues and design of the variants impaired in binding

A) Electrostatic potential distribution was calculated using Adaptive Poisson-Boltzmann Solver (Jurrus et al., 2018) module in PyMOL (DeLano, 2002) and plotted on the solvent accessible surface of the RBD, with red corresponding to the negative, and blue to positive potentials (2 left panels). The ensemble of HS molecules modeled by ClusPro (Kozakov et al., 2017) map to the lower subdomain and are displayed in sticks on the two right panels, which show the RBD in cartoon model and in two orientations to illustrate the location of predicted HS binding secondary structure elements. **B)** Predicted number of contacts per residue and per side chain atoms calculated by ClusPro and plotted for each RBD residue, revealing the most likely candidates to be engaged in HS binding. **C)** Structure of RBD is shown in cartoon, with the region containing $\alpha 2$ and $\eta 4$ helices highlighted in grey. Magnification of the grey boxed region is shown on the right panel, with the relevant secondary structure elements and predicted HS binding residues shown in sticks. Two disulfide bonds are indicated with yellow circles. The figure was created with PyMOL (DeLano, 2002) and BioRender.com.

Based on the ClusPro predictions, we produced two GII RBD variants (K342/R343, termed ‘mut1’, and R359/R369, termed ‘mut2’) and tested their binding to HS immobilized on a Sepharose matrix (Fig. IV-6A). The two RBD variants eluted at the same volume on size exclusion chromatography consistent with the expected size of a monomer (Fig. S.IV-11), indicating that the introduced mutations did not cause protein misfolding. The WT RBD was retained on the column and eluted at 300 mM sodium chloride concentration, while mut1 and mut2 variants were not retained by the column and eluted in the flow-through fraction. The observed loss of heparin binding capacity strongly suggests that residues K342, K343, R359, and R369 are directly involved in interactions with HS.

Next, we used flow cytometry to investigate the interaction between the GII RBD and HS on cells (Fig. S.IV-12A). We found that the monomeric RBD did not bind to HT1080 cells even at high protein concentrations (Fig. IV-6B). We therefore tested a longer construct, the GII Env ectodomain, which spontaneously form trimers, hypothesizing that an oligomer would yield higher signal due to avidity effects. The trimeric ectodomain bound to HT1080 cells (Fig. IV-

6B), and the mutations K342A/R343A and R356A/R369A (mut1 and mut2, respectively) were introduced into the ectodomain background to render them suitable for flow cytometry experiments. We assayed the binding of the Env ectodomains to HT1080 and to BHK-21 cells (Fig. S.IV-12B), which are susceptible to infection by gorilla FVs (Couteaudier et al., 2019). We quantified HS expression levels by flow cytometry concomitantly with the binding experiments, and verified that BHK-21 cells expressed lower HS levels than HT1080 cells, as had been reported (Plochmann et al., 2012) (Fig. S.IV-12C). The HS expression levels were 10 to 30-fold lower on BHK-21 cells compared to HT1080 cells (Fig. IV-6C). The binding of the WT ectodomain was lower on BHK-21 than to HT1080 cells at the highest protein concentrations tested. The binding signal was dose-dependent and one log lower for mut1 and mut2 ectodomain variants in comparison with the WT protein on both cell lines (Fig. IV-6C).

To prove that the designed mutations specifically affected the interaction with cellular HS, we measured binding to HT1080 cells that were pre-treated with heparinase, which removed more than 90% of HS from the cells (Fig. S.IV-12D). Binding of the WT ectodomain to heparinase-treated cells was diminished about 100-fold when compared to buffer-treated cells, while the binding of the mut1 and mut2 variants was not affected by heparinase treatment (Fig. IV-6D).

The importance of residues K342, R343, R356, R369 for viral entry into susceptible cells was tested using FVVs that express either GII WT, mut1 or mut2 Env on their surface. The total number of FVV particles released by the transfected cells, measured by RT-qPCR, was ~6-fold lower for the mut1 compared to WT FVVs, while mut2 had the same particle production as WT (Fig. S.IV-13A). The infectious titers were 34- and 65-fold lower for mut1 and mut2, respectively, compared to WT (Fig. S.IV-13B). The proportion of infectious particles, defined as the infectious titer (Fig. S.IV-13B), divided by the total number of FVVs (Fig. S.IV-13A) was 0.7% for WT Env FVVs, while the values for mut1 and mut2 FVVs were 3- and 22-fold lower, respectively (Fig. IV-6E). We measured the binding of FVVs to cells by RT-qPCR, and found that the binding was also reduced 3- and 23-fold for FVVs carrying mut1 and mut2 Envs, respectively, compared to the WT Env FVVs (Fig. IV-6F). Thus, binding to cells and entry levels were decreased to the same extent for the FVVs carrying Env proteins with mutations in the HS binding site.

The results described for the recombinant Env proteins and FVVs carrying full-length Env agree with the biochemical data (Fig. IV-6A) and demonstrate that residues K342, R343, R356, R369 play a crucial role in virus interaction with HS.

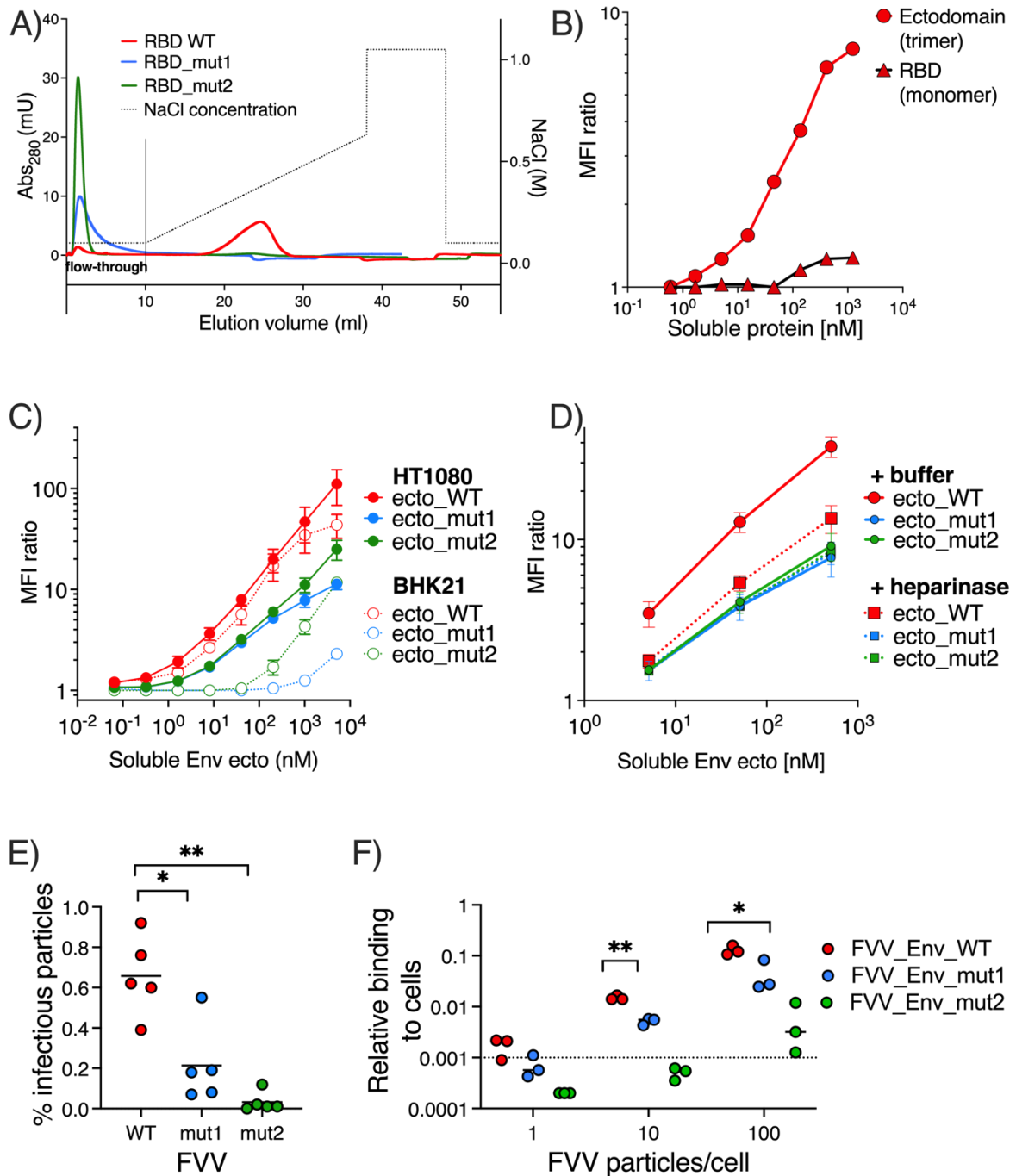


Figure IV-6 – The SFV RBD residues K342, R343, R356 and R369 mediate Env binding to HS

A) Chromatogram of the recombinant SFV RBD, WT (red line) and variants with mutations in HS binding residues: mut1 (K342A/R343A) in blue, and mut2 (R356A/R369A) in green on a heparin-Sepharose column. Dotted line shows salt concentration, which is plotted on the right y-axis. **B)** Binding of recombinant WT RBD and ectodomains to HT1080 cells. To be comparable with the RBD, the concentration for the ectodomain is calculated

and plotted for the monomeric protein. **C)** Binding of WT, mut1 (K342A/R343A), and mut2 (R356A/R369A) recombinant Env ectodomains to HT1080 cells and BHK-21 cells. SFV Env binding level was expressed as the ratio of MFI from protein treated to untreated cells (Fig. S.IV-12B). Mean and SD from two independent experiments are shown. Cell HS expression levels were monitored on the day of each of the 2 experiments (the Env binding levels were 85.4 and 61.6 for HT1080 cells, 8.40 and 2.68 for BHK-21 cells (Fig. S.IV-12C)). **D)** Binding of WT, mut1 (K342A/R343A), and mut2 (R356A/R369A) recombinant Env ectodomain variants to HT1080 cells treated with heparinase or buffer was quantified at increasing ectodomain concentrations. Ectodomain binding level was expressed as the ratio of MFI from protein treated to untreated cells (Fig. S.IV-12D). Mean and SD from two independent experiments are shown. **E)** Percentage of infectious FVV particles carrying WT, mut1 or mut2 Env. The percentage was calculated from the ratio between the number of infectious particles (determined by titration of susceptible cells) (Fig. S.IV-13A) and the amount of vector particles obtained by RT-qPCR (Fig. S.IV-13B). The different FVVs were compared using the paired t-test, * $p < 0.05$, ** $p < 0.01$. **F)** Binding of FVVs carrying the WT, mut1 or mut2 Env to HT1080 cells. The FVVs were incubated with HT1080 cells on ice for 1 hour at different particle/cell ratios, before washing and quantification of the remaining vector particles by RT-PCR. Lines represent mean values from tested FVV batches. The dotted line represents the quantification threshold. The different FVVs were compared using the paired t-test, * $p < 0.05$, ** $p < 0.01$.

4.4 Discussion

FV RBD adopts a novel fold and is composed of two subdomains. We determined the X-ray structure of the RBD from a gorilla FV, revealing a fold (Fig. IV-1, Fig. IV-2) distinct from the available orthoretroviral RBD structures i.e. from the Friend murine leukemia virus, feline leukemia virus, human endogenous retrovirus EnvP(b)1 (gammaretrovirus genus) (Fass et al., 1997; Fass et al., 1996; McCarthy et al., 2020), and gp120 from HIV (lentivirus genus) (Kwong et al., 1998) (Fig. S.IV-4). This finding expands the repertoire of unique FV features (assembly, particle release (Lindemann et al., 2021), replication (Rethwilm, 2003)) that are not shared with Orthoretroviruses, and is consistent with the lack of Env sequence conservation between Orthoretroviruses and FVs.

The gammaretroviral RBDs are relatively small (~200 residues) and fold into an antiparallel β -sandwich with two extended loops that give rise to a helical subdomain that sits on top of the sandwich (Fass et al., 1997; Fass et al., 1996) (Fig. S.IV-4). The helical subdomain defines the tropism for cellular receptors (Battini et al., 1992) and shows high sequence variability within the genus. HIV interacts with its cognate receptor CD4 through gp120, its SU, which is larger (~450 residues) and has two subdomains, inner and outer. The receptor binding surface of gp120 is formed by secondary structure elements from both subdomains (Kwong et al., 1998). Variable loops project out from the gp120 core, and participate in receptor binding and immune invasion (Chen, 2019). It is possible to argue that the FV RBD global organization into two subdomains – the lower, which is better conserved, and upper, which contains the protruding loops and is variable in sequence – is reminiscent of the characteristics described above for the Orthoretrovirus RBDs. Whether the presence of similar features implies similar function remains to be investigated.

The RBDs form a cage-like structure at the membrane-distal side of Env. We fitted the experimentally determined RBD structure into the low-resolution density map (Fig. IV-4A) obtained by cryo-EM single particle reconstruction of trimeric PFV Env expressed on FVV particles (Effantin et al., 2016). The resulting model of the RBD trimer arrangement is consistent with the biochemical and functional data presented here - as expected, the HS binding residues (K342, R343, R356, R369) and seven N-linked carbohydrates map to the Env surface that is exposed to the solvent (Fig. IV-4C). According to our model, the L1-L4 loops, located at the top of the upper subdomain of each protomer, form the inter-protomer

interface (Fig. S.IV-10) leaving, just below, a cavity that was clearly observable in the cryo-EM maps (Effantin et al., 2016). The loop sequences are poorly conserved across the FV family (Fig. S.IV-10), and the superposition of the AF models of 11 FV RBDs reveal only slight structural differences, which are mostly limited to this variable region containing the loops (Fig. S.IV-8, Fig. S.IV-9). Based on these observations we speculate that the inter-protomer interactions mediated by the loops maintain a closed Env conformation, stabilizing the Env protein in its metastable pre-fusion form that is displayed on the virion surface. It is possible to envisage that different sets of interacting residues in the loops in different FVs stabilize the RBDs within the trimeric Env sufficiently well to maintain its native state. We hypothesize that the RBDs are loosely bound within native Env to enable them to readily dissociate upon a fusion trigger, which could be delivered in the endosome (acidic pH) and / or by a specific cellular receptor. In that respect, the FV upper domain loops could play a role equivalent to V1/V2/V3 loops in HIV Env (Wang et al., 2016a). It will be also important to discern the RBD molecular determinants, if any, that drive the membrane fusion at the plasma membrane, as used by PFV, in comparison to all the other FVs that fuse in the endosomes (Dupont et al., 2020).

The structure explains why upper RBD domain is tolerant to deletions or substitutions.

Based on the ability of Env truncated variants to bind to cells, Duda *et al.* defined the RBD of PFV Env as a region spanning residues 225-555 (residues 226-552 in gorilla GII Env (Fig. S.IV-14A)) (Duda et al., 2006). Within the proposed region, the terminal segments were found to be essential for the RBD to retain its cell binding activity, while the central region was dispensable. This RBD region, which is not essential for binding to cells (Duda et al., 2006), termed also RBDjoin (Dynesen et al., 2022, submitted), maps to the top of the RBD, is clamped by two intra-region DS bonds, and encompasses L3 and L4 (Fig. S.IV-5). Its location, away from the HS binding residues, is consistent with the ability of the PFV SU truncation lacking the “non-essential” region to bind to cells at the levels measured for WT protein (Duda et al., 2006). The AF model of the PFV RBD lacking this RBDjoin region reveals a 3D fold very similar to that of the complete RBD (Fig. S.IV-14B). Considering the RBD arrangement within trimeric Env, which we show is maintained by the loops in the RBDjoin region (Fig. IV-4), we hypothesized that the loop deletions, while tolerated by isolated, monomeric RBD, would likely be detrimental for the integrity of the trimeric Env and its function in fusion and entry.

Dynesen *et al.* indeed show that the virus with Env carrying deletion in loop regions lead to the loss of infectivity (Dynesen *et al.*, 2022, submitted).

The lower RBD subdomain carries the residues involved in HS binding. Our data demonstrate that K342/R343 and R356/R369 are the key residues for the RBD interaction with HS immobilized on an inert matrix or expressed on cells (Fig. IV-6) and that HS is an attachment factor for SFV expands upon previous reports for PFV (Plochmann *et al.*, 2012). In SFV Envs, the residue at position equivalent to 343 in gorilla GII Env is always an arginine or lysine, while arginine is strictly conserved at position 356 (Fig. S.IV-5). Residues at positions 342 and 369 are less conserved among SFV Envs, although they are usually surrounded by positive or polar residues. This suggests that the R343 and R356 may be important for HS binding in all FVs, while other positively charged residues, specific to each virus, can be dispersed in the patch with high positive electrostatic potential (Fig. IV-5A) contributing to the HS binding in a virus-specific context. Existence of an FV receptor had been proposed by Plochmann *et al.* since a total lack of HS did not abolish FV infection, but HS has also been proposed to function as a true FV receptor (Nasimuzzaman and Persons, 2012). The residual Env binding to cells devoid of HS, which we observed both for the WT and the HS-binding impaired variants (Fig. IV-6D), is consistent with the existence of another cell receptor(s) in FV entry. These HS-binding defective Env variants will be useful tools in the research of the potential proteinaceous receptor, as they eliminate binding to HS, which is a widely expressed attachment factor.

Concluding remarks. In this manuscript we have described the first X-ray structure of a FV RBD and validated that the novel fold is the one adopted in the native Env. We identified, within the RBD, two subdomains in terms of their structure, conservation, and function: the upper subdomain, which encompasses the majority of the genotype-specific region, and is likely involved in maintaining the closed prefusion Env conformation, and a more conserved, lower subdomain, important for binding to the attachment factor HS. We generated AF models for 11 additional FV RBDs, highlighting its conserved three-dimensional conformation. This information is critical for understanding virus-cell interactions and provides a framework for structure-driven mutagenesis studies necessary for establishing the molecular basis of FV entry and recognition by neutralizing antibodies as described in Dynesen *et al.* (Dynesen *et al.*, 2022, submitted). The AlphaFold algorithm (Jumper *et al.*, 2021) cannot predict the arrangement of oligosaccharides at the surface of glycoproteins. The previously reported

functional observations on FV Envs, along with the role of N8 can now be understood in light of the experimentally derived structure, underscoring the necessity for structure determination by experimental means. Identification of HS binding residues will aid the search for additional putative FV receptor(s). Insights into the structure-function relationship of the metastable, multimeric and heavily glycosylated FV Env, as well as unraveling the molecular basis of receptor activation and membrane fusion, will require integrated biology efforts and experimental structural methods.

4.5 Materials and Methods

4.5.1 Expression construct design (SFV RBD and ectodomains for HS binding studies)

A flow-cytometry assay was developed by Duda *et al.* to detect binding of recombinantly expressed foamy virus Env variants to cells (Duda *et al.*, 2006). By using a panel of SU truncations fused to the Fc region of murine IgG (immunoadhesins) the authors showed that the RBD – defined as the minimal region of the PFV Env sufficient for binding to cells - encompassed residues 225 to 555 (corresponding to residues 226 to 552 in gorilla FV RBD (GII-K74 strain, accession number JQ867464) (Rua *et al.*, 2012a) (Fig. S.IV-5). When designing the expression construct for SFV RBD, we also considered the secondary prediction generated by the Phyre2 webserver (Kelley *et al.*, 2015). Residue I225 was in the middle of a putative helix (residues 220-230), leading us to choose an upstream residue R218 as the N-terminus of the construct (Fig. IV-1A, Fig. S.IV-5).

The Phyre2 webserver was also used to design the ectodomain construct, which starts after the first predicted transmembrane helix (S91) and encompasses residues up to I905.

4.5.2 Recombinant SFV RBD and ectodomain production and purification

For structural studies the RBD (residues 218-552, GII-K74 strain, Env accession number JQ867464) (Krey *et al.*, 2010) was cloned into a modified pMT/BiP insect cell expression plasmid (Invitrogen) designated pT350, which contains a divalent-cation inducible metallothionein promoter, the BiP signal peptide at the N-terminus (MKLCILLAVVAFVGLSLG), and a double strep tag (DST) (AGWSHPQFEKGGGSGGGSGGGSWHPQFEK) at the C-terminus, as previously described (Krey *et al.*, 2010). This plasmid was co-transfected to *Drosophila* Schneider line 2 cells (S2) with the pCoPuro plasmid for puromycin selection (Backovic and Krey, 2016). The cell line has undergone selection in serum-free insect cell medium (HyClone, GE Healthcare) containing 7 µg/ml puromycin and 1% penicillin/streptomycin. For the protein production stage, the cells were grown in spinner flasks until the density reached approximately 1×10^7 cells/ml, at which point the protein expression was induced with 4 µM CdCl₂. After 6 days, the cells were separated by centrifugation, and the supernatant was concentrated and used for affinity purification using a Streptactin column (IBA). Approximately 20 milligrams of recombinant RBD were obtained per liter of S2 cell culture.

The DST was removed by incubating the protein with 64 units of Enterokinase light chain (BioLabs) in 10 mM Tris-HCl, 100 mM NaCl, 2 mM CaCl₂, pH 8.0, at room temperature, overnight. The proteolysis reaction was buffer exchanged into 10 mM Tris-HCl, 100mM NaCl, pH 8.0, and subjected to another affinity purification, recovering the flow-through fraction containing the untagged RBD. The protein was concentrated and its enzymatic deglycosylation with EndoD and EndoH was set up at room-temperature following overnight incubation with 1000 units of each glycosidase in 50 mM Na-acetate, 200 mM NaCl, pH 5.5. The protein was further purified on a size exclusion chromatography (SEC) column Superdex 200 16/60 (Cytiva) in 10 mM Tris-HCl, 100 mM NaCl, pH 8.0, concentrated in VivaSpin concentrators to 8.2 mg/ml and used as such for crystallization trials.

For cell binding experiments the RBD construct was cloned in a pcDNA3.1(+) derived plasmid, for expression in mammalian cells. The expression plasmid was modified by inserting a CMV exon-intron-exon sequence that increases the expression of recombinant proteins. The RBD was cloned downstream of the CD5 signal peptide (MPMGSLQPLATLYLLGMLVASCLG) with an enterokinase cleavage site and a DST tag in the C-terminus. The HS mutants were generated by site-directed mutagenesis. The plasmids coding for the recombinant proteins were transiently transfected in Expi293F™ cells (Thermo Fischer) using FectroPRO® DNA transfection reagent (Polyplus), according to the manufacturer's instructions. The cells were incubated at 37 °C for 5 days after which the cultures were centrifuged. The protein was purified from the supernatants by affinity chromatography using a StrepTactin column (IBA), followed by SEC on a Superdex 200 10/300 column (Cytiva) equilibrated in 10 mM Tris-HCl, 100 mM NaCl, pH 8.0. The peak corresponding to the monomeric protein was concentrated and stored at -80 °C until used.

The wild-type gorilla GII FV ectodomain was cloned into the pT350 vector and used as a template for generating the heparan-sulphate binding mutants by site-directed mutagenesis. *Drosophila* S2 cells were stably transfected with all the vectors, as previously mentioned. The ectodomains expression followed the same steps reported for the RBD production and after 6 days they were purified from the cell supernatants by affinity chromatography using a StrepTactin column (IBA) and SEC on a Superose 6 10/300 column (Cytiva) in 10mM Tris-HCl, 100 mM NaCl, pH 8.0. The fractions within the peak corresponding to the trimeric ectodomain were concentrated in VivaSpin concentrators and stored at -80 °C until used.

4.5.3 Crystallization

Crystallization trials were performed in 200 nanoliter sitting drops formed by mixing equal volumes of the protein and reservoir solution in the format of 96 Greiner plates, using a Mosquito robot, and monitored by a Rock-Imager at the Core Facility for Protein Crystallization at Institut Pasteur in Paris, France (Weber et al., 2019). The native RBD^D crystal used for data collection was grown in 0.1M Tris pH 8.5, 3.5M sodium formate (NaCOOH). For the derivative data, the RBD^D crystal, grown in 0.1M Tris pH 8.5, 3.25M sodium formate, was soaked overnight in the same crystallization solution supplemented with 0.5M sodium iodide and directly frozen using the mother liquor containing 33% ethylene glycol as cryo-buffer. The RBD^G crystals were obtained from a solution containing 0.2M ammonium tartarate ((NH₄)₂ C₄H₄O₆) and 20% w/v PEG 3350.

4.5.4 X-ray diffraction data collection and SFV RBD structure determination

The native, the derivative (iodine-soaked) and the 'glycosylated' data were all collected at 100K on the Proxima-1 (Chavas et al., 2021) or Proxima-2A beamlines at the SOLEIL synchrotron source (Saint Aubin, France), using the Pilatus Eiger X 16M or Eiger X 9M detectors (Dectris), respectively.

We obtained trigonal crystals, space group 322₁ for the RBD^D (2.6 Å), P3₁21 (later found to be P3₂21) for the derivative RBD^D (3.2 Å), and hexagonal crystals for the RBD^G protein (2.8 Å, space group P6₁). Diffraction data were processed using XDS (Kabsch, 2010) and scaled and merged with AIMLESS (Evans and Murshudov, 2013). The high-resolution cut-off was based on the statistical indicator CC1/2 (Karplus and Diederichs, 2012). Several applications from the CCP4 suite were used throughout processing (Winn et al., 2011). The statistics are given in Table S.IV-1.

To solve the structure of the RBD^D, the AutoSol pipeline from the Phenix suite (Adams et al., 2010; Terwilliger et al., 2009) was employed, using the anomalous data set, searching for 20 iodine sites and specifying two NCS copies in the asymmetric unit (ASU). AutoSol reliably determined the substructure, composed of 20 iodine sites. The refined anomalous phases were internally used to phase the entire protein with the aid of density modification. The result of the process was a structure with a low R-factor; moreover, the density modified map showed a good contrast between the protein and the solvent and helical features clearly

discernible. The initial assignment of the space group of the anomalous data was tentative, as the screw axis that is present in the cell allows for two alternatives ($P3_121$ or $P3_221$). The enantiomorph ambiguity was resolved after density modification with the anomalous phases and model building by looking at the map and its quality. AutoSol unambiguously selected the correct space group, which is $P3_221$. The structure was further improved in Buccaneer (Cowtan, 2006) in 'experimental phases' mode, using the density modified map from AutoSol and the refined substructure from AutoSol. Finally, the BUCCANEER model was refined against the native data at 2.6 Å by iterative rounds of phenix.refine (Adams et al., 2010), BUSTER (Blanc et al., 2004; Bricogne et al., 2009) and Coot (Emsley and Cowtan, 2004), which was used throughout all model building and refinement to inspect and manually correct the model.

To solve the structure of the RBD^G, the RBD^D was used as a search-model in Molecular Replacement in Phaser (McCoy et al., 2007) from the Phenix suite. In this case, the ASU was found to contain two molecules, which were again refined using a combination of BUSTER and phenix.refine.

For both models, the $2|F|_o - |F|_c$ and $|F|_o - |F|_c$ electron density maps were used to unambiguously identify the carbohydrate moieties and built them. For both models, the final stereochemistry was assessed by MolProbity (<http://molprobity.biochem.duke.edu/>) (Chen et al., 2010).

The final maps showed clear, interpretable electron density, except for a region comprising residues 419-427 precluding building on these 9 amino acids and indicating inherent flexibility of the region. The atomic models were refined to R_{work}/R_{free} of 0.21/0.25 and 0.19/0.23, for the RBD^D and RBD^G crystals, respectively.

4.5.5 Cells, viral sequences and production of foamy virus viral vectors

Baby Hamster Kidney (BHK)-21 cells (ATCC-CLL-10) were cultured in DMEM-glutamax-5% fetal bovine serum (FBS) (PAA Laboratories). HT1080 cells (ECACC 85111505) were cultured in EMEM-10% FBS supplemented with 1x L-glutamine and 1x non-essential amino acids (NEAA). Human embryonic kidney 293T cells (CRL-3216) were cultured in DMEM-glutamax-10% FBS.

Foamy virus isolates were named according to the revised taxonomy (Khan et al., 2018) and short names were used for gorilla and chimpanzee strains (Lambert et al., 2018). The four-component FVV system (plasmids pcoPG, pcoPP, pcoPE, pcu2MD9-BGAL (a transfer plasmid

encoding for β -galactosidase)) and the gorilla Env construct containing sequences from the zoonotic and GI-D468 (JQ867465) and GII-K74 (JQ867464) *env* genes (EnvGI-SUGII) have been described (Hütter et al., 2013; Lambert et al., 2018), also in Dynesen *et al.* (Dynesen et al., 2022, submitted). Briefly, the genotype II Env construct we used (EnvGI-SUGII) is comprised of the SU is from the GII-BAK74 genotype, and the LP and TM from the GI strain BAD468, the latter two being very conserved between GI and GII (Lambert et al., 2018).

Mutations in the RBD predicted heparan sulfate binding site (K342A/R343A and R356A/R369A) were introduced to this gorilla Env plasmid containing full-length GII SU. FVVs were produced by co-transfection of four plasmids (gag:env:pol:transgene (β -galactosidase) ratio of 8:2:3:32). Three μ g total DNA and eight μ l polyethyleneimine (JetPEI, #101-10N, Polyplus, Ozyme) were added to 0.5×10^6 HEK 293T cells seeded in 6-well plates. Supernatants were collected 48 hours post transfection, clarified at $1,500 \times g$ for 10 min, and stored as single-use aliquots at -80°C . Vector infectivity was determined by transducing BHK-21 cells with serial five-fold dilutions of vectors and detecting β -galactosidase expression after 72 hours of culture at 37°C . Plates were fixed with 0.5% glutaraldehyde in PBS for 10 min at room temperature (RT), washed with PBS and stained with 150 μ l X-gal solution containing 2 mM MgCl_2 , 10 mM potassium ferricyanide, 10 mM potassium ferrocyanide and 0.8 mg/ml 5-bromo-4-chloro-3-indolyl-B-D-galactopyranoside in PBS for 3 hours at 37°C . Plates were counted on a S6 Ultimate Image UV analyzer (CTL Europe, Bonn, Germany). One blue cell was defined as one infectious unit. Cell transduction by FVV is a surrogate for viral infectivity and FVV titers were expressed as infectious units/ml.

The yield of FVV particles was estimated by the quantification of particle-associated transgene RNA. FVVs RNAs were extracted from raw cell supernatants with QIAamp Viral RNA Extraction Kit (Qiagen). RNAs were treated with DNA free kit (Life Technologies), retro-transcribed with Maxima H Minus Reverse Transcriptase (Thermo Fischer Scientific) using random primers (Thermo Fischer Scientific), according to manufacturer's instructions. qPCR was performed on cDNA using BGAL primers (BGAL_F 5' AAACCTCGCAAGCCGACTGAT 3' and BGAL_R 5' ATATCGCGGCTCAGTTCGAG 3') with a 10-min-long denaturation step at 95°C and 40 amplification cycles (15s at 95°C , 20s at 60°C and 30s at 72°C) carried out with an Eppendorf realplex2 Mastercycler (Eppendorf). A standard curve prepared with serial dilutions of pcu2MD9-BGAL plasmid was used to determine the copy number of FVVs. Results were

expressed as vector particles/ml, considering that each particle carries 2 copies of the transgene.

4.5.6 Prediction of RBD heparan-binding site and mutant design

The server ClusPro (<https://cluspro.org/login.php>) was used for identifying a potential heparin-binding site (Desta et al., 2020; Kozakov et al., 2017; Mottarella et al., 2014; Vajda et al., 2017). The server generated 13 models of a fully sulfated tetra-saccharide heparin fragment docked to the FV RBD and a list of atom-atom contacts between the heparin chain and the protein residues that was used to generate the plots on Fig. IV-5B.

4.5.7 Env interactions with heparan sulfate assayed by binding to heparin-sepharose

100 µg of recombinant FV RBDs (wild-type, R356A/R369A, K342A/R343A) were injected at 1 ml/min onto a Heparin-Sepharose column (Cytiva) previously equilibrated with running buffer (10 mM Tris-HCl, 100 mM NaCl, pH 8.0). After washing, a linear gradient (50% in 30 minutes) of elution buffer (10 mM Tris-HCl, 2M NaCl, pH 8.0) was applied.

4.5.8 Env interactions with heparan sulfate on cells (*in vitro*): Env protein binding assay

HT1080 and BHK-21 adherent cells were detached with Trypsin-EDTA and 5 x 10⁵ cells were used per condition. Cell washing and staining steps were performed in PBS-0.1% BSA at 4°C. SFV Env ectodomains were added to the cell pellet for 1 hour. Cells were washed twice, incubated with anti-StrepMAB-Classic-HRP antibody that recognizes the strep tag at the C-terminus of the SFV Env ectodomain (7.5 µg/ml, IBA Lifesciences #2-1509-001) for 1 hour, washed twice and incubated with the secondary antibody coupled to fluorophore AF488, anti-HRP-AF488 (0.75 µg/ml, Jackson ImmunoResearch, #123-545-021) for 30 min. Cells were washed and fixed in PBS-2% PFA at RT for 10 min and kept at 4°C until acquisition. A minimum of 25,000 cells were acquired on a CytoFLEX cytometer (Beckman Coulter). Data were analyzed using Kaluza software (Beckman Coulter). Viable single cells were selected by the sequential application of gates on FSC-A/SSC-A and SSC-A/SSC-H dot-plots (Fig. S.IV-12A). Cells labelled with the two secondary antibodies only were used as a reference. SFV Env binding was expressed as the ratio of mean fluorescence intensity (MFI) from the cells that were incubated with the recombinant ectodomains vs untreated cells (Fig. S.IV-12B).

4.5.9 Heparan sulfate removal and detection

Cells were treated with Trypsin-EDTA and 5×10^5 cells were labelled per condition. Cells were washed once with PBS-0.1% BSA prior to incubation with 0.1 mIU/ml heparinase III from *Flavobacterium heparinum* (Sigma-Aldrich, #H8891) in 20 mM Tris-HCl, 0.1 mg/mL BSA and 4 mM CaCl_2 , pH 7.45 for 15 min. at 37°C. Heparan sulfate was detected by staining with F58-10E4 antibody (5 µg/ml, AmsBio, UK #370255-S) and anti-mouse IgM-AF488 antibodies (2 µg/ml, Invitrogen #A-21042). The neoantigen generated by HS removal (Δ HS) was detected with the F69-3G10 antibody (10 µg/ml, AmsBio #370260-S) and anti-mIgG-AF647 antibodies (4 µg/ml, Invitrogen #A-31571). Cell staining and washing were performed in PBS-0.1% BSA at 4°C. Incubation times were 60 and 30 min for primary and secondary antibodies, respectively. Cytometer acquisition, and data analysis were performed as described for Env binding (Fig. S.IV-12). Cells labelled with secondary antibodies only were used as a reference. Levels of HS and Δ HS staining were expressed as the ratio of MFI from labelled to unlabeled cells (Fig. S.IV-12C).

4.5.10 FVVs binding assay

HT1080 cells were incubated with FVV particles (1, 10 and 100 particles/cell) on ice for 1h. Cells were washed 3 times with PBS to eliminate unbound FVVs and RNAs were extracted using RNeasy plus mini Kit (Qiagen) according to manufacturer's protocol. RT was performed as described for FVVs RNA quantification. Bound FVV were quantified by qPCR of *bgal* gene as described for vector titration; cells were quantified by a qPCR amplifying the *hgapdh* gene with the following primers: hGAPDH_F 5' GGAGCGAGATCCCTCCAAAAT 3' and hGAPDH_R 5' GGCTGTTGTCATACTTCTCATGG 3'. The qPCR reaction conditions were the same as those used to amplify the *bgal* gene. Relative mRNA expression of *bgal* versus *hgapdh* was calculated using the $-\Delta\Delta\text{Ct}$ method, and relative binding as $2^{-\Delta\Delta\text{Ct}}$.

4.5.11 Statistics

The infectious titers, particle concentration, percentages of infectious particles and quantity of bound FVVs carrying wild-type and mutant SU were compared using the paired t-test.

4.5.12 Data availability

The data related to the X-ray structures determined for the SFV GII RBD^D and RBD^G have been deposited to the RCSB protein databank under PDB accession codes 8AEZ and 8AIZ, respectively.

4.6 Acknowledgements

This work was supported by the ‘Agence Nationale de la Recherche’ [ANR-10-LABX62-IBEID, Intra-Labex Grant, M.B] and the ‘Programme de recherche transversal from Institut Pasteur’ [PTR2020-353 ZOOFOAMENV, F.B.]. The funding agencies had no role in the study design, generation of results, or writing of the manuscript. We thank the staff from the Utechs Cytometry & Biomarkers and Crystallography platform at the Institut Pasteur, the synchrotron source Soleil (Saint-Aubin, France) for granting access to the facility, and to the staff of Proxima 1 and Proxima 2A beamlines for helpful assistance during X-ray data collection. We are grateful to Jan Hellert, Pablo Guardado-Calvo and Philippe Afonso for the discussions and advice, with special thanks to Max Baker for reading the manuscript and English language corrections.

4.7 Author contributions

Conceptualization: MB, FB

Realization of the assays: IF, **LTD**, YC, DB, RP, AH

Resources: MB, FB, FAR, AG

Supervision: MB, FB

Writing—original draft: MB

Writing—review & editing: IF, FB, FAR, **LTD**, AG

Funding acquisition: MB, FB

4.8 Competing interests

The authors have no competing interests to declare.

CHAPTER V

MANUSCRIPT II

5 | MANUSCRIPT II

Neutralization of zoonotic simian foamy viruses: genotype-specific epitopes within the receptor-binding domain

Lasse Toftdal Dynesen^a, Ignacio Fernandez^b, Youna Coquin^a, Manon Delaplace^a, Thomas Montange^a, Richard Njouom^c, Chanceline Bilonga-Ndongo^d, Felix A. Rey^b, Antoine Gessain^a, Marija Backovic^b, and Florence Buseyne^{a,*}

^aInstitut Pasteur, Université Paris Cité, CNRS UMR3569, Unité d'Epidémiologie et Physiopathologie des Virus Oncogènes, 75015 Paris, France

^bInstitut Pasteur, Université Paris Cité, CNRS UMR3569, Unité de Virologie Structurale, 75015 Paris, France

^cCentre Pasteur du Cameroun, Yaoundé, Cameroon

^dMinistère de la Santé Publique, Yaoundé, Cameroon

*Corresponding author: Florence Buseyne, florence.buseyne@pasteur.fr

5.1 Abstract

Simian foamy viruses (SFVs) are retroviruses that are frequently cross-transmitted to humans. SFVs establish life-long infection in their human hosts, with the persistence of replication-competent virus. Zoonotic SFVs do not induce severe pathology and are not transmitted between humans. Infected individuals develop potent neutralizing antibodies (nAbs) that targets the SFV envelope protein (Env). Env carries a variable region that defines two SFV genotypes and is the exclusive target of nAbs. However, its antigenic determinants are not understood. Here, we characterized nAbs from SFV-infected individuals living in Central Africa. The nAbs target conformational epitopes within two major antigenic areas located at the Env apex: One mediates the interaction between Env protomers to form Env trimers and one harbors several determinants of Env binding to susceptible cells. One binding determinant is genotype-specific. We propose a model integrating structural, genetic, functional, and immunological knowledge on the SFV receptor binding domain.

5.2 Introduction

Foamy viruses (FVs) are the most ancient of retroviruses (Pinto-Santini et al., 2017; Rethwilm and Bodem, 2013). Simian foamy viruses (SFVs) are widespread in nonhuman primates (NHPs), replicate in the buccal cavity, and are transmitted to humans mostly through bites by infected NHPs (Betsem et al., 2011; Filippone et al., 2015; Pinto-Santini et al., 2017). Such cross-species transmission events currently occur in Asia, Africa, and the Americas. Most individuals known to be infected with zoonotic SFV live in Central Africa, the region at the epicenter of the emergence of HIV-1 and HTLV-1 from their simian reservoirs. In their human hosts, SFVs establish a life-long persistent infection associated with subclinical pathophysiological alterations (Buseyne et al., 2018; Gessain et al., 2019). Thus far, neither severe disease nor human-to-human transmission have been described, suggesting efficient control of SFV replication and transmission in humans.

SFV infection elicits envelope (Env)-specific neutralizing antibodies (nAbs) that block the entry of viral particles into susceptible cells *in vitro* (Lambert et al., 2018). Although they do not block cell-to-cell infection *in vitro*, antibodies prevent cell-associated SFV transmission by transfusion in monkeys (Couteaudier et al., 2022; Williams and Khan, 2010). SFV Env is cleaved into three subunits, the leader peptide (LP), the surface subunit (SU), which binds to cells, and the transmembrane (TM) subunit, which carries out fusion. In several SFV species, there are two variants of the *env* gene, defining two genotypes (Aiewsakun et al., 2019a; Galvin et al., 2013; Richard et al., 2015). The two variants differ in a discrete region encoding 250 residues, named SUvar, located at the center of the SU and overlapping with most of the receptor-binding domain (RBD) (Duda et al., 2006). The RBD is thus bimorphic and the exclusive target of genotype-specific nAbs (Lambert et al., 2018).

We have determined the RBD structure, which we describe in a co-submitted paper (Fernandez et al., 2022, submitted). Here, we present the epitopic sites that were concomitantly defined by the use of plasma samples from SFV-infected African hunters. These individuals were infected by SFV of gorilla origin through bites (Betsem et al., 2011). We have previously described the infecting strains, *ex vivo* blood target cells, antibody response, and medical status of these individuals (Buseyne et al., 2018; Couteaudier et al., 2019; Couteaudier et al., 2022; Gessain et al., 2019; Lambert et al., 2018; Richard et al., 2015; Rua et al., 2014). We expressed the SU as a soluble recombinant protein that competes with SU present on viral

vector particles for binding to plasma nAbs in a neutralization assay. We defined the regions targeted by the nAbs using mutant SU protein modified at the glycosylation sites (Luftenegger et al., 2005), RBD functional subregions (Duda et al., 2006), genotype-specific sequences that present properties of B-cell epitopes, and structural information (Fernandez et al., 2022, submitted). Finally, we tested whether immunodominant epitopes recognized by nAbs are involved in SU binding to and viral entry into susceptible cells.

5.3 Results

5.3.1 Infrequent binding of plasma antibodies to linear epitopes located on the SUvar domain

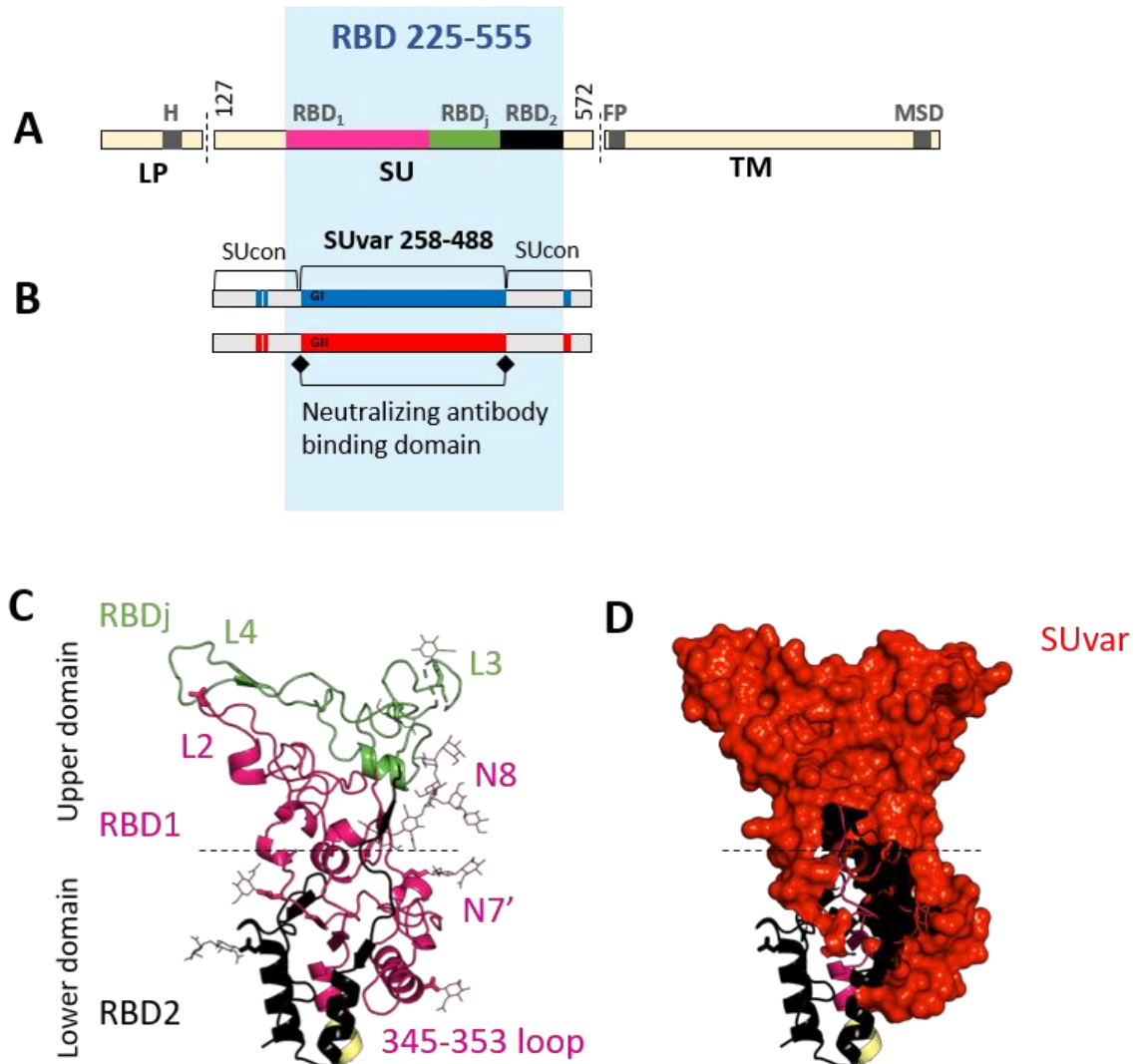
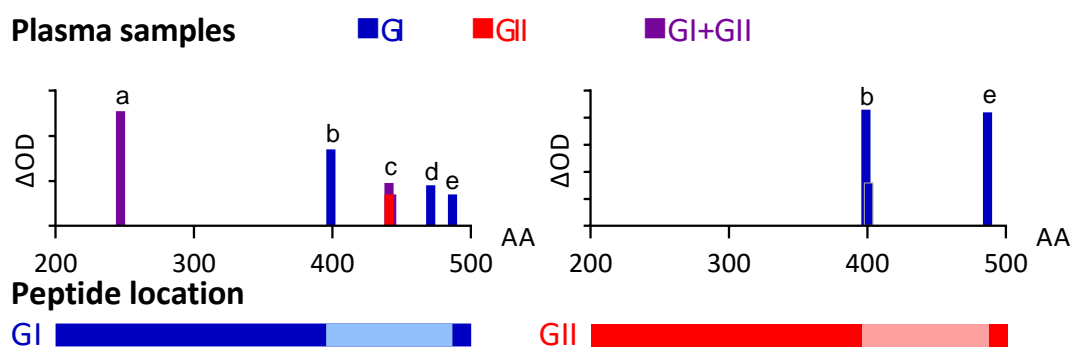


Figure V-1 – SFV Env

A. Schematic representation of SFV Env. The precursor Env protein is cleaved by furin-like protease(s) at two sites (vertical bars) to generate LP, SU, and TM. The dark sections highlight the transmembrane regions of LP (H) and TM (MSD), and the fusion peptide (F). The minimal continuous RBD (aa 225-555, blue background) comprises two regions essential for SU binding to cells, RBD₁ (aa 225-396) and RBD₂ (aa 484-555) (Duda et al., 2006). The intervening region (aa 397-483), named RBD_j, can be deleted without abrogating binding to susceptible cells. **B.** The genotype-specific variable SU region (SUvar, aa 248-488) partially overlaps with the RBD and is the exclusive target of nAbs (Lambert et al., 2018). **C.** The structure of the GII-K74 RBD monomer (aa 218-552, PDB code 8AEZ, (Fernandez et al., 2022, submitted)) is presented in cartoon with glycans shown as sticks. RBD₁, RBD₂, and RBD_j regions are color-coded as on panel A. Structural elements relevant for the present study are indicated, and the full description of the structure is available in (Fernandez et al., 2022, submitted). **D.** The SUvar region (red) is rendered as solvent accessible surface. The conserved region (SUcon) is displayed in cartoon. The dashed line indicates the boundary between the lower and upper RBD subdomains.

We started the epitope mapping project by screening plasma samples for binding to 37 synthetic peptides spanning the SUvar domain from three viral strains (Fig. V-1, Table S.V-1 and S.V-2, Fig. S.V-1). By ELISA, seven of 17 (41%) plasma samples from SFV-infected individuals reacted against at least one peptide; five locations represented by peptides with GI and/or GII sequences were recognized by at least one plasma sample (Fig. V-2). In comparison, 76%, and 71% of plasma samples displayed binding activity against immunodominant viral peptides used as positive controls (see Materials and Methods). Plasma antibodies bound to GI and/or GII peptides irrespective of the SFV genotype against which they were raised. In conclusion, the binding study showed that most SFV-specific antibodies do not recognize genotype-specific linear epitopes.



CI-PFV	LVKYKEPKPW	PKEGLIADQC	PLPGYHAGLT	276
	YNRQSIWDYY			
		BAD468[g1g2]		
GI-D468	LVKYKTPQPW	PSEELIADQC	PLPGYHAGVE	276
	YTTQAIWDYY			
GII-K74	LVKYKTPQPW	PNEGLIADQC	PLPGLADVSE	276
	YPYQAIWDYY			
IKVESIRPAN	WTKSKYGQA	RLGSFYIPSS	LRQINVSHVL	326
FCSDQLYSKW				
IKVEITRPKN	WTSYAQYGNA	RLGSFFIPPH	VRK-NFTHVL	325
FCSDQLYAKW				
AKIENIRPAN	WTSSKLYGKA	RMGSYYIPKR	LRNINNTHIL	326
FCSDVLYSKW				
YNIENTIEQN	ERFLLNKLNN	LTSGTSVLKK	RALPKDWSSQ	376
GKNALFREIN				
YNIENTLLKN	EELLQKKLNN	LTELTSLLKK	RALPRTWTTQ	375
GKNNLFRNIT				
YNLQNSILQN	ENELTKRLSN	LT-IGNKLKN	RALPYEWAKG	375
GLNRLFRNIS				

VLDICSKPES	VILLNTSYYS	<i>FSLWEGDCNF</i>	<i>TKDMISQLVP</i>	426
<u>ECDGFYNN</u> SK				
		b-BAK56[g1]		
VLDVCNRPEM	VLLLNISYDL	<i>FSLWEGDCNY</i>	<i>TKDKISEIVP</i>	425
<u>OCKGFYNN</u> SK				
		b-BAK56[g1] BAK82[g1]		
VLDVCSRPEM	VLLLNKTYYT	<i>FSLWEGDCNI</i>	<i>TRYNVNETVP</i>	424
<u>ECKDFPHRR</u> -				
WMHMHPYACR	FWRSKNEKEE	TKCRDGETKR	CLYYPLWDSP	476
<u>ESTYDFGYLA</u>				
		c-BAD551[g2] BAK55[g1g2] BAK74[g1g2]		
WMHMHPYACR	FWRNKNEKEE	<i>TKCDGRDDNK</i>	<i>CLYYPLWDSP</i>	475
<u>EATYDFGFLA</u>				
-FNDHPYSCR	LWRYREGKEE	VKCLTSDHTR	CLYYPEYSNP	473
<u>EALFDFGF</u> LS				
		d-BAK132[g1]		
YQNNFSPIC	IEQQKIRDQD	YEVYSLYQER	KIASKAYGID	526
<u>TVLFSLKNFL</u>				
		e-BAK56[g1]		
YQNNFSPIC	ISSKOIROOD	YEVYSIYOEC	KLASRIHGID	525
<u>SVLFSLKNFL</u>				
		e-BAK56[g1]		
YMRNFPGPQC	IESTSIRQOD	YEVYSIYOEC	KLASKTYGID	523
<u>SVLFSLKNFL</u>				

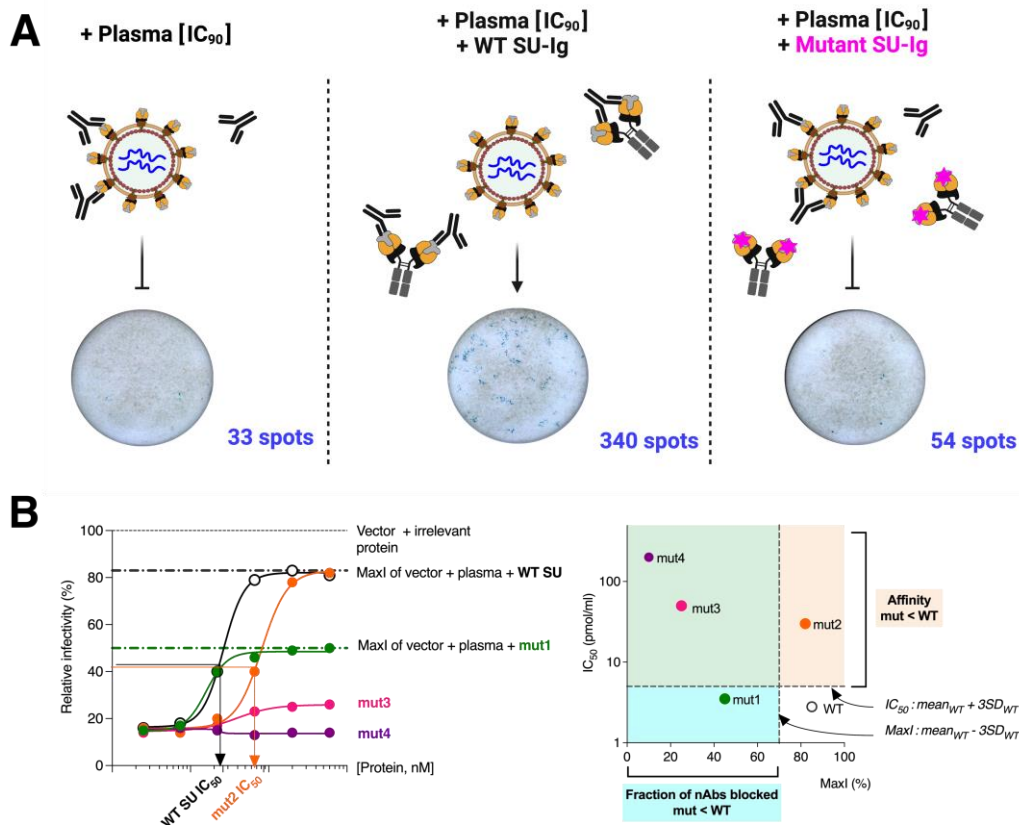
Figure V-2 – Only a small proportion of plasma samples bind to peptides covering the SUvar domain

Seventeen plasma samples from African hunters were tested for binding to 37 peptides located in the SUvar domain (Table S.V-2). The summary graph shows positive responses (Δ_{OD} , y-axis) plotted against peptides identified by the position of their first aa (x-axis). Plasma samples are identified by a color code corresponding to the genotype(s) of the infecting strains (blue: infected with a GI strain, red: infected with a GII strain, purple: infected by strains of both genotypes (Lambert et al., 2018)). Left, peptides spanning GI SUvar; right, peptides spanning GII SUvar; the RBDj region is indicated by the lighter color. Detailed binding activity is shown on the aligned SU sequences; the RBDj sequence is highlighted in italic characters; the sequence covered by peptides is highlighted by grey background. Recognized peptides are underscored and designated by the same letters as those used in panel A. Reactive plasma samples are indicated above the sequence and colored according to the genotype(s) of the infecting strains. Six plasma samples from SFV-infected individuals reacted against seven peptides located in the RBDj region (BAD551, BAK55, BAK56, BAK74, BAK82, and BAK132) and two samples reacted against a peptide located in the RBD1 or RBD2 subdomains (BAD468 and BAK56, respectively). Plasma antibody binding to the peptides was not genotype-specific. For example, sample BAK56 reacted against peptide b (399W-K418) from the GI-D468 and GII-K74 strains.

5.3.2 SFV SU protein competes with the virus for binding to nAbs

We sought to define nAb epitopes by performing neutralization assays in the presence of recombinant SU protein that competes with the SU within Env present at the surface of foamy viral vector (FVV) particles. While wild-type (WT) SU bound to the nAbs, allowing cell infection to proceed, SU mutants with altered nAb epitopes did not (Fig. V-3A and V-3B). We tested

several recombinant Env and SU expression constructs, of which the production level and stability varied according to the genotype: Gorilla genotype II (GII) Env-derived constructs were expressed at high levels, whereas gorilla genotype I (GI) Env-derived counterparts were poorly expressed and aggregated (Fig. S.V-2A). The immunoglobulin Fc domain acts as a secretion carrier for the SU, giving the construct high stability. Such chimeric proteins – referred to as immunoadhesins – have been used to produce soluble SFV SU (Duda et al., 2006). The GI SU immunoadhesin was expressed at insufficient levels, but we readily produced the chimpanzee genotype I (CI) and GII SU immunoadhesins. We therefore studied epitopes recognized by GII-specific nAbs with the GII immunoadhesin (referred to as ^{GII}SU for the WT sequence) and those recognized by GI-specific nAbs with the CI immunoadhesin (^{CI}SU), as allowed by the frequent cross-neutralization of gorilla and chimpanzee strains belonging to the same genotype (Lambert et al., 2018) and CI and GI SUvar sequence identity of 70% (Richard et al., 2015).



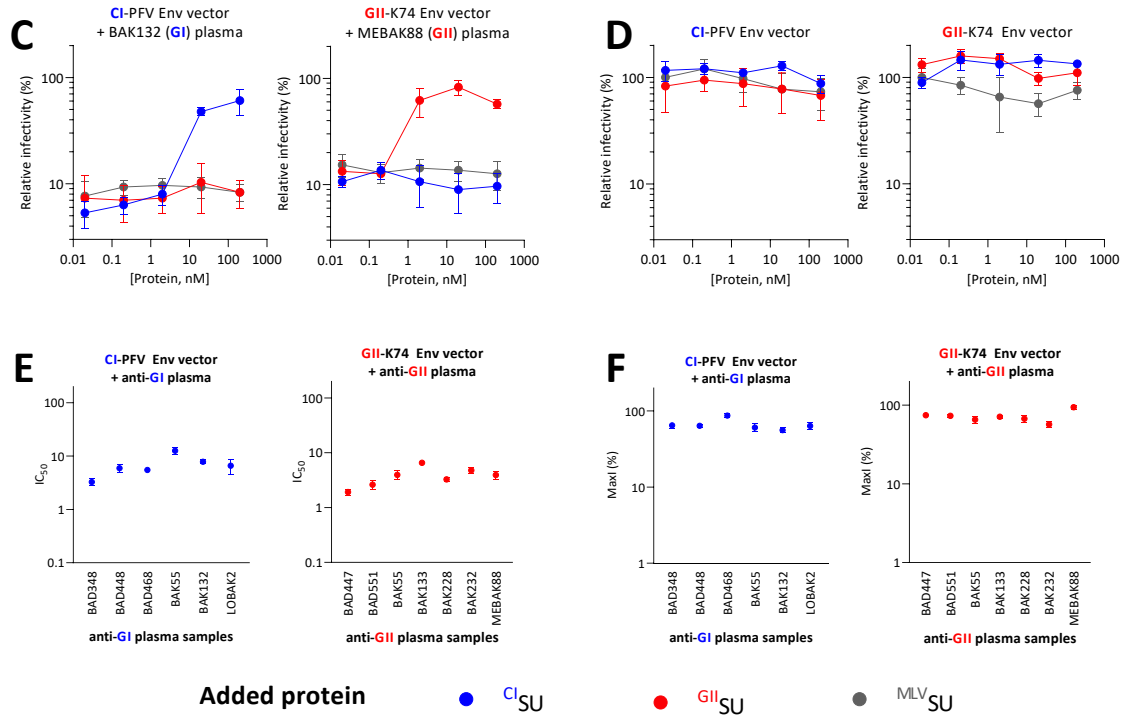


Figure V-3 – The SFV SU block nAbs without affecting viral entry

A. Schematic presentation of the neutralization assay using SU immunoadhesin as competitor. Plasma samples were diluted to achieve a reduction in the number of FVV-transduced cells by 90%. WT immunoadhesins compete with Env on FVV for binding by nAbs, resulting in a higher number of FVV-transduced cells; mutations in SU that affect binding by nAbs result in inefficient competition and reduced FVV transduction. Representative images of wells with FVV-transduced cells stained by X-gal are shown. **B.** Schematic representation of titration curves corresponding to SU mutants that lose their capacity to block a fraction of nAbs (mut1, green), block all nAbs with reduced affinity (mut2 SU, orange), or block a fraction of nAbs with reduced affinity (mut 3, pink) or those with no blocking activity (mut4, purple). The curves are summarized by two parameters, MaxI and IC₅₀, which were compared to those obtained with WT SU (panel C and D) to define significant differences in binding (see Materials and Methods). **C.** The BAK132 (anti-GI) and MEBAK88 (anti-GII) plasma samples were incubated with immunoadhesins and the mix added to FVVs expressing matched Env before titration. The relative proportion of transduced cells is expressed as the percentage of cells transduced by untreated FVVs (no plasma and no protein), is referred to as the relative infectivity, and is presented as a function of protein concentration. The addition of Cl^ISU (blue symbols) inhibited the action of nAbs from sample BAK132, as shown by increased CI-PFV Env FVV relative infectivity, whereas GII^ISU (red symbols) had no effect. Conversely, GII^ISU inhibited the action of nAbs from sample MEBAK88. MLV^ISU (grey symbols) had no effect on the plasma antibodies. **D.** The infectivity of the CI-PFV and GII-K74 Env vectors was quantified in the presence of Cl^ISU, GII^ISU, and MLV^ISU; the relative infectivity is presented as a function of protein concentration. **E and F.** Thirteen pairs of plasma samples and genotype-matched immunoadhesins were tested at least five times for their activity against FFVs. The mean and standard error of the mean of the IC₅₀ (panel E) and MaxI (panel F) are shown for the CI-PFV Env vectors and anti-GI plasma samples (blue symbols) and the GII-K74 Env vectors and anti-GII plasma samples (red symbols).

We validated the competition strategy with genotype-matched and mismatched immunoadhesins (Fig. V-3, Table S.V-3 and S.V-4). We tested plasma samples from gorilla SFV-infected hunters at the dilution required for 90% reduction of FVV infectivity (IC₉₀) to allow Env-specific antibody saturation by the competitor immunoadhesin. Thus, plasma

samples were tested at the same nAb concentration and responses from different individuals could be compared. We incubated immunoadhesins with plasma samples before addition to a FVV expressing the matching envelope protein and titration of residual infectivity. Both ^CISU and ^{GII}SU blocked the action of nAbs present in genotype-matched plasma samples in a concentration-dependent manner but failed to block the activity of genotype-mismatched samples (Fig. V-3C). Importantly, the immunoadhesins did not affect SFV entry (Fig. V-3D, (Berg et al., 2003)), allowing their use as competitors for binding to nAbs in an infectivity assay. The unrelated MLV SU construct (^{MLV}SU) had no impact on either the neutralizing activity of plasma samples or SFV infectivity (Fig. V-3C and V-3D). We titrated 12 samples against matched ^CISU and ^{GII}SU, including one from a coinfecting individual which was tested against both immunoadhesins, leading to 13 sample-immunoadhesin pairs tested. Immunoadhesin's effect on nAb can be described by its affinity and by the fraction of plasma nAb blocked. The IC₅₀, a measure of affinity, ranged between 3.3 and 12.6 nM for ^CISU and 2.9 and 12.5 nM for ^{GII}SU, depending on the plasma sample (Fig. V-3E). Taking FVV treated with ^{MLV}SU without plasma as a reference value for full infectivity (100%), ^CISU and ^{GII}SU restored the infectivity of plasma-treated FVV to between 56% and 94% of infectivity. This value is referred to as maximum infectivity (MaxI) and quantifies the proportion of nAb blocked by the immunoadhesin (Fig. V-3B and V-3F). We used the values from at least five independent experiments to calculate the IC₅₀ and MaxI threshold values to define the nAb blocking activity of mutated recombinant proteins as being significantly different from that of WT SU (Fig. V-3B).

We evaluated the impact of SU oligomerization and mammalian-type glycosylation on its capacity to block nAbs by testing the following constructs: SU monomers produced in mammalian and insect cells, trimeric Env ectodomains produced in insect cells, and dimeric SU (i.e., immunoadhesin) produced in mammalian cells. All had the same capacity to block the nAbs (Fig. S.V-2B). Therefore, we used the only recombinant proteins available for both genotypes, the SU immunoadhesins. We first studied GII-specific nAbs using ^{GII}SU before testing GI-specific nAbs using ^CISU.

5.3.3 Certain nAbs target glyco-epitopes

The GII SUvar domain carries seven of the 11 SU glycosylation sites (Fig. V-4A and V-4B). We assessed whether these glycans are recognized by nAbs or whether they shield epitopes

from nAb recognition. We produced ^{GII}SU in the presence of the mannosidase inhibitor kifunensine, which prevents complex-type glycan addition, or treated it with endo-H to remove all glycans. The absence of complex glycans had no impact on nAb blockade by ^{GII}SU (Fig. V-4C), confirming data obtained with GII Env constructs expressed in insect cells, which also lack complex glycans (Fig. S.V-2). By contrast, the removal of all glycans decreased nAb blockade and protein titration showed lower affinity for the nAbs present in three out of four plasma samples (Fig. V-4D). Endo-H treatment did not induce protein aggregation (Fig. S.V-4) but may have a global effect on the SU affecting SFV-specific nAbs. Conversely, glycans did not shield major nAb epitopes on SFV Env, as their removal did not enhance nAb blockade in the samples tested.

The N10 glycosylation site is located at different positions for the two genotypes and may be part of a potential epitopic region (N422/N423 on GI-D468/CI-PFV strains, N411 on the GII-K74 strain). The N10 glycosylation knock-down mutant (^{GII}ΔN10) was as efficient as ^{GII}SU in blocking nAbs from all plasma samples (Fig. V-4E). N10 belongs to a stretch of seven genotype-specific residues that were replaced by those from the GI-D468 strain. The chimeric protein (^{GII}swap407) blocked nAbs as efficiently as ^{GII}SU for three samples and showed decreased affinity against nAbs for one sample (Fig. V-4F). Thus, GII-specific nAbs occasionally target the N10 glycosylation site.

To identify other glycosylation sites targeted by nAbs, we knocked them down one by one, except for N8, which is critical for SU expression (Luftenegger et al., 2005). The ^{GII}ΔN7' mutant showed reduced capacity to block nAbs from five of the seven samples (Fig. V-4J). ^{GII}ΔN5 and ^{GII}ΔN9 showed reduced capacity to block nAbs from one or two plasma samples (Fig. V-4G and V-4K). Knock down of N6 and N7 had no impact (Fig. V-4H and V-4I). Overall, our data support that most glycans are not part of glyco-epitopes, except those at the N7' glycosylation site.

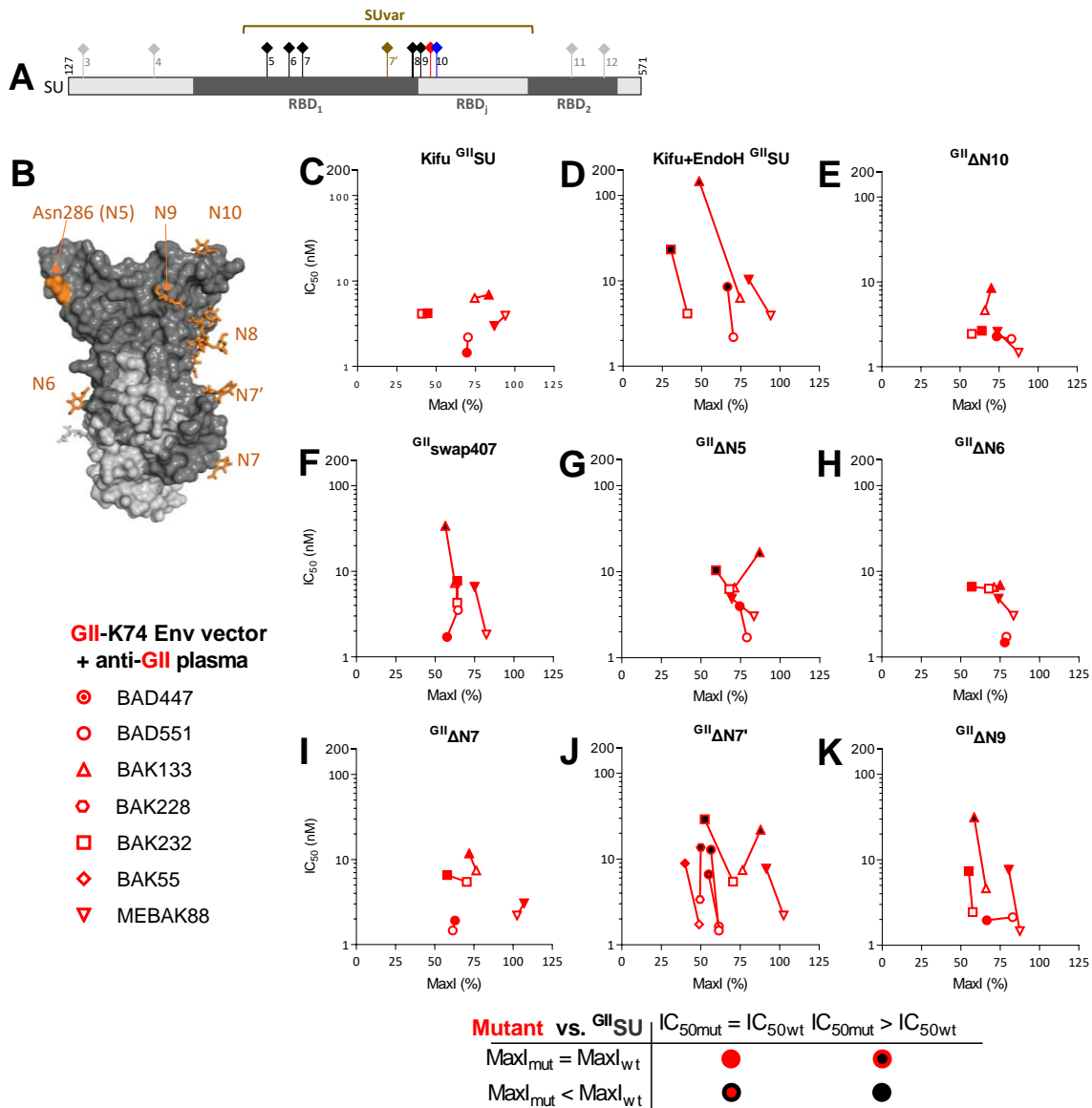


Figure V-4 – SFV-specific nAbs recognize glycans on SUvar

A. Schematic representation of N-glycosylation sites on the SUvar domain. The N7' site (position 374, brown symbol) is absent from CI-PFV but present in zoonotic gorilla SFV and several chimpanzee SFVs (Richard et al., 2015). The N8 site (position 391, bold stem) is required for SU expression (Luftenegger et al., 2005). The N10 site has a genotype-specific location (N411 in GII strains, red symbol; N422 or 423 in GI/CI strains, blue symbol). The glycosylation sites outside SUvar are shown in grey. **B.** The RBD is shown as a solvent accessible surface, with SUvar in dark grey and SUcon in light grey. Side chains of the glycans are shown in orange and were identified on deglycosylated RBD; the N5 glycan was poorly resolved and N286 is colored to indicate the localization of its anchor. **C and D.** To determine whether SFV-specific nAbs target residue glycosylated epitopes, vectors carrying CI-PFV or GII-K74 Env were mixed with four genotype-matched plasma samples previously incubated with untreated, kifunensine (C), or kifunensine and endo-H treated (D) ^{GII}SU at several concentrations. **E.** To test whether nAbs target the genotype-specific N10 glycosylation site, the immunoadhesin in which N10 was inactivated (^{GII}ΔN10) was incubated with four genotype-matched plasma samples. **F.** Residues 407-413 were swapped with those from the GI-D468 strain and the resulting ^{GII}swap407 was tested for its ability to block four anti-GII plasma samples. **G to K.** The glycosylation sites located on the immunoadhesins were inactivated one by one (except N8) and tested for their inability to block four GII-specific plasma samples. ^{GII}ΔN7' was tested against

three additional samples to confirm its impact on nAbs (J). For each plasma sample, the IC₅₀ is presented as a function of MaxI for untreated and enzyme-treated GII^ISU (C and D) or GII^ISU and mutated immunoadhesins (E to K). The IC₅₀ and MaxI values for untreated GII^ISU are presented as open symbols and are from the same experiment in which the mutant immunoadhesins were tested. For the enzyme-treated and mutated immunoadhesins, the symbols are colored according to the IC₅₀ and MaxI thresholds that were used to statistically define significant differences from GII^ISU.

5.3.4 SFV-specific nAbs target loops at the RBD apex

Next, we aimed to locate nAb epitopes on the SU subdomains involved in binding to susceptible cells (Aiewsakun et al., 2019a). Two regions of the RBD were identified as being essential for binding (RBD1 and RBD2) and the region in between (RBDj) could be deleted without fully compromising cell binding (Fig. V-1A, V-1C, V-5A and V-5B). The SUvar region encompasses RBD1 (except its first 16 N-term residues), RBDj, and the seven N-terminal residues of RBD2 (Fig. V-1B, V-1D). We first constructed a mutant immunoadhesin with RBDj deleted. GII^IΔRBDj was highly impaired in blocking nAbs from three individuals: the IC₅₀ values were above the highest concentration tested (200 nM) and the MaxI values were close to 10%, the value of plasma samples incubated with the irrelevant M^{LV}SU (Fig. V-5C). By contrast, GII^IΔRBDj blocked nAbs from the BAD551 plasma sample as efficiently as GII^ISU.

Then, we used the recently discovered RBD structural elements. In the lower subdomain, the main candidate epitopic region was the heparan sulfate glycosaminoglycan binding site (HBS). The GII Env ectodomain mutated on HBS residues (GII^IK342A/R343A or GII^IR356A/R369A, (Dynesen et al., 2022, submitted)) blocked nAbs from three samples as efficiently as their WT counterpart and showed lower affinity for the MEBAK88 plasma sample (Fig. V-5D and V-5E). Thus, nAb activity is modestly affected by mutated HBS residues.

The X-ray structure of the RBD showed that four loops emanate from the upper domain (Fernandez et al., 2022, submitted). L1 is shielded at the center of the trimer and is probably not accessible to nAbs, whereas L2 (276-281), L3 (416-436), and L4 (446-453) are exposed to solvent, mobile, and therefore considered to be candidate epitopic regions. Furthermore, L3 and L4 are located in the RBDj region, which is a major target of nAbs (Fig. V-5C). We deleted the loops individually (Fig. V-5F-H). GII^IΔL3 blocked all GII-specific samples but one, although with lower affinity. GII^IΔL2 and GII^IΔL4 showed plasma-dependent effects, with three patterns: (1) full activity (such as against BAD551) (2), full loss or a strong reduction of activity (for example, against BAK133), (3) or reduction of the MaxI with unchanged affinity (such as

MEBAK88). The last pattern probably reflects the presence of nAbs targeting different epitopes within the same plasma sample, some epitopes being altered on mutant immunoadhesins while others are not.

Even though L2, L3, and L4 are mobile in the structure of the RBD monomer (Fernandez et al., 2022, submitted), the plasma samples did not recognize synthetic peptides spanning these loops (Fig. S.V-5), indicating that they may be part of conformational epitopes. Overall, we show that nAbs from most samples target conformational epitopes at the RBD apex, some being carried by L2, L3, and L4.

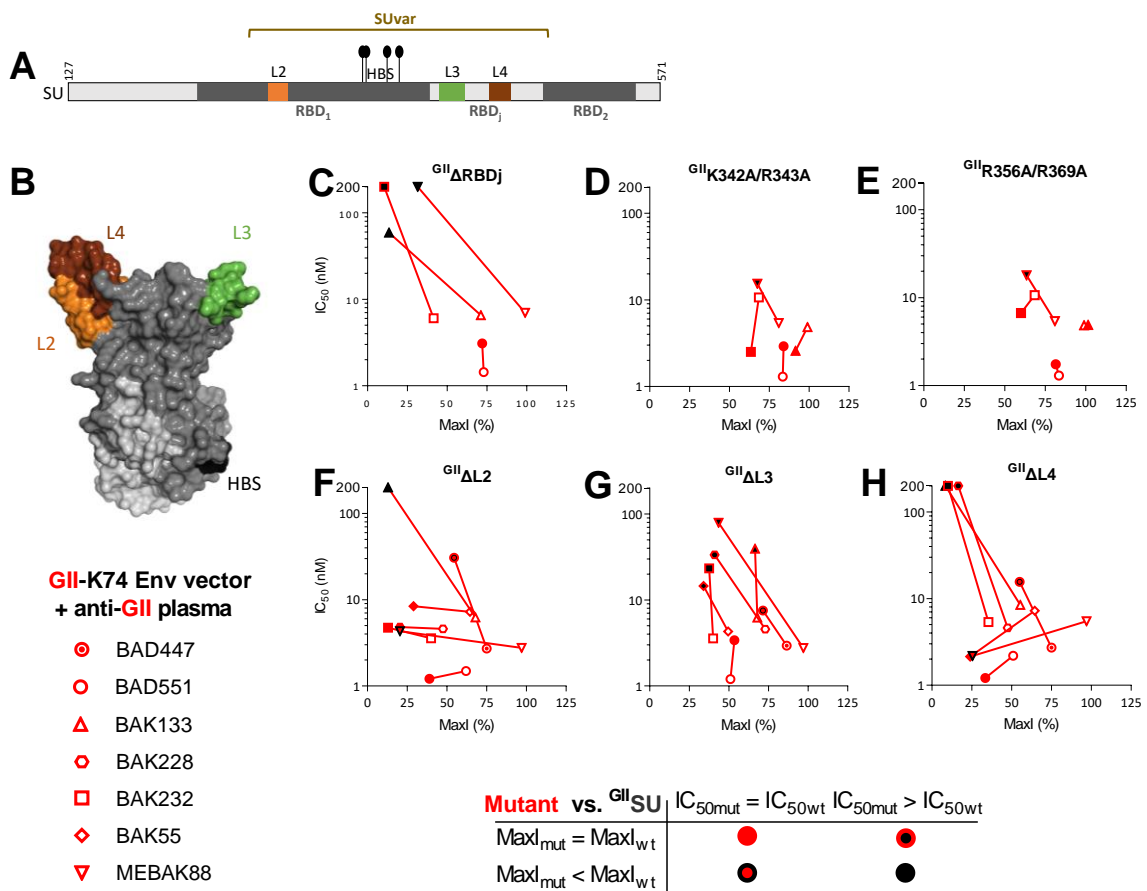


Figure V-5 – Most SFV-specific nAbs recognize the RBDj domain

A. Schematic representation of functional RBD subdomains (Duda et al., 2006), loops, and HBS identified in (Fernandez et al., 2022, submitted). **B.** The RBD is shown as a solvent accessible surface with SUvar in dark grey, SUcon in light grey, L2 in orange, L3 in green, L4 in maroon, and HBS in black. To locate SFV-specific nAb epitopes on SU functional domains, vectors carrying GII-K74 Env were treated with GII-specific plasma samples previously incubated with $G^{II}SU$ and mutant immunoadhesin with RBDj deleted ($G^{II}\Delta RBD_j$, **C**), the Env ectodomain with WT or mutated HBS ($G^{II}K342A/R343A$ in panel **D** and $G^{II}K356A/R369A$ in panel **E**), and immunoadhesins with deleted loops ($G^{II}\Delta L2$, $G^{II}\Delta L3$, and $G^{II}\Delta L4$ in panels **F** to **H**). For each plasma sample, the IC_{50} is presented as a function of $MaxI$ for $G^{II}SU$ and the mutated immunoadhesins. The IC_{50} and $MaxI$ values for $G^{II}SU$ are presented as open

symbols and are from the same experiment in which the mutant immunoadhesins were tested. Symbols are colored according to the IC₅₀ and MaxI thresholds used to define statistically significant differences from GII^{WT}SU; we applied the same threshold values for the analyses of the Env ectodomain, which had the same inhibitory activity as GII^{WT}SU (Fig. S.V-2).

5.3.5 SFV-specific nAbs target the base of the SUvar region

Before the 3D structure was available, we used the insertion of N-linked glycosylation sequences (NXS/T) to disrupt potential epitopes. We selected seven genotype-specific sequences predicted to have a disordered secondary structure or to contain a B-cell epitope and built mutant immunoadhesins with a glycosylation site inserted in the targeted sequence (Fig. V-6A, V-6B, Table S.V-5). Four of the seven glycans were inserted in the upper subdomain and resulted in decreased affinity against certain plasma nAbs: GII⁴²⁶_{glyc} in L3, GII⁴⁵⁰_{glyc} in L4, GII⁴⁵⁹_{glyc} after L4, and GII⁴⁸⁵_{glyc} in RBDj (Fig. V-6C-F). GII²⁶³_{glyc} had no or only a modest effect on nAb activity, which is consistent with its location at the center of the trimer (Fig. V-6G, (Fernandez et al., 2022, submitted)). Overall, glycan insertions at five sites of the RBD upper subdomain confirmed its frequent recognition by nAbs.

One immunoadhesin with glycans inserted in the lower RBD subdomain (GII³⁵¹_{glyc}) showed a strongly reduced capacity to block the nAbs (Fig. V-6H). The modified residue is located on a solvent-exposed loop at the base of the SUvar region (aa 345-353) (Fig. V-6B and V-6B'). GII³⁵¹_{glyc} was the first mutant to indicate that nAbs recognize a region of the RBD to which no function has yet been attributed. We therefore focused the following experiments on this novel epitopic region.

As GII³⁵¹_{glyc} was prone to aggregation (Fig. S.V-4H), we produced a second batch, half of which was purified by affinity chromatography (standard protocol) and the other half further purified by size exclusion chromatography (SEC) to eliminate aggregates. Both GII³⁵¹_{glyc} preparations were unable to block nAbs from the plasma samples (Fig. S.V-6A-E). Glycan insertion at an adjacent position in GII³⁵⁰_{glyc} led to the loss of nAb blockade and reduced aggregation (Fig. V-6I). The GII 345-353 loop is one residue shorter than that of the GI-D468 and CI-PFV strains (Fig. V-6B'). The mutant immunoadhesin with an extra E at position 349 (GII^{349+E}) showed a strongly reduced capacity to block the nAbs (Fig. V-6J). We replaced the seven GII residues by the eight residues from the GI-D468 strain; GII^{swap345} showed a reduced ability to block nAbs from five of the seven plasma samples (Fig. V-6K). By contrast, swapping

the $\alpha 3$ -helix located N-terminal to the loop (G^{II} swap333) had no impact on the capacity to block the nAbs (Fig. V-6L). Finally, we tested the substitution of residues on the $\alpha 8$ -helix facing the 345-353 loop; G^{II} E502A and G^{II} L505N showed a reduced capacity to block the nAbs (Fig. V-6M-N). Overall, these experiments define the 345-353 loop and adjacent $\alpha 8$ -helix as a major epitopic region on GII RBD.

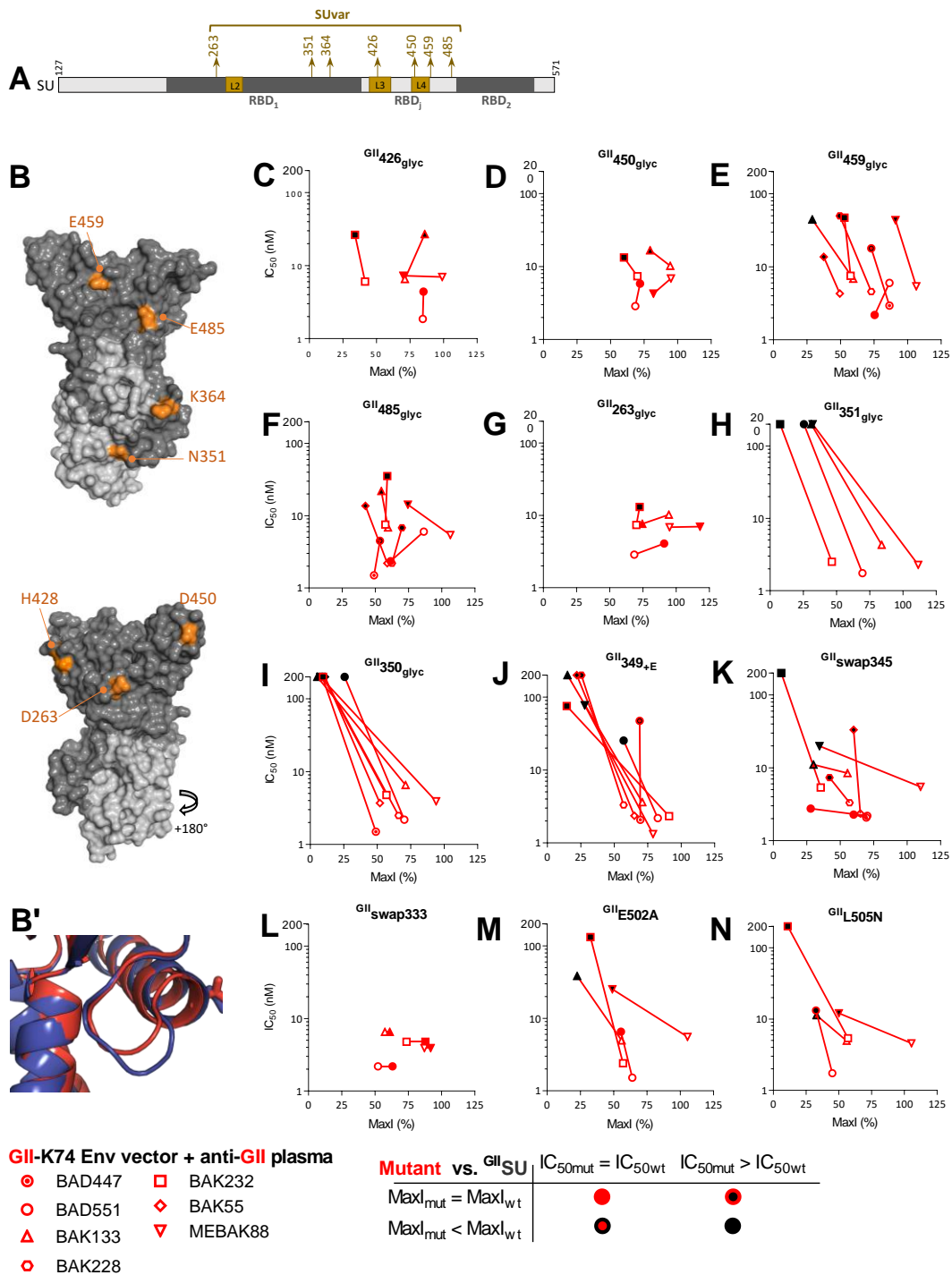


Figure V-6 – Epitope disruption by glycan insertion revealed additional sites recognized by nAbs

A. Schematic representation of the seven sites of glycan insertion on SU. Functional RBD subdomains and loops are indicated using the same color code as in Fig. V-5. **B.** The RBD is shown as a solvent accessible surface with SUvar in dark grey, SUcon in light grey, and the seven glycan insertion sites in orange; front (top) and back (bottom) views are shown. **B'.** The 345-353 loop and adjacent helix are presented as ribbons and side chains for GII-K74 (red) and CI-PFV (blue, AlphaFold2-predicted structure). **C to I.** Seven candidate genotype-specific sequences (Table S.V-5) were disrupted by inserting glycans in the immunoadhesins that were tested for their capacity to block nAbs. **J to M.** Five mutant immunoadhesins were tested to characterize the epitopic region in the 345-353 loop. All mutants were tested against at least four plasma samples. Those for which the capacity to block nAbs was the most altered were then tested on additional samples. For each plasma sample, the IC_{50} is presented as a function of MaxI for ^{GII}SU and the mutant SUs. The IC_{50} and MaxI values of ^{GII}SU are presented as open symbols and are those from the same experiment in which the mutated immunoadhesins were tested. Symbols are colored according to the IC_{50} and MaxI thresholds used to statistically define significant differences from ^{GII}SU . $^{GII}swap333$ was tested twice at three concentrations and showed similar blocking capacity as ^{GII}SU ; the IC_{50} values were arbitrarily set to the same level as those of ^{GII}SU (see Materials and Methods).

5.3.6 GI and GII-specific nAbs target different epitopes

We applied a similar strategy using GI-specific plasma samples and ^{CI}SU harboring the mutations with the greatest impact on GII-specific epitopes. We present these data with a comparison with those obtained with the GII-specific samples (Fig. V-7, blue symbols over light red lines). GI-specific nAbs targeted glycans removed by endo-H but not complex glycans and did not recognize N10, for which the presence is genotype-specific (Fig. V-7A-7C). We could not test the recognition of N7', as it is absent from the CI-PFV strain.

The most striking difference between GI and GII epitopes was around residue 350: in sharp contrast to $^{GII}351_{glyc}$ (Fig. V-6H) and $^{GII}350_{glyc}$ (Fig. V-6I), $^{CI}350_{glyc}$ fully blocked GI-specific nAbs (Fig. V-7D). Neither $^{CI}\Delta RBDj$ nor $^{CI}\Delta L3$ proteins blocked the nAbs (Fig. V-7E and V-7G). Thus, L3 is more important for GI- than GII-specific nAbs. Indeed, $^{GII}\Delta L3$ blocked GII-specific nAbs, although with lower affinity than ^{GII}SU . $^{CI}\Delta L2$ and $^{CI}\Delta L4$ showed sample-dependent effects, as their GII counterparts (Fig. V-7F and V-7H). $^{CI}463_{glyc}$ blocked GI-specific nAbs, with a reduced MaxI (Fig. V-7I), indicating that a fraction of GI-specific nAbs was not blocked, whereas the other was blocked as efficiently as by ^{CI}SU . The corresponding $^{GII}459_{glyc}$ mutant blocked GII-specific nAbs, but with lower affinity than ^{GII}SU (Fig. V-6E). Overall, nAbs from GI- and GII-specific plasma samples target different epitopes.

The mutations on the SU immunoadhesins may have induced epitope-specific or nonspecific conformational changes. The RBDj deletion had a likely epitope-specific effect on the GII backbone, as $^{GII}\Delta RBDj$ retained its capacity to block one sample containing nAbs that preferentially targeted epitopes outside the RBDj (Fig. V-5C). However, $^{CI}\Delta RBDj$ and $^{CI}\Delta L3$ did

not display any nAb blocking activity. Thus, we confirmed the results using chimeric immunoadhesins: ^{GII}swapRBDj (i.e., GI RBDj in ^{GII}SU) blocked nAbs from the four anti-GI plasma samples with a similar or modestly reduced capacity relative to that of ^{CI}SU (Fig. V-7J), whereas ^{GII}SU had no blocking activity (Fig. V-7K). ^{CI}swapL3 (GII L3 in ^{CI}SU) did not block the nAbs (Fig. V-7L). These data suggest that either GI-specific nAbs recognize the L3 loop or that the L3 loop requires a matching interaction to adopt its native conformation.

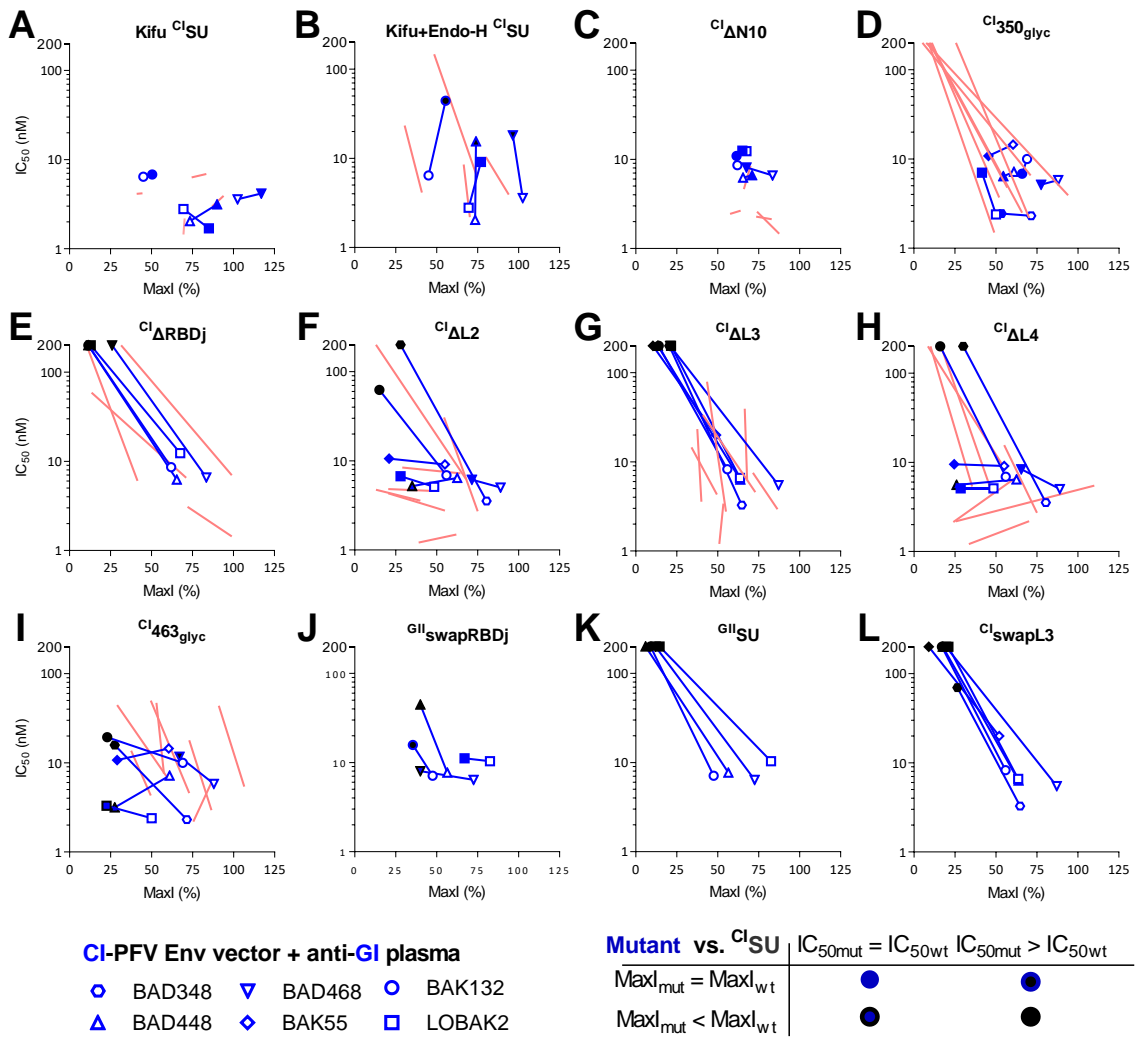


Figure V-7 – GI and GII-specific nAbs target different epitopes

CI SU immunoadhesins with mutations matching the most informative GII-K74 mutations were tested for their capacity to block nAbs from GI-specific plasma samples. **A**, Kifunensin-treated ^{CI}SU; **B**, Kifunensin and endoH-treated ^{CI}SU; **C**, ^{CI}ΔN10; **D**, ^{CI}350_{glyc}; **E**, ^{CI}ΔRBDj; **F**, ^{CI}ΔL2; **G**, ^{CI}ΔL3; **H**, ^{CI}ΔL4; **I**, ^{CI}463_{glyc}; **J**, ^{GII}swapRBDj; **K**, ^{GII}SU; **L**, ^{CI}swapL3. All mutants were tested against four plasma samples. Those for which the capacity to block nAbs was the most altered were then tested on additional samples. For each plasma sample, the IC₅₀ is presented as a function of MaxI for the ^{CI}SU and mutant immunoadhesins. The IC₅₀ and MaxI values of ^{CI}SU are presented as open symbols and are those from the same experiment in which the mutant immunoadhesins were tested. For mutant immunoadhesins, the symbols are colored according to the IC₅₀ and MaxI thresholds used to statistically

define significant differences from ^{C1}SU. The red lines correspond to data obtained with GII-specific plasma samples against equivalent constructs (Panels V-4C, 4D, 4E, 5C, 5F, 5H, 6E, and 6H match panels V-7A to 7H, respectively).

5.3.7 Human plasma samples contain nAbs targeting a variable number of epitopic regions

The effect of the mutant SU on each plasma sample can be summarized as recognition similar to that as for WT SU, recognition with a reduced affinity (i.e., increased IC₅₀), blocking a smaller fraction of nAbs than WT SU (i.e., reduced MaxI), or having both effects (Fig. V-8). We grouped the most relevant mutants according to their location: the RBD apex, the 345-353 loop, and the N7' region. We tested the recognition of the N7' region by GII-specific samples only. This summary highlights the two genotype-specific and immunodominant epitopic regions that we identified: loop 345-353 on ^{GII}SU (Fig. V-8A) and L3 on ^{C1}SU (Fig. V-8B). Within the RBD apex, four mutant immunoadhesins correspond to different epitopic sites (L2, L3, L4, and 459/463^{glyc}). GI-specific plasma samples contained nAbs focused on a single subdomain (such as BAK55 and ^{C1}L3) or epitopes on up to four sites (BAD348 and BAK132). Similarly, GII-specific plasma samples presented interindividual variations in their specificity.

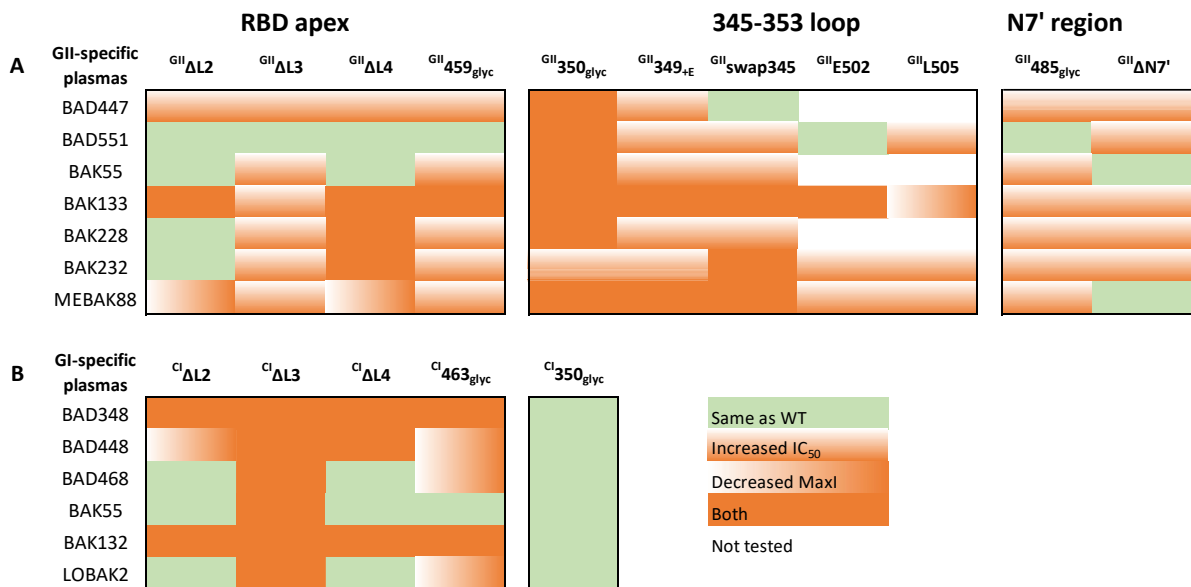


Figure V-8 – Most samples contain nAbs that recognize several epitopic regions on SUvar

The results from competition experiments were summarized for each plasma sample and for the mutant immunoadhesins from the most targeted regions (apex, 345-353 loop, and the N7' region). Four outcomes are presented: same recognition as WT SU (green), recognition with reduced affinity (i.e., increased IC₅₀, orange vertical shading), blocking a smaller fraction of nAbs than WT SU (i.e., reduced MaxI, orange horizontal shading),

or having both effects, orange. Black squares indicate the major epitopic regions of the GII- and GI-specific samples (panels A and B, respectively). Within each epitopic region defined by several mutant immunoadhesins, nAb specificity varied between individuals.

We examined the sequence of the identified epitopes and found that all were conserved on the SFV strains infecting individuals from this study or circulating in Central Africa (Fig. S.V-7). Overall, we identified three immunodominant epitopic regions (RBD apex, 345-353 loop, and N7' region), of which the sequences are conserved within each genotype. We provide evidence that SFV-infected individuals have nAbs that target several epitopes and recognize epitopes that differ between individuals.

5.3.8 Functional studies

5.3.8.1 Protein binding to susceptible cells

All immunoadhesins used for epitope mapping were tested for their capacity to bind to human HT1080 cells, which are highly susceptible to gorilla and chimpanzee SFVs (Couteaudier et al., 2019) (Fig. V-9A, Fig. S.V-8). Immunoadhesin binding was enhanced after glycan removal, possibly through reduced steric hindrance. Deletion of the RBDj reduced binding to susceptible cells, while one-by-one deletion of loops L2, L3, and L4 abolished it. We observed genotype-specific differences; the RBDj deletion had a stronger impact on GII than on CI immunoadhesins (6- vs. 2.5-fold reduction). Conversely, glycan insertion after L4 had only a moderate impact on the GII immunoadhesin (GII^{459}_{glyc} , 6-fold reduction) but abolished binding of the CI immunoadhesin (CI^{463}_{glyc} , ≈ 100 -fold reduction). In the 345-353 loop, glycan insertion strongly affected the binding of GII immunoadhesins (GII^{350}_{glyc} and GII^{351}_{glyc} , ≈ 50 -fold reduction), but there was no effect on CI immunoadhesins, mirroring the recognition by the nAbs. Overall, our data suggest that certain residues involved in cell binding may be genotype-specific.

The binding data were also considered for the interpretation of nAb blocking experiments. The mutant immunoadhesins that retained their capacity to bind cells were considered to likely be properly folded and loss of nAb blockade could be considered as being due to mutation of the epitope. Overall, a single mutated adhesins failed to bind cells and block the nAbs from all samples tested and related data are not presented.

5.3.8.2 The epitopic regions targeted by nAbs are involved in viral infectivity

We then tested the impact of RBDj and loop deletions in the context of FVVs. We produced FVVs with Env mutants corresponding to the immunoadhesins most affected in blocking genotype-specific nAbs (i.e., Δ RBDj and Δ L3 CI-PFV, Δ RBDj, Δ L2, and Δ L4 GII-K74 Env). The quantity of FVV particles carrying deletions was strongly reduced, over 1000-fold for CI-PFV Δ RBDj, over 100-fold for CI-PFV Δ L3 and GII-K74 Δ RBDj, and over 50-fold GII-K74 Δ L2 and Δ L4 (Fig. V-9B), despite all mutant Env being expressed in transfected cells (Fig. S.V-9). Moreover, none of the FVVs with mutant Env were infectious (Fig. V-9C). However, most bound to susceptible cells at levels 2 to 4-fold below those of FVVs with WT Env, except the CI-PFV Δ RBDj mutant, for which the binding was reduced \approx 30-fold) (Fig. V-9D). In conclusion, the regions from the upper RBD subdomain targeted by nAbs are required for viral infectivity independently of their capacity to bind to susceptible cells.

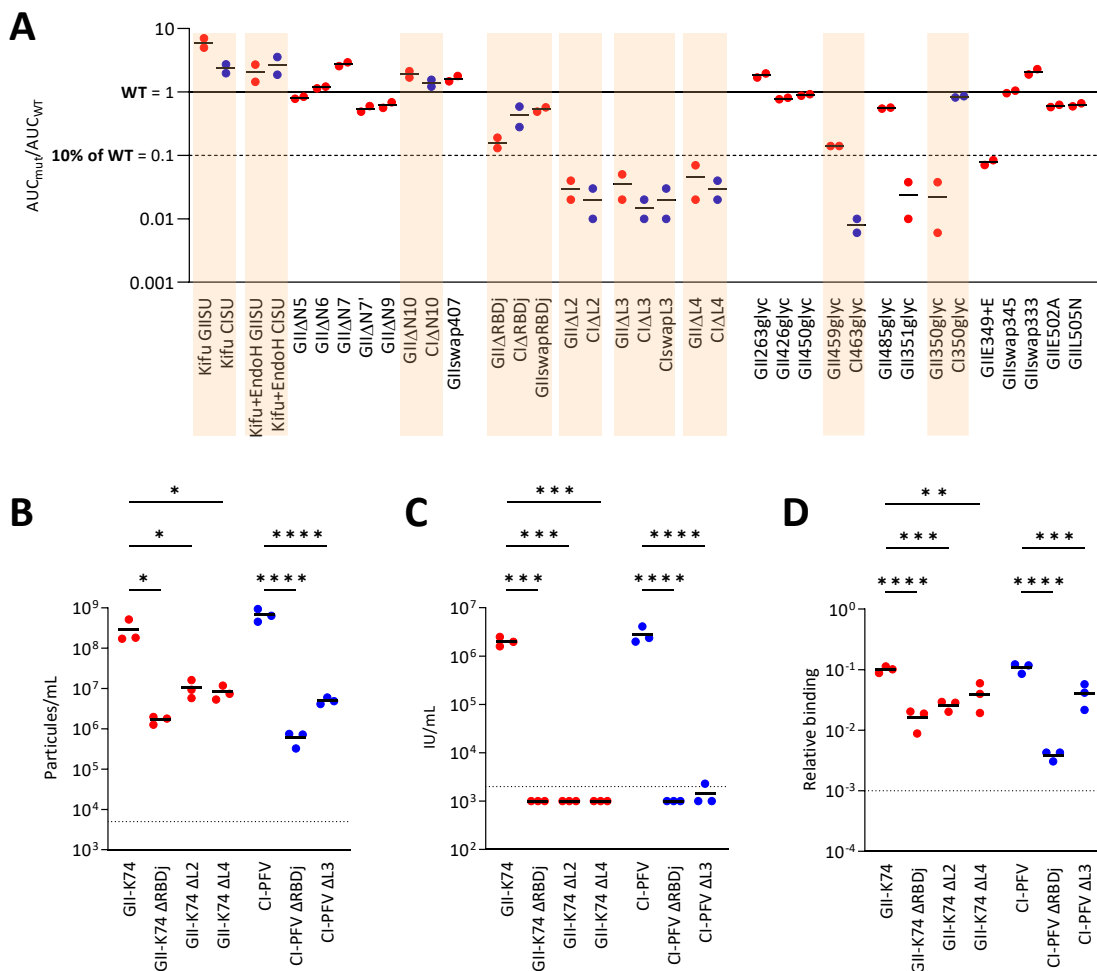


Figure V-9 – nAbs target epitopic regions involved in SU binding to susceptible cells or required for viral infectivity

A. HT1080 cells were incubated with the panel of tested immunoadhesins (Fig. V-4 to V-7). Cell-bound immunoadhesins were detected by staining with a fluorescently labeled antibody targeting the murine IgG Fc fragment. Stained cells were analyzed on a flow cell cytometer. Fig. S.V-8 presents the gating strategy and normalization of the results to the levels of bound WT immunoadhesins (^{GII}SU and ^{CI}SU). Binding levels of GII mutants (red symbols) are presented in the same order as in Fig. V-4, V-5 and V-6. CI mutants (blue symbols) are presented side-by-side with the corresponding and related GII mutants, with a colored background. Mutated HBS shows reduced binding to susceptible cells, as shown in (Fernandez et al., 2022, submitted). **B to D.** Three batches of FVVs carrying WT or mutated Env were produced. The concentration of vector particles was quantified by RT-qPCR amplification of the *bgal* transgene. Each batch was titrated twice and the mean titers are presented; lines represent the mean values from the three FVV batches. FVV infectious titers were quantified on BHK-21 cells. Each batch was titrated twice and the mean titers are presented; lines represent the mean values from the three FVV batches. FVVs carrying WT and mutated Env were incubated with HT1080 cells on ice for 1 h before washing and quantification of *bgal* mRNA incorporated in the vector particles and the *gapdh* gene of susceptible cells. The FVV dose was 10 FVV particles per cell. The levels of *bgal* and cellular *gapdh* mRNA were quantified by RT-qPCR; the $\Delta\Delta C_t$ method was used to calculate the relative amount of FVV particles bound to cells. Values below the threshold were arbitrarily set at 0.0005. Lines represent the mean values from tested FVV batches. The dotted lines in panels B to D represent the quantification threshold. The infectious titers, particle concentration, and levels of bound particles from FVVs carrying mutant or WT SU were compared using the ANOVA test and Sidak's multiple comparison test, * $p < 0.05$, ** $p < 0.01$, *** $p < 0.001$, **** $p < 0.0001$.

5.3.9 Three-dimensional map of epitopic regions

We built a model integrating the current knowledge on Env structure, genetic variability, function, and our findings on the recognition by nAbs (Fig. V-10). According to our model for the arrangement of the RBD within the trimeric Env, the RBD occupies the space at the top of Env spike (Effantin et al., 2016; Fernandez et al., 2022, submitted); each RBD has two subdomains, referred to as upper and lower (Fernandez et al., 2022, submitted) (Fig. V-10A). The genotype-specific SUvar region is targeted by nAbs (Aiewsakun et al., 2019a; Lambert et al., 2018; Richard et al., 2015) and comprises the entire upper RBD subdomain (SUvar^{Up}) and one third of its lower subdomain (SUvar^{Lo}) (Fig. V-10B). SUvar^{Lo} wraps around a stem formed by the conserved part of the RBD (SUcon region). The functionally defined bipartite RBD (Duda et al., 2006) could be located as follows: RBD1 forms half of the SUvar^{Up} and the SUvar^{Lo} region wrapping around the conserved RBD2, while the RBDj forms the top of SUvar^{Up}.

Here, we show that nAbs recognize the three solvent-exposed loops on SUvar^{Up} (Fig. V-10C). We also identified mutations located C-terminal (^{GII}459_{glyc} and ^{CI}463_{glyc}) that may affect nAb binding or the SU folding. For SUvar^{Lo}, we show the 345-353 loop to be an immunodominant epitope exclusively recognized by GII-specific nAbs and that it has a role in binding to cells. The glycosylation site N7' had the greatest impact on the nAbs. It is located at the opening of the cavity in which the essential N8 glycan is buried (Fernandez et al., 2022, submitted). Of

note, the glycan inserted in ^{GII}485_{glyc} may interfere with N8 function and/or accessibility to nAbs. SUvar^{Lo} comprises the HBS, which was not frequently recognized. In conclusion, the nAbs bound to the loops on SUvar^{Up} might interfere with trimer integrity or the conformational changes required for the triggering of fusion, whereas those that bound to SUvar^{Lo} may prevent viral attachment and/or binding.

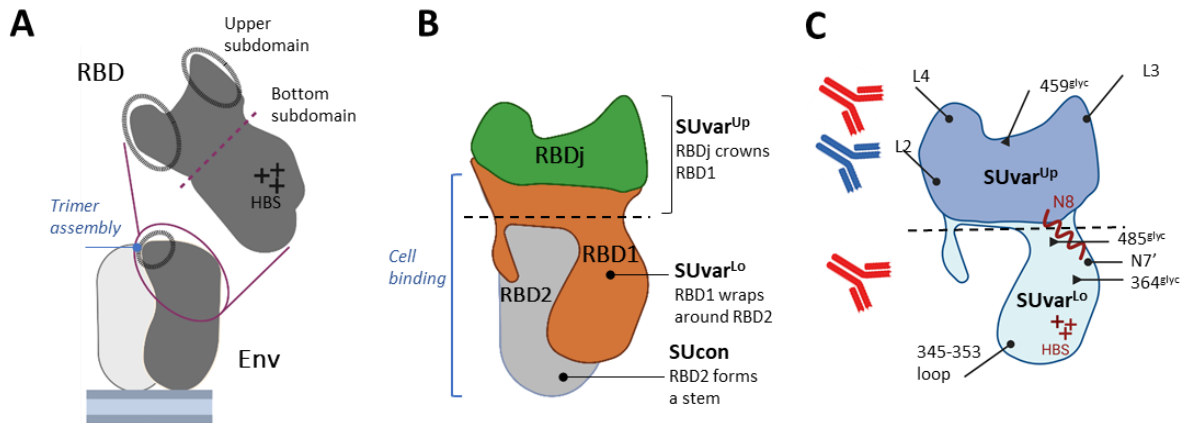


Figure V-10 – Schematic summary of current knowledge on SFV Env

A. The RBD domain is composed of two subdomains located at the top of Env trimers; the drawing highlights the region involved in trimer assembly and the HBS (Effantin et al., 2016; Fernandez et al., 2022, submitted). **B.** Genetic studies on SFV strains circulating in Central Africa have identified two genotypes that differ in the sequence encoding the central part of the SU (SUvar) domain (Aiewsakun et al., 2019a; Richard et al., 2015). The SUvar domain forms the upper part of the RBD (SUvar^{Up}) prolonged, in the lower subdomain, by an arm (SUvar^{Lo}) wrapping around the stem of which the sequence is conserved (SUcon). Binding studies defined the RBD as being bipartite, with two essential binding regions (RBD1 and RBD2) separated by RBDj (Duda et al., 2006). These regions form the bottom of SUvar^{Up} and SUvar^{Lo} (variable part of RBD1), the top of SUvar^{Up} (RBDj), and the stem (short conserved fragment of RBD1 and RBD2). **C.** nAbs exclusively target the SUvar domain (Lambert et al., 2018). In the present paper, we identified GII-specific epitopes in the SUvar^{Up} and SUvar^{Lo} domains and GI-specific epitopes in SUvar^{Up} only. nAbs recognized L2, L3, and L4 of SUvar^{Up} and the N7' region and 345-353 loop of SUvar^{Lo} (lines ending with a dot). Glycans inserted in both domains revealed additional epitopic sites (lines ending with a triangle).

5.4 Discussion

Here, we demonstrate that SFV GII-specific nAbs raised by infected humans recognize two antigenic regions in the genotype-specific region of the SU and that GI-specific nAbs target at least one of these regions. Based on previous knowledge (Duda et al., 2006; Effantin et al., 2016), the X-ray structure presented in the co-submitted paper (Fernandez et al., 2022, submitted), and our functional data, the SFV-specific nAbs most likely target sites involved in either Env trimer formation or cell binding.

We identified conformational epitopes only, despite several attempts to capture linear epitopes using peptides (Fig. V-2, Fig. S.V-5 and (Lambert et al., 2019)). Our data are consistent with the low reactivity of NHP and human immune sera to denatured Env in immunoblot assays, which contain antibodies that bind to native Env in radio-immunoprecipitation and neutralization assays (Cummins et al., 2005; Hahn et al., 1994; Herchenroder et al., 1999; Netzer et al., 1990). Linear epitopes are usually located in mobile regions of the polypeptide chains. Such mobile segments are absent from the RBD lower subdomain formed by the compact assembly of α -helices and β -sheets (Fernandez et al., 2022, submitted). In RBD monomers, the upper subdomain loops appear to be mobile, but inter-protomer interactions probably impose specific conformations in full-length Env. The loops likely form a number of discontinuous epitopes; L2 and L4 are in proximity in the monomer and L3 and L4 in the trimer (Fernandez et al., 2022, submitted).

Twelve plasma samples were used in this study, including one from an individual infected by strains belonging to both genotypes. Overall, the epitopic regions were recognized by all or most donors and can be considered to be immunodominant (Fig. V-8). Importantly, within each genotype, sequences from the epitopic regions were identical among SFV strains infecting the studied individuals and those circulating in the same geographical area. This observation is consistent with the genetic stability of SFV (Switzer et al., 2005). The use of polyclonal plasma samples was key to providing a global picture of nAbs raised upon infection with zoonotic SFV, but only epitopes recognized by a significant fraction of plasma antibodies can be detected. Thus, future studies may identify subdominant epitopes and provide a more precise definition of those that are immunodominant.

Immunoadhesins fully blocked nAbs from certain samples. However, for most tested samples, the infectivity was maintained but at levels lower than those observed for FVVs not exposed to plasma samples (Fig. V-3). The heterogeneous glycosylation of the immunoadhesins could explain the partial blockade of nAbs (Herchenroder et al., 1999), as proposed for the incomplete neutralization of HIV (Doores and Burton, 2010; Kim et al., 2014; Mangala Prasad et al., 2022; McCoy et al., 2015). The SU antigenicity of soluble monomeric proteins probably differed from those contained within viral particles due to the lack of the intra- and interprotomer interactions that form quaternary structures. Thus, our data identify nAb epitopes presented on the monomeric SU domain and indirectly suggest the existence of quaternary epitopes.

We have provided experimental evidence for the targeting of different epitopes by nAbs raised after infection by the two SFV genotypes. The RBD fold from different genotypes and FV from different host species is highly conserved (Fernandez et al., 2022, submitted). In superinfection-resistance experiments, the CI Env inhibited entry from genotype II strains, indicating that SFV from different genotypes share the use of at least one molecule for entry into target cells; this molecule could act as an attachment factor or receptor (Hill et al., 1999). The SUvar^{UP} domain was recognized by both GI- and GII-specific nAbs and the SUvar^{LO} by GII-specific nAbs only. GI-specific nAbs may, nevertheless, recognize epitopes on SUvar^{LO} that are yet to be identified. Indeed, the biochemical properties of GI Env protein resulted in low expression and protein aggregation. Therefore, we used an SU from chimpanzee genotype I SFV to map epitopes recognized by antibodies induced by a gorilla genotype I SFV. We previously reported that plasma samples cross-neutralize both SFV species, with a strong correlation between nAb titers; however, nAb titers were globally higher against the GI than CI strain (Lambert et al., 2018). Thus, we may have missed a number of GI-specific epitopes.

Relative to other viruses, SFV-specific nAbs target a limited region on Env, i.e., they do not recognize epitopes on the TM nor non-RBD sites of the SU (Burkhart et al., 2003; Chuang et al., 2019; Murin et al., 2019). Based on the inhibition mechanisms described for other viruses (Murin et al., 2019), we can propose a number of possible modes of action. The targeting of RBD loops by nAbs may prevent the fusogenic conformational transition and exposure of the fusion peptide, which is located at the center of the trimer and shielded by the RBD, as visualized on viral particles (Effantin et al., 2016). It is possible that certain loop-specific nAbs

bind several protomers, as described for HIV- and Ebola-specific nAbs (McLellan et al., 2011; Milligan et al., 2022). An alternative neutralization mechanism could be the targeting of epitopes located close to the protomer interface, resulting in trimer disruption, as described for HIV- and Flu-specific nAbs (Bangaru et al., 2019; Turner et al., 2021).

Many nAbs interfere with particle binding to susceptible cells. The existence of a *bona fide* receptor for SFV is yet to be demonstrated. Consequently, the molecular determinants of Env binding to susceptible cells within SUvar^{Lo} are still only roughly defined. Certain nAbs recognize attachment factors, such as an HBS on SARS-CoV-2 spike (Bermejo-Jambrina et al., 2021). The SFV HBS is a patch of residues located in SUvar^{Lo}. The mutants deficient for HS binding efficiently blocked most plasma samples, indicating that HBS is either not a major nAb target or that the antigenicity of these mutants is preserved. Of note, the N7' site located in the vicinity of HBS was recognized. All immunoadhesins designed to map potential B-cell epitopes were tested for their capacity to bind susceptible cells. SU from the two genotypes differed in certain residues involved in cell binding. Most notably, nAbs recognizing the 345-353 loop may prevent GII Env binding, whereas the loop on GI Env is not involved in cell binding and is not targeted by nAbs (Fig. V-9). This last observation highlights, for the first time, genotype-specific differences in SFV binding to susceptible cells and could be a starting point for further studies on identifying attachment factors and receptors for SFV.

Our choice of a functional strategy to map the epitopes targeted by nAbs proved to be critical due to the lack of linear epitopes. Overall, the use of human samples and soluble SU as competitor allowed us to create the first map of targeted regions. We considered several caveats (polyspecificity of plasma samples, absence of quaternary epitopes). We also carefully considered the possible nonspecific effect of mutations on protein folding, which could generate misleading results. Certain mutants were, indeed, poorly expressed and could not be used (Table S.V-3). A number of these limitations may be overcome in the future with the use of alternative tools, such as human monoclonal antibodies and subviral particles.

Human infection with zoonotic SFV represents a model for cross-species transmission of retroviruses leading to persistent infection that is successfully controlled by the immune system. We have previously reported the presence of potent nAbs in most infected individuals (Lambert et al., 2019). Here, we have mapped major antigenic sites. Concerning the control of

SFV in humans, a notable result from the present study is that two immune escape mechanisms, sequence variation and glycan shielding, were observed. The SFV RBD is structurally different from known and modelled retroviral RBDs (Hötzel, 2022). We have provided a novel model integrating structural, genetic, functional, and immunological knowledge on the bimorphic SFV RBD. We have thus gained information on the two SFV genotypes that have persisted for over 30 million years of evolution with their animal hosts. Through the study of SFV and its unique properties, we should also gain fundamental knowledge on the structural basis for the inhibition of viruses by nAbs.

5.5 Materials and Methods

5.5.1 Human plasma samples

Blood samples were drawn from adult populations living in villages and settlements throughout the rainforests of Cameroon. Participants gave written informed consent. Ethics approval was obtained from the relevant national authorities in Cameroon (the Ministry of Health and the National Ethics Committee) and France (Commission Nationale de l'Informatique et des Libertés, Comité de Protection des Personnes Ile de France IV). The study was registered at www.clinicaltrials.gov, <https://clinicaltrials.gov/ct2/show/NCT03225794/>. SFV infection was diagnosed by a clearly positive Gag doublet on Western blots using plasma samples from the participants and the amplification of the integrase gene and/or LTR DNA fragments by PCR using cellular DNA isolated from blood buffy-coats (Betsem et al., 2011). We identified the SFV origin by phylogenetic analysis of the integrase gene sequence (Betsem et al., 2011). The SFV genotype was determined by amplification of the SUvar DNA fragment by PCR (Lambert et al., 2018). Plasma samples from 24 participants were used for this study (Tables S.V-1 and S.V-4). Four participants were not infected with SFV and 20 were infected with a gorilla SFV.

5.5.2 Viral strains, amino-acid numbering, and Env domain nomenclature

We used sequences from primary zoonotic gorilla SFVs, SFVggo_huBAD468 (GI-D468, JQ867465) and SFVggo_huBAK74 (GII-K74, JQ867464) (Rua et al., 2012a) and the laboratory-adapted chimpanzee SFV, SFVpsc_huPFV (CI-PFV, KX087159) (Wagner and Bodem, 2017) for the synthesis of foamy viral vectors (FVV) and envelope proteins and peptides. For simple reference to previously described Env sequences and functions, we used the amino-acid positions from the CI-PFV strain, unless otherwise stated. The GI-D468, GII-K74, and CI-PFV sequence alignment are shown in Fig. S.V-1. When referring to infecting SFV strains and the antibodies raised against them, gorilla and chimpanzee genotype I SFV are referred to as GI and CI, respectively; gorilla genotype II SFV is referred to as GII.

5.5.3 Cells

Baby hamster kidney (BHK)-21 cells (ATCC-CLL-10, hamster kidney fibroblast) were cultured in DMEM-5% fetal bovine serum (FBS). HT1080 cells (ECACC 85111505, human fibrosarcoma)

were cultured in Eagle's Minimum Essential Medium with Earle's Balanced Salts and L-glutamine supplemented with 10% FBS and 1% L-glutamine. Human embryonic kidney 293T cells (Cat. N° 12022001, Sigma) were cultured in DMEM-10% FBS. FreeStyle 293-F cells (Life Technologies) were cultured in Ex-cell 293 HEK serum-free medium supplemented with 5 µg/mL phenol red sodium salt, 2% L-glutamine, and 0.2x penicillin-streptomycin.

5.5.4 Peptides

At the beginning of the project, the SUvar (aa 248-488) sequences from the GI-D468 and GII-K74 strains were analyzed using linear B-cell epitope prediction software available on the Immune Epitope Data Base (<http://tools.iedb.org/bcell/>), which are based on known B-cell epitopes (LBtope, (Singh et al., 2013)), hydrophilicity (Parker prediction replaced by Bepipred software, (Larsen et al., 2006)), and protrusion outside of globular proteins (Ellipro, (Ponomarenko et al., 2008)). In addition, we manually inspected viral sequences for stretches of genotype-specific epitopes. We selected 14 sequences and tested the corresponding GI-D468 and GII-K74 peptides, as well as nine CI-PFV peptides from a previously synthesized peptide set (Lambert et al., 2019) (Table S.V-2). After resolution of the RBD crystal structure, we designed a novel peptide set corresponding to the four loops located in the RBD upper subdomain (Fernandez et al., 2022, submitted). As positive controls, we used the N₉₆-V₁₁₀ (NKDIQVLGPVIDWNV from SFV Env LP) and I₁₇₆-I₁₉₉ (INTEPSQLPPTAPLLPHSNLDHI from HTLV-1 gp46) peptides containing immunodominant epitopes (Lambert et al., 2019). Peptides were synthesized by Smartox SAS (Saint-Martin d'Hères, France) or Genscript (Leiden, The Netherlands) and were tested individually.

5.5.5 ELISA

The protocol was described in (Lambert et al., 2019). Briefly, peptides diluted in carbonate buffer at 1 µg/mL were coated on clear high-binding polystyrene 96-well microplates (Biotechne) overnight (ON) at +4°C. Plasma samples were diluted at 1:200 in phosphate buffered saline (PBS)-0.1% bovine serum albumin (BSA)-0.1% Tween20. Bound plasma antibodies were detected with horseradish peroxidase (HRP)-conjugated goat anti-human IgG H+L (0.02 µg/mL, #109-035-008, Jackson Immuno Research Europe). The peptide diluent was used as the negative control and antibody binding to peptides is expressed as the difference in OD ($\Delta_{OD} = OD_{test} - OD_{control}$). Plasma samples from three SFV-uninfected individuals were

tested for binding to the 37 peptides. The mean + 2 SD of Δ_{OD} (0.14) was used to define the positivity cutoff. The proportion of responding individuals was calculated among those infected with a given virus (SFV, n = 17; HTLV-1, n = 7).

5.5.6 Plasmids

The four-component CI-PFV FVV system (pcoPG, pcoPP, pcoPE, and pcu2MD9) and the gorilla SFV Env constructs containing sequence from the zoonotic GI-D468 and GII-K74 *env* genes have already been described (Hütter et al., 2013; Lambert et al., 2018). Novel plasmids were synthesized by Genscript (Piscataway, NJ, USA). We built a FVV expressing β -galactosidase with a nuclear localization signal (puc2MD9-B-GAL) by replacement of the *gfp* gene in the puc2MD9 backbone for easier image analysis on our quantification device. CI-PFV Env deleted of RBDj or L3, GII-K74 Env deleted of RBDj or L2 or L4 were constructed with the boundaries used for immunoadhesins (Table S.V-3).

Immunoadhesin constructs express a fusion protein formed by the murine IgK signal peptide, SFV SU with deleted furin cleavage site (aa 127-567), and the heavy chain (hinge-CH2-CH3) of murine IgG2a. A Twin-Strep-tag was fused after the mIgG2a to facilitate immunoadhesin purification, except for the first immunoadhesin constructs (^{GI} Δ RBDj, ^{GI}swapRBDj and ^{GI} Δ N10). The murine leukemia virus (MLV) gp70 SU (aa 34-475, strain FB29, NP_040334.1) was fused to the Twin-Strep-tag. All genes were codon optimized for expression in mammalian cells and placed under the control of a CMV promoter and intron in the pcZI plasmid (Heinkelein et al., 2002).

The codon-optimized synthetic genes encoding GII-K74 SU (aa 127-566) and ectodomain (aa 91-907) were cloned into the already described pT350 plasmid (Krey et al., 2010), which contains the *Drosophila* metallothionein promoter, which is inducible by divalent cations (Bunch et al., 1988), the *Drosophila* BiP signal peptide (MKLCILLAVVAFVGLSLG) at the N-terminus and a Twin-Strep-tag (AGWSHPQFEKGGGSGGGSGGGWSHPQFEK) for affinity purification at the C-terminus. Stable S2 cell lines were generated by antibiotic resistance and protein production was induced by the addition of 2 μ M CaCl₂. For expression in mammalian cells, the murine IgK signal peptide was fused at the N-terminus of codon-optimized genes encoding GII-K74 SU (aa 127-566). The genes were placed under the control of the CMV promoter and intron (Heinkelein et al., 2002) by insertion into the pcDNA3.1 vector.

5.5.7 Protein expression and purification

293-F cells were seeded at 2.5×10^6 cells/mL in FreeStyle 293 Expression medium and transfected by the addition of plasmid DNA (2 $\mu\text{g}/\text{mL}$) and LipoD293 (6 $\mu\text{g}/\text{mL}$ #SL100668, Tebu-bio). After 24 h, cells were diluted 1:1 in Ex-cell culture media and cultivated for another 48 h and the supernatants collected and stored at -80°C . For the expression of immunoadhesins with high-mannose-type glycans, transfected cells were cultivated in the presence of 5 μM Kifunensine mannosidase inhibitor (#BML-S114-0005, Enzo Life Sciences). Glycans were removed by incubating the immunoadhesins ON at room temperature (RT) with endoglycosidase H (endo-H, 0.8 U/mL, #P0702L, New England Biolabs) in 50 mM Na acetate-50 mM NaCl, pH 6. Supernatants were thawed and filtrated through a 0.2 μm filter before centrifugation at $4500 \times g$ at 4°C in VivaSpin tubes (Sartorius). The first-generation immunoadhesins do not carry the Twin-Strep-tag and were purified using Protein A Mag Sepharose™ Xtra beads (50 μL beads/mL of supernatant; #28-9670-62, GE Healthcare) using binding Buffer pH 7, 0.2 M Na_3PO_4 (#28-9030-59, Ab Buffer Kit, GE Healthcare). Beads were incubated at 4°C on a rotator ON. Proteins were eluted with a pH 2.5 elution buffer containing 0.2 M Glycine-HCl and neutralized with 1 M Tris-HCl, pH 9 (#PUR004, NEO Biotech, CliniSciencesProteus). Immunoadhesins and ^{MLV}SU fused to Twin-Strep-tag were purified using Gravity Flow Strep-Tactin XT Superflow High-Capacity columns (#2-4031-001, Iba Lifescience). Concentrated proteins were resuspended in buffer W at pH 8 and incubated with BioLock (#2-0205-050, Iba Life sciences) for 15 min at RT to neutralize biotin. Loading onto the columns and elution were performed according to manufacturer's instructions.

GII-K74 SU, WT, and mutated ectodomains were expressed in *Drosophila* Schneider's cell line 2 (S2) cells following the standard protocol (Backovic and Krey, 2016). GII monomeric SU and trimeric ectodomain proteins were purified by affinity chromatography on a Streptactin column (IBA Biosciences), followed by size-exclusion chromatography on Superdex 200, using standard methods provided by the manufacturers.

Protein concentrations were measured by NanoDrop. To verify protein purity and aggregate formation, 1.5 μg of purified proteins was heat-denatured at 70°C for 10 min in NuPAGE LDS sample buffer (#NP0007, Introgen), with or without NuPAGE reducing buffer (50 mM DTT; #NP0009, Invitrogen). Samples were loaded onto a precast NuPAGE 4-12% Bis-Tris gel

(#NP0322, Invitrogen). The gel was incubated with Bio-Safe Coomassie staining solution (#1610786, Bio-Rad) for 2 h with gentle shaking, rinsed in H₂O ON, and imaged using a G:BOX (Syngene) (Fig. S.V-4).

5.5.8 Western-blot

Western-blot analysis of protein expression was performed on cell supernatants. Samples were heat-denatured and reduced as described for purified proteins before loading onto precast NuPAGE 4-12% Bis-Tris gels (#NP0322, Invitrogen). Proteins were migrated for 2-3 h at 120 V in NuPAGE MOPS SDS running buffer (#NP0001, Invitrogen) and transferred onto a PVDF membrane (#1704156, Bio-Rad) using a Trans-Blot Turbo transfer system (Bio-Rad). Membranes were blocked and antibody labeled in Tris-buffered saline (TBS)-0.1%Tween-5% BSA. For Strep-tag detection, membranes were incubated with StrepMAB-Classic monoclonal antibody conjugated to HRP (0.05 µg/mL, #2-1509-001, Iba Lifesciences) for 2 h at RT. For SFV SU detection, membranes were incubated with a biotinylated anti-SU murine antibody ON at 4°C (3E10, 1 µg/mL), washed three times in TBS-0.1% Tween for 10 min and incubated with Streptavidin-HRP (1:2000, #DY998, Biotechne). Membranes were washed three times in TBS-0.1% Tween for 10 min before revelation with SuperSignal West Pico PLUS chemiluminescence substrate (#34579, ThermoFischer Scientific) and signal acquisition using a G:BOX.

5.5.9 Foamy viral vectors (FVVs)

FVV particles were produced by co-transfection of HEK293T cells by the four plasmids. Fifteen µg total DNA (gag:env:pol:transgene ratio of 8:2:3:32) and 45 µl polyethyleneimine (#101-10N, JetPEI, Polyplus) were added to a 10 cm² culture dish seeded with 4 x 10⁶ 293T cells. Supernatants were collected 48 h post-transfection, clarified at 500 x g for 10 min, filtered using a 0.45 µm filter, and stored as single-use aliquots at -80°C. FVVs were titrated as described (Lambert et al., 2018; Lambert et al., 2016), with minor modifications to optimize X-Gal staining of transduced cells, which was lighter than that of infected cells. Briefly, FVV samples were thawed and clarified by spinning at 10,000 x g at 4°C for 10 min. Serial five-fold dilutions were added in triplicate to sub-confluent BHK-21 cells seeded in 96-well plates and cultured for 72 h at 37°C. Plates were fixed with 0.5% glutaraldehyde in PBS for 10 min at RT, washed with PBS, and stained with 150 µl X-gal solution containing 2 mM MgCl₂, 10 mM potassium ferricyanide, 10 mM potassium ferrocyanide, and 0.8 mg/mL 5-bromo-4-chloro-3-

indolyl-B-D-galactopyranoside in PBS for 3 h at 37°C. Blue-stained cells were counted using an S6 Ultimate Image UV analyzer (CTL Europe, Bonn, Germany). One infectious unit was defined as one blue cell. Cell transduction by FVV is a surrogate for viral infectivity and FVV titers are expressed as infectious units (IU)/mL.

5.5.10 Neutralization assays

Prior to use in neutralization assays, plasma samples were diluted 1:10 in DMEM + 1 mM MgCl₂, decomplexed by heating at 56°C for 30 min, and frozen at -80°C as single-use aliquots. Thawed plasma samples were clarified by spinning at 10,000 x g for 10 min at 4°C. Serial two-fold dilutions were incubated with FVV for 1 h at 37°C before titration in triplicate and residual infectivity quantified using the 96-well plate microtitration assay described above. P96-well plates seeded with 5,000 BHK-21 cells were exposed to 300 IUs of FVV. Plasma samples were initially titrated against replicating virus (Lambert et al., 2018). We selected those with neutralization titers > 1:100 against the virus and performed plasma titration against the FVV. We defined the plasma dilution required for a 90% reduction of FVV infectivity and used it as the fixed concentration for the nAbs. Plasma samples were incubated with serial dilutions of recombinant Env proteins for 1 h at 37°C. FVV was then mixed with the plasma/protein preparation and incubated 1 h at 37°C before addition to BHK-21 cells. FVV infectivity was quantified 72 h later as described for their titration. All conditions were tested in triplicate and the mean IU/well calculated. Cells transduced with mock treated FVV (i.e., incubated with ^{MLV}SU at 20 nM or with medium) were quantified on each plate and this value used as a reference. Relative infectivity was calculated for wells treated with the plasma/protein mix and is expressed as the percentage of the reference value. The WT immunoadhesin (^{GII}SU or ^{CI}SU) matched with the FVV Env was titrated along with the tested mutant immunoadhesins on every plate in every experiment for each plasma tested. All immunoadhesins were tested against each plasma at least twice and against at least four plasma samples. In the first assay (screening), immunoadhesins were added at three concentrations, ranging from 200 to 2 nM. In the second assay (confirmation), immunoadhesins with activity similar to that of WT or with no activity were tested a second time at three dilutions. Mutant immunoadhesins with intermediate activity were titrated in a three-fold serial dilution setting starting at 60 nM. We used two parameters to define the action of the immunoadhesins on the nAbs from each plasma sample: maximum infectivity

(MaxI) and 50% inhibitory concentration (IC₅₀). MaxI corresponds to the maximal infectivity in the presence of immunoadhesin-blocking nAb and is defined as the mean relative infectivity at the two highest doses tested. The IC₅₀ values were calculated by plotting the relative infectivity as a function of immunoadhesin concentration and a four parameters regression modeling of the Prism software (Version 9, GraphPad). Mutant immunoadhesins with nAb activity similar to the WT one were given its IC₅₀, and those with minimal or no activity were given an arbitrary IC₅₀ value of 200 nM, corresponding to the highest concentration of immunoadhesin tested.

5.5.11 SFV Env binding to cells

Immunoadhesins were thawed at RT and clarified at 10,000 x g for 10 min. HT1080 cells were treated with trypsin-EDTA and 5 x 10⁵ cells resuspended in 0.1 mL FACS buffer (PBS-0.1% BSA) containing the immunoadhesins and incubated on ice for 1 h. Cells were washed twice and incubated with donkey anti-murine IgG-(H+L)-AF488 (20 µg/mL, #A21202, Invitrogen) on ice for 30 min. Cells were washed and resuspended in 0.2 mL PBS-2% PFA. Data were acquired on a CytoFlex cytometer (Beckman Coulter) and analyzed using Kaluza software. A minimum of 25,000 cells were acquired. Single cells were selected by sequential gating on FSC-A/SSC-A and SSC-A/SSC-H dot-plots (Fig. S.V-8A). Immunoadhesin binding is expressed as the ratio of mean fluorescence intensity (MFI) of immunoadhesin-treated over untreated cells. Each immunoadhesin was tested twice at 3, 30, and 300 nM. The MFI ratios were plotted as a function of immunoadhesin concentration and the area under the curve was calculated (Fig. S.V-8B and S.V-8C). To limit inter-experimental variation, WT immunoadhesins were included in every experiment and the binding level of mutant immunoadhesins normalized to that of the WT.

5.5.12 Analysis of FVVs carrying mutated Env

The yield of FVV particles was estimated by quantifying particle-associated transgene RNA. FVV RNA was extracted from raw cell supernatants using a QIAamp Viral RNA Extraction Kit (Qiagen), treated with a DNA-free kit (Life Technologies), and retro-transcribed with Maxima H Minus Reverse Transcriptase (Thermo Fischer Scientific) using random primers (Thermo Fischer Scientific) according to the manufacturers' instructions. qPCR was performed on cDNA using BGAL primers (BGAL_F 5' AAACCTCGCAAGCCGACTGAT 3' and BGAL_R 5'

ATATCGCGGCTCAGTTCGAG 3') with a 10-min denaturation step at 95°C and 40 amplification cycles (15 s at 95°C, 20 s at 60°C, and 30 s at 72°C) carried out using an Eppendorf realplex2 Mastercycler (Eppendorf). A standard curve prepared with serial dilutions of pcu2MD9-BGAL plasmid was used to determine the FVV copy number. Results are expressed as vector particles/mL, considering that each particle carries two copies of the transgene.

The expression level of mutated Env proteins in producer cells was assessed by western-blot analysis. 293T cells transfected to produce FVVs were collected and lysed in RIPA buffer (#R0278, Sigma) containing protease inhibitors (#11140920, Roche) for 2 h at 4°C. Samples were heat-denatured at 70°C for 10 min in LDS sample buffer (NuPage) and 50 mM DTT before loading onto a precast NuPAGE 4-12% Bis-Tris gel (Invitrogen) and migration for 2 h at 120 V in MOPS running buffer. The content of \approx one million cells was analyzed. Samples were transferred onto a PVDF membrane using a Trans-Blot Turbo transfer system (Bio-Rad, Hercules, CA, USA). Membrane blockade and antibody labelling were performed in TBS-0.1%Tween-5%BSA. Membranes were incubated with an anti-LP antibody ON at 4°C (clone P6G11-G11, 1 μ g/mL), washed, and incubated with a goat anti-mouse secondary antibody HRP conjugate (1:10000, #31430, Invitrogen). Membranes were washed three times in TBS-0.1% Tween for 10 min before revelation using Immobilon ECL Ultra Western HRP Substrate (WBULS0100, Merck) and signal acquisition on an Amersham Imager 680 (GE Healthcare).

To test the capacity of mutated Env to mediate the binding of vector particles to cells, HT1080 cells were incubated with the FVV particles (1, 10 and 100 particles/cell) on ice for 1 h. The cells were washed three times with PBS to eliminate unbound FVV and RNA was extracted using an RNeasy plus mini-Kit (Qiagen) according to manufacturer's protocol and RT performed as described for FVV RNA quantification. Bound FVV was quantified by qPCR of the *bgal* gene as described for vector titration; cells were quantified by qPCR amplification of the *hgapdh* gene with the following primers: hGAPDH_F 5' GGAGCGAGATCCCTCCAAAAT 3' and hGAPDH_R 5' GGCTGTTGTCATACTTCTCATGG 3'. The qPCR reaction conditions were the same as those used to amplify the *bgal* gene. The relative mRNA expression of *bgal* versus *hgapdh* was calculated using the $-\Delta\Delta C_t$ method, and relative binding as $2^{-\Delta\Delta C_t}$.

5.5.13 Statistical analysis

Mutations in the immunoadhesins modified their ability to block the nAbs in two ways: either by reducing avidity, leading to a higher IC_{50} , or by the fraction of plasma nAb blocked, leading to lower maximal infectivity. For each plasma sample, the IC_{50} and MaxI were tested for the WT immunoadhesin in at least five experiments. The threshold value defining a statistically significant change relative to WT was defined as the mean + 3*SD for the IC_{50} and the mean - 3*SD for MaxI. Thresholds were defined for each plasma sample. The infectious titers, particle concentration, percentage of infectious particles, and quantity of bound FVV carrying WT and mutant immunoadhesins were compared using the ANOVA test for paired samples and Sidak's multiple comparisons test (GraphPad Prism 9 software).

5.6 Acknowledgements

We thank H. Mouquet and V. Lorin for sharing the 293-F cells and advice. We are grateful to Mathilde Couteaudier for mentoring MD and LTD in their performance of the experimental work. We used devices from the Cytometry and Biomarker Utechs at the Institut Pasteur and we thank their staff for their support and advice. We thank Delphine Brun from the Unité de Virologie Structurale for technical assistance. The manuscript has been edited by a native English speaker.

5.7 Funding

This work was supported by the Agence Nationale de la Recherche (ANR-10-LABX62-IBEID, Intra-Labex Grant (M.B.)), and the Programme de Recherche Transversal from the Institut Pasteur (PTR2020-353 ZOOFOAMENV, F.B.). SFV protein production was supported by the European Virus Archive-GLOBAL project, which has received funding from the EU Horizon 2020 Research and Innovation Programme (grant agreement number 871029). **L.T.D.** was supported by the Pasteur-Paris-University (PPU) International Doctoral Program and the Fondation pour la Recherche Médicale, including additional supportive funding from the Danish Pasteur Society, Augustinus Fonden, Knud-Højgaards Fond, and Viet-Jacobsen Fonden. The funding agencies had no role in the study design, generation of results, or writing of the manuscript.

5.8 Authors contribution

FB, MB, FR, and AG designed the project. FB and MB supervised the project and acquired funding. **LTD**, IF, YC, MD, and TM performed the experiments. **LTD**, IF, FB, and MB analyzed the data. AG, RN, and CBN collected the human samples. **LTD** and YC provided figures and text elements for the draft. FB wrote the initial and final drafts. All authors participated in reviewing the drafts.

CHAPTER VI

DISCUSSION AND PERSPECTIVES

6 | DISCUSSION AND PERSPECTIVES

6.1 Achievements on nAb epitopes

6.1.1 SFV nAb epitopes are conformational

We report limited recognition of linear peptides spanning the SUvar region by plasma nAbs, in agreement with previous work by our lab (Lambert et al., 2019). While linear epitopes appear rare, one study on FFV-specific feline antibodies reported strong plasma reactivities to a peptide (residues 441-463) within the SU domain of FFV Env that correlated with genotype-specific neutralization (Mühle et al., 2017), as I will discuss below. Peptides used in the previous study by our lab might be suboptimal to detect antibody binding due to their short size (15-mers) and because their sequence was from the chimpanzee CI-PFV strain, while plasma antibodies were from individuals infected with gorilla SFV strains. In contrast, the peptides used in my current study were longer to match the usual sizes of B cell epitopes and their sequences were derived from homologous gorilla strains. Nevertheless, few antibodies bind to these peptides and binding did not match with the genotype of their infecting strain (Fig. V-2). Accordingly, these results highlight that the majority of nAb epitopes are conformational. Once the RBD structure was known, we indeed observed that the major epitopic regions on the RBD structure located to disordered outer regions rather than the more structurally conserved ‘common core’ of the RBD. Indeed, peptide sequences spanning the mobile loops on the RBD apex from homologous gorilla SFV strains were not recognized by plasma antibodies (Fig. S.V-5). This observation goes in line with what has been observed for plasma antibodies directed against HTLV, which also mostly target conformational epitopes (Hadlock et al., 1999). Similarly, nAbs against MLV target variable loops on the RBD and conformational epitopes have been reported (Evans et al., 2014; Fass et al., 1997).

6.1.2 Localization of nAb epitopes on RBD and possible mode of actions

While some epitopes were found at the core and lower domain of the structure (N7', base loop residues 345-351 and adjacent helices), the vast majority located to the upper apex of the RBD, in particular within three mobile loops (Fig. VI-1). Moreover, it is worth notice that the nAb epitopes I identified fall to one face of the RBD, consistent with the orientation of the RBD within the SFV Env trimer as demonstrated by our collaborators (Fig. IV-4).

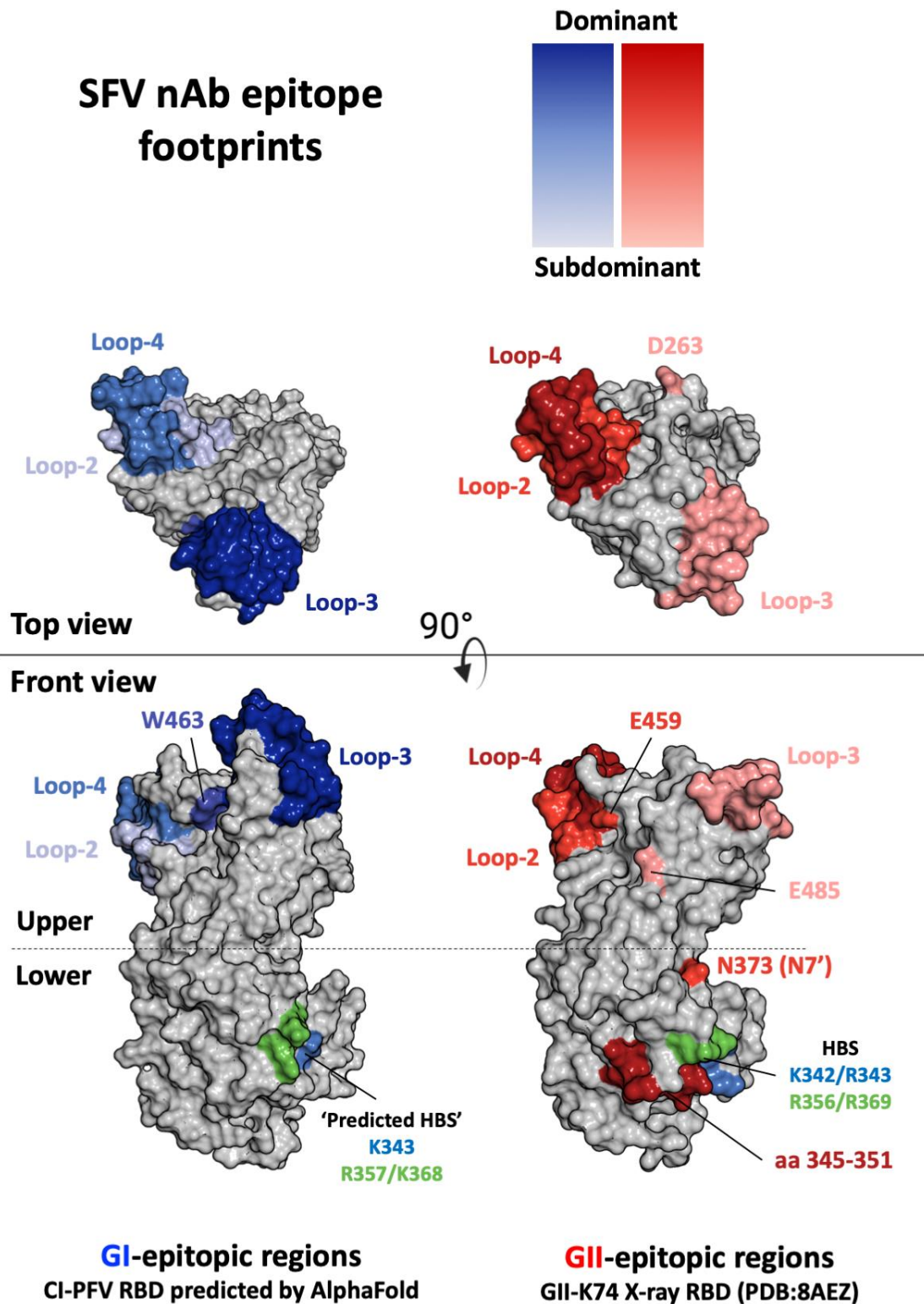


Figure VI-1 – Summary of discovered genotype-specific epitopic regions

SFV nAb epitope footprints determined in the current study with use of human plasma samples from SFV-infected donors are presented on CI-PFV (AlphaFold predicted) and GII-K74 (experimentally determined) RBD structures. Immunodominance of GI- and GII-specific epitopes is highlighted according to spectrum of blue and red shades, respectively. For the purpose of location to adjacent discovered epitopes, the determined HBS of GII-K74 and its equivalent site predicted on CI-PFV is highlighted in blue and green for the specific residues, respectively. Figure created in PyMOL.

6.1.2.1 Epitopes on the Upper domain

Most of the tested plasma samples target epitopes on the three mobile/flexible loops (L2/3/4) located at the RBD apex. These loops are likely to form interfaces between RBD protomers in the trimer and may potentially be key for the stabilization of the trimeric Env in a pre-fusion conformation (Fig. S.IV-2). Indeed, superposition of the GII-K74 RBD onto the cryo-EM density map of CI-PFV Env trimer showed an overall good fit, and clearly support that the apex loops form protomer-protomer interfaces (Fig. IV-4).

Despite their dominance, we have not defined these apex epitopes at the residue level. However, some mutations based on removal and insertion of glycosylation sites and sequence swaps allow us to exclude or specify certain residues from the discovered epitopes. For instance, mutation of glycan N5 within the central part of GII-L2 had minimal effect on block of nAbs. Similarly, deletion of N10 had no effect on block of nAbs specific for either genotype from eight donors, for which this glycan locates in the N-ter of L3 in GII. In line with those results, a chimeric mutant spanning glycan N10 and its upstream region swapped from GI into GII (swap407) blocked three of four samples from GII-donors to same extend as WT. Those results exclude this region as part of a dominant epitope within GII-L3, although one donor may have nAbs that recognize the N-ter of L3 (Fig. V-4E vs V-4F). In contrast, glycan insertion on residue N426 at the C-ter of L3 demonstrated similar loss of activity as for deletion of L3 for two of three GII-donors (Fig. V-5G vs V-6C). Those results imply that the central part of L3 may form a more common epitope.

Within L4, glycan insertion mutant D450 only slightly affected block of nAbs from two of four GII-infected donors tested. Thus, we may exclude this region as part of a major GII-specific epitope within L4 (Fig. V-5H vs V-6D). Interestingly, we noticed an overlap between the FFV-genotype specific peptide (residues 441-463) recognized by plasma antibodies from FFV-infected cats and the sequence location of L4 in our study with SFVs (Mühle et al., 2017).

FFV-FUV peptide: ⁴⁴⁰ **ESV**QCYNN--DM**CY**R**PLYD**GT**ENT**E⁴⁶³
 GII-K74 Loop-4: ⁴⁴² **E**.K.LTS**DH**TR.L.Y.**E**.SNP.ALF⁴⁶⁷
 CI-PFV Loop-4: ⁴⁴⁵ **E**TK.RDGETKR.L.Y.**W**.SP.S.Y⁴⁷⁰

Six residues (**E-C-C-Y-P-E**, highlighted in bold with grey background on sequences) within this region are conserved between FFV and both SFV strains (respective peptide sequences

shown with underline). Moreover, five residues in this region are conserved between FFV and either the CI or the GII SFV strains (highlighted in bold with grey background and residue letters in color according to SFV genotype; blue = CI, red = GII). The D450N glycan insert mutation which had limited effect on block of GII-specific nAbs is located in a central region of the peptides that is most divergent between FFV and SFV sequences (highlighted in bold with residue letter in orange on GII-K74 sequence). Furthermore, the two SFV peptides border the glycan insert mutations GII-E459N and CI-W463N (highlighted in bold with residue letters in green on respective sequences). These mutations largely affected block of plasma nAbs from 11 of 13 plasma-protein pairs tested (Fig. V-6E vs V-7I). Those data suggest that the SFV genotype-specific L4 epitopes may locate to the C-ter region, which was not fully covered by our L4 loop peptides – or that the glycan insert mutations next to the C-ter of the peptides may disrupt a distinct epitope. The latter seems more likely since the six residues at the C-ter of both L4-peptides are 100% conserved between the two SFV strains, making this an unlikely genotype-specific epitope. However, we cannot exclude that these residues fold in genotype-specific conformations on Env from the respective strains.

Importantly, these mobile regions were crucial for infectivity of viral vectors when substituting individual loops by glycine residue linkers matched to those on loop mutant SU-Ig proteins (Fig. V-9C). Our results support that the nAbs target epitopes with functional importance. A possible mode of action could be maintenance of the Env trimer in a pre-fusion conformation unable to undergo conformational changes necessary for transition to a post-fusion conformation and fusion of viral and cellular membranes. Such apex epitope location is frequently observed for Flu-specific antibodies targeting the head domain of the hemagglutinin on influenza viruses (Bangaru et al., 2019). Another potential mechanism of action in nAb block of viral entry is the disassembly of Env trimers into protomers which has been observed for anti-HIV-1 nAbs and bnAbs (Lee et al., 2015; Pancera et al., 2014).

Our approach to map nAb epitopes with SU-Igs did not include quaternary structures formed by distinct protomers within an Env trimer, however such epitopes are likely to exist. Indeed, for most donors tested the WT SU-Ig proteins rarely reverted vector infectivity in presence of plasma to a level observed in the absence of plasma (Fig. V-3B and V-3F). Those data indicate that some nAbs were not blocked by the SU-Igs and indirectly suggest the presence of nAbs targeting quaternary epitopes. These may represent a proportion of neutralizing activity ranging from 5% to 40% (Fig. V-3F). The apex loops may form most of the quaternary epitopes based on their placement in the trimer. Indeed, quaternary epitopes have been observed for nAbs

targeting the Ebola GP trimer and one of such neutralizing mAbs engaged in interactions with residues from all three protomers in a GP trimer at once (Milligan et al., 2022). A possibility to map such quaternary epitopes would be the use of Env trimers in a pre-fusion conformation or sub-viral particles which only contain Env (Stanke et al., 2005).

The quaternary epitope mapping has not been initiated during my thesis because the conformation of the apex loops is still unknown. Indeed, some parts of L3 could not be resolved in the RBD crystal structure. Furthermore, structural prediction tools were not able to give confident answers to the folding of these loops. In general, our use of prediction tools was not very informative in regards to discovery of novel genotype-specific epitopes. These included tools for both linear (BepiPred 2.0, (Jespersen et al., 2017)) as well as conformational epitopes (DiscoTope 2.0, (Kringelum et al., 2012)) which failed to pinpoint obvious genotype-specific epitopic regions. In fact, we discovered genotype-specific epitopes not predicted by these *in silico* tools such as the base loop by manually inspecting genotype-specific sequences.

In summary, we have discovered genotype-specific conformational epitopes at the upper domain of the RBD. These epitopes are located at mobile loops forming protomer interfaces at the trimer apex that may stabilize the pre-fusion conformation important for viral infectivity. One loop (L3) appears dominantly targeted by plasma nAbs from GI-infected donors, while a second loop (L4) overlaps in sequence and location with a previously reported FFV genotype-specific linear epitope. Further studies are needed to precisely map these epitopes.

6.1.2.2 Epitopes on the Lower domain

While the SFV receptor is yet to be identified, HS is a well-established attachment factor (Nasimuzzaman and Persons, 2012; Plochmann et al., 2012). In this study, we identified four residues essential for SFV Env binding to HS located on the CC of the GII-K74 RBD (Fig. IV-5 and IV-6). Mutation of these residues only affected block of plasma nAbs to some extent for one of four GII-infected donors tested (Fig. V-5D and V-5E). These results show that the HBS is not a dominant target for GII-specific nAbs. Additionally, we know that HS is an attachment factor for CI-PFV and thus this strain must also harbor an HBS. However, currently we do not have structural insights to a GI/CI RBD hence we did not explore if this site is a target for GI-specific nAbs. In the current absence of experimental CI/GI-RBD structures, AF prediction could provide a useful tool as it gives high confidence structures for the CC of the RBD (Fig. S.IV-8 and S.IV-9). Thus, mutations in an AF predicted HBS on CI-PFV SU-Ig could be designed to test whether a potential GI-specific HBS is recognized by nAbs from GI-infected

individuals. Mutations could also be introduced in Env on FVVs to test if the predicted residues impact binding and entry into cells.

While our data suggest that the HBS does not form a common nAb epitope itself, regions surrounding the HBS potentially constitute important targets. Indeed, residues around glycan N7' located above the HBS were identified as common targets of plasma nAbs from most GII-infected donors (Fig. V-4J). Moreover, N8 is located just above N7' where it arises from a cavity, thus one could speculate if N8 takes part of an epitope formed by N7'. The buried location of N8 renders it resistant to removal by glycosidases as observed on the solved RBD structure and explains its essential role for Env expression (Fig. IV-3). For those reasons we could not mutate this glycan and directly investigate this question. In line with this, one could speculate if N8 is masking nAb epitopes. We assume this to be unlikely since the glycan is necessary for expression and the residues masked on the protein surface underneath this glycan forms a hydrophobic patch (Fig. IV-3A). Instead to answer these questions, I would design mutations surrounding the N8 glycan. Indeed, the glycan insertion mutant E485N which is located close to N8 had a notable effect on block of GII-specific nAbs (Fig. V-6F), which indirectly suggests the presence of epitopes in near proximity to this evolutionary conserved glycan.

GI-specific nAbs target the L3 loop, which is clearly an immunodominant epitope. For this reason, I have not intensively searched for epitopes on the lower domain as these would probably be subdominant and likely difficult to study with polyclonal plasma samples. To build a more comprehensive study on nAb epitopes on GI Env, some additional mutants could be tested on CI-PFV SU-Ig. HBS mutations could be determined through AF structural prediction as discussed above. Moreover, the N7' glycosylation site is absent on CI-PFV. Thus, a mutant with glycan insertion on this position would indicate if GI-specific nAbs are targeting this glycan as was observed for GII-specific plasma nAbs. In such case, N7' insertion should enhance the block of nAbs compared to WT CI-PFV SU-Ig.

My data support that one prominent and genotype-specific epitopic region is located on base loop (residues 345-353) within the lower domain of the GII-K74 RBD. Insertion of a glycan at residue G350 completely abrogated block of nAbs from seven GII-infected donors (Fig. V-6I). Repositioning of the inserted glycan one residue downstream at position N351 resulted in same effect as observed for the glycan at position G350 (Fig. V-6H). Although these proteins tended to form more aggregates compared to WT, we excluded this as reason for lack of mutant activity through size exclusion chromatography (Fig. S.V-6). Moreover, swapping of base loop residues

345-351 from GI-D468 into GII-K74 SU supported the location of an epitope (Fig. V-6K). Interestingly, sequence alignments and structural predictions by AF found substantial variation in this loop, primarily due to an additional residue present in CI/GI strains compared to GII strains (Fig. V-6B'). Insertion of this missing residue (E349) from the GI-D468 strain into the backbone of GII-K74 SU confirmed our results (Fig. V-6J). Lastly, we showed that insertion of a glycan on the helix adjacent to the base loop also disrupted binding of most nAbs (Fig. V-6N). Collectively, these results support that the base loop residues 345-351 are part of a GII-specific nAb epitope.

Although we did not find evidence of nAb recognition of the base loop among six GI-infected donors tested against the CI-PFV G350N mutant, this result remains to be confirmed with additional mutants. For example, the swap345 mutant (Fig. V-6K) containing the majority of the GI base loop sequence in GII SU backbone could be tested for acquired activity against GI-specific plasma samples. CI-PFV base loop deletion and swapping with GII-K74 in SU-Iggs were tested but resulted in low protein expression. Importantly, studies on SFV strains from other species including macaques and mandrills found that our inserted N350 glycosylation site exists and circulates in nature in genotype I strains (Aiewsakun et al., 2019a). While we cannot confirm the actual attachment of a glycan on this position, these data suggest that this glycan is not deleterious for genotype I SU binding to susceptible cells or entry (Fig. V-9). In addition, we have observed another GI-specific polymorphism just upstream at position 346 within the base loop resulting in the presence or absence of glycosylation site N7 (Fig. S.IV-7B).

In summary, we have identified two epitopic regions on the lower RBD subdomain targeted by GII-specific nAbs. Further studies are required to obtain a more precise location of these epitopes. GI-specific nAbs mostly target the upper domain and therefore we have limited the investigations on epitopes at the lower subdomain because these are likely subdominant.

6.1.3 Limitations of current data and opportunities to address them in future studies

Our study has some limitations for which most are related to our experimental settings. Some of these has already been addressed in the sections above, while other important limitations were not addressed yet. Firstly, while we have performed a broad mapping of GII-specific epitopes using a homologous protein to the strain of infection, our mapping of GI-specific epitopes was performed using a heterologous protein from the laboratory adapted CI-PFV strain. Although this strain is cross-neutralized by most GI-infected donors (Lambert et al.,

2018), nAb titers to this strain are usually lower compared to the homologous GI-D468 strain isolated from a zoonotically infected donor. Unfortunately, the GI-D468 SU was poorly expressed, tended to aggregate and for that reason we only mapped the best candidate epitopes using the CI-PFV SU-Ig which was well expressed. This could influence our data and we have likely missed GI-strain specific epitopes not present at the CI-PFV strain. For example, this strain does not carry the N7' glycan which is present in most other CI and GI strains as already mentioned. An insert of N7' within CI SU or chimeras with GI-CI sequence swaps could be used to address some of these missed GI-specific epitopes.

Secondly, the use of polyclonal plasma samples for mapping of nAb epitopes hampers the precise definition of epitopes. Our results are likely reflecting a mapping of dominant epitopes. We would expect to observe stronger negative effects on block of nAbs by mutations affecting a larger fraction of nAbs targeting similar sites or epitopes, compared to a mutation affecting a smaller fraction of nAbs. For those reasons, it is likely that we have missed some subdominant epitopes. A solution to this would be isolation of monoclonal antibodies that recognize subdominant epitopes (see perspective section 6.3).

Other limitations include introduction of mutations with detrimental effects for protein expression and/or folding. We observed such effects for certain mutants as mentioned in supplementary table S.V-3. Moreover, our glycan insertion strategy has some drawbacks that includes uncertainty in regards to actual glycan insertion on the desired location. Such glycan differences are difficult to observe by size of protein bands on gels. Instead, a solution would be to perform mass-spectrometry on protein samples to confirm the actual insertion of a glycan. The glycan insert approach has been used by others for mapping of HIV-1 nAbs on viral particles (Dingens et al., 2017; Dingens et al., 2021). We chose our strategy with protein competitors since this was the simplest and we indeed identified important epitopes using this strategy. Glycan insertion might be used as a screening tool to be confirmed with additional constructs and design of mutations which may preserve folding, such as swapping stretches of residues or aa substitutions. The model for this approach is the experiments performed to define the epitope on the base loop on the lower RBD (aa 345-351). This epitope was the easiest to study because the structure was known with high confidence and the loop size was genotype-specific.

6.1.4 Epitope comparison to nAbs targeting orthoretroviruses

MLV and HTLV: The majority of characterized nAbs against MLV, for which the RBD structure has been solved, are strain-specific and target epitopes located on the variable loops VRA -B and -C (Fig. I-23). These loops define the viral tropism as they are critical for receptor binding. Our work on SFV also shows the targeting of variable loops on the RBD by human antibodies. In contrast to MLV, the three loops in the upper domain are not involved in cell binding. Indeed, deletion of RBDj and loops on recombinant SU and Env expressed on SFV vectors had minor effects on binding to cells (Fig. V-9). Our data also confirms that most SFV-specific nAb epitopes are conformational which goes in line with what has been reported for HTLV-specific human antibodies (Hadlock et al., 1999).

HIV: A wide range of bnAb epitopes have been defined on the HIV-1 Env, including the CD4-receptor binding site. This site is a critical target of bnAbs because it is more conserved and allows fewer mutations due to its functional role across all major HIV strains (Scheid et al., 2011; Zhou et al., 2015) and reviewed by (Georgiev et al., 2013). In addition, many epitopes formed by glycans have been well characterized for the heavily glycosylated HIV-1 Env. Glycans on HIV Env themselves often participate in bnAb contact but can also modulate epitope focus as seen for nAbs targeting the glycan hole super site (Dingens et al., 2021; Klasse et al., 2020; McCoy et al., 2016). Despite less extensive glycosylation, our results pinpoint glycan N7' as a nAb target on SFV GII Env (Fig. V-4J). In contrast to HIV-1, SFV Env does not seem to use glycan masking of epitopes, which likely also participates to the lack of immune escape variants observed in SFV-infections. Moreover, our results confirm that the major nAb epitopes are located on the RBD within SU and not on the LP or TM domains of SFV Env. This is in contrast to HIV-1, for which its TM domain has been shown targeted by bnAbs as well as the SU/TM subunit interface. Lastly, HIV-1 nAb epitopes frequently undergo deep immune escape through sequence variations which is in stark contrast to the highly stable genome of SFVs.

6.2 Achievements regarding the two genotypes

6.2.1 Discovery of genotype-specific epitopes

Based on previous work from our lab showing that the majority of SFV single-infected individuals neutralize only one SFV genotype (Lambert et al., 2018), we expected and directly searched for epitopes within SUvar. Indeed, I identified key epitopic regions that appear distinctly recognized by GI vs GII-infected donors.

Firstly, I identified a potent nAb epitopic region around residues 345-351 targeted by most GII-infected donors. Glycan insertion at position G350 in the base loop of the RBD resulted in strong decrease in block of nAbs from GII-infected donors but not GI-infected donors (Fig. V-7D). Secondly, the apex loops L2, -3 and -4 appear as major targets of nAbs for all donors, however substantial differences were observed. In particular, L3 was a dominant target of GI-specific nAbs, while all three loops were targeted by GII-specific nAbs (Fig. V-7G and V-7L). Further studies to precisely narrow down these genotype-specific epitopes and potentially identify novel ones may expand the list of differences.

6.2.2 Genotype-specific determinants of binding

While the receptor for SFV is still unknown, our results on SU-Ig binding to cells described one genotype-specific region critical for SU binding to its entry receptor(s) expressed on HT1080 cells (Fig. V-9). In line with block of nAbs, the base loop appears important for binding of SFV Env to cells for the GII-K74 strain but not for CI-PFV. Indeed, glycan insertion into this base loop only impacted binding of SU-Ig from the GII strain (Fig. V-9A). Interestingly, I also observed overall higher level of SU binding for the CI-PFV strain compared to that of GII-K74 (Fig. S.V-8B). In line with those results, our structural predictions highlight with strong confidence a clear difference in fold of this loop for which CI/GI strains harbor an additional residue as mentioned above (Fig. V-6B'). Thus, our data support that the base loop located at the lower domain of RBD may be involved in receptor binding. One could speculate that this loop interacts directly with a cellular receptor, which is different for the two genotypes. However, this goes against published data supporting that all FVs use the same entry receptor or attachment factors (Berg et al., 2003). Alternatively, each genotype may bind the same cellular receptor in a different way. Currently, we cannot exclude the existence of several molecules required for SFV entry, including some common to all genotypes and others specific for a certain genotype.

6.2.3 A similar global fold of RBD among distinct FVs

The SFV RBD structure solved by our collaborators represents the first high-resolution structure of a FV RBD and adds to the list of solved exogenous retroviral RBD structures from HIV, MLV and FeLV (Fig. S.IV-4). This RBD structure represent a novel fold with no precedents and shows limited similarity to these other retroviral RBDs. Based on AF structural predictions, sequence alignments and the novel gorilla SFV RBD structure, an RBD 'common core' was shown structurally conserved across all FVs. In contrast, outer regions of the RBD

were found to be more divergent between FVs – including among SFV strains from distinct genotypes (Fig. S.IV-9). Although the AF neural network predicts the CC with high precision for a wide range of FVs, it fails to obtain confident predictions of the outer apex loops (Fig. S.IV-8). For those reasons, experimental structures are still crucial in order to obtain and validate native protein conformations. We mainly found genotype-specific epitopes on the outer RBD regions, but epitopes located on the CC are expected and we should search for more GI epitopes in this region. Antibodies able to cross-neutralize both genotypes would likely target more ‘structurally’ conserved epitopes within the genotype-specific SUvar region.

6.2.4 Genotype-specific ELISA assay and tools to identify co-infected individuals

Our lab has previously identified co-infection by strains from two genotypes. The neutralization assay identified one third of individuals whose plasma samples neutralized both strains. The genotype-specific PCR identified only half of these infections based on SUvar directed primers (Lambert et al., 2018; Richard et al., 2015). Thus, PCR may be less sensitive than serologic assays. For those reasons, methods for detection of genotype-specific infection by serological means would be of great interest. I tested the recognition of SU-Ig immunoadhesins by human plasma samples in ELISA and found that SU-Ig binding by plasma antibodies matched the genotype of infection. Those findings support the use of the CI-PFV and GII-K74 SU-Ig as a diagnostic tool for serological identification of genotype of infection. Such genotype specific binding to SU was unexpected, as nearly half of its sequence (44%) is well conserved between the two strains used, and suggest that the SUvar (aa identity = 58%) region is more immunogenic than the SUcon (aa identity = 87%). For comparison and in support of this, the aa identity of SUcon is 97.2% between the zoonotic GII-K74 and GI-D468 strains homologous to those viruses infecting our cohort of donors. In contrast, SUvar from the heterologous CI-PFV strain used in the assay present only 71.4% aa identity to SUvar from the gorilla GI-D468 strain. Thus, most antibodies recognizing SU are directed against the genotype-defining SUvar region.

6.3 Next step on epitope mapping

While we chose a functional assay for mapping of nAb epitopes, other approaches would be ideal to use in the future for mapping of polyclonal antibody epitopes. One recently emerged technique for that exact purpose is negative-stain electron microscopy. This tool was used for the mapping of polyclonal antibody epitopes on HIV-1 Env in sera from immunized animals (Bianchi et al., 2018). That approach, in combination with other classical epitope mapping strategies nicely recapitulated findings from other studies and gave a broad overview of major Env targets (Dingens et al., 2021). However, this technique requires large amounts of plasma which is currently not available in our biobank from SFV-infected donors.

The more precise mapping of nAb epitopes would be through structural obtainment of antigen-antibody complexes. However, this requires monoclonal antibodies which are currently not available. If such mAbs were at hand, solving the structure of a mAb Fab bound to the SFV Env would directly identify the epitope and residues of contact. A Fab arm complexed to Env could potentially also favor Env in a pre-fusion state, in particular if the mAb binds a quaternary epitope. Thus, the obtainment of SFV Env-specific mAbs may help our collaborators obtain an Env structure in its pre-fusion conformation.

To obtain mAbs from SFV-infected individuals, I set up the assay for the isolation of memory B cells and subsequent screening for SFV Env-reactive antibodies in ELISA based largely on a published protocol (Huang et al., 2013). This approach relies on fluorescence activated cell sorting (FACS) based isolation of single CD19⁺IgG⁺ memory B cells from frozen PBMCs. Single-sorted memory B cells are cultured for two weeks in P384-well plates seeded with irradiated 3T3-msCD40L feeder cells in presence of IL-2 and -21. After two weeks of culture, supernatants are harvested and screened for IgG and binding to SFV antigens. The first cloning of memory B cells from a GI-infected donor has been initiated.

6.4 Env mutations useful for selecting Env-specific B cells

A commonly used method for isolation of monoclonal antibodies relies on sorting of antigen-specific memory B cells with fluorescently conjugated protein baits. Such methods have been used for isolation of potent nAbs against a broad range of pathogenic viruses including HIV, influenza, ebola and more (Gieselmann et al., 2021). In the case of SFV, using the Env protein as a bait would likely result in high background binding to all major B cell populations expressing the ubiquitous receptor yet to be identified. Indeed, my preliminary data showed high binding of trimeric Env and SU-Ig proteins to all major B cell, T cell, NK cell and

monocyte populations from healthy donor PBMCs (data not shown). For those reasons, I initiated B cell isolation strategies that does not rely on Env baits as described above. Interestingly, the monomeric RBD proteins showed limited binding compared to SU-Ig and trimeric Env on the HT1080 cell line, despite the RBD blocking nAbs as efficiently as SU immunoadhesin. This knowledge is valuable for the use of SFV Env as a protein bait. Moreover, the identification of mutations which lowered cell binding but retained nAb block such as the HBS mutant pairs (K342/R343 and R356/R369) may further diminish Env background binding to HS expressed on unspecific B cells. These mutant proteins have to be tested for their binding to human primary B cells before their use to isolate SFV-specific B cells.

6.5 Next step on SFV Env structure

At the present moment, we do not have a pre-fusion Env trimer structure from SFV available. As mentioned above, an Env structure in its pre-fusion conformation would be highly valuable and needed for the characterization of quaternary nAb epitopes as well as decoding the SFV fusion machinery. Vice versa, isolation of mAbs targeting a quaternary epitope may allow the obtainment of a stabilized Env trimer 3D-structure. In absence of mAbs, a pre-fusion Env trimer could be obtained through introduction of stabilizing mutations preventing the Env from folding into a post-fusion state. Such mutations were successfully introduced into HIV-1 Env (Julien et al., 2013) and CoV spike (Hsieh et al., 2020; Kirchdoerfer et al., 2016) among other viral fusogenic glycoproteins, and these stabilized trimers are the preferred use as vaccine antigens since they favor induction of nAbs compared to non-stabilized trimers, reviewed by (Sliепен and Sanders, 2016).

While we have structural details of the GII-K74 strain, its opposite genotype is lacking such information. Prediction tools like AF did not give clues to differences in fold of RBD from GI strains vs our X-ray RBD structure from the GII-K74 strain. Thus, obtaining high-resolution structures of an RBD or pre-fusion trimer from a GI strain to compare major differences between SFV genotypes would be valuable and help to find key regions that can explain genotype-specific epitopes. Moreover, obtaining trimeric Env structures would validate our results on location of the RBD within the pre-fusion trimer. It is expected that the flexible apex loops will have distinct conformations, which may only be visible within a trimeric context – or may only be visible upon nAb binding.

6.6 Next step on SFV receptor

6.6.1 HBS

Our results identified residues K342, R343, R356 and R369 as essential for SFV Env binding to HS expressed on cells. However, binding was readily observed for HBS mutant proteins despite removal of surface expressed HS. It is currently unclear whether residual HS mediates the low level of binding or whether the results indirectly support the presence of an additional receptor. HT1080 cells express an excessive amount of HS compared to BHK cells (approx. 10-fold higher), and HS surface expression is correlated with the susceptibility to infection in cell lines (Plochmann et al., 2012). Indeed, one study concluded that HS acts as a direct entry receptor for PFV (Nasimuzzaman and Persons, 2012), while another study concluded that an additional receptor must be present since FVV transduction of HS^{neg} cells was possible, albeit at lower levels compared to its parental HS^{pos} clone (Plochmann et al., 2012). Indeed, the study of SFV entry and the search of a FV-specific receptor may require the use of HS-deficient cell lines. Several studies have used Raji B cells as control due to their overall resistance to PFV-infection and low transduction by FVVs which correlate with their near absence of surface expressed HS. In my experiments Raji cells are stained by SFV Env proteins at low level. Similarly, HS staining is very low but treatment with heparinase yields a clear staining with the control antibody against the neo-epitope present post HS cleavage (data not shown). These results suggest a low but detectable level of HS on Raji cells.

Our definition of the HS binding site and the mutant proteins will likely be useful for the experiments on SFV entry in the future.

6.7 Next step on antiviral role of antibodies

Lastly, my study has focused solely on nAbs and thus, we did not assess other functionalities beyond neutralization. Fc-mediated functions and complement may play important roles in antibody-mediated control of SFV infection, as has been observed for HIV-1 nAbs in protection against SHIV challenge in macaques (Hessell et al., 2007). In addition to block of viral entry, nAbs may prevent dissemination of virus *in vivo* and could potentially mediate reduction or elimination of viral reservoirs through ADCC or ADCP by binding to surface expressed Env on infected cells (Barin and Braibant, 2019). In the case of HIV-1, experimental intravenous use of bnAbs in NHP models have shown that these potent antibodies can suppress viral replication in anatomical sites distant from the site of viral inoculation (Liu et al., 2016). This study also suggested that the V3-glycan recognizing bnAb PGT121 permits mucosal

translocation of SHIV. In relation to this, another possible mode of action is block of viral budding from infected cells as has been observed *in vitro* (Dufloo et al., 2022).

For SFV, two small studies have addressed the role of antibodies in protection against infection and establishment of chronic SFV-infection in NHPs (Khan and Kumar, 2006; Williams and Khan, 2010). Experimental SFV-infection in rhesus macaques upon whole blood transfusion from an SFV-infected donor monkey to an SFV-naïve recipient monkey demonstrated that infection only occurred when low nAb titers were present, or when the plasma was removed from the whole blood transfusion (Khan and Kumar, 2006; Williams and Khan, 2010). Although only few animals were studied, those results suggest that antibodies play a role in protection against SFV-infection. Non-neutralizing antibody functionalities were not investigated in these studies. Importantly, a recent paper from our lab showed that SFV-specific plasma antibodies from infected humans can bind to the surface of infected cells, possibly allowing the recruitment of innate effector cells (Couteaudier et al., 2022). Currently, the obstacle to test antibody-mediated elimination of SFV-infected cells is the low Env surface expression on infected cells and the relatively narrow window of Env expression prior to syncytia formation and cell death upon *in vitro* infection with replication competent virus. Instead, target cells transduced with an Env expression vector for stable Env surface presentation or surrogate assays using recombinant Env and reporter effector cells could be applied to circumvent this issue for the future. Such assays can be used with polyclonal plasma samples from SFV-infected individuals. Moreover, and beyond neutralization, this would also be ideal to test for any isolated mAbs specific for SFV Env.

CHAPTER VII

CONCLUSIONS

7 | CONCLUSIONS

Our collaborators describe the first high-resolution structure of a FV RBD from a zoonotic gorilla SFV strain. This 3D structure shows the organization of the RBD in an upper and a lower subdomain. The upper domain is involved in inter-trimer contacts and likely stabilizes the trimeric Env. Moreover, we discovered a potent HBS within the lower domain and demonstrated that four residues K342, R343, R356 and R369 are directly involved in SFV Env binding to immobilized heparin and cell surface-expressed HS.

I demonstrated that nAb epitopes are mainly conformational and I discovered epitopes on both domains of the RBD with evidence for genotype-specific targets. In addition, we demonstrated that mobile loops at the RBD apex likely involved in trimer stabilization are targeted by nAbs in a genotype-specific manner, for which L3 is dominantly targeted by GI-infected donors. We confirmed that these loops are necessary for viral entry or fusion and that they are not recognized as linear peptides by plasma antibodies. Moreover, a dominant genotype-specific epitope was defined around residues 345-351 in the lower domain targeted only by plasma antibodies from GII-infected donors. My results do not support the HBS as a dominant epitope, however other targets in its proximity were discovered including the N7' glycan on GII-RBD.

In conclusion, the work presented in this thesis highlights the first comprehensive mapping of conformational epitopes on the SFV Env targeted by human polyclonal plasma antibodies. My work contributes substantially to knowledge on immune responses to SFVs and I provide evidence that human nAbs target epitopes with functional importance for the virus. This knowledge may aid the ongoing work on understanding SFV impact on human health, the subsequent control in the human host upon zoonotic spill-over from NHP reservoirs and prevention of viral emergence in the human population. Our work may also guide the future design and use of FVs as gene therapy tools.

CHAPTER VIII

LIST OF REFERENCES

8 | LIST OF REFERENCES

1. Achong, B.G., Mansell, P.W., Epstein, M.A., and Clifford, P. (1971). An unusual virus in cultures from a human nasopharyngeal carcinoma. *J Natl Cancer Inst* 46, 299-307.
2. Adams, P.D., Afonine, P.V., Bunkóczi, G., Chen, V.B., Davis, I.W., Echols, N., Headd, J.J., Hung, L.W., Kapral, G.J., Grosse-Kunstleve, R.W., *et al.* (2010). PHENIX: a comprehensive Python-based system for macromolecular structure solution. *Acta Crystallogr D Biol Crystallogr* 66, 213-221.
3. Aiewsakun, P. (2020). Avian and serpentine endogenous foamy viruses, and new insights into the macroevolutionary history of foamy viruses. *Virus evolution* 6, vez057.
4. Aiewsakun, P., and Katzourakis, A. (2017). Marine origin of retroviruses in the early Palaeozoic Era. *Nature communications* 8, 13954.
5. Aiewsakun, P., Richard, L., Gessain, A., Mouinga-Ondeme, A., Vicente Afonso, P., and Katzourakis, A. (2019a). Modular nature of simian foamy virus genomes and their evolutionary history. *Virus evolution* 5, vez032.
6. Aiewsakun, P., Simmonds, P., and Katzourakis, A. (2019b). The First Co-Opted Endogenous Foamy Viruses and the Evolutionary History of Reptilian Foamy Viruses. *Viruses* 11.
7. Alais, S., Pasquier, A., Jegado, B., Journo, C., Rua, R., Gessain, A., Tobaly-Tapiero, J., Lacoste, R., Turpin, J., and Mahieux, R. (2018). STLV-1 co-infection is correlated with an increased SFV proviral load in the peripheral blood of SFV/STLV-1 naturally infected non-human primates. *PLoS Negl Trop Dis* 12, e0006812.
8. Alamgir, A.S., Owens, N., Lavignon, M., Malik, F., and Evans, L.H. (2005). Precise identification of endogenous proviruses of NFS/N mice participating in recombination with moloney ecotropic murine leukemia virus (MuLV) to generate polytropic MuLVs. *J Virol* 79, 4664-4671.
9. Albritton, L.M., Tseng, L., Scadden, D., and Cunningham, J.M. (1989). A putative murine ecotropic retrovirus receptor gene encodes a multiple membrane-spanning protein and confers susceptibility to virus infection. *Cell* 57, 659-666.
10. Alke, A., Schwantes, A., Zemba, M., Flugel, R.M., and Lochelt, M. (2000). Characterization of the humoral immune response and virus replication in cats experimentally infected with feline foamy virus. *Virology* 275, 170-176.
11. Amanna, I.J., Carlson, N.E., and Slifka, M.K. (2007). Duration of humoral immunity to common viral and vaccine antigens. *N Engl J Med* 357, 1903-1915.
12. Amborski, G.F., Storz, J., Keney, D., Lo, J., and McChesney, A.E. (1987). Isolation of a retrovirus from the American bison and its relation to bovine retroviruses. *J Wildl Dis* 23, 7-11.
13. Ansari, H.R., and Raghava, G.P. (2010). Identification of conformational B-cell Epitopes in an antigen from its primary sequence. *Immunome Res* 6, 6.
14. Ayoub, A., Akoua-Koffi, C., Calvignac-Spencer, S., Esteban, A., Locatelli, S., Li, H., Li, Y., Hahn, B.H., Delaporte, E., Leendertz, F.H., *et al.* (2013). Evidence for continuing cross-species transmission of SIVsmm to humans: characterization of a new HIV-2 lineage in rural Cote d'Ivoire. *AIDS* 27, 2488-2491.
15. Baba, E., Nakamura, M., Tanaka, Y., Kuroki, M., Itoyama, Y., Nakano, S., and Niho, Y. (1993). Multiple neutralizing B-cell epitopes of human T-cell leukemia virus type 1 (HTLV-1) identified by human monoclonal antibodies. A basis for the design of an HTLV-1 peptide vaccine. *J Immunol* 151, 1013-1024.
16. Backovic, M., and Krey, T. (2016). Stable Drosophila Cell Lines: An Alternative Approach to Exogenous Protein Expression. *Methods Mol Biol* 1350, 349-358.
17. Bahr, A., Singer, A., Hain, A., Vasudevan, A.A., Schilling, M., Reh, J., Riess, M., Panitz, S., Serrano, V., Schweizer, M., *et al.* (2016). Interferon but not MxB inhibits foamy retroviruses. *Virology* 488, 51-60.
18. Baldwin, D.N., and Linial, M.L. (1998). The roles of Pol and Env in the assembly pathway of human foamy virus. *J Virol* 72, 3658-3665.
19. Bangaru, S., Lang, S., Schotsaert, M., Vandervan, H.A., Zhu, X., Kose, N., Bombardi, R., Finn, J.A., Kent, S.J., Gilchuk, P., *et al.* (2019). A Site of Vulnerability on the Influenza Virus Hemagglutinin Head Domain Trimer Interface. *Cell* 177, 1136-1152.e1118.

List of References

20. Bansal, A., Shaw, K.L., Edwards, B.H., Goepfert, P.A., and Mulligan, M.J. (2000). Characterization of the R572T point mutant of a putative cleavage site in human foamy virus. *Env. J Virol* *74*, 2949-2954.
21. Bao, Q., Hipp, M., Hugo, A., Lei, J., Liu, Y., Kehl, T., Hechler, T., and Löchelt, M. (2015). In Vitro Evolution of Bovine Foamy Virus Variants with Enhanced Cell-Free Virus Titers and Transmission. *Viruses* *7*, 5855-5874.
22. Bao, Q., Hotz-Wagenblatt, A., Betts, M.J., Hipp, M., Hugo, A., Pougialis, G., Lei-Rossmann, J., and Löchelt, M. (2020). Shared and cell type-specific adaptation strategies of Gag and Env yield high titer bovine foamy virus variants. *Infect Genet Evol* *82*, 104287.
23. Bar-On, Y., Gruell, H., Schoofs, T., Pai, J.A., Nogueira, L., Butler, A.L., Millard, K., Lehmann, C., Suarez, I., Oliveira, T.Y., *et al.* (2018). Safety and antiviral activity of combination HIV-1 broadly neutralizing antibodies in viremic individuals. *Nat Med* *24*, 1701-1707.
24. Bar, K.J., Tsao, C.Y., Iyer, S.S., Decker, J.M., Yang, Y., Bonsignori, M., Chen, X., Hwang, K.K., Montefiori, D.C., Liao, H.X., *et al.* (2012). Early low-titer neutralizing antibodies impede HIV-1 replication and select for virus escape. *PLoS Pathog* *8*, e1002721.
25. Barbalat, R., Lau, L., Locksley, R.M., and Barton, G.M. (2009). Toll-like receptor 2 on inflammatory monocytes induces type I interferon in response to viral but not bacterial ligands. *Nat Immunol* *10*, 1200-1207.
26. Barin, F., and Braibant, M. (2019). HIV-1 antibodies in prevention of transmission. *Curr Opin HIV AIDS* *14*, 273-278.
27. Barnett, A.L., Wensel, D.L., Li, W., Fass, D., and Cunningham, J.M. (2003). Structure and mechanism of a coreceptor for infection by a pathogenic feline retrovirus. *J Virol* *77*, 2717-2729.
28. Barouch, D.H., Whitney, J.B., Moldt, B., Klein, F., Oliveira, T.Y., Liu, J., Stephenson, K.E., Chang, H.W., Shekhar, K., Gupta, S., *et al.* (2013). Therapeutic efficacy of potent neutralizing HIV-1-specific monoclonal antibodies in SHIV-infected rhesus monkeys. *Nature* *503*, 224-228.
29. Battini, J.L., Danos, O., and Heard, J.M. (1995). Receptor-binding domain of murine leukemia virus envelope glycoproteins. *J Virol* *69*, 713-719.
30. Battini, J.L., Heard, J.M., and Danos, O. (1992). Receptor choice determinants in the envelope glycoproteins of amphotropic, xenotropic, and polytropic murine leukemia viruses. *J Virol* *66*, 1468-1475.
31. Benson, J., Tschachler, E., Gessain, A., Yanagihara, R., Gallo, R.C., and Franchini, G. (1994). Cross-neutralizing antibodies against cosmopolitan and Melanesian strains of human T cell leukemia/lymphotropic virus type I in sera from inhabitants of Africa and the Solomon Islands. *AIDS Res Hum Retroviruses* *10*, 91-96.
32. Berg, A., Pietschmann, T., Rethwilm, A., and Lindemann, D. (2003). Determinants of foamy virus envelope glycoprotein mediated resistance to superinfection. *Virology* *314*, 243-252.
33. Bergez, M., Weber, J., Riess, M., Erdbeer, A., Seifried, J., Stanke, N., Munz, C., Hornung, V., König, R., and Lindemann, D. (2019). Insights into Innate Sensing of Prototype Foamy Viruses in Myeloid Cells. *Viruses* *11*.
34. Berka, U., Hamann, M.V., and Lindemann, D. (2013). Early events in foamy virus-host interaction and intracellular trafficking. *Viruses* *5*, 1055-1074.
35. Bermejo-Jambrina, M., Eder, J., Kaptein, T.M., van Hamme, J.L., Helgers, L.C., Vlaming, K.E., Brouwer, P.J.M., van Nuenen, A.C., Spaargaren, M., de Bree, G.J., *et al.* (2021). Infection and transmission of SARS-CoV-2 depend on heparan sulfate proteoglycans. *EMBO J* *40*, e106765.
36. Betsem, E., Rua, R., Tortevoeye, P., Froment, A., and Gessain, A. (2011). Frequent and recent human acquisition of simian foamy viruses through apes' bites in central Africa. *PLoS Pathog* *7*, e1002306.
37. Bianchi, M., Turner, H.L., Nogal, B., Cottrell, C.A., Oyen, D., Pauthner, M., Bastidas, R., Nedellec, R., McCoy, L.E., Wilson, I.A., *et al.* (2018). Electron-Microscopy-Based Epitope Mapping Defines Specificities of Polyclonal Antibodies Elicited during HIV-1 BG505 Envelope Trimer Immunization. *Immunity* *49*, 288-300.e288.
38. Bieniasz, P.D., Rethwilm, A., Pitman, R., Daniel, M.D., Chrystie, I., and McClure, M.O. (1995a). A comparative study of higher primate foamy viruses, including a new virus from a gorilla. *Virology* *207*, 217-228.
39. Bieniasz, P.D., Weiss, R.A., and McClure, M.O. (1995b). Cell cycle dependence of foamy retrovirus infection. *J Virol* *69*, 7295-7299.

40. Blanc, E., Roversi, P., Vonrhein, C., Flensburg, C., Lea, S.M., and Bricogne, G. (2004). Refinement of severely incomplete structures with maximum likelihood in BUSTER-TNT. *Acta Crystallogr D Biol Crystallogr* *60*, 2210-2221.
41. Blanchard, S., Astier-Gin, T., Tallet, B., Moynet, D., Londos-Gagliardi, D., and Guillemain, B. (1999). Amino acid changes at positions 173 and 187 in the human T-cell leukemia virus type 1 surface glycoprotein induce specific neutralizing antibodies. *J Virol* *73*, 9369-9376.
42. Blasse, A., Calvignac-Spencer, S., Merkel, K., Goffe, A.S., Boesch, C., Mundry, R., and Leendertz, F.H. (2013). Mother-offspring transmission and age-dependent accumulation of simian foamy virus in wild chimpanzees. *J Virol* *87*, 5193-5204.
43. Blewett, E.L., Black, D.H., Lerche, N.W., White, G., and Eberle, R. (2000). Simian foamy virus infections in a baboon breeding colony. *Virology* *278*, 183-193.
44. Bloom, D.E., Black, S., and Rappuoli, R. (2017). Emerging infectious diseases: A proactive approach. *Proc Natl Acad Sci U S A* *114*, 4055-4059.
45. Bodem, J. (2011). Regulation of foamy viral transcription and RNA export. *Adv Virus Res* *81*, 1-31.
46. Bodem, J., Schied, T., Gabriel, R., Rammling, M., and Rethwilm, A. (2011). Foamy virus nuclear RNA export is distinct from that of other retroviruses. *J Virol* *85*, 2333-2341.
47. Bogerd, H.P., Skalsky, R.L., Kennedy, E.M., Furuse, Y., Whisnant, A.W., Flores, O., Schultz, K.L., Putnam, N., Barrows, N.J., Sherry, B., *et al.* (2014). Replication of many human viruses is refractory to inhibition by endogenous cellular microRNAs. *J Virol* *88*, 8065-8076.
48. Boneva, R.S., Grindon, A.J., Orton, S.L., Switzer, W.M., Shanmugam, V., Hussain, A.I., Bhullar, V.B., Chamberland, M.E., Heneine, W., Folks, T.M., *et al.* (2002). Simian foamy virus infection in a blood donor. *Transfusion* *42*, 886-891.
49. Boneva, R.S., Switzer, W.M., Spira, T.J., Bhullar, V.B., Shanmugam, V., Cong, M.E., Lam, L., Heneine, W., Folks, T.M., and Chapman, L.E. (2007). Clinical and virological characterization of persistent human infection with simian foamy viruses. *AIDS Res Hum Retroviruses* *23*, 1330-1337.
50. Bouvin-Pley, M., Morgand, M., Moreau, A., Jestin, P., Simonnet, C., Tran, L., Goujard, C., Meyer, L., Barin, F., and Braibant, M. (2013). Evidence for a continuous drift of the HIV-1 species towards higher resistance to neutralizing antibodies over the course of the epidemic. *PLoS Pathog* *9*, e1003477.
51. Boyer, P.L., Stenbak, C.R., Hoberman, D., Linial, M.L., and Hughes, S.H. (2007). In vitro fidelity of the prototype primate foamy virus (PFV) RT compared to HIV-1 RT. *Virology* *367*, 253-264.
52. Bricogne, G., Blanc, E., Brandl, M., Flensburg, C., Keller, P., Paciorek, W., Roversi, P., Smart, O.S., Vonrhein, C., and Womack, T.O. (2009). BUSTER. 2.8.0 edn (Global Phasing Ltd., Cambridge, United Kingdom).
53. Brooks, J.I., Rud, E.W., Pilon, R.G., Smith, J.M., Switzer, W.M., and Sandstrom, P.A. (2002). Cross-species retroviral transmission from macaques to human beings. *Lancet* *360*, 387-388.
54. Brown, P., Nemo, G., and Gajdusek, D.C. (1978). Human foamy virus: further characterization, seroepidemiology, and relationship to chimpanzee foamy viruses. *J Infect Dis* *137*, 421-427.
55. Bruhns, P., and Jonsson, F. (2015). Mouse and human FcR effector functions. *Immunol Rev* *268*, 25-51.
56. Bunch, T.A., Grinblat, Y., and Goldstein, L.S. (1988). Characterization and use of the *Drosophila* metallothionein promoter in cultured *Drosophila melanogaster* cells. *Nucleic Acids Res* *16*, 1043-1061.
57. Bunnik, E.M., Euler, Z., Welkers, M.R., Boeser-Nunnink, B.D., Grijsen, M.L., Prins, J.M., and Schuitemaker, H. (2010). Adaptation of HIV-1 envelope gp120 to humoral immunity at a population level. *Nat Med* *16*, 995-997.
58. Burkhart, M.D., Kayman, S.C., He, Y., and Pinter, A. (2003). Distinct mechanisms of neutralization by monoclonal antibodies specific for sites in the N-terminal or C-terminal domain of murine leukemia virus SU. *J Virol* *77*, 3993-4003.
59. Burtner, C.R., Beard, B.C., Kennedy, D.R., Wohlfahrt, M.E., Adair, J.E., Trobridge, G.D., Scharenberg, A.M., Torgerson, T.R., Rawlings, D.J., Felsburg, P.J., *et al.* (2014). Intravenous injection of a foamy virus vector to correct canine SCID-X1. *Blood* *123*, 3578-3584.
60. Buseyne, F., Betsem, E., Montange, T., Njouom, R., Bilounga Ndongo, C., Hermine, O., and Gessain, A. (2018). Clinical Signs and Blood Test Results Among Humans Infected With Zoonotic Simian Foamy Virus: A Case-Control Study. *J Infect Dis* *218*, 144-151.

List of References

61. Cabasso, V.J., Loofbourow, J.C., Roby, R.E., and Anuskiewicz, W. (1971). Rabies immune globulin of human origin: preparation and dosage determination in non-exposed volunteer subjects. *Bull World Health Organ* 45, 303-315.
62. Caillat, C., Guilligay, D., Sulbaran, G., and Weissenhorn, W. (2020). Neutralizing Antibodies Targeting HIV-1 gp41. *Viruses* 12.
63. Calattini, S., Betssem, E., Bassot, S., Chevalier, S.A., Tortevoeye, P., Njouom, R., Mahieux, R., Froment, A., and Gessain, A. (2011). Multiple retroviral infection by HTLV type 1, 2, 3 and simian foamy virus in a family of Pygmies from Cameroon. *Virology* 410, 48-55.
64. Calattini, S., Betssem, E.B., Froment, A., Mauclere, P., Tortevoeye, P., Schmitt, C., Njouom, R., Saib, A., and Gessain, A. (2007). Simian foamy virus transmission from apes to humans, rural Cameroon. *Emerg Infect Dis* 13, 1314-1320.
65. Calattini, S., Nerrienet, E., Mauclère, P., Georges-Courbot, M.C., Saib, A., and Gessain, A. (2006a). Detection and molecular characterization of foamy viruses in Central African chimpanzees of the Pan troglodytes troglodytes and Pan troglodytes vellerosus subspecies. *J Med Primatol* 35, 59-66.
66. Calattini, S., Nerrienet, E., Mauclère, P., Georges-Courbot, M.C., Saib, A., and Gessain, A. (2004). Natural simian foamy virus infection in wild-caught gorillas, mandrills and drills from Cameroon and Gabon. *J Gen Virol* 85, 3313-3317.
67. Calattini, S., Wanert, F., Thierry, B., Schmitt, C., Bassot, S., Saib, A., Herrenschmidt, N., and Gessain, A. (2006b). Modes of transmission and genetic diversity of foamy viruses in a *Macaca tonkeana* colony. *Retrovirology* 3, 23.
68. Cao, W., Bover, L., Cho, M., Wen, X., Hanabuchi, S., Bao, M., Rosen, D.B., Wang, Y.H., Shaw, J.L., Du, Q., *et al.* (2009). Regulation of TLR7/9 responses in plasmacytoid dendritic cells by BST2 and ILT7 receptor interaction. *J Exp Med* 206, 1603-1614.
69. Carlson, C.J., Albery, G.F., Merow, C., Trisos, C.H., Zipfel, C.M., Eskew, E.A., Olival, K.J., Ross, N., and Bansal, S. (2022). Climate change increases cross-species viral transmission risk. *Nature*.
70. Cartellieri, M., Herchenröder, O., Rudolph, W., Heinkelein, M., Lindemann, D., Zentgraf, H., and Rethwilm, A. (2005). N-terminal Gag domain required for foamy virus particle assembly and export. *J Virol* 79, 12464-12476.
71. Caskey, M. (2020). Broadly neutralizing antibodies for the treatment and prevention of HIV infection. *Curr Opin HIV AIDS* 15, 49-55.
72. Chai, N., Chang, H.E., Nicolas, E., Han, Z., Jarnik, M., and Taylor, J. (2008). Properties of subviral particles of hepatitis B virus. *J Virol* 82, 7812-7817.
73. Chan, D.C., Fass, D., Berger, J.M., and Kim, P.S. (1997). Core structure of gp41 from the HIV envelope glycoprotein. *Cell* 89, 263-273.
74. Chareza, S., Slavkovic Lukic, D., Liu, Y., Räthe, A.M., Münk, C., Zabogli, E., Pistello, M., and Löchel, M. (2012). Molecular and functional interactions of cat APOBEC3 and feline foamy and immunodeficiency virus proteins: different ways to counteract host-encoded restriction. *Virology* 424, 138-146.
75. Chavas, L.M.G., Gourhant, P., Guimaraes, B.G., Isabet, T., Legrand, P., Lener, R., Montaville, P., Sirigu, S., and Thompson, A. (2021). PROXIMA-1 beamline for macromolecular crystallography measurements at Synchrotron SOLEIL. *J Synchrotron Radiat* 28, 970-976.
76. Chen, B. (2019). Molecular Mechanism of HIV-1 Entry. *Trends Microbiol* 27, 878-891.
77. Chen, V.B., Arendall, W.B., 3rd, Headd, J.J., Keedy, D.A., Immormino, R.M., Kapral, G.J., Murray, L.W., Richardson, J.S., and Richardson, D.C. (2010). MolProbity: all-atom structure validation for macromolecular crystallography. *Acta Crystallogr D Biol Crystallogr* 66, 12-21.
78. Chen, Z., Telfier, P., Gettie, A., Reed, P., Zhang, L., Ho, D.D., and Marx, P.A. (1996). Genetic characterization of new West African simian immunodeficiency virus SIVsm: geographic clustering of household-derived SIV strains with human immunodeficiency virus type 2 subtypes and genetically diverse viruses from a single feral sooty mangabey troop. *J Virol* 70, 3617-3627.
79. Choudhary, A., Galvin, T.A., Williams, D.K., Beren, J., Bryant, M.A., and Khan, A.S. (2013). Influence of naturally occurring simian foamy viruses (SFVs) on SIV disease progression in the rhesus macaque (*Macaca mulatta*) model. *Viruses* 5, 1414-1430.

List of References

80. Chuang, G.Y., Zhou, J., Acharya, P., Rawi, R., Shen, C.H., Sheng, Z., Zhang, B., Zhou, T., Bailer, R.T., Dandey, V.P., *et al.* (2019). Structural Survey of Broadly Neutralizing Antibodies Targeting the HIV-1 Env Trimer Delineates Epitope Categories and Characteristics of Recognition. *Structure* 27, 196-206.e196.
81. Clapham, P., Nagy, K., and Weiss, R.A. (1984). Pseudotypes of human T-cell leukemia virus types 1 and 2: neutralization by patients' sera. *Proc Natl Acad Sci U S A* 81, 2886-2889.
82. Clarke, J.K., Attridge, J.T., and Gay, F.W. (1969). The morphogenesis of simian foamy agents. *J Gen Virol* 4, 183-188.
83. Colomer-Lluch, M., Ruiz, A., Moris, A., and Prado, J.G. (2018). Restriction Factors: From Intrinsic Viral Restriction to Shaping Cellular Immunity Against HIV-1. *Front Immunol* 9, 2876.
84. Cordonnier, A., Casella, J.F., and Heidmann, T. (1995). Isolation of novel human endogenous retrovirus-like elements with foamy virus-related pol sequence. *J Virol* 69, 5890-5897.
85. Couteaudier, M., Calzada-Fraile, D., Montange, T., Gessain, A., and Buseyne, F. (2019). Inhibitors of the interferon response increase the replication of gorilla simian foamy viruses. *Virology* 541, 25-31.
86. Couteaudier, M., Montange, T., Njouom, R., Bilounga-Ndongo, C., Gessain, A., and Buseyne, F. (2022). Plasma antibodies from humans infected with zoonotic simian foamy virus do not inhibit cell-to-cell transmission of the virus despite binding to the surface of infected cells. *PLoS Pathog* 18, e1010470.
87. Cowtan, K. (2006). The Buccaneer software for automated model building. 1. Tracing protein chains. *Acta Crystallogr D Biol Crystallogr* 62, 1002-1011.
88. Craig, K.L., Hasan, M.K., Jackson, D.L., Engel, G.A., Soliven, K., Feeroz, M.M., Wang, X., Jones-Engel, L., and Linial, M.L. (2015). A Semimadic Population in Bangladesh with Extensive Exposure to Macaques Does Not Exhibit High Levels of Zoonotic Simian Foamy Virus Infection. *J Virol* 89, 7414-7416.
89. Crotty, S. (2019). T Follicular Helper Cell Biology: A Decade of Discovery and Diseases. *Immunity* 50, 1132-1148.
90. Cullen, B.R. (2003). Nuclear mRNA export: insights from virology. *Trends Biochem Sci* 28, 419-424.
91. Cullen, B.R. (2013). How do viruses avoid inhibition by endogenous cellular microRNAs? *PLoS Pathog* 9, e1003694.
92. Cummins, J.E., Jr., Boneva, R.S., Switzer, W.M., Christensen, L.L., Sandstrom, P., Heneine, W., Chapman, L.E., and Dezzutti, C.S. (2005). Mucosal and systemic antibody responses in humans infected with simian foamy virus. *J Virol* 79, 13186-13189.
93. D'Arc, M., Ayouba, A., Esteban, A., Learn, G.H., Boué, V., Liegeois, F., Etienne, L., Tagg, N., Leendertz, F.H., Boesch, C., *et al.* (2015). Origin of the HIV-1 group O epidemic in western lowland gorillas. *Proc Natl Acad Sci U S A* 112, E1343-1352.
94. Daszak, P., Cunningham, A.A., and Hyatt, A.D. (2000). Emerging infectious diseases of wildlife--threats to biodiversity and human health. *Science* 287, 443-449.
95. Davey, R.A., Zuo, Y., and Cunningham, J.M. (1999). Identification of a receptor-binding pocket on the envelope protein of friend murine leukemia virus. *J Virol* 73, 3758-3763.
96. Davies, T.J., and Pedersen, A.B. (2008). Phylogeny and geography predict pathogen community similarity in wild primates and humans. *Proc Biol Sci* 275, 1695-1701.
97. DeLano, W.L. (2002). The PyMOL Molecular Graphics System. (DeLano Scientific, San Carlos, CA, USA).
98. Delebecque, F., Suspène, R., Calattini, S., Casartelli, N., Saïb, A., Froment, A., Wain-Hobson, S., Gessain, A., Vartanian, J.P., and Schwartz, O. (2006). Restriction of foamy viruses by APOBEC cytidine deaminases. *J Virol* 80, 605-614.
99. Delelis, O., Lehmann-Che, J., and Saib, A. (2004). Foamy viruses--a world apart. *Curr Opin Microbiol* 7, 400-406.
100. Delelis, O., Saïb, A., and Sonigo, P. (2003). Biphasic DNA synthesis in spumaviruses. *J Virol* 77, 8141-8146.
101. Desgranges, C., Souche, S., Vernant, J.C., Smadja, D., Vahlne, A., and Horal, P. (1994). Identification of novel neutralization-inducing regions of the human T cell lymphotropic virus type I envelope glycoproteins with human HTLV-I-seropositive sera. *AIDS Res Hum Retroviruses* 10, 163-173.
102. Desta, I.T., Porter, K.A., Xia, B., Kozakov, D., and Vajda, S. (2020). Performance and Its Limits in Rigid Body Protein-Protein Docking. *Structure* 28, 1071-1081.e1073.

103. Diebold, S.S., Kaisho, T., Hemmi, H., Akira, S., and Reis e Sousa, C. (2004). Innate antiviral responses by means of TLR7-mediated recognition of single-stranded RNA. *Science* *303*, 1529-1531.
104. Dingens, A.S., Haddox, H.K., Overbaugh, J., and Bloom, J.D. (2017). Comprehensive Mapping of HIV-1 Escape from a Broadly Neutralizing Antibody. *Cell host & microbe* *21*, 777-787.e774.
105. Dingens, A.S., Pratap, P., Malone, K., Hilton, S.K., Ketas, T., Cottrell, C.A., Overbaugh, J., Moore, J.P., Klasse, P.J., Ward, A.B., *et al.* (2021). High-resolution mapping of the neutralizing and binding specificities of polyclonal sera post-HIV Env trimer vaccination. *eLife* *10*.
106. Dong, L., Cheng, Q., Wang, Z., Yuan, P., Li, Z., Sun, Y., Han, S., Yin, J., Peng, B., He, X., *et al.* (2015). Human Pirh2 is a novel inhibitor of prototype foamy virus replication. *Viruses* *7*, 1668-1684.
107. Dong, R., Pan, S., Peng, Z., Zhang, Y., and Yang, J. (2018a). mTM-align: a server for fast protein structure database search and multiple protein structure alignment. *Nucleic Acids Res* *46*, W380-w386.
108. Dong, R., Peng, Z., Zhang, Y., and Yang, J. (2018b). mTM-align: an algorithm for fast and accurate multiple protein structure alignment. *Bioinformatics* *34*, 1719-1725.
109. Doores, K.J., and Burton, D.R. (2010). Variable loop glycan dependency of the broad and potent HIV-1-neutralizing antibodies PG9 and PG16. *J Virol* *84*, 10510-10521.
110. Dubrovskaya, V., Tran, K., Ozorowski, G., Guenaga, J., Wilson, R., Bale, S., Cottrell, C.A., Turner, H.L., Seabright, G., O'Dell, S., *et al.* (2019). Vaccination with Glycan-Modified HIV NFL Envelope Trimer-Liposomes Elicits Broadly Neutralizing Antibodies to Multiple Sites of Vulnerability. *Immunity*.
111. Duda, A., Luftenegger, D., Pietschmann, T., and Lindemann, D. (2006). Characterization of the prototype foamy virus envelope glycoprotein receptor-binding domain. *J Virol* *80*, 8158-8167.
112. Duda, A., Stange, A., Lüftenegger, D., Stanke, N., Westphal, D., Pietschmann, T., Eastman, S.W., Linial, M.L., Rethwilm, A., and Lindemann, D. (2004). Prototype foamy virus envelope glycoprotein leader peptide processing is mediated by a furin-like cellular protease, but cleavage is not essential for viral infectivity. *J Virol* *78*, 13865-13870.
113. Dufloo, J., Planchais, C., Frémont, S., Lorin, V., Guivel-Benhassine, F., Stefic, K., Casartelli, N., Echard, A., Roingeard, P., Mouquet, H., *et al.* (2022). Broadly neutralizing anti-HIV-1 antibodies tether viral particles at the surface of infected cells. *Nature communications* *13*, 630.
114. Dupont, A., Glück, I.M., Ponti, D., Stirnagel, K., Hütter, S., Perrotton, F., Stanke, N., Richter, S., Lindemann, D., and Lamb, D.C. (2020). Identification of an Intermediate Step in Foamy Virus Fusion. *Viruses* *12*.
115. Dynesen, L.T., Fernandez, I., Coquin, Y., Delaplace, M., Montange, T., Njouom, R., Bilounga Ndongo, C., Rey, F., Gessain, A., Backovic, M., *et al.* (2022, submitted). Neutralization of zoonotic simian foamy viruses: genotype-specific epitopes within the receptor-binding domain.
116. Effantin, G., Estrozi, L.F., Aschman, N., Renesto, P., Stanke, N., Lindemann, D., Schoehn, G., and Weissenhorn, W. (2016). Cryo-electron Microscopy Structure of the Native Prototype Foamy Virus Glycoprotein and Virus Architecture. *PLoS Pathog* *12*, e1005721.
117. Elder, J.H., Gautsch, J.W., Jensen, F.C., Lerner, R.A., Hartley, J.W., and Rowe, W.P. (1977). Biochemical evidence that MCF murine leukemia viruses are envelope (env) gene recombinants. *Proc Natl Acad Sci U S A* *74*, 4676-4680.
118. Emsley, P., and Cowtan, K. (2004). Coot: model-building tools for molecular graphics. *Acta Crystallogr D Biol Crystallogr* *60*, 2126-2132.
119. Enders, J.F., and Peebles, T.C. (1954). Propagation in tissue cultures of cytopathogenic agents from patients with measles. *Proc Soc Exp Biol Med* *86*, 277-286.
120. Engel, G., Hungerford, L.L., Jones-Engel, L., Travis, D., Eberle, R., Fuentes, A., Grant, R., Kyes, R., and Schillaci, M. (2006). Risk assessment: A model for predicting cross-species transmission of simian foamy virus from macaques (*M. fascicularis*) to humans at a monkey temple in Bali, Indonesia. *Am J Primatol* *68*, 934-948.
121. Engel, G.A., Pizarro, M., Shaw, E., Cortes, J., Fuentes, A., Barry, P., Lerche, N., Grant, R., Cohn, D., and Jones-Engel, L. (2008). Unique pattern of enzootic primate viruses in Gibraltar macaques. *Emerg Infect Dis* *14*, 1112-1115.
122. Engel, G.A., Small, C.T., Soliven, K., Feeroz, M.M., Wang, X., Kamrul Hasan, M., Oh, G., Rabiul Alam, S.M., Craig, K.L., Jackson, D.L., *et al.* (2013). Zoonotic simian foamy virus in Bangladesh reflects diverse patterns of transmission and co-infection. *Emerging microbes & infections* *2*, e58.

List of References

123. Enssle, J., Fischer, N., Moebes, A., Mauer, B., Smola, U., and Rethwilm, A. (1997). Carboxy-terminal cleavage of the human foamy virus Gag precursor molecule is an essential step in the viral life cycle. *J Virol* *71*, 7312-7317.
124. Enssle, J., Moebes, A., Heinkelein, M., Panhuysen, M., Mauer, B., Schweizer, M., Neumann-Haefelin, D., and Rethwilm, A. (1999). An active foamy virus integrase is required for virus replication. *J Gen Virol* *80* (Pt 6), 1445-1452.
125. Evans, L.H., Alamgir, A.S., Owens, N., Weber, N., Virtaneva, K., Barbian, K., Babar, A., Malik, F., and Rosenke, K. (2009). Mobilization of endogenous retroviruses in mice after infection with an exogenous retrovirus. *J Virol* *83*, 2429-2435.
126. Evans, L.H., Boi, S., Malik, F., Wehrly, K., Peterson, K.E., and Chesebro, B. (2014). Analysis of two monoclonal antibodies reactive with envelope proteins of murine retroviruses: one pan specific antibody and one specific for Moloney leukemia virus. *J Virol Methods* *200*, 47-53.
127. Evans, L.H., and Cloyd, M.W. (1985). Friend and Moloney murine leukemia viruses specifically recombine with different endogenous retroviral sequences to generate mink cell focus-forming viruses. *Proc Natl Acad Sci U S A* *82*, 459-463.
128. Evans, L.H., Morrison, R.P., Malik, F.G., Portis, J., and Britt, W.J. (1990). A neutralizable epitope common to the envelope glycoproteins of ecotropic, polytropic, xenotropic, and amphotropic murine leukemia viruses. *J Virol* *64*, 6176-6183.
129. Evans, P.R., and Murshudov, G.N. (2013). How good are my data and what is the resolution? *Acta Crystallogr D Biol Crystallogr* *69*, 1204-1214.
130. Falcone, V., Leupold, J., Clotten, J., Urbanyi, E., Herchenroder, O., Spatz, W., Volk, B., Bohm, N., Toniolo, A., Neumann-Haefelin, D., *et al.* (1999a). Sites of simian foamy virus persistence in naturally infected African green monkeys: latent provirus is ubiquitous, whereas viral replication is restricted to the oral mucosa. *Virology* *257*, 7-14.
131. Falcone, V., Schweizer, M., Toniolo, A., Neumann-Haefelin, D., and Meyerhans, A. (1999b). Gamma interferon is a major suppressive factor produced by activated human peripheral blood lymphocytes that is able to inhibit foamy virus-induced cytopathic effects. *J Virol* *73*, 1724-1728.
132. Faria, N.R., Rambaut, A., Suchard, M.A., Baele, G., Bedford, T., Ward, M.J., Tatem, A.J., Sousa, J.D., Arinaminpathy, N., Pépin, J., *et al.* (2014). HIV epidemiology. The early spread and epidemic ignition of HIV-1 in human populations. *Science* *346*, 56-61.
133. Fass, D., Davey, R.A., Hamson, C.A., Kim, P.S., Cunningham, J.M., and Berger, J.M. (1997). Structure of a murine leukemia virus receptor-binding glycoprotein at 2.0 angstrom resolution. *Science* *277*, 1662-1666.
134. Fass, D., Harrison, S.C., and Kim, P.S. (1996). Retrovirus envelope domain at 1.7 angstrom resolution. *Nat Struct Biol* *3*, 465-469.
135. Feeroz, M.M., Soliven, K., Small, C.T., Engel, G.A., Andreina Pacheco, M., Yee, J.L., Wang, X., Kamrul Hasan, M., Oh, G., Levine, K.L., *et al.* (2013). Population dynamics of rhesus macaques and associated foamy virus in Bangladesh. *Emerging microbes & infections* *2*, e29.
136. Fernandez, I., Dynesen, L.T., Coquin, Y., Pederzoli, R., Brun, D., Haouz, A., Gessain, A., Rey, F., Buseyne, F., and Backovic, M. (2022, submitted). The crystal structure of a simian foamy virus receptor binding domain provides clues about entry into host cells.
137. Ferruz, N., Schmidt, S., and Höcker, B. (2021). ProteinTools: a toolkit to analyze protein structures. *Nucleic Acids Res* *49*, W559-w566.
138. Fevrier, M., Dorgham, K., and Rebollo, A. (2011). CD4+ T cell depletion in human immunodeficiency virus (HIV) infection: role of apoptosis. *Viruses* *3*, 586-612.
139. Filippone, C., Betsem, E., Tortevoeye, P., Cassar, O., Bassot, S., Froment, A., Fontanet, A., and Gessain, A. (2015). A Severe Bite From a Nonhuman Primate Is a Major Risk Factor for HTLV-1 Infection in Hunters From Central Africa. *Clin Infect Dis* *60*, 1667-1676.
140. Fischer, N., Heinkelein, M., Lindemann, D., Enssle, J., Baum, C., Werder, E., Zentgraf, H., Müller, J.G., and Rethwilm, A. (1998). Foamy virus particle formation. *J Virol* *72*, 1610-1615.
141. Flanagan, M. (1992). Isolation of a spumavirus from a sheep. *Aust Vet J* *69*, 112-113.
142. Flügel, R.M., and Pfrepper, K.I. (2003). Proteolytic processing of foamy virus Gag and Pol proteins. *Curr Top Microbiol Immunol* *277*, 63-88.

List of References

143. Fujii, H., Shimizu, M., Miyagi, T., Kunihiro, M., Tanaka, R., Takahashi, Y., and Tanaka, Y. (2016). A Potential of an Anti-HTLV-I gp46 Neutralizing Monoclonal Antibody (LAT-27) for Passive Immunization against Both Horizontal and Mother-to-Child Vertical Infection with Human T Cell Leukemia Virus Type-I. *Viruses* 8.
144. Gaebler, C., Nogueira, L., Stoffel, E., Oliveira, T.Y., Breton, G., Millard, K.G., Turroja, M., Butler, A., Ramos, V., Seaman, M.S., *et al.* (2022). Prolonged viral suppression with anti-HIV-1 antibody therapy. *Nature*.
145. Gajdusek, D.C., Rogers, N.G., Basnight, M., Gibbs, C.J., Jr., and Alpers, M. (1969). Transmission experiments with kuru in chimpanzees and the isolation of latent viruses from the explanted tissues of affected animals. *Ann N Y Acad Sci* 162, 529-550.
146. Galvin, T.A., Ahmed, I.A., Shahabuddin, M., Bryan, T., and Khan, A.S. (2013). Identification of recombination in the envelope gene of simian foamy virus serotype 2 isolated from *Macaca cyclopis*. *J Virol* 87, 8792-8797.
147. Garten, R.J., Davis, C.T., Russell, C.A., Shu, B., Lindstrom, S., Balish, A., Sessions, W.M., Xu, X., Skepner, E., Deyde, V., *et al.* (2009). Antigenic and genetic characteristics of swine-origin 2009 A(H1N1) influenza viruses circulating in humans. *Science* 325, 197-201.
148. Gautam, R., Nishimura, Y., Gaughan, N., Gazumyan, A., Schoofs, T., Buckler-White, A., Seaman, M.S., Swihart, B.J., Follmann, D.A., Nussenzweig, M.C., *et al.* (2018). A single injection of crystallizable fragment domain-modified antibodies elicits durable protection from SHIV infection. *Nat Med* 24, 610-616.
149. Geiselhart, V., Bastone, P., Kempf, T., Schnölzer, M., and Löchelt, M. (2004). Furin-mediated cleavage of the feline foamy virus Env leader protein. *J Virol* 78, 13573-13581.
150. Geiselhart, V., Schwantes, A., Bastone, P., Frech, M., and Löchelt, M. (2003). Features of the Env leader protein and the N-terminal Gag domain of feline foamy virus important for virus morphogenesis. *Virology* 310, 235-244.
151. Georgiev, I.S., Gordon Joyce, M., Zhou, T., and Kwong, P.D. (2013). Elicitation of HIV-1-neutralizing antibodies against the CD4-binding site. *Curr Opin HIV AIDS* 8, 382-392.
152. Gessain, A., and Cassar, O. (2012). Epidemiological Aspects and World Distribution of HTLV-1 Infection. *Front Microbiol* 3, 388.
153. Gessain, A., Montange, T., Betsem, E., Ndongo, C.B., Njouom, R., and Buseyne, F. (2019). Case-control study of the immune status of humans infected with zoonotic gorilla simian foamy viruses. *J Infect Dis*.
154. Gessain, A., Rua, R., Betsem, E., Turpin, J., and Mahieux, R. (2013). HTLV-3/4 and simian foamy retroviruses in humans: discovery, epidemiology, cross-species transmission and molecular virology. *Virology* 435, 187-199.
155. Ghersi, B.M., Jia, H., Aiewsakun, P., Katzourakis, A., Mendoza, P., Bausch, D.G., Kasper, M.R., Montgomery, J.M., and Switzer, W.M. (2015). Wide distribution and ancient evolutionary history of simian foamy viruses in New World primates. *Retrovirology* 12, 89.
156. Ghez, D., Lepelletier, Y., Lambert, S., Fourneau, J.M., Blot, V., Janvier, S., Arnulf, B., van Endert, P.M., Heveker, N., Pique, C., *et al.* (2006). Neuropilin-1 is involved in human T-cell lymphotropic virus type 1 entry. *J Virol* 80, 6844-6854.
157. Gieselmann, L., Kreer, C., Ercanoglu, M.S., Lehnen, N., Zehner, M., Schommers, P., Potthoff, J., Gruell, H., and Klein, F. (2021). Effective high-throughput isolation of fully human antibodies targeting infectious pathogens. *Nat Protoc* 16, 3639-3671.
158. Gliniak, B.C., Kozak, S.L., Jones, R.T., and Kabat, D. (1991). Disulfide bonding controls the processing of retroviral envelope glycoproteins. *J Biol Chem* 266, 22991-22997.
159. Goepfert, P.A., Shaw, K.L., Ritter, G.D., Jr., and Mulligan, M.J. (1997). A sorting motif localizes the foamy virus glycoprotein to the endoplasmic reticulum. *J Virol* 71, 778-784.
160. Goepfert, P.A., Wang, G., and Mulligan, M.J. (1995). Identification of an ER retrieval signal in a retroviral glycoprotein. *Cell* 82, 543-544.
161. Goldstone, D.C., Flower, T.G., Ball, N.J., Sanz-Ramos, M., Yap, M.W., Ogrodowicz, R.W., Stanke, N., Reh, J., Lindemann, D., Stoye, J.P., *et al.* (2013). A unique spumavirus Gag N-terminal domain with functional properties of orthoretroviral matrix and capsid. *PLoS Pathog* 9, e1003376.

List of References

162. Goujon, C., Moncorgé, O., Bauby, H., Doyle, T., Ward, C.C., Schaller, T., Hué, S., Barclay, W.S., Schulz, R., and Malim, M.H. (2013). Human MX2 is an interferon-induced post-entry inhibitor of HIV-1 infection. *Nature* 502, 559-562.
163. Gramberg, T., Kahle, T., Bloch, N., Wittmann, S., Müllers, E., Daddacha, W., Hofmann, H., Kim, B., Lindemann, D., and Landau, N.R. (2013). Restriction of diverse retroviruses by SAMHD1. *Retrovirology* 10, 26.
164. Grange, M.P., Rosenberg, A.R., Horal, P., and Desgranges, C. (1998). Identification of exposed epitopes on the envelope glycoproteins of human T-cell lymphotropic virus type I (HTLV-I). *Int J Cancer* 75, 804-813.
165. Gruell, H., and Schommers, P. (2022). Broadly neutralizing antibodies against HIV-1 and concepts for application. *Curr Opin Virol* 54, 101211.
166. Guo, G., Wang, Y., Hu, X.M., Li, Z.R., Tan, J., and Qiao, W.T. (2021). Human Schlafen 11 exploits codon preference discrimination to attenuate viral protein synthesis of prototype foamy virus (PFV). *Virology* 555, 78-88.
167. Gärtner, K., Wiktorowicz, T., Park, J., Mergia, A., Rethwilm, A., and Scheller, C. (2009). Accuracy estimation of foamy virus genome copying. *Retrovirology* 6, 32.
168. Hadlock, K.G., Rowe, J., and Fong, S.K. (1999). The humoral immune response to human T-cell lymphotropic virus type 1 envelope glycoprotein gp46 is directed primarily against conformational epitopes. *J Virol* 73, 1205-1212.
169. Hadlock, K.G., Rowe, J., Perkins, S., Bradshaw, P., Song, G.Y., Cheng, C., Yang, J., Gascon, R., Halmos, J., Rehman, S.M., *et al.* (1997). Neutralizing human monoclonal antibodies to conformational epitopes of human T-cell lymphotropic virus type 1 and 2 gp46. *J Virol* 71, 5828-5840.
170. Hadlock, K.G., Yang, Q., Rowe, J., and Fong, S.K. (2002). Epitope mapping of human monoclonal antibodies recognizing conformational epitopes within HTLV type 1 gp46, employing HTLV type 1/2 envelope chimeras. *AIDS Res Hum Retroviruses* 18, 57-70.
171. Hahn, H., Baunach, G., Bräutigam, S., Mergia, A., Neumann-Haefelin, D., Daniel, M.D., McClure, M.O., and Rethwilm, A. (1994). Reactivity of primate sera to foamy virus Gag and Bet proteins. *J Gen Virol* 75 (Pt 10), 2635-2644.
172. Halbrook, M., Gadoth, A., Shankar, A., Zheng, H., Campbell, E.M., Hoff, N.A., Muyembe, J.J., Wemakoy, E.O., Rimoin, A.W., and Switzer, W.M. (2021). Human T-cell lymphotropic virus type 1 transmission dynamics in rural villages in the democratic republic of the congo with high nonhuman primate exposure. *PLoS Negl Trop Dis* 15, e0008923.
173. Hamann, M.V., and Lindemann, D. (2016). Foamy Virus Protein-Nucleic Acid Interactions during Particle Morphogenesis. *Viruses* 8.
174. Hamann, M.V., Müllers, E., Reh, J., Stanke, N., Effantin, G., Weissenhorn, W., and Lindemann, D. (2014). The cooperative function of arginine residues in the Prototype Foamy Virus Gag C-terminus mediates viral and cellular RNA encapsidation. *Retrovirology* 11, 87.
175. Han, G.Z., and Worobey, M. (2012a). An endogenous foamy-like viral element in the coelacanth genome. *PLoS Pathog* 8, e1002790.
176. Han, G.Z., and Worobey, M. (2012b). An endogenous foamy virus in the aye-aye (*Daubentonia madagascariensis*). *J Virol* 86, 7696-7698.
177. Hansda, A., Biswas, D., Bhatta, A., Chakravorty, N., and Mukherjee, G. (2022). Plasma therapy: a passive resistance against the deadliest. *Hum Vaccin Immunother* 18, 2006026.
178. Hare, S., Gupta, S.S., Valkov, E., Engelman, A., and Cherepanov, P. (2010a). Retroviral intasome assembly and inhibition of DNA strand transfer. *Nature* 464, 232-236.
179. Hare, S., Vos, A.M., Clayton, R.F., Thuring, J.W., Cummings, M.D., and Cherepanov, P. (2010b). Molecular mechanisms of retroviral integrase inhibition and the evolution of viral resistance. *Proc Natl Acad Sci U S A* 107, 20057-20062.
180. Harrison, S.C. (2015). Viral membrane fusion. *Virology* 479-480, 498-507.
181. Hashimoto-Gotoh, A., Yoshikawa, R., Nakagawa, S., Okamoto, M., and Miyazawa, T. (2020). Phylogenetic analyses reveal that simian foamy virus isolated from Japanese Yakushima macaques (*Macaca fuscata yakui*) is distinct from most of Japanese Hondo macaques (*Macaca fuscata fuscata*). *Gene* 734, 144382.

List of References

182. Heinkelstein, M., Dressler, M., Jármy, G., Rammling, M., Imrich, H., Thurow, J., Lindemann, D., and Rethwilm, A. (2002). Improved primate foamy virus vectors and packaging constructs. *J Virol* 76, 3774-3783.
183. Heinkelstein, M., Rammling, M., Juretzek, T., Lindemann, D., and Rethwilm, A. (2003). Retrotransposition and cell-to-cell transfer of foamy viruses. *J Virol* 77, 11855-11858.
184. Heneine, W., Switzer, W.M., Sandstrom, P., Brown, J., Vedapuri, S., Schable, C.A., Khan, A.S., Lerche, N.W., Schweizer, M., Neumann-Haefelin, D., *et al.* (1998). Identification of a human population infected with simian foamy viruses. *Nat Med* 4, 403-407.
185. Herchenroder, O., Moosmayer, D., Bock, M., Pietschmann, T., Rethwilm, A., Bieniasz, P.D., McClure, M.O., Weis, R., and Schneider, J. (1999). Specific binding of recombinant foamy virus envelope protein to host cells correlates with susceptibility to infection. *Virology* 255, 228-236.
186. Herchenroder, O., Renne, R., Loncar, D., Cobb, E.K., Murthy, K.K., Schneider, J., Mergia, A., and Luciw, P.A. (1994). Isolation, cloning, and sequencing of simian foamy viruses from chimpanzees (SFVcpz): high homology to human foamy virus (HFV). *Virology* 201, 187-199.
187. Hessel, A.J., Hangartner, L., Hunter, M., Havenith, C.E., Beurskens, F.J., Bakker, J.M., Lanigan, C.M., Landucci, G., Forthal, D.N., Parren, P.W., *et al.* (2007). Fc receptor but not complement binding is important in antibody protection against HIV. *Nature* 449, 101-104.
188. Hill, C.L., Bieniasz, P.D., and McClure, M.O. (1999). Properties of human foamy virus relevant to its development as a vector for gene therapy. *J Gen Virol* 80 (Pt 8), 2003-2009.
189. Hirsch, V.M., Olmsted, R.A., Murphey-Corb, M., Purcell, R.H., and Johnson, P.R. (1989). An African primate lentivirus (SIVsm) closely related to HIV-2. *Nature* 339, 389-392.
190. Holm, L. (2020). DALI and the persistence of protein shape. *Protein Sci* 29, 128-140.
191. Hooks, J.J., and Gibbs, C.J., Jr. (1975). The foamy viruses. *Bacteriol Rev* 39, 169-185.
192. Hooks, J.J., Gibbs, C.J., Jr., Chou, S., Howk, R., Lewis, M., and Gajdusek, D.C. (1973). Isolation of a new simian foamy virus from a spider monkey brain culture. *Infect Immun* 8, 804-813.
193. Hooks, J.J., Gibbs, C.J., Jr., Cutchins, E.C., Rogers, N.G., Lampert, P., and Gajdusek, D.C. (1972). Characterization and distribution of two new foamy viruses isolated from chimpanzees. *Arch Gesamte Virusforsch* 38, 38-55.
194. Hoshino, H., Shimoyama, M., Miwa, M., and Sugimura, T. (1983). Detection of lymphocytes producing a human retrovirus associated with adult T-cell leukemia by syncytia induction assay. *Proc Natl Acad Sci U S A* 80, 7337-7341.
195. Hsieh, C.L., Goldsmith, J.A., Schaub, J.M., DiVenere, A.M., Kuo, H.C., Javanmardi, K., Le, K.C., Wrapp, D., Lee, A.G., Liu, Y., *et al.* (2020). Structure-based design of prefusion-stabilized SARS-CoV-2 spikes. *Science* 369, 1501-1505.
196. Hu, X., Yang, W., Liu, R., Geng, Y., Qiao, W., and Tan, J. (2014). N-Myc interactor inhibits prototype foamy virus by sequestering viral Tas protein in the cytoplasm. *J Virol* 88, 7036-7044.
197. Huang, F., Wang, H., Jing, S., and Zeng, W. (2012). Simian foamy virus prevalence in *Macaca mulatta* and zookeepers. *AIDS Res Hum Retroviruses* 28, 591-593.
198. Huang, J., Doria-Rose, N.A., Longo, N.S., Laub, L., Lin, C.L., Turk, E., Kang, B.H., Migueles, S.A., Bailer, R.T., Mascola, J.R., *et al.* (2013). Isolation of human monoclonal antibodies from peripheral blood B cells. *Nat Protoc* 8, 1907-1915.
199. Hussain, A.I., Shanmugam, V., Bhullar, V.B., Beer, B.E., Vallet, D., Gautier-Hion, A., Wolfe, N.D., Karesh, W.B., Kilbourn, A.M., Tooze, Z., *et al.* (2003). Screening for simian foamy virus infection by using a combined antigen Western blot assay: evidence for a wide distribution among Old World primates and identification of four new divergent viruses. *Virology* 309, 248-257.
200. Hutter, S., Zurnic, I., and Lindemann, D. (2013). Foamy virus budding and release. *Viruses* 5, 1075-1098.
201. Hütter, S., Müllers, E., Stanke, N., Reh, J., and Lindemann, D. (2013). Prototype foamy virus protease activity is essential for intraparticle reverse transcription initiation but not absolutely required for uncoating upon host cell entry. *J Virol* 87, 3163-3176.
202. Hötzel, I. (2022). Deep-Time Structural Evolution of Retroviral and Filoviral Surface Envelope Proteins. *J Virol*, e0006322.
203. Imrich, H., Heinkelstein, M., Herchenröder, O., and Rethwilm, A. (2000). Primate foamy virus Pol proteins are imported into the nucleus. *J Gen Virol* 81, 2941-2947.

List of References

204. Inoue, T., Moran, I., Shinnakasu, R., Phan, T.G., and Kurosaki, T. (2018). Generation of memory B cells and their reactivation. *Immunol Rev* 283, 138-149.
205. Iwahara, Y., Sawada, T., Taguchi, H., Hoshino, H., Umemoto, M., Take, H., Fong, S., and Miyoshi, I. (1993). Neutralizing antibody to vesicular stomatitis virus (HTLV-I) pseudotype in infants born to seropositive mothers. *Jpn J Cancer Res* 84, 114-116.
206. Jaguva Vasudevan, A.A., Becker, D., Luedde, T., Gohlke, H., and Münk, C. (2021). Foamy Viruses, Bet, and APOBEC3 Restriction. *Viruses* 13.
207. Jaguva Vasudevan, A.A., Perkovic, M., Bulliard, Y., Cichutek, K., Trono, D., Häussinger, D., and Münk, C. (2013). Prototype foamy virus Bet impairs the dimerization and cytosolic solubility of human APOBEC3G. *J Virol* 87, 9030-9040.
208. Jegado, B., Kashanchi, F., Dutartre, H., and Mahieux, R. (2019). STLTV-1 as a model for studying HTLV-1 infection. *Retrovirology* 16, 41.
209. Jespersen, M.C., Peters, B., Nielsen, M., and Marcatili, P. (2017). BepiPred-2.0: improving sequence-based B-cell epitope prediction using conformational epitopes. *Nucleic Acids Res* 45, W24-w29.
210. Jin, Q., Agrawal, L., VanHorn-Ali, Z., and Alkhatib, G. (2006). Infection of CD4+ T lymphocytes by the human T cell leukemia virus type 1 is mediated by the glucose transporter GLUT-1: evidence using antibodies specific to the receptor's large extracellular domain. *Virology* 349, 184-196.
211. Johnston, E.R., Albritton, L.M., and Radke, K. (2002). Envelope proteins containing single amino acid substitutions support a structural model of the receptor-binding domain of bovine leukemia virus surface protein. *J Virol* 76, 10861-10872.
212. Johnston, P.B. (1961). A second immunologic type of simian foamy virus: monkey throat infections and unmasking by both types. *J Infect Dis* 109, 1-9.
213. Johnston, P.B. (1971). Taxonomic features of seven serotypes of simian and ape foamy viruses. *Infect Immun* 3, 793-799.
214. Jones-Engel, L., Engel, G.A., Heidrich, J., Chalise, M., Poudel, N., Viscidi, R., Barry, P.A., Allan, J.S., Grant, R., and Kyes, R. (2006). Temple monkeys and health implications of commensalism, Kathmandu, Nepal. *Emerg Infect Dis* 12, 900-906.
215. Jones-Engel, L., Engel, G.A., Schillaci, M.A., Rompis, A., Putra, A., Suaryana, K.G., Fuentes, A., Beer, B., Hicks, S., White, R., *et al.* (2005). Primate-to-human retroviral transmission in Asia. *Emerg Infect Dis* 11, 1028-1035.
216. Jones-Engel, L., May, C.C., Engel, G.A., Steinkraus, K.A., Schillaci, M.A., Fuentes, A., Rompis, A., Chalise, M.K., Aggimarangsee, N., Feeroz, M.M., *et al.* (2008). Diverse contexts of zoonotic transmission of simian foamy viruses in Asia. *Emerg Infect Dis* 14, 1200-1208.
217. Jones-Engel, L., Steinkraus, K.A., Murray, S.M., Engel, G.A., Grant, R., Aggimarangsee, N., Lee, B.P., May, C., Schillaci, M.A., Somgird, C., *et al.* (2007). Sensitive assays for simian foamy viruses reveal a high prevalence of infection in commensal, free-ranging Asian monkeys. *J Virol* 81, 7330-7337.
218. Jones, K.E., Patel, N.G., Levy, M.A., Storeygard, A., Balk, D., Gittleman, J.L., and Daszak, P. (2008). Global trends in emerging infectious diseases. *Nature* 451, 990-993.
219. Jones, K.S., Fugo, K., Petrow-Sadowski, C., Huang, Y., Bertolette, D.C., Lisinski, I., Cushman, S.W., Jacobson, S., and Ruscetti, F.W. (2006). Human T-cell leukemia virus type 1 (HTLV-1) and HTLV-2 use different receptor complexes to enter T cells. *J Virol* 80, 8291-8302.
220. Jones, K.S., Lambert, S., Bouttier, M., Bénit, L., Ruscetti, F.W., Hermine, O., and Pique, C. (2011). Molecular aspects of HTLV-1 entry: functional domains of the HTLV-1 surface subunit (SU) and their relationships to the entry receptors. *Viruses* 3, 794-810.
221. Jones, K.S., Petrow-Sadowski, C., Bertolette, D.C., Huang, Y., and Ruscetti, F.W. (2005). Heparan sulfate proteoglycans mediate attachment and entry of human T-cell leukemia virus type 1 virions into CD4+ T cells. *J Virol* 79, 12692-12702.
222. Jouvenet, N., Neil, S.J., Zhadina, M., Zang, T., Kratovac, Z., Lee, Y., McNatt, M., Hatzioannou, T., and Bieniasz, P.D. (2009). Broad-spectrum inhibition of retroviral and filoviral particle release by tetherin. *J Virol* 83, 1837-1844.
223. Julien, J.P., Cupo, A., Sok, D., Stanfield, R.L., Lyumkis, D., Deller, M.C., Klasse, P.J., Burton, D.R., Sanders, R.W., Moore, J.P., *et al.* (2013). Crystal structure of a soluble cleaved HIV-1 envelope trimer. *Science* 342, 1477-1483.

List of References

224. Jumper, J., Evans, R., Pritzel, A., Green, T., Figurnov, M., Ronneberger, O., Tunyasuvunakool, K., Bates, R., Žídek, A., Potapenko, A., *et al.* (2021). Highly accurate protein structure prediction with AlphaFold. *Nature* *596*, 583-589.
225. Jurrus, E., Engel, D., Star, K., Monson, K., Brandi, J., Felberg, L.E., Brookes, D.H., Wilson, L., Chen, J., Liles, K., *et al.* (2018). Improvements to the APBS biomolecular solvation software suite. *Protein Sci* *27*, 112-128.
226. Kabsch, W. (2010). XDS. *Acta Crystallogr D Biol Crystallogr* *66*, 125-132.
227. Kaewchot, S., Tangsudjai, S., Sariya, L., Mongkolphan, C., Saechin, A., Sariwongchan, R., Panpeth, N., Thongsahuan, S., and Suksai, P. (2022). Zoonotic pathogens survey in free-living long-tailed macaques in Thailand. *International journal of veterinary science and medicine* *10*, 11-18.
228. Kane, M., Mele, V., Liberatore, R.A., and Bieniasz, P.D. (2020). Inhibition of spumavirus gene expression by PHF11. *PLoS Pathog* *16*, e1008644.
229. Kane, M., Yadav, S.S., Bitzegeio, J., Kutluay, S.B., Zang, T., Wilson, S.J., Schoggins, J.W., Rice, C.M., Yamashita, M., Hatzioannou, T., *et al.* (2013). MX2 is an interferon-induced inhibitor of HIV-1 infection. *Nature* *502*, 563-566.
230. Kane, M., Zang, T.M., Rihn, S.J., Zhang, F., Kueck, T., Alim, M., Schoggins, J., Rice, C.M., Wilson, S.J., and Bieniasz, P.D. (2016). Identification of Interferon-Stimulated Genes with Antiretroviral Activity. *Cell host & microbe* *20*, 392-405.
231. Karplus, P.A., and Diederichs, K. (2012). Linking crystallographic model and data quality. *Science* *336*, 1030-1033.
232. Kataoka, R., Takehara, N., Iwahara, Y., Sawada, T., Ohtsuki, Y., Dawei, Y., Hoshino, H., and Miyoshi, I. (1990). Transmission of HTLV-I by blood transfusion and its prevention by passive immunization in rabbits. *Blood* *76*, 1657-1661.
233. Katzourakis, A., Aiewsakun, P., Jia, H., Wolfe, N.D., LeBreton, M., Yoder, A.D., and Switzer, W.M. (2014). Discovery of prosimian and afrotherian foamy viruses and potential cross species transmissions amidst stable and ancient mammalian co-evolution. *Retrovirology* *11*, 61.
234. Katzourakis, A., Gifford, R.J., Tristem, M., Gilbert, M.T., and Pybus, O.G. (2009). Macroevolution of complex retroviruses. *Science* *325*, 1512.
235. Kazanji, M., Mouinga-Ondeme, A., Lekana-Douki-Etenna, S., Caron, M., Makuwa, M., Mahieux, R., and Gessain, A. (2015). Origin of HTLV-1 in hunters of nonhuman primates in Central Africa. *J Infect Dis* *211*, 361-365.
236. Kechejian, S.R., Dannemiller, N., Kraberger, S., Ledesma-Feliciano, C., Malmberg, J., Roelke Parker, M., Cunningham, M., McBride, R., Riley, S.P.D., Vickers, W.T., *et al.* (2019). Feline Foamy Virus is Highly Prevalent in Free-Ranging Puma concolor from Colorado, Florida and Southern California. *Viruses* *11*.
237. Keele, B.F., Van Heuverswyn, F., Li, Y., Bailes, E., Takehisa, J., Santiago, M.L., Bibollet-Ruche, F., Chen, Y., Wain, L.V., Liegeois, F., *et al.* (2006). Chimpanzee reservoirs of pandemic and nonpandemic HIV-1. *Science* *313*, 523-526.
238. Kehl, T., Tan, J., and Materniak, M. (2013). Non-simian foamy viruses: molecular virology, tropism and prevalence and zoonotic/interspecies transmission. *Viruses* *5*, 2169-2209.
239. Keller, A., Partin, K.M., Löchelt, M., Bannert, H., Flügel, R.M., and Cullen, B.R. (1991). Characterization of the transcriptional trans activator of human foamy retrovirus. *J Virol* *65*, 2589-2594.
240. Kelley, L.A., Mezulis, S., Yates, C.M., Wass, M.N., and Sternberg, M.J.E. (2015). The Phyre2 web portal for protein modeling, prediction and analysis. *Nat Protoc* *10*, 845-858.
241. Khan, A.S., Bodem, J., Buseyne, F., Gessain, A., Johnson, W., Kuhn, J.H., Kuzmak, J., Lindemann, D., Linial, M.L., Lochelt, M., *et al.* (2018). Spumaretroviruses: Updated taxonomy and nomenclature. *Virology* *516*, 158-164.
242. Khan, A.S., and Kumar, D. (2006). Simian foamy virus infection by whole-blood transfer in rhesus macaques: potential for transfusion transmission in humans. *Transfusion* *46*, 1352-1359.
243. Kim, A.S., Leaman, D.P., and Zwick, M.B. (2014). Antibody to gp41 MPER alters functional properties of HIV-1 Env without complete neutralization. *PLoS Pathog* *10*, e1004271.
244. Kim, F.J., Battini, J.L., Manel, N., and Sitbon, M. (2004). Emergence of vertebrate retroviruses and envelope capture. *Virology* *318*, 183-191.

List of References

245. Kim, F.J., Seiliez, I., Denesvre, C., Lavillette, D., Cosset, F.L., and Sitbon, M. (2000). Definition of an amino-terminal domain of the human T-cell leukemia virus type 1 envelope surface unit that extends the fusogenic range of an ecotropic murine leukemia virus. *J Biol Chem* 275, 23417-23420.
246. Kim, J., and Shin, C.G. (2020). IFITM proteins inhibit the late step of feline foamy virus replication. *Anim Cells Syst (Seoul)* 24, 282-288.
247. Kincaid, R.P., Chen, Y., Cox, J.E., Rethwilm, A., and Sullivan, C.S. (2014). Noncanonical microRNA (miRNA) biogenesis gives rise to retroviral mimics of lymphoproliferative and immunosuppressive host miRNAs. *mBio* 5, e00074.
248. Kirchdoerfer, R.N., Cottrell, C.A., Wang, N., Pallesen, J., Yassine, H.M., Turner, H.L., Corbett, K.S., Graham, B.S., McLellan, J.S., and Ward, A.B. (2016). Pre-fusion structure of a human coronavirus spike protein. *Nature* 531, 118-121.
249. Kirchhoff, F. (2010). Immune evasion and counteraction of restriction factors by HIV-1 and other primate lentiviruses. *Cell host & microbe* 8, 55-67.
250. Kirisawa, R., Toishi, Y., Hashimoto, H., and Tsunoda, N. (2019). Isolation of an Equine Foamy Virus and Sero-Epidemiology of the Viral Infection in Horses in Japan. *Viruses* 11.
251. Klasse, P.J., Ozorowski, G., Sanders, R.W., and Moore, J.P. (2020). Env Exceptionalism: Why Are HIV-1 Env Glycoproteins Atypical Immunogens? *Cell host & microbe* 27, 507-518.
252. Klein, F., Diskin, R., Scheid, J.F., Gaebler, C., Mouquet, H., Georgiev, I.S., Pancera, M., Zhou, T., Incesu, R.B., Fu, B.Z., *et al.* (2013). Somatic mutations of the immunoglobulin framework are generally required for broad and potent HIV-1 neutralization. *Cell* 153, 126-138.
253. Klose, D.P., Wallace, B.A., and Janes, R.W. (2010). 2Struc: the secondary structure server. *Bioinformatics* 26, 2624-2625.
254. Kozak, C.A. (2014). Origins of the endogenous and infectious laboratory mouse gammaretroviruses. *Viruses* 7, 1-26.
255. Kozakov, D., Hall, D.R., Xia, B., Porter, K.A., Padhorny, D., Yueh, C., Beglov, D., and Vajda, S. (2017). The ClusPro web server for protein-protein docking. *Nat Protoc* 12, 255-278.
256. Krey, T., d'Alayer, J., Kikuti, C.M., Saulnier, A., Damier-Piolle, L., Petitpas, I., Johansson, D.X., Tawar, R.G., Baron, B., Robert, B., *et al.* (2010). The disulfide bonds in glycoprotein E2 of hepatitis C virus reveal the tertiary organization of the molecule. *PLoS Pathog* 6, e1000762.
257. Kringelum, J.V., Lundegaard, C., Lund, O., and Nielsen, M. (2012). Reliable B cell epitope predictions: impacts of method development and improved benchmarking. *PLoS Comput Biol* 8, e1002829.
258. Krissinel, E., and Henrick, K. (2007). Inference of macromolecular assemblies from crystalline state. *J Mol Biol* 372, 774-797.
259. Kwong, P.D., Doyle, M.L., Casper, D.J., Cicala, C., Leavitt, S.A., Majeed, S., Steenbeke, T.D., Venturi, M., Chaiken, I., Fung, M., *et al.* (2002). HIV-1 evades antibody-mediated neutralization through conformational masking of receptor-binding sites. *Nature* 420, 678-682.
260. Kwong, P.D., and Mascola, J.R. (2012). Human antibodies that neutralize HIV-1: identification, structures, and B cell ontogenies. *Immunity* 37, 412-425.
261. Kwong, P.D., Wyatt, R., Robinson, J., Sweet, R.W., Sodroski, J., and Hendrickson, W.A. (1998). Structure of an HIV gp120 envelope glycoprotein in complex with the CD4 receptor and a neutralizing human antibody. *Nature* 393, 648-659.
262. Kyte, J., and Doolittle, R.F. (1982). A simple method for displaying the hydropathic character of a protein. *J Mol Biol* 157, 105-132.
263. Lambert, C., Batale, D., Montange, T., Betsem, E., Mouinga-Ondeme, A., Njouom, R., Gessain, A., and Buseyne, F. (2019). An Immunodominant and Conserved B-Cell Epitope in the Envelope of Simian Foamy Virus Recognized by Humans Infected with Zoonotic Strains from Apes. *J Virol* 93.
264. Lambert, C., Couteaudier, M., Gouzil, J., Richard, L., Montange, T., Betsem, E., Rua, R., Tobaly-Tapiero, J., Lindemann, D., Njouom, R., *et al.* (2018). Potent neutralizing antibodies in humans infected with zoonotic simian foamy viruses target conserved epitopes located in the dimorphic domain of the surface envelope protein. *PLoS Pathog* 14, e1007293.
265. Lambert, C., Rua, R., Gessain, A., and Buseyne, F. (2016). A new sensitive indicator cell line reveals cross-transactivation of the viral LTR by gorilla and chimpanzee simian foamy viruses. *Virology* 496, 219-226.

List of References

266. Lambert, S., Bouttier, M., Vassy, R., Seigneuret, M., Petrow-Sadowski, C., Janvier, S., Heveker, N., Ruscetti, F.W., Perret, G., Jones, K.S., *et al.* (2009). HTLV-1 uses HSPG and neuropilin-1 for entry by molecular mimicry of VEGF165. *Blood* 113, 5176-5185.
267. Larsen, J.E., Lund, O., and Nielsen, M. (2006). Improved method for predicting linear B-cell epitopes. *Immunome Res* 2, 2.
268. Lavignon, M., Walker, J.L., Perryman, S.M., Malik, F.G., Khan, A.S., Theodore, T.S., and Evans, L.H. (1994). Characterization of epitopes defining two major subclasses of polytropic murine leukemia viruses (MuLVs) which are differentially expressed in mice infected with different ecotropic MuLVs. *J Virol* 68, 5194-5203.
269. Lavillette, D., Maurice, M., Roche, C., Russell, S.J., Sitbon, M., and Cosset, F.L. (1998). A proline-rich motif downstream of the receptor binding domain modulates conformation and fusogenicity of murine retroviral envelopes. *J Virol* 72, 9955-9965.
270. Lavillette, D., Ruggieri, A., Boson, B., Maurice, M., and Cosset, F.L. (2002). Relationship between SU subdomains that regulate the receptor-mediated transition from the native (fusion-inhibited) to the fusion-active conformation of the murine leukemia virus glycoprotein. *J Virol* 76, 9673-9685.
271. Lecellier, C.H., Dunoyer, P., Arar, K., Lehmann-Che, J., Eyquem, S., Himber, C., Saïb, A., and Voinnet, O. (2005). A cellular microRNA mediates antiviral defense in human cells. *Science* 308, 557-560.
272. Ledesma-Feliciano, C., Troyer, R.M., Zheng, X., Miller, C., Cianciolo, R., Bordicchia, M., Dannemiller, N., Gagne, R., Beatty, J., Quimby, J., *et al.* (2019). Feline Foamy Virus Infection: Characterization of Experimental Infection and Prevalence of Natural Infection in Domestic Cats with and without Chronic Kidney Disease. *Viruses* 11.
273. Lee, E.G., Stenbak, C.R., and Linial, M.L. (2013). Foamy virus assembly with emphasis on pol encapsidation. *Viruses* 5, 886-900.
274. Lee, J.H., Leaman, D.P., Kim, A.S., Torrents de la Peña, A., Sliepen, K., Yasmeen, A., Derking, R., Ramos, A., de Taeye, S.W., Ozorowski, G., *et al.* (2015). Antibodies to a conformational epitope on gp41 neutralize HIV-1 by destabilizing the Env spike. *Nature communications* 6, 8167.
275. Lee, J.H., Ozorowski, G., and Ward, A.B. (2016). Cryo-EM structure of a native, fully glycosylated, cleaved HIV-1 envelope trimer. *Science* 351, 1043-1048.
276. Leendertz, F.H., Zirkel, F., Couacy-Hymann, E., Ellerbrok, H., Morozov, V.A., Pauli, G., Hedemann, C., Formenty, P., Jensen, S.A., Boesch, C., *et al.* (2008). Interspecies transmission of simian foamy virus in a natural predator-prey system. *J Virol* 82, 7741-7744.
277. Leendertz, S.A., Junglen, S., Hedemann, C., Goffe, A., Calvignac, S., Boesch, C., and Leendertz, F.H. (2010). High prevalence, coinfection rate, and genetic diversity of retroviruses in wild red colobus monkeys (*Piliocolobus badius badius*) in Tai National Park, Cote d'Ivoire. *J Virol* 84, 7427-7436.
278. Lehmann-Che, J., Giron, M.L., Delelis, O., Löchelt, M., Bittoun, P., Tobaly-Tapiero, J., de Thé, H., and Saïb, A. (2005). Protease-dependent uncoating of a complex retrovirus. *J Virol* 79, 9244-9253.
279. Lesbats, P., Serrao, E., Maskell, D.P., Pye, V.E., O'Reilly, N., Lindemann, D., Engelman, A.N., and Cherepanov, P. (2017). Structural basis for spumavirus GAG tethering to chromatin. *Proc Natl Acad Sci U S A* 114, 5509-5514.
280. Lindel, F., Dodt, C.R., Weidner, N., Noll, M., Bergemann, F., Behrendt, R., Fischer, S., Dietrich, J., Cartellieri, M., Hamann, M.V., *et al.* (2019). TraFo-CRISPR: Enhanced Genome Engineering by Transient Foamy Virus Vector-Mediated Delivery of CRISPR/Cas9 Components. *Molecular therapy Nucleic acids* 18, 708-726.
281. Lindemann, D., Hütter, S., Wei, G., and Löchelt, M. (2021). The Unique, the Known, and the Unknown of Spumaretrovirus Assembly. *Viruses* 13.
282. Lindemann, D., Pietschmann, T., Picard-Maureau, M., Berg, A., Heinkelein, M., Thurow, J., Knaus, P., Zentgraf, H., and Rethwilm, A. (2001). A particle-associated glycoprotein signal peptide essential for virus maturation and infectivity. *J Virol* 75, 5762-5771.
283. Lindemann, D., and Rethwilm, A. (2011). Foamy virus biology and its application for vector development. *Viruses* 3, 561-585.
284. Liu, J., Ghneim, K., Sok, D., Bosche, W.J., Li, Y., Chipriano, E., Berkemeier, B., Oswald, K., Borducchi, E., Cabral, C., *et al.* (2016). Antibody-mediated protection against SHIV challenge includes systemic clearance of distal virus. *Science* 353, 1045-1049.

List of References

- 285.Liu, W., Worobey, M., Li, Y., Keele, B.F., Bibollet-Ruche, F., Guo, Y., Goepfert, P.A., Santiago, M.L., Ndjango, J.B., Neel, C., *et al.* (2008). Molecular ecology and natural history of simian foamy virus infection in wild-living chimpanzees. *PLoS Pathog* 4, e1000097.
- 286.Llorens, C., Muñoz-Pomer, A., Bernad, L., Botella, H., and Moya, A. (2009). Network dynamics of eukaryotic LTR retroelements beyond phylogenetic trees. *Biol Direct* 4, 41.
- 287.Lo, Y.T., Tian, T., Nadeau, P.E., Park, J., and Mergia, A. (2010). The foamy virus genome remains unintegrated in the nuclei of G1/S phase-arrested cells, and integrase is critical for preintegration complex transport into the nucleus. *J Virol* 84, 2832-2842.
- 288.Locatelli, S., and Peeters, M. (2012). Cross-species transmission of simian retroviruses: how and why they could lead to the emergence of new diseases in the human population. *AIDS* 26, 659-673.
- 289.Lu, L.L., Suscovich, T.J., Fortune, S.M., and Alter, G. (2018). Beyond binding: antibody effector functions in infectious diseases. *Nat Rev Immunol* 18, 46-61.
- 290.Luftenegger, D., Picard-Maureau, M., Stanke, N., Rethwilm, A., and Lindemann, D. (2005). Analysis and function of prototype foamy virus envelope N glycosylation. *J Virol* 79, 7664-7672.
- 291.Lukic, D.S., Hotz-Wagenblatt, A., Lei, J., Räthe, A.M., Mühle, M., Denner, J., Münk, C., and Löchelt, M. (2013). Identification of the feline foamy virus Bet domain essential for APOBEC3 counteraction. *Retrovirology* 10, 76.
- 292.Löchelt, M., Flügel, R.M., and Aboud, M. (1994). The human foamy virus internal promoter directs the expression of the functional Bel 1 transactivator and Bet protein early after infection. *J Virol* 68, 638-645.
- 293.Löchelt, M., Muranyi, W., and Flügel, R.M. (1993). Human foamy virus genome possesses an internal, Bel-1-dependent and functional promoter. *Proc Natl Acad Sci U S A* 90, 7317-7321.
- 294.Löchelt, M., Romen, F., Bastone, P., Muckenfuss, H., Kirchner, N., Kim, Y.B., Truyen, U., Rösler, U., Battenberg, M., Saib, A., *et al.* (2005). The antiretroviral activity of APOBEC3 is inhibited by the foamy virus accessory Bet protein. *Proc Natl Acad Sci U S A* 102, 7982-7987.
- 295.Löchelt, M., Yu, S.F., Linial, M.L., and Flügel, R.M. (1995). The human foamy virus internal promoter is required for efficient gene expression and infectivity. *Virology* 206, 601-610.
- 296.Maertens, G.N., Hare, S., and Cherepanov, P. (2010). The mechanism of retroviral integration from X-ray structures of its key intermediates. *Nature* 468, 326-329.
- 297.Malleret, B., Manéglier, B., Karlsson, I., Lebon, P., Nascimbeni, M., Perié, L., Brochard, P., Delache, B., Calvo, J., Andrieu, T., *et al.* (2008). Primary infection with simian immunodeficiency virus: plasmacytoid dendritic cell homing to lymph nodes, type I interferon, and immune suppression. *Blood* 112, 4598-4608.
- 298.Malmquist, W.A., Van der Maaten, M.J., and Boothe, A.D. (1969). Isolation, immunodiffusion, immunofluorescence, and electron microscopy of a syncytial virus of lymphosarcomatous and apparently normal cattle. *Cancer Res* 29, 188-200.
- 299.Malvy, D., McElroy, A.K., de Clerck, H., Gunther, S., and van Griensven, J. (2019). Ebola virus disease. *Lancet* 393, 936-948.
- 300.Manel, N., Kim, F.J., Kinet, S., Taylor, N., Sitbon, M., and Battini, J.L. (2003). The ubiquitous glucose transporter GLUT-1 is a receptor for HTLV. *Cell* 115, 449-459.
- 301.Mangala Prasad, V., Leaman, D.P., Lovendahl, K.N., Croft, J.T., Benhaim, M.A., Hodge, E.A., Zwick, M.B., and Lee, K.K. (2022). Cryo-ET of Env on intact HIV virions reveals structural variation and positioning on the Gag lattice. *Cell* 185, 641-653.e617.
- 302.Marston, H.D., Folkers, G.K., Morens, D.M., and Fauci, A.S. (2014). Emerging viral diseases: confronting threats with new technologies. *Sci Transl Med* 6, 253ps210.
- 303.Martínez, V.P., Di Paola, N., Alonso, D.O., Pérez-Sautu, U., Bellomo, C.M., Iglesias, A.A., Coelho, R.M., López, B., Periolo, N., Larson, P.A., *et al.* (2020). "Super-Spreaders" and Person-to-Person Transmission of Andes Virus in Argentina. *N Engl J Med* 383, 2230-2241.
- 304.Materniak-Kornas, M., Tan, J., Heit-Mondrzyk, A., Hotz-Wagenblatt, A., and Löchelt, M. (2019). Bovine Foamy Virus: Shared and Unique Molecular Features In Vitro and In Vivo. *Viruses* 11.
- 305.Matsen, F.A.t., Small, C.T., Soliven, K., Engel, G.A., Feeroz, M.M., Wang, X., Craig, K.L., Hasan, M.K., Emerman, M., Linial, M.L., *et al.* (2014). A novel Bayesian method for detection of APOBEC3-mediated hypermutation and its application to zoonotic transmission of simian foamy viruses. *PLoS Comput Biol* 10, e1003493.

List of References

306. Matthes, D., Wiktorowicz, T., Zahn, J., Bodem, J., Stanke, N., Lindemann, D., and Rethwilm, A. (2011). Basic residues in the foamy virus Gag protein. *J Virol* *85*, 3986-3995.
307. McCarthy, K.R., Timpona, J.L., Jenni, S., Bloyet, L.M., Brusica, V., Johnson, W.E., Whelan, S.P.J., and Robinson-McCarthy, L.R. (2020). Structure of the Receptor Binding Domain of EnvP(b)1, an Endogenous Retroviral Envelope Protein Expressed in Human Tissues. *mBio* *11*.
308. McClure, M.O., Bieniasz, P.D., Schulz, T.F., Chrystie, I.L., Simpson, G., Aguzzi, A., Hoad, J.G., Cunningham, A., Kirkwood, J., and Weiss, R.A. (1994). Isolation of a new foamy retrovirus from orangutans. *J Virol* *68*, 7124-7130.
309. McCoy, A.J., Grosse-Kunstleve, R.W., Adams, P.D., Winn, M.D., Storoni, L.C., and Read, R.J. (2007). Phaser crystallographic software. *J Appl Crystallogr* *40*, 658-674.
310. McCoy, L.E. (2018). The expanding array of HIV broadly neutralizing antibodies. *Retrovirology* *15*, 70.
311. McCoy, L.E., Falkowska, E., Doores, K.J., Le, K., Sok, D., van Gils, M.J., Euler, Z., Burger, J.A., Seaman, M.S., Sanders, R.W., *et al.* (2015). Incomplete Neutralization and Deviation from Sigmoidal Neutralization Curves for HIV Broadly Neutralizing Monoclonal Antibodies. *PLoS Pathog* *11*, e1005110.
312. McCoy, L.E., van Gils, M.J., Ozorowski, G., Messmer, T., Briney, B., Voss, J.E., Kulp, D.W., Macauley, M.S., Sok, D., Pauthner, M., *et al.* (2016). Holes in the Glycan Shield of the Native HIV Envelope Are a Target of Trimer-Elicited Neutralizing Antibodies. *Cell reports* *16*, 2327-2338.
313. McLellan, J.S., Pancera, M., Carrico, C., Gorman, J., Julien, J.P., Khayat, R., Louder, R., Pejchal, R., Sastry, M., Dai, K., *et al.* (2011). Structure of HIV-1 gp120 V1/V2 domain with broadly neutralizing antibody PG9. *Nature* *480*, 336-343.
314. Meiering, C.D., and Linial, M.L. (2001). Historical perspective of foamy virus epidemiology and infection. *Clin Microbiol Rev* *14*, 165-176.
315. Meiering, C.D., and Linial, M.L. (2003). The promyelocytic leukemia protein does not mediate foamy virus latency in vitro. *J Virol* *77*, 2207-2213.
316. Mendoza, P., Gruell, H., Nogueira, L., Pai, J.A., Butler, A.L., Millard, K., Lehmann, C., Suarez, I., Oliveira, T.Y., Lorenzi, J.C.C., *et al.* (2018). Combination therapy with anti-HIV-1 antibodies maintains viral suppression. *Nature* *561*, 479-484.
317. Mergia, A., Leung, N.J., and Blackwell, J. (1996). Cell tropism of the simian foamy virus type 1 (SFV-1). *J Med Primatol* *25*, 2-7.
318. Mesin, L., Ersching, J., and Vitoria, G.D. (2016). Germinal Center B Cell Dynamics. *Immunity* *45*, 471-482.
319. Mikovits, J.A., Hoffman, P.M., Rethwilm, A., and Ruscetti, F.W. (1996). In vitro infection of primary and retrovirus-infected human leukocytes by human foamy virus. *J Virol* *70*, 2774-2780.
320. Milligan, J.C., Davis, C.W., Yu, X., Ilinykh, P.A., Huang, K., Halfmann, P.J., Cross, R.W., Borisevich, V., Agans, K.N., Geisbert, J.B., *et al.* (2022). Asymmetric and non-stoichiometric glycoprotein recognition by two distinct antibodies results in broad protection against ebolaviruses. *Cell* *185*, 995-1007.e1018.
321. Miyoshi, I., Takehara, N., Sawada, T., Iwahara, Y., Kataoka, R., Yang, D., and Hoshino, H. (1992). Immunoglobulin prophylaxis against HTLV-I in a rabbit model. *Leukemia* *6 Suppl 1*, 24-26.
322. Moebes, A., Enssle, J., Bieniasz, P.D., Heinkelstein, M., Lindemann, D., Bock, M., McClure, M.O., and Rethwilm, A. (1997). Human foamy virus reverse transcription that occurs late in the viral replication cycle. *J Virol* *71*, 7305-7311.
323. Moir, S., and Fauci, A.S. (2017). B-cell responses to HIV infection. *Immunol Rev* *275*, 33-48.
324. Moldt, B., Rakasz, E.G., Schultz, N., Chan-Hui, P.Y., Swiderek, K., Weisgrau, K.L., Piaskowski, S.M., Bergman, Z., Watkins, D.I., Pognard, P., *et al.* (2012). Highly potent HIV-specific antibody neutralization in vitro translates into effective protection against mucosal SHIV challenge in vivo. *Proc Natl Acad Sci U S A* *109*, 18921-18925.
325. Morens, D.M., Folkers, G.K., and Fauci, A.S. (2008). Emerging infections: a perpetual challenge. *Lancet Infect Dis* *8*, 710-719.
326. Mottarella, S.E., Beglov, D., Beglova, N., Nugent, M.A., Kozakov, D., and Vajda, S. (2014). Docking server for the identification of heparin binding sites on proteins. *J Chem Inf Model* *54*, 2068-2078.
327. Mouinga-Ondeme, A., Betsem, E., Caron, M., Makuwa, M., Salle, B., Renault, N., Saib, A., Telfer, P., Marx, P., Gessain, A., *et al.* (2010). Two distinct variants of simian foamy virus in naturally infected mandrills (*Mandrillus sphinx*) and cross-species transmission to humans. *Retrovirology* *7*, 105.

List of References

328. Mouinga-Ondémé, A., Caron, M., Nkoghé, D., Telfer, P., Marx, P., Saïb, A., Leroy, E., Gonzalez, J.P., Gessain, A., and Kazanji, M. (2012). Cross-species transmission of simian foamy virus to humans in rural Gabon, Central Africa. *J Virol* 86, 1255-1260.
329. Mouinga-Ondeme, A., and Kazanji, M. (2013). Simian foamy virus in non-human primates and cross-species transmission to humans in Gabon: an emerging zoonotic disease in central Africa? *Viruses* 5, 1536-1552.
330. Mouquet, H., Scharf, L., Euler, Z., Liu, Y., Eden, C., Scheid, J.F., Halper-Stromberg, A., Gnanapragasam, P.N., Spencer, D.I., Seaman, M.S., *et al.* (2012). Complex-type N-glycan recognition by potent broadly neutralizing HIV antibodies. *Proc Natl Acad Sci U S A* 109, E3268-3277.
331. Muniz, C.P., Cavalcante, L.T.F., Jia, H., Zheng, H., Tang, S., Augusto, A.M., Pissinatti, A., Fedullo, L.P., Santos, A.F., Soares, M.A., *et al.* (2017). Zoonotic infection of Brazilian primate workers with New World simian foamy virus. *PLoS One* 12, e0184502.
332. Muniz, C.P., Jia, H., Shankar, A., Troncoso, L.L., Augusto, A.M., Farias, E., Pissinatti, A., Fedullo, L.P., Santos, A.F., Soares, M.A., *et al.* (2015). An expanded search for simian foamy viruses (SFV) in Brazilian New World primates identifies novel SFV lineages and host age-related infections. *Retrovirology* 12, 94.
333. Muniz, C.P., Troncoso, L.L., Moreira, M.A., Soares, E.A., Pissinatti, A., Bonvicino, C.R., Seuanez, H.N., Sharma, B., Jia, H., Shankar, A., *et al.* (2013). Identification and characterization of highly divergent simian foamy viruses in a wide range of new world primates from Brazil. *PLoS One* 8, e67568.
334. Munro, J.B., Gorman, J., Ma, X., Zhou, Z., Arthos, J., Burton, D.R., Koff, W.C., Courter, J.R., Smith, A.B., 3rd, Kwong, P.D., *et al.* (2014). Conformational dynamics of single HIV-1 envelope trimers on the surface of native virions. *Science* 346, 759-763.
335. Murin, C.D., Wilson, I.A., and Ward, A.B. (2019). Antibody responses to viral infections: a structural perspective across three different enveloped viruses. *Nature microbiology* 4, 734-747.
336. Murray, S.M., and Linial, M.L. (2019). Simian Foamy Virus Co-Infections. *Viruses* 11.
337. Murray, S.M., Picker, L.J., Axthelm, M.K., Hudkins, K., Alpers, C.E., and Linial, M.L. (2008). Replication in a superficial epithelial cell niche explains the lack of pathogenicity of primate foamy virus infections. *J Virol* 82, 5981-5985.
338. Murray, S.M., Picker, L.J., Axthelm, M.K., and Linial, M.L. (2006). Expanded tissue targets for foamy virus replication with simian immunodeficiency virus-induced immunosuppression. *J Virol* 80, 663-670.
339. Mühle, M., Bleiholder, A., Kolb, S., Hübner, J., Löchelt, M., and Denner, J. (2011). Immunological properties of the transmembrane envelope protein of the feline foamy virus and its use for serological screening. *Virology* 412, 333-340.
340. Mühle, M., Bleiholder, A., Löchelt, M., and Denner, J. (2017). Epitope Mapping of the Antibody Response Against the Envelope Proteins of the Feline Foamy Virus. *Viral Immunol* 30, 388-395.
341. Mänz, B., Dornfeld, D., Götz, V., Zell, R., Zimmermann, P., Haller, O., Kochs, G., and Schwemmle, M. (2013). Pandemic influenza A viruses escape from restriction by human MxA through adaptive mutations in the nucleoprotein. *PLoS Pathog* 9, e1003279.
342. Nagy, K., Clapham, P., Cheingsong-Popov, R., and Weiss, R.A. (1983). Human T-cell leukemia virus type I: induction of syncytia and inhibition by patients' sera. *Int J Cancer* 32, 321-328.
343. Nandi, J.S., Rathore, S.S., and Mathur, B.R. (2021). Transmission of infectious viruses in the natural setting at human-animal interface. *Current research in virological science* 2, 100008.
344. Nasimuzzaman, M., and Persons, D.A. (2012). Cell Membrane-associated heparan sulfate is a receptor for prototype foamy virus in human, monkey, and rodent cells. *Mol Ther* 20, 1158-1166.
345. Nemo, G.J., Brown, P.W., Gibbs, C.J., Jr., and Gajdusek, D.C. (1978). Antigenic relationship of human foamy virus to the simian foamy viruses. *Infect Immun* 20, 69-72.
346. Nethe, M., Berkhout, B., and van der Kuyl, A.C. (2005). Retroviral superinfection resistance. *Retrovirology* 2, 52.
347. Netzer, K.O., Rethwilm, A., Maurer, B., and ter Meulen, V. (1990). Identification of the major immunogenic structural proteins of human foamy virus. *J Gen Virol* 71 (Pt 5), 1237-1241.
348. O'Brien, T.C., Albrecht, P., Hannah, J.E., Tauraso, N.M., Robbins, B., and Trimmer, R.W. (1972). Foamy virus serotypes 1 and 2 in rhesus monkey tissues. *Arch Gesamte Virusforsch* 38, 216-224.

349. Okamoto, M., Oguma, K., Yamashita-Kawanishi, N., Ichijo, T., Hatama, S., Endo, M., Ishikawa, M., and Haga, T. (2020). Genomic characterization and distribution of bovine foamy virus in Japan. *J Vet Med Sci* 82, 1607-1613.
350. Opstelten, D.J., Wallin, M., and Garoff, H. (1998). Moloney murine leukemia virus envelope protein subunits, gp70 and Pr15E, form a stable disulfide-linked complex. *J Virol* 72, 6537-6545.
351. Pacheco, B., Finzi, A., McGee-Estrada, K., and Sodroski, J. (2010). Species-specific inhibition of foamy viruses from South American monkeys by New World Monkey TRIM5{alpha} proteins. *J Virol* 84, 4095-4099.
352. Pancera, M., Changela, A., and Kwong, P.D. (2017). How HIV-1 entry mechanism and broadly neutralizing antibodies guide structure-based vaccine design. *Curr Opin HIV AIDS* 12, 229-240.
353. Pancera, M., Zhou, T., Druz, A., Georgiev, I.S., Soto, C., Gorman, J., Huang, J., Acharya, P., Chuang, G.Y., Ofek, G., *et al.* (2014). Structure and immune recognition of trimeric pre-fusion HIV-1 Env. *Nature* 514, 455-461.
354. Pang, I.K., and Iwasaki, A. (2012). Control of antiviral immunity by pattern recognition and the microbiome. *Immunol Rev* 245, 209-226.
355. Paris, J., Tobaly-Tapiero, J., Giron, M.L., Burlaud-Gaillard, J., Buseyne, F., Roingeard, P., Lesage, P., Zamborlini, A., and Saib, A. (2018). The invariant arginine within the chromatin-binding motif regulates both nucleolar localization and chromatin binding of Foamy virus Gag. *Retrovirology* 15, 48.
356. Parker Miller, E., Finkelstein, M.T., Erdman, M.C., Seth, P.C., and Fera, D. (2021). A Structural Update of Neutralizing Epitopes on the HIV Envelope, a Moving Target. *Viruses* 13.
357. Patton, G.S., Erlwein, O., and McClure, M.O. (2004). Cell-cycle dependence of foamy virus vectors. *J Gen Virol* 85, 2925-2930.
358. Peeters, M., and Delaporte, E. (2012). Simian retroviruses in African apes. *Clin Microbiol Infect* 18, 514-520.
359. Percher, F., Jeannin, P., Martin-Latil, S., Gessain, A., Afonso, P.V., Vidy-Roche, A., and Ceccaldi, P.E. (2016). Mother-to-Child Transmission of HTLV-1 Epidemiological Aspects, Mechanisms and Determinants of Mother-to-Child Transmission. *Viruses* 8.
360. Perkovic, M., Schmidt, S., Marino, D., Russell, R.A., Stauch, B., Hofmann, H., Kopietz, F., Kloke, B.P., Zielonka, J., Ströver, H., *et al.* (2009). Species-specific inhibition of APOBEC3C by the prototype foamy virus protein bet. *J Biol Chem* 284, 5819-5826.
361. Pertel, T., Hausmann, S., Morger, D., Züger, S., Guerra, J., Lascano, J., Reinhard, C., Santoni, F.A., Uchil, P.D., Chatel, L., *et al.* (2011). TRIM5 is an innate immune sensor for the retrovirus capsid lattice. *Nature* 472, 361-365.
362. Petit, C., Giron, M.L., Tobaly-Tapiero, J., Bittoun, P., Real, E., Jacob, Y., Tordo, N., De The, H., and Saib, A. (2003). Targeting of incoming retroviral Gag to the centrosome involves a direct interaction with the dynein light chain 8. *J Cell Sci* 116, 3433-3442.
363. Pettersen, E.F., Goddard, T.D., Huang, C.C., Couch, G.S., Greenblatt, D.M., Meng, E.C., and Ferrin, T.E. (2004). UCSF Chimera--a visualization system for exploratory research and analysis. *J Comput Chem* 25, 1605-1612.
364. Phung, H.T., Ikeda, Y., Miyazawa, T., Nakamura, K., Mochizuki, M., Izumiya, Y., Sato, E., Nishimura, Y., Tohya, Y., Takahashi, E., *et al.* (2001). Genetic analyses of feline foamy virus isolates from domestic and wild feline species in geographically distinct areas. *Virus Res* 76, 171-181.
365. Phung, H.T., Tohya, Y., Miyazawa, T., and Akashi, H. (2005). Characterization of Env antigenicity of feline foamy virus (FeFV) using FeFV-infected cat sera and a monoclonal antibody. *Vet Microbiol* 106, 201-207.
366. Piantadosi, A., Chohan, B., Chohan, V., McClelland, R.S., and Overbaugh, J. (2007). Chronic HIV-1 infection frequently fails to protect against superinfection. *PLoS Pathog* 3, e177.
367. Picard-Maureau, M., Jarmy, G., Berg, A., Rethwilm, A., and Lindemann, D. (2003). Foamy virus envelope glycoprotein-mediated entry involves a pH-dependent fusion process. *J Virol* 77, 4722-4730.
368. Pietschmann, T., Zentgraf, H., Rethwilm, A., and Lindemann, D. (2000). An evolutionarily conserved positively charged amino acid in the putative membrane-spanning domain of the foamy virus envelope protein controls fusion activity. *J Virol* 74, 4474-4482.

List of References

369. Piñon, J.D., Klasse, P.J., Jassal, S.R., Welson, S., Weber, J., Brighty, D.W., and Sattentau, Q.J. (2003). Human T-cell leukemia virus type 1 envelope glycoprotein gp46 interacts with cell surface heparan sulfate proteoglycans. *J Virol* 77, 9922-9930.
370. Pinto-Santini, D.M., Stenbak, C.R., and Linial, M.L. (2017). Foamy virus zoonotic infections. *Retrovirology* 14, 55.
371. Plantier, J.C., Leoz, M., Dickerson, J.E., De Oliveira, F., Cordonnier, F., Leme, V., Damond, F., Robertson, D.L., and Simon, F. (2009). A new human immunodeficiency virus derived from gorillas. *Nat Med* 15, 871-872.
372. Plataniias, L.C. (2005). Mechanisms of type-I- and type-II-interferon-mediated signalling. *Nat Rev Immunol* 5, 375-386.
373. Plochmann, K., Horn, A., Gschmack, E., Armbruster, N., Krieg, J., Wiktorowicz, T., Weber, C., Stirnagel, K., Lindemann, D., Rethwilm, A., *et al.* (2012). Heparan sulfate is an attachment factor for foamy virus entry. *J Virol* 86, 10028-10035.
374. Plotkin, S.A. (2010). Correlates of protection induced by vaccination. *Clin Vaccine Immunol* 17, 1055-1065.
375. Poesz, B.J., Ruscetti, F.W., Gazdar, A.F., Bunn, P.A., Minna, J.D., and Gallo, R.C. (1980). Detection and isolation of type C retrovirus particles from fresh and cultured lymphocytes of a patient with cutaneous T-cell lymphoma. *Proc Natl Acad Sci U S A* 77, 7415-7419.
376. Pollard, V.W., and Malim, M.H. (1998). The HIV-1 Rev protein. *Annu Rev Microbiol* 52, 491-532.
377. Ponomarenko, J., Bui, H.H., Li, W., Fusseder, N., Bourne, P.E., Sette, A., and Peters, B. (2008). ElliPro: a new structure-based tool for the prediction of antibody epitopes. *BMC Bioinformatics* 9, 514.
378. Potter, C.W. (2001). A history of influenza. *J Appl Microbiol* 91, 572-579.
379. Pritchard, L.K., Spencer, D.I., Royle, L., Bonomelli, C., Seabright, G.E., Behrens, A.J., Kulp, D.W., Menis, S., Krumm, S.A., Dunlop, D.C., *et al.* (2015a). Glycan clustering stabilizes the mannose patch of HIV-1 and preserves vulnerability to broadly neutralizing antibodies. *Nature communications* 6, 7479.
380. Pritchard, L.K., Vasiljevic, S., Ozorowski, G., Seabright, G.E., Cupo, A., Ringe, R., Kim, H.J., Sanders, R.W., Doores, K.J., Burton, D.R., *et al.* (2015b). Structural Constraints Determine the Glycosylation of HIV-1 Envelope Trimers. *Cell reports* 11, 1604-1613.
381. Rajawat, Y.S., Humbert, O., and Kiem, H.P. (2019). In-Vivo Gene Therapy with Foamy Virus Vectors. *Viruses* 11.
382. Ramdas, P., Bhardwaj, V., Singh, A., Vijay, N., and Chande, A. (2021). Coelacanth SERINC2 Inhibits HIV-1 Infectivity and Is Counteracted by Envelope Glycoprotein from Foamy Virus. *J Virol* 95, e0022921.
383. Regad, T., Saib, A., Lallemand-Breitenbach, V., Pandolfi, P.P., de Thé, H., and Chelbi-Alix, M.K. (2001). PML mediates the interferon-induced antiviral state against a complex retrovirus via its association with the viral transactivator. *EMBO J* 20, 3495-3505.
384. Reh, J., Stange, A., Götz, A., Rönitz, M., Große, A., and Lindemann, D. (2013). An N-terminal domain helical motif of Prototype Foamy Virus Gag with dual functions essential for particle egress and viral infectivity. *Retrovirology* 10, 45.
385. Renault, N., Tobaly-Tapiero, J., Paris, J., Giron, M.L., Coiffic, A., Roingeard, P., and Saïb, A. (2011). A nuclear export signal within the structural Gag protein is required for prototype foamy virus replication. *Retrovirology* 8, 6.
386. Rethwilm, A. (1996). Unexpected replication pathways of foamy viruses. *J Acquir Immune Defic Syndr Hum Retrovirol* 13 Suppl 1, S248-253.
387. Rethwilm, A. (2003). The replication strategy of foamy viruses. *Curr Top Microbiol Immunol* 277, 1-26.
388. Rethwilm, A., and Bodem, J. (2013). Evolution of foamy viruses: the most ancient of all retroviruses. *Viruses* 5, 2349-2374.
389. Rey, F.A., and Lok, S.M. (2018). Common Features of Enveloped Viruses and Implications for Immunogen Design for Next-Generation Vaccines. *Cell* 172, 1319-1334.
390. Rhodes-Feuillette, A., Lasneret, J., Paulien, S., Ogunkolade, W., Periés, J., and Canivet, M. (1990). Effects of human recombinant alpha and gamma and of highly purified natural beta interferons on simian Spumavirinae prototype (simian foamy virus 1) multiplication in human cells. *Res Virol* 141, 31-43.

List of References

391. Rhodes-Feuillette, A., Saal, F., Lasneret, J., Dubouch, P., and Périès, J. (1979). Isolation and characterization of a new simian foamy virus serotype from lymphocytes of a *Papio cynocephalus* baboon. *J Med Primatol* 8, 308-320.
392. Rhodes-Feuillette, A., Saal, F., Lasneret, J., Santillana-Hayat, M., and Peries, J. (1987). Studies on in vitro interferon induction capacity and interferon sensitivity of simian foamy viruses. *Arch Virol* 97, 77-84.
393. Rich, R.R., and Chaplin, D.D. (2019). The Human Immune Response. In *Clin Immunol*, R.R. Rich, T.A. Fleisher, W.T. Shearer, H. Schroeder, A.J. Frew, and C.M. Weyand, eds. (Elsevier), pp. Pages 3-17.e11.
394. Richard, L., Rua, R., Betsem, E., Mouinga-Ondeme, A., Kazanji, M., Leroy, E., Njouom, R., Buseyne, F., Afonso, P.V., and Gessain, A. (2015). Cocirculation of Two env Molecular Variants, of Possible Recombinant Origin, in Gorilla and Chimpanzee Simian Foamy Virus Strains from Central Africa. *J Virol* 89, 12480-12491.
395. Riggs, J.L., Oshirls, Taylor, D.O., and Lennette, E.H. (1969). Syncytium-forming agent isolated from domestic cats. *Nature* 222, 1190-1191.
396. Robert, X., and Gouet, P. (2014). Deciphering key features in protein structures with the new ENDscript server. *Nucleic Acids Res* 42, W320-324.
397. Rogers, N.G., Basnight, M., Gibbs, C.J., and Gajdusek, D.C. (1967). Latent viruses in chimpanzees with experimental kuru. *Nature* 216, 446-449.
398. Romen, F., Backes, P., Materniak, M., Sting, R., Vahlenkamp, T.W., Riebe, R., Pawlita, M., Kuzmak, J., and Löchel, M. (2007). Serological detection systems for identification of cows shedding bovine foamy virus via milk. *Virology* 364, 123-131.
399. Romen, F., Pawlita, M., Sehr, P., Bachmann, S., Schröder, J., Lutz, H., and Löchel, M. (2006). Antibodies against Gag are diagnostic markers for feline foamy virus infections while Env and Bet reactivity is undetectable in a substantial fraction of infected cats. *Virology* 345, 502-508.
400. Rua, R., Betsem, E., Calattini, S., Saib, A., and Gessain, A. (2012a). Genetic characterization of simian foamy viruses infecting humans. *J Virol* 86, 13350-13359.
401. Rua, R., Betsem, E., and Gessain, A. (2013). Viral latency in blood and saliva of simian foamy virus-infected humans. *PLoS One* 8, e77072.
402. Rua, R., Betsem, E., Montange, T., Buseyne, F., and Gessain, A. (2014). In vivo cellular tropism of gorilla simian foamy virus in blood of infected humans. *J Virol* 88, 13429-13435.
403. Rua, R., and Gessain, A. (2015). Origin, evolution and innate immune control of simian foamy viruses in humans. *Curr Opin Virol* 10, 47-55.
404. Rua, R., Lepelley, A., Gessain, A., and Schwartz, O. (2012b). Innate sensing of foamy viruses by human hematopoietic cells. *J Virol* 86, 909-918.
405. Rupprecht, C.E., and Gibbons, R.V. (2004). Clinical practice. Prophylaxis against rabies. *N Engl J Med* 351, 2626-2635.
406. Ruscetti, S., Davis, L., Feild, J., and Oliff, A. (1981). Friend murine leukemia virus-induced leukemia is associated with the formation of mink cell focus-inducing viruses and is blocked in mice expressing endogenous mink cell focus-inducing xenotropic viral envelope genes. *J Exp Med* 154, 907-920.
407. Russell, R.A., Wiegand, H.L., Moore, M.D., Schäfer, A., McClure, M.O., and Cullen, B.R. (2005). Foamy virus Bet proteins function as novel inhibitors of the APOBEC3 family of innate antiretroviral defense factors. *J Virol* 79, 8724-8731.
408. Rustigian, R., Johnston, P., and Reihart, H. (1955). Infection of monkey kidney tissue cultures with virus-like agents. *Proc Soc Exp Biol Med* 88, 8-16.
409. Sabile, A., Rhodes-Feuillette, A., Jaoui, F.Z., Tobaly-Tapiero, J., Giron, M.L., Lasneret, J., Périès, J., and Canivet, M. (1996). In vitro studies on interferon-inducing capacity and sensitivity to IFN of human foamy virus. *Res Virol* 147, 29-37.
410. Sabouri, Z., Schofield, P., Horikawa, K., Spierings, E., Kipling, D., Randall, K.L., Langley, D., Roome, B., Vazquez-Lombardi, R., Rouet, R., *et al.* (2014). Redemption of autoantibodies on anergic B cells by variable-region glycosylation and mutation away from self-reactivity. *Proc Natl Acad Sci U S A* 111, E2567-2575.
411. Sáez-Cirión, A., and Manel, N. (2018). Immune Responses to Retroviruses. *Annu Rev Immunol* 36, 193-220.

List of References

- 412.Saïb, A., Puvion-Dutilleul, F., Schmid, M., Périès, J., and de Thé, H. (1997). Nuclear targeting of incoming human foamy virus Gag proteins involves a centriolar step. *J Virol* *71*, 1155-1161.
- 413.Saito, M., Tanaka, R., Fujii, H., Kodama, A., Takahashi, Y., Matsuzaki, T., Takashima, H., and Tanaka, Y. (2014). The neutralizing function of the anti-HTLV-1 antibody is essential in preventing in vivo transmission of HTLV-1 to human T cells in NOD-SCID/ γ cnul (NOG) mice. *Retrovirology* *11*, 74.
- 414.Sandstrom, P.A., Phan, K.O., Switzer, W.M., Fredeking, T., Chapman, L., Heneine, W., and Folks, T.M. (2000). Simian foamy virus infection among zoo keepers. *Lancet* *355*, 551-552.
- 415.Sanjuán, R., and Domingo-Calap, P. (2016). Mechanisms of viral mutation. *Cell Mol Life Sci* *73*, 4433-4448.
- 416.Santiago, M.L., Range, F., Keele, B.F., Li, Y., Bailes, E., Bibollet-Ruche, F., Fruteau, C., Noe, R., Peeters, M., Brookfield, J.F., *et al.* (2005). Simian immunodeficiency virus infection in free-ranging sooty mangabeys (*Cercocebus atys atys*) from the Tai Forest, Cote d'Ivoire: implications for the origin of epidemic human immunodeficiency virus type 2. *J Virol* *79*, 12515-12527.
- 417.Santos, A.F., Cavalcante, L.T.F., Muniz, C.P., Switzer, W.M., and Soares, M.A. (2019). Simian Foamy Viruses in Central and South America: A New World of Discovery. *Viruses* *11*.
- 418.Sauerbrei, A. (2016). Diagnosis, antiviral therapy, and prophylaxis of varicella-zoster virus infections. *Eur J Clin Microbiol Infect Dis* *35*, 723-734.
- 419.Saunders, P.M., Vivian, J.P., O'Connor, G.M., Sullivan, L.C., Pymm, P., Rossjohn, J., and Brooks, A.G. (2015). A bird's eye view of NK cell receptor interactions with their MHC class I ligands. *Immunol Rev* *267*, 148-166.
- 420.Sawada, T., Iwahara, Y., Ishii, K., Taguchi, H., Hoshino, H., and Miyoshi, I. (1991). Immunoglobulin prophylaxis against milkborne transmission of human T cell leukemia virus type I in rabbits. *J Infect Dis* *164*, 1193-1196.
- 421.Schartl, M., Walter, R.B., Shen, Y., Garcia, T., Catchen, J., Amores, A., Braasch, I., Chalopin, D., Volff, J.N., Lesch, K.P., *et al.* (2013). The genome of the platyfish, *Xiphophorus maculatus*, provides insights into evolutionary adaptation and several complex traits. *Nat Genet* *45*, 567-572.
- 422.Scheid, J.F., Mouquet, H., Ueberheide, B., Diskin, R., Klein, F., Oliveira, T.Y., Pietzsch, J., Fenyo, D., Abadir, A., Velinzon, K., *et al.* (2011). Sequence and structural convergence of broad and potent HIV antibodies that mimic CD4 binding. *Science* *333*, 1633-1637.
- 423.Schillaci, M.A., Jones-Engel, L., Engel, G.A., Paramastri, Y., Iskandar, E., Wilson, B., Allan, J.S., Kyes, R.C., Watanabe, R., and Grant, R. (2005). Prevalence of enzootic simian viruses among urban performance monkeys in Indonesia. *Trop Med Int Health* *10*, 1305-1314.
- 424.Schliephake, A.W., and Rethwilm, A. (1994). Nuclear localization of foamy virus Gag precursor protein. *J Virol* *68*, 4946-4954.
- 425.Schweizer, M., Falcone, V., Gange, J., Turek, R., and Neumann-Haefelin, D. (1997). Simian foamy virus isolated from an accidentally infected human individual. *J Virol* *71*, 4821-4824.
- 426.Schweizer, M., Schleer, H., Pietrek, M., Liegibel, J., Falcone, V., and Neumann-Haefelin, D. (1999). Genetic stability of foamy viruses: long-term study in an African green monkey population. *J Virol* *73*, 9256-9265.
- 427.Schweizer, M., Turek, R., Hahn, H., Schliephake, A., Netzer, K.O., Eder, G., Reinhardt, M., Rethwilm, A., and Neumann-Haefelin, D. (1995). Markers of foamy virus infections in monkeys, apes, and accidentally infected humans: appropriate testing fails to confirm suspected foamy virus prevalence in humans. *AIDS Res Hum Retroviruses* *11*, 161-170.
- 428.Seabright, G.E., Doores, K.J., Burton, D.R., and Crispin, M. (2019). Protein and Glycan Mimicry in HIV Vaccine Design. *J Mol Biol* *431*, 2223-2247.
- 429.Sharp, P.M., and Hahn, B.H. (2011). Origins of HIV and the AIDS pandemic. *Cold Spring Harb Perspect Med* *1*, a006841.
- 430.Shaw, K.L., Lindemann, D., Mulligan, M.J., and Goepfert, P.A. (2003). Foamy virus envelope glycoprotein is sufficient for particle budding and release. *J Virol* *77*, 2338-2348.
- 431.Shingai, M., Nishimura, Y., Klein, F., Mouquet, H., Donau, O.K., Plishka, R., Buckler-White, A., Seaman, M., Piatak, M., Jr., Lifson, J.D., *et al.* (2013). Antibody-mediated immunotherapy of macaques chronically infected with SHIV suppresses viraemia. *Nature* *503*, 277-280.

List of References

432. Singh, H., Ansari, H.R., and Raghava, G.P. (2013). Improved method for linear B-cell epitope prediction using antigen's primary sequence. *PLoS One* 8, e62216.
433. Sitbon, M., Denesvre, C., Dardalhon, V., Battini, J.L., and Mougel, M. (2001). Les rétrovirus leucémogènes murins : pathogènes, gènes et outils génétiques. *Virologie* 5, 265-293.
434. Slipeen, K., and Sanders, R.W. (2016). HIV-1 envelope glycoprotein immunogens to induce broadly neutralizing antibodies. *Expert review of vaccines* 15, 349-365.
435. Smiley Evans, T., Barry, P.A., Gilardi, K.V., Goldstein, T., Deere, J.D., Fike, J., Yee, J., Ssebide, B.J., Karmacharya, D., Cranfield, M.R., *et al.* (2015). Optimization of a Novel Non-invasive Oral Sampling Technique for Zoonotic Pathogen Surveillance in Nonhuman Primates. *PLoS Negl Trop Dis* 9, e0003813.
436. Smiley Evans, T., Gilardi, K.V., Barry, P.A., Ssebide, B.J., Kinani, J.F., Nizeyimana, F., Noheri, J.B., Byarugaba, D.K., Mudakikwa, A., Cranfield, M.R., *et al.* (2016). Detection of viruses using discarded plants from wild mountain gorillas and golden monkeys. *Am J Primatol* 78, 1222-1234.
437. Soliven, K., Wang, X., Small, C.T., Feeroz, M.M., Lee, E.G., Craig, K.L., Hasan, K., Engel, G.A., Jones-Engel, L., Matsen, F.A.t., *et al.* (2013). Simian foamy virus infection of rhesus macaques in Bangladesh: relationship of latent proviruses and transcriptionally active viruses. *J Virol* 87, 13628-13639.
438. Stange, A., Luftenegger, D., Reh, J., Weissenhorn, W., and Lindemann, D. (2008). Subviral particle release determinants of prototype foamy virus. *J Virol* 82, 9858-9869.
439. Stange, A., Mannigel, I., Peters, K., Heinkelein, M., Stanke, N., Cartellieri, M., Göttlinger, H., Rethwilm, A., Zentgraf, H., and Lindemann, D. (2005). Characterization of prototype foamy virus gag late assembly domain motifs and their role in particle egress and infectivity. *J Virol* 79, 5466-5476.
440. Stanke, N., Stange, A., Luftenegger, D., Zentgraf, H., and Lindemann, D. (2005). Ubiquitination of the prototype foamy virus envelope glycoprotein leader peptide regulates subviral particle release. *J Virol* 79, 15074-15083.
441. Stapleton, J.T. (1992). Passive immunization against hepatitis A. *Vaccine* 10 Suppl 1, S45-47.
442. Stenbak, C.R., Craig, K.L., Ivanov, S.B., Wang, X., Soliven, K.C., Jackson, D.L., Gutierrez, G.A., Engel, G., Jones-Engel, L., and Linal, M.L. (2014). New World simian foamy virus infections in vivo and in vitro. *J Virol* 88, 982-991.
443. Stewart-Jones, G.B., Soto, C., Lemmin, T., Chuang, G.Y., Druz, A., Kong, R., Thomas, P.V., Wagh, K., Zhou, T., Behrens, A.J., *et al.* (2016). Trimeric HIV-1-Env Structures Define Glycan Shields from Clades A, B, and G. *Cell* 165, 813-826.
444. Stiles, G.E., Bittle, J.L., and Cabasso, V.J. (1964). COMPARISON OF SIMIAN FOAMY VIRUS STRAINS INCLUDING A NEW SEROLOGICAL TYPE. *Nature* 201, 1350-1351.
445. Stirnagel, K., Lüftenegger, D., Stange, A., Swiersy, A., Müllers, E., Reh, J., Stanke, N., Grosse, A., Chiantia, S., Keller, H., *et al.* (2010). Analysis of prototype foamy virus particle-host cell interaction with autofluorescent retroviral particles. *Retrovirology* 7, 45.
446. Stoye, J.P., and Coffin, J.M. (1987). The four classes of endogenous murine leukemia virus: structural relationships and potential for recombination. *J Virol* 61, 2659-2669.
447. Streeck, H., Jolin, J.S., Qi, Y., Yassine-Diab, B., Johnson, R.C., Kwon, D.S., Addo, M.M., Brumme, C., Routy, J.P., Little, S., *et al.* (2009). Human immunodeficiency virus type 1-specific CD8+ T-cell responses during primary infection are major determinants of the viral set point and loss of CD4+ T cells. *J Virol* 83, 7641-7648.
448. Sun, Y., Wen, D.D., Liu, Q.M., Yi, X.F., Wang, T.T., Wei, L.L., Li, Z., Liu, W.H., and He, X.H. (2012). Comparative analysis of the envelope glycoproteins of foamy viruses. *Acta Virol* 56, 283-291.
449. Switzer, W.M., Bhullar, V., Shanmugam, V., Cong, M.E., Parekh, B., Lerche, N.W., Yee, J.L., Ely, J.J., Boneva, R., Chapman, L.E., *et al.* (2004). Frequent simian foamy virus infection in persons occupationally exposed to nonhuman primates. *J Virol* 78, 2780-2789.
450. Switzer, W.M., Garcia, A.D., Yang, C., Wright, A., Kalish, M.L., Folks, T.M., and Heneine, W. (2008). Coinfection with HIV-1 and simian foamy virus in West Central Africans. *J Infect Dis* 197, 1389-1393.
451. Switzer, W.M., Salemi, M., Shanmugam, V., Gao, F., Cong, M.E., Kuiken, C., Bhullar, V., Beer, B.E., Vallet, D., Gautier-Hion, A., *et al.* (2005). Ancient co-speciation of simian foamy viruses and primates. *Nature* 434, 376-380.

List of References

452. Switzer, W.M., Tang, S., Ahuka-Mundeke, S., Shankar, A., Hanson, D.L., Zheng, H., Ayouba, A., Wolfe, N.D., LeBreton, M., Djoko, C.F., *et al.* (2012). Novel simian foamy virus infections from multiple monkey species in women from the Democratic Republic of Congo. *Retrovirology* 9, 100.
453. Switzer, W.M., Tang, S., Zheng, H., Shankar, A., Sprinkle, P.S., Sullivan, V., Granade, T.C., and Heneine, W. (2016). Dual Simian Foamy Virus/Human Immunodeficiency Virus Type 1 Infections in Persons from Cote d'Ivoire. *PLoS One* 11, e0157709.
454. Takahashi, K., Takezaki, T., Oki, T., Kawakami, K., Yashiki, S., Fujiyoshi, T., Usuku, K., Mueller, N., Osame, M., Miyata, K., *et al.* (1991). Inhibitory effect of maternal antibody on mother-to-child transmission of human T-lymphotropic virus type I. The Mother-to-Child Transmission Study Group. *Int J Cancer* 49, 673-677.
455. Takehisa, J., Kraus, M.H., Ayouba, A., Bailes, E., Van Heuverswyn, F., Decker, J.M., Li, Y., Rudicell, R.S., Learn, G.H., Neel, C., *et al.* (2009). Origin and biology of simian immunodeficiency virus in wild-living western gorillas. *J Virol* 83, 1635-1648.
456. Takenouchi, N., Jones, K.S., Lisinski, I., Fugo, K., Yao, K., Cushman, S.W., Ruscetti, F.W., and Jacobson, S. (2007). GLUT1 is not the primary binding receptor but is associated with cell-to-cell transmission of human T-cell leukemia virus type 1. *J Virol* 81, 1506-1510.
457. Taylor, L.H., Latham, S.M., and Woolhouse, M.E. (2001). Risk factors for human disease emergence. *Philos Trans R Soc Lond B Biol Sci* 356, 983-989.
458. Terwilliger, T.C., Adams, P.D., Read, R.J., McCoy, A.J., Moriarty, N.W., Grosse-Kunstleve, R.W., Afonine, P.V., Zwart, P.H., and Hung, L.W. (2009). Decision-making in structure solution using Bayesian estimates of map quality: the PHENIX AutoSol wizard. *Acta Crystallogr D Biol Crystallogr* 65, 582-601.
459. Tobaly-Tapiero, J., Bittoun, P., Lehmann-Che, J., Delelis, O., Giron, M.L., de Thé, H., and Saïb, A. (2008). Chromatin tethering of incoming foamy virus by the structural Gag protein. *Traffic (Copenhagen, Denmark)* 9, 1717-1727.
460. Tobaly-Tapiero, J., Bittoun, P., Neves, M., Guillemin, M.C., Lecellier, C.H., Puvion-Dutilleul, F., Gicquel, B., Zientara, S., Giron, M.L., de Thé, H., *et al.* (2000). Isolation and characterization of an equine foamy virus. *J Virol* 74, 4064-4073.
461. Trobridge, G., Josephson, N., Vassilopoulos, G., Mac, J., and Russell, D.W. (2002). Improved foamy virus vectors with minimal viral sequences. *Mol Ther* 6, 321-328.
462. Trobridge, G., and Russell, D.W. (2004). Cell cycle requirements for transduction by foamy virus vectors compared to those of oncovirus and lentivirus vectors. *J Virol* 78, 2327-2335.
463. Trobridge, G.D., Allen, J., Peterson, L., Ironside, C., Russell, D.W., and Kiem, H.P. (2009). Foamy and lentiviral vectors transduce canine long-term repopulating cells at similar efficiency. *Hum Gene Ther* 20, 519-523.
464. Trobridge, G.D., Beard, B.C., Wu, R.A., Ironside, C., Malik, P., and Kiem, H.P. (2012). Stem cell selection in vivo using foamy vectors cures canine pyruvate kinase deficiency. *PLoS One* 7, e45173.
465. Tumas, K.M., Poszgay, J.M., Avidan, N., Ksiazek, S.J., Overmoyer, B., Blank, K.J., and Prystowsky, M.B. (1993). Loss of antigenic epitopes as the result of env gene recombination in retrovirus-induced leukemia in immunocompetent mice. *Virology* 192, 587-595.
466. Turner, H.L., Andrabi, R., Cottrell, C.A., Richey, S.T., Song, G., Callaghan, S., Anzanello, F., Moyer, T.J., Abraham, W., Melo, M., *et al.* (2021). Disassembly of HIV envelope glycoprotein trimer immunogens is driven by antibodies elicited via immunization. *Sci Adv* 7.
467. Vajda, S., Yueh, C., Beglov, D., Bohnuud, T., Mottarella, S.E., Xia, B., Hall, D.R., and Kozakov, D. (2017). New additions to the ClusPro server motivated by CAPRI. *Proteins* 85, 435-444.
468. Viant, C., Weymar, G.H.J., Escolano, A., Chen, S., Hartweg, H., Cipolla, M., Gazumyan, A., and Nussenzweig, M.C. (2020). Antibody Affinity Shapes the Choice between Memory and Germinal Center B Cell Fates. *Cell* 183, 1298-1311.e1211.
469. Victora, G.D., and Nussenzweig, M.C. (2022). Germinal Centers. *Annu Rev Immunol* 40, 413-442.
470. Victora, G.D., Schwickert, T.A., Fooksman, D.R., Kamphorst, A.O., Meyer-Hermann, M., Dustin, M.L., and Nussenzweig, M.C. (2010). Germinal center dynamics revealed by multiphoton microscopy with a photoactivatable fluorescent reporter. *Cell* 143, 592-605.
471. Visseaux, B., Damond, F., Matheron, S., Descamps, D., and Charpentier, C. (2016). Hiv-2 molecular epidemiology. *Infect Genet Evol.*

472. von Laer, D., Neumann-Haefelin, D., Heeney, J.L., and Schweizer, M. (1996). Lymphocytes are the major reservoir for foamy viruses in peripheral blood. *Virology* *221*, 240-244.
473. Wagh, K., Hahn, B.H., and Korber, B. (2020). Hitting the sweet spot: exploiting HIV-1 glycan shield for induction of broadly neutralizing antibodies. *Curr Opin HIV AIDS* *15*, 267-274.
474. Wagner, T.C., and Bodem, J. (2017). Sequence errors in foamy virus sequences in the GenBank database: resequencing of the prototypic foamy virus proviral plasmids. *Arch Virol* *162*, 1141-1144.
475. Wang, H., Cohen, A.A., Galimidi, R.P., Gristick, H.B., Jensen, G.J., and Bjorkman, P.J. (2016a). Cryo-EM structure of a CD4-bound open HIV-1 envelope trimer reveals structural rearrangements of the gp120 V1V2 loop. *Proc Natl Acad Sci U S A* *113*, E7151-e7158.
476. Wang, M., Zhang, H., Liu, Q.M., Sun, Y., Li, Z., Liu, W.H., He, X.H., Song, J., and Wang, Y.X. (2016b). Structure of transmembrane subunits gp47 of the foamy virus envelope glycoproteins. *Acta Virol* *60*, 181-189.
477. Weber, P., Pissis, C., Navaza, R., Mechaly, A.E., Saul, F., Alzari, P.M., and Haouz, A. (2019). High-Throughput Crystallization Pipeline at the Crystallography Core Facility of the Institut Pasteur. *Molecules* *24*.
478. Weissenhorn, W., Dessen, A., Harrison, S.C., Skehel, J.J., and Wiley, D.C. (1997). Atomic structure of the ectodomain from HIV-1 gp41. *Nature* *387*, 426-430.
479. White, J.M., and Whittaker, G.R. (2016). Fusion of Enveloped Viruses in Endosomes. *Traffic (Copenhagen, Denmark)* *17*, 593-614.
480. Wilk, T., de Haas, F., Wagner, A., Rutten, T., Fuller, S., Flügel, R.M., and Löchelt, M. (2000). The intact retroviral Env glycoprotein of human foamy virus is a trimer. *J Virol* *74*, 2885-2887.
481. Wilk, T., Geiselhart, V., Frech, M., Fuller, S.D., Flügel, R.M., and Löchelt, M. (2001). Specific interaction of a novel foamy virus Env leader protein with the N-terminal Gag domain. *J Virol* *75*, 7995-8007.
482. Williams, D.K., and Khan, A.S. (2010). Role of neutralizing antibodies in controlling simian foamy virus transmission and infection. *Transfusion* *50*, 200-207.
483. Winkler, I.G., Flügel, R.M., Lochelt, M., and Flower, R.L. (1998). Detection and molecular characterisation of feline foamy virus serotypes in naturally infected cats. *Virology* *247*, 144-151.
484. Winkler, I.G., Löchelt, M., and Flower, R.L. (1999). Epidemiology of feline foamy virus and feline immunodeficiency virus infections in domestic and feral cats: a seroepidemiological study. *J Clin Microbiol* *37*, 2848-2851.
485. Winn, M.D., Ballard, C.C., Cowtan, K.D., Dodson, E.J., Emsley, P., Evans, P.R., Keegan, R.M., Krissinel, E.B., Leslie, A.G., McCoy, A., *et al.* (2011). Overview of the CCP4 suite and current developments. *Acta Crystallogr D Biol Crystallogr* *67*, 235-242.
486. Wolfe, N.D., Dunavan, C.P., and Diamond, J. (2007). Origins of major human infectious diseases. *Nature* *447*, 279-283.
487. Wolfe, N.D., Heneine, W., Carr, J.K., Garcia, A.D., Shanmugam, V., Tamoufe, U., Torimiro, J.N., Prosser, A.T., Lebreton, M., Mpoudi-Ngole, E., *et al.* (2005). Emergence of unique primate T-lymphotropic viruses among central African bushmeat hunters. *Proc Natl Acad Sci U S A* *102*, 7994-7999.
488. Wolfe, N.D., Switzer, W.M., Carr, J.K., Bhullar, V.B., Shanmugam, V., Tamoufe, U., Prosser, A.T., Torimiro, J.N., Wright, A., Mpoudi-Ngole, E., *et al.* (2004). Naturally acquired simian retrovirus infections in central African hunters. *Lancet* *363*, 932-937.
489. Wu, F., Zhao, S., Yu, B., Chen, Y.M., Wang, W., Song, Z.G., Hu, Y., Tao, Z.W., Tian, J.H., Pei, Y.Y., *et al.* (2020). A new coronavirus associated with human respiratory disease in China. *Nature* *579*, 265-269.
490. Wu, Z., Ren, X., Yang, L., Hu, Y., Yang, J., He, G., Zhang, J., Dong, J., Sun, L., Du, J., *et al.* (2012). Virome analysis for identification of novel mammalian viruses in bat species from Chinese provinces. *J Virol* *86*, 10999-11012.
491. Xu, F., Tan, J., Liu, R., Xu, D., Li, Y., Geng, Y., Liang, C., and Qiao, W. (2011). Tetherin inhibits prototypic foamy virus release. *Virol J* *8*, 198.
492. Yan, J., Zheng, Y., Yuan, P., Wang, S., Han, S., Yin, J., Peng, B., Li, Z., Sun, Y., He, X., *et al.* (2021). Novel Host Protein TBC1D16, a GTPase Activating Protein of Rab5C, Inhibits Prototype Foamy Virus Replication. *Front Immunol* *12*, 658660.
493. Yan, N., and Chen, Z.J. (2012). Intrinsic antiviral immunity. *Nat Immunol* *13*, 214-222.

List of References

494. Yap, M.W., Lindemann, D., Stanke, N., Reh, J., Westphal, D., Hanenberg, H., Ohkura, S., and Stoye, J.P. (2008). Restriction of foamy viruses by primate Trim5alpha. *J Virol* 82, 5429-5439.
495. Yu, S.F., Baldwin, D.N., Gwynn, S.R., Yendapalli, S., and Linial, M.L. (1996). Human foamy virus replication: a pathway distinct from that of retroviruses and hepadnaviruses. *Science* 271, 1579-1582.
496. Yu, S.F., Eastman, S.W., and Linial, M.L. (2006). Foamy virus capsid assembly occurs at a pericentriolar region through a cytoplasmic targeting/retention signal in Gag. *Traffic (Copenhagen, Denmark)* 7, 966-977.
497. Yu, S.F., Lujan, P., Jackson, D.L., Emerman, M., and Linial, M.L. (2011). The DEAD-box RNA helicase DDX6 is required for efficient encapsidation of a retroviral genome. *PLoS Pathog* 7, e1002303.
498. Yu, S.F., Sullivan, M.D., and Linial, M.L. (1999). Evidence that the human foamy virus genome is DNA. *J Virol* 73, 1565-1572.
499. Zamborlini, A., Renault, N., Saïb, A., and Delelis, O. (2010). Early reverse transcription is essential for productive foamy virus infection. *PLoS One* 5, e11023.
500. Zemba, M., Alke, A., Bodem, J., Winkler, I.G., Flower, R.L., Pfrepper, K., Delius, H., Flügel, R.M., and Löchelt, M. (2000). Construction of infectious feline foamy virus genomes: cat antisera do not cross-neutralize feline foamy virus chimera with serotype-specific Env sequences. *Virology* 266, 150-156.
501. Zhang, J., Han, C., Xiong, Z., Qiu, M., Tuo, X., Wang, C., Qiao, W., and Tan, J. (2022). SGK1, a Serine/Threonine Kinase, Inhibits Prototype Foamy Virus Replication. *Microbiology spectrum*, e0199521.
502. Zhang, S., Liu, X., Liang, Z., Bing, T., Qiao, W., and Tan, J. (2019). The Influence of Envelope C-Terminus Amino Acid Composition on the Ratio of Cell-Free to Cell-Cell Transmission for Bovine Foamy Virus. *Viruses* 11.
503. Zhang, Y., and Skolnick, J. (2004). Scoring function for automated assessment of protein structure template quality. *Proteins* 57, 702-710.
504. Zhang, Z., Perković, M., Gu, Q., Balakrishnan, K., Sangwiman, A., Häussinger, D., Lindemann, D., and Münk, C. (2021). HIV-2 Vif and foamy virus Bet antagonize APOBEC3B by different mechanisms. *Virology* 554, 17-27.
505. Zhou, P., Yang, X.L., Wang, X.G., Hu, B., Zhang, L., Zhang, W., Si, H.R., Zhu, Y., Li, B., Huang, C.L., *et al.* (2020). A pneumonia outbreak associated with a new coronavirus of probable bat origin. *Nature* 579, 270-273.
506. Zhou, T., Doria-Rose, N.A., Cheng, C., Stewart-Jones, G.B.E., Chuang, G.Y., Chambers, M., Druz, A., Geng, H., McKee, K., Kwon, Y.D., *et al.* (2017). Quantification of the Impact of the HIV-1-Glycan Shield on Antibody Elicitation. *Cell reports* 19, 719-732.
507. Zhou, T., Lynch, R.M., Chen, L., Acharya, P., Wu, X., Doria-Rose, N.A., Joyce, M.G., Lingwood, D., Soto, C., Bailer, R.T., *et al.* (2015). Structural Repertoire of HIV-1-Neutralizing Antibodies Targeting the CD4 Supersite in 14 Donors. *Cell* 161, 1280-1292.
508. Zhou, T., Zheng, A., Baxa, U., Chuang, G.Y., Georgiev, I.S., Kong, R., O'Dell, S., Shahzad-Ul-Hussan, S., Shen, C.H., Tsybovsky, Y., *et al.* (2018). A Neutralizing Antibody Recognizing Primarily N-Linked Glycan Targets the Silent Face of the HIV Envelope. *Immunity* 48, 500-513.e506.

CHAPTER IX

APPENDICES

9 | APPENDICES

9.1 Supplementary Tables - Manuscript I

Table S.IV-1 – X-ray crystallography data collection and refinement statistics

	SFV GII RBD ^D (native) data (PBD 8AEZ)	RBD ^D (derivative) data	SFV GII RBD ^G (native) data (PBD 8AIC)
Data collection			
Wavelength	0.9786	1.907	0.9786
Space group	P3 ₂ 21	P3 ₁ 21	P6 ₁
Cell dimensions			
<i>a</i> , <i>b</i> , <i>c</i> (Å)	99.5, 99.5, 120.6	99.6, 99.6, 120.9	123.6, 123.6, 191.6
α , β , γ (°)	90, 90, 120	90, 90, 120	90, 90, 120
Resolution range (Å)	49.73 - 2.574 (2.666 - 2.574) ^a	46.06 - 3.171 (3.284 - 3.171)	46.73 - 2.8 (2.9 - 2.8)
Total reflections	453419 (44048)	238580 (24149)	875971 (87278)
Unique reflections	22363 (2191)	12192 (1165)	40619 (4041)
Completeness (%)	99.91 (99.50)	99.60 (96.75)	99.58 (99.14)
Redundancy	20.3 (20.1)	19.6 (20.1)	21.6 (21.6)
<i>R</i> _{merge} ^b	0.2051 (0.9362)	0.1776 (0.9898)	0.199 (1.705)
<i>R</i> _{pim}	0.04701 (0.2117)	0.04098 (0.2256)	0.04364 (0.3719)
<i>I</i> / σ (<i>I</i>)	10.10 (1.85)	20.30 (5.19)	13.35 (1.45)
CC _{1/2}	0.986 (0.846)	0.998 (0.917)	0.997 (0.689)
Refinement			
No. reflections	22355 (2190)	/	40615 (4040)
No. of reflections for <i>R</i> _{free} ^c	1052 (110)	/	2111 (208)
<i>R</i> _{work} / <i>R</i> _{free} ^d	0.213/0.253	/	0.194/0.229
No. non-hydrogen atoms	2945	/	6086
Macromolecules	2711	/	5448
Ligands	203	/	531
Water	93	/	321
Mean B value (Å²)			

Appendices

Protein and sugar	73.88	/	65.44
Ligand/Ion	94.16	/	114.49
Water	60.68	/	55.18
R.m.s. deviations			
Bond lengths (Å)	0.012	/	0.004
Bond angles (°)	1.62	/	0.77
Ramachandran favored/outliers (%)	95.99/0.31	/	95.69/0.00

^a Values in parentheses are for highest-resolution shell.

^b $R_{\text{merge}} = \frac{\sum_{hkl} \sum_i |I_i(hkl) - \langle I(hkl) \rangle|}{\sum_{hkl} \sum_i I_i(hkl)}$, where $I_i(hkl)$ is the i th observation of reflection hkl and $\langle I(hkl) \rangle$ is the weighted average intensity for all observations i of reflection hkl .

^c The free set represents a random 5% of reflections not included in refinement

^d $R = \frac{\sum_{hkl} (||F_{\text{obs}}| - |F_{\text{calc}}||)}{\sum_{hkl} |F_{\text{obs}}|}$, where $|F_{\text{obs}}|$ and $|F_{\text{calc}}|$ are the observed and calculated structure factor amplitudes, respectively.

Table S.IV-2 – Secondary structure content in GII RBD

Domain	Helical [†] (%)	β-strands (%)	Other [‡] (%)
RBD	30	14	56
Lower	45	17	38
Upper	20	12	68

[†] - α- and 3₁₀ helices

[‡] - B, S, T, X

The secondary structure content was calculated using 2StrucCompare webserver (Klose et al., 2010) at <https://2struccompare.cryst.bbk.ac.uk/index.php>.

Table S.IV-3 – Intramolecular interactions within GII RBD

The intramolecular interactions were analyzed by ProteinTools program <https://proteintools.uni-bayreuth.de> (Ferruz et al., 2021).

Van der Waals contacts in the SFV RBD			
Cluster #	Area (Å ²)	# of residues	Location (domain)
1	153	4	Lower
2	1002	22	
3	2543	51	Lower + upper
4	82	2	Upper
5	77	2	
6	86	2	

Polar contacts in the SFV RBD		
Lower subdomain		
Cluster	Donor - Acceptor	Distance (Å)
1	HIS225-ND1 -- GLN222-OE1	3.3
2	ARG226-NH1 -- GLU337-OE1	3.1
	ARG226-NH2 -- GLU337-OE2	2.4
3	HIS234-ND1 -- TYR323-OH	3.1
4	THR242-OG1 -- GLN492-OE1	3.4
5	HIS314-ND1 -- THR313-OG1	2.9
6	TYR327-OH -- ASP320-OD2	2.5
7	ASN331-ND2 -- ASN336-OD1	3.4
8	LYS342-NZ -- GLU339-OE1	3.3
	ARG343-NE -- GLU339-OE2	2.8
	ARG343-NH2 -- GLU339-OE2	3.2
9	ASN351-ND2 -- GLU502-OE1	2.5
	TYR551-OH -- GLU502-OE2	2.5
10	LYS352-NZ -- GLU495-OE2	3.2
	TYR497-OH -- GLU495-OE1	3.1
11	ASN368-ND2 -- ASN373-OD1	3.0

Appendices

Upper subdomain		
Cluster	Donor - Acceptor	Distance (Å)
12	GLN244-NE2 -- GLN491-OE1	2.6
	GLN491-NE2 -- SER488-OG	3.0
13	TYR267-OH -- ASP468-OD2	2.9
14	THR288-OG1 -- GLU442-OE1	2.9
	THR288-OG1 -- GLU442-OE2	3.4
	TYR456-OH -- GLU442-OE2	3.2
15	ARG297-NH1 -- ASP402-OD2	2.9
	ARG297-NH2 -- ASP402-OD1	2.6
	ARG297-NH2 -- ASP402-OD2	2.9
	SER397-OG -- ASP402-OD2	2.8
	ARG372-NH1 -- ASP378-OD2	2.8
16	ARG372-NH2 -- ASP378-OD1	2.9
	ARG382-NH1 -- ASP378-OD1	2.8
	SER375-OG -- ASP378-OD2	2.9
	TRP399-NE1 -- ASP254-OD1	2.7
17	TRP399-NE1 -- ASP254-OD1	2.7
18	THR406-OG1 -- ASN409-OD1	3.4
19	ARG407-NE -- GLU400-OE2	3.1
20	ARG433-NH2 -- GLU464-OE2	2.7
21	TRP435-NE1 -- ASN462-OD1	3.0
22	ARG436-NH2 -- ASP254-OD1	2.6
23	THR452-OG1 -- ASP450-OD1	2.9
24	SER461-OG -- GLU439-OE2	2.5
25	GLN482-NE2 -- SER473-OG	3.1
26	ARG537-NE -- GLU384-OE1	3.0
	ARG537-NH1 -- TYR269-OH	3.4
	ARG537-NH2 -- GLU384-OE2	2.8
	ARG537-NH2 -- ASP274-OD2	2.8
	TYR269-OH -- ASP274-OD1	2.6
	TYR275-OH -- GLU384-OE2	2.6

9.2 Supplementary Figures - Manuscript I

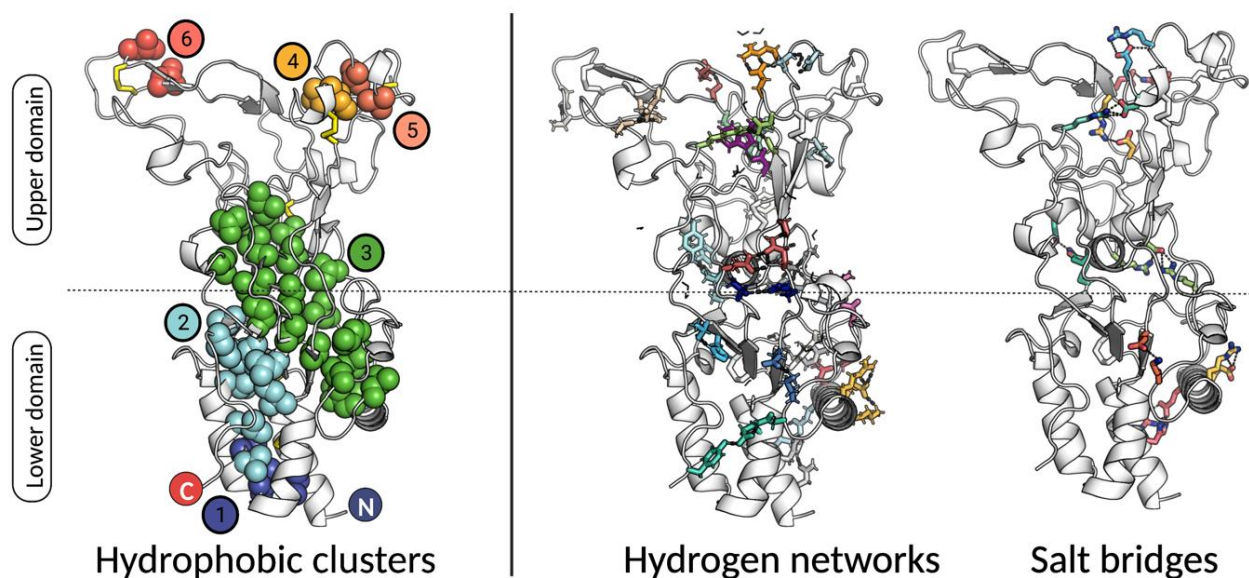


Figure S.IV-1 – The fold of the FV RBD is maintained by hydrophobic and polar interactions

The FV RBD core is formed by the hydrophobic residues grouped in 6 clusters - 2 in the lower subdomain (clusters #1 and #2), 3 in the upper subdomain (clusters #4, #5, #6), and the largest hydrophobic cluster (BSA=2451 Å² with 51 participating residues; cluster #3 shown in green) running in the direction of the longer axis of the RBD and containing residues from both domains. There are 24 networks of residues whose side chains contribute to 43 hydrogen bonds, with 21 charged residues forming 9 salt bridges. The area of the hydrophobic interfaces in the lower subdomain is about 6 times larger than in the upper subdomain, while the hydrogen bonds and salt bridges are more prevalent in the upper subdomain. The full list of intramolecular interactions and relevant details are given in Table S.IV-3. The intramolecular interactions were analyzed by ProteinTools program <https://proteintools.uni-bayreuth.de> (Ferruz et al., 2021).

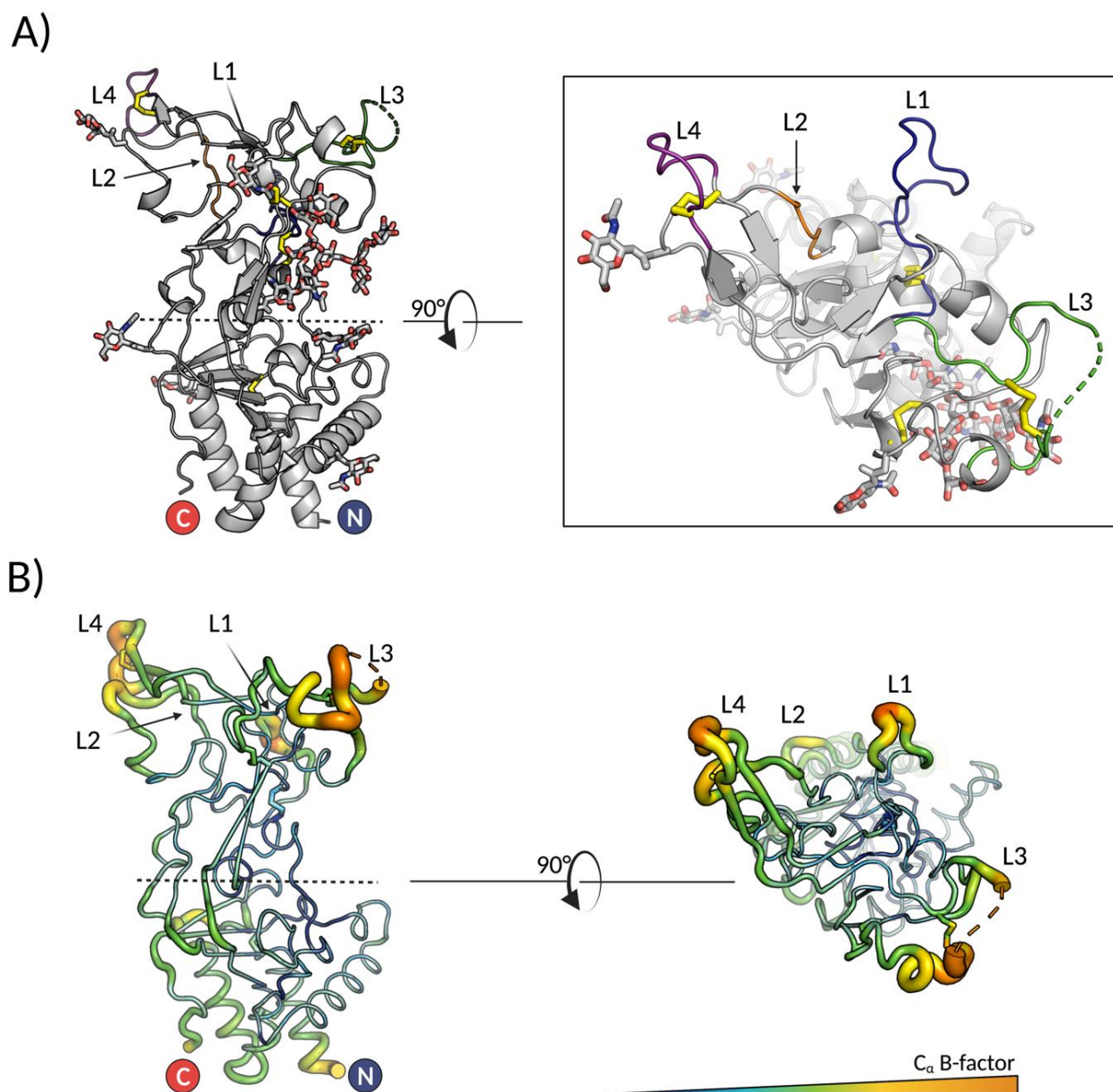


Figure S.IV-2 – Mobile loops decorate the apex of the RBD

A) The upper subdomains loops are designated as follows: loop 1 (L1, residues 253-270, connecting $\beta 2$ and $\eta 1$) in blue, loop 2 (L2, residues 276-281, connecting $\eta 1$ and $\beta 3$) in orange, loop 3 (L3, residues 414-436, connecting $\alpha 6$ and $\beta 9$) in green, and loop 4 (L4, residues 446-453, connecting $\beta 10$ and $\beta 11$) in dark purple. **B)** The RBD structure is shown in ‘tube’ presentation to illustrate the mobility, with the more flexible regions shown as thicker tubes. Coloring scheme corresponds to the C_{α} atomic B-factors (low to high B factors shown in blue to orange spectrum). The images were generated in PyMOL (DeLano, 2002).

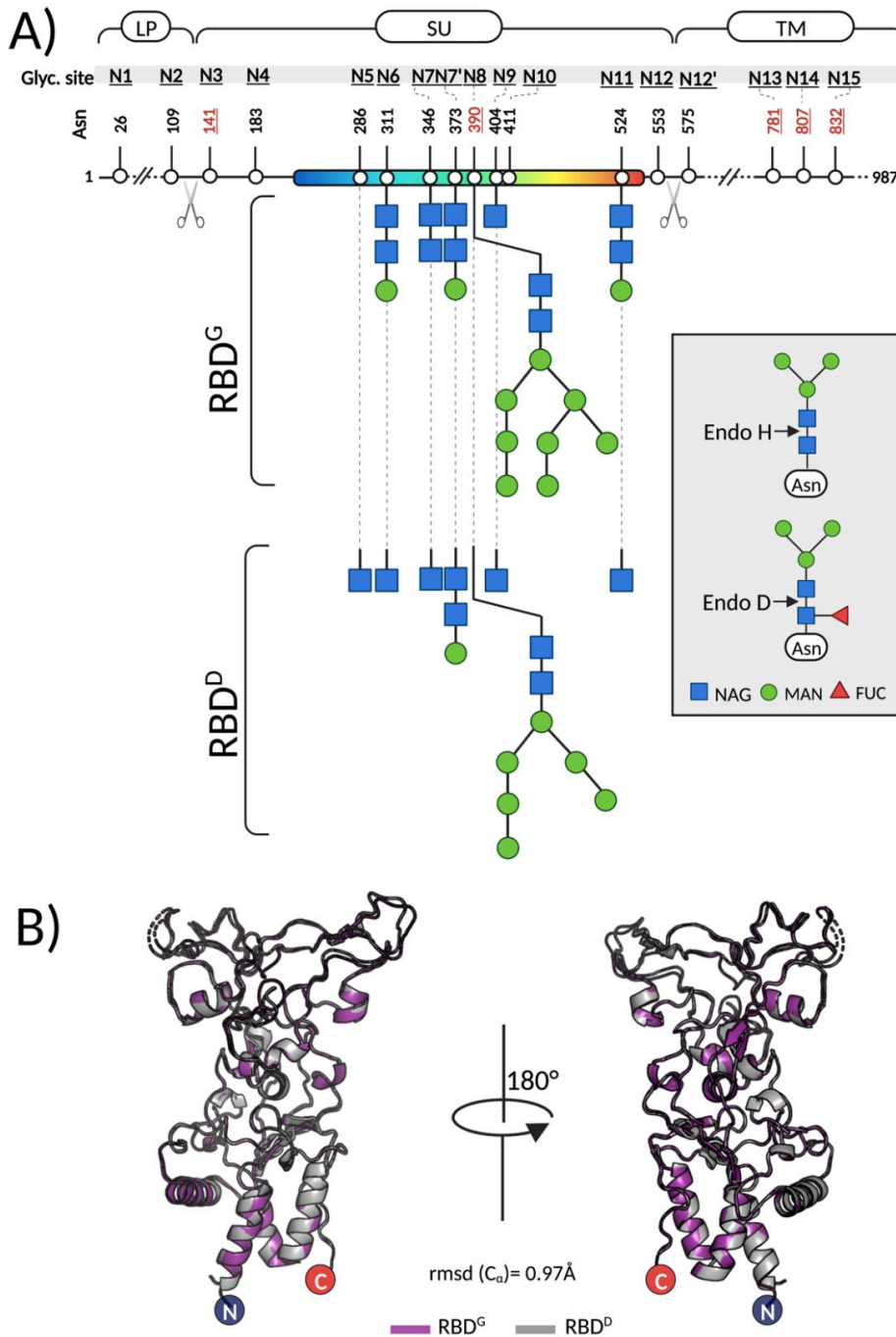


Figure S.IV-3 – Comparison of glycosylated vs deglycosylated RBD structures

A) Schematic representation of SFV Env and the 17 predicted N-glycosylation sites, labeled as N1 to N15 (Luftenecker et al., 2005). The sites that are 100% conserved in all FV Envs (Asn¹⁴¹ (N3), Asn³⁹⁰ (N8), Asn⁷⁸¹ (N13), Asn⁸⁰⁷ (N14), Asn⁸³² (N15)) are indicated with red underscored letters. The two furin sites are represented by scissors. LP, SU and TM are the abbreviations for the leader peptide, surface subunit and transmembrane subunit, respectively. The sugar residues, N-acetyl glucosamine (NAG) and mannose (MAN) that could be resolved in RBD^D or RBD^G are shown. The N-linked oligosaccharide core is shown in the grey inset, with the cleavage sites indicated for the EndoD and EndoH glycosyades. A fraction of proteins expressed in insect cells contains an α 1-6 fucose bound to the first NAG, rendering the sugar sensitive to cleavage by EndoD, but resistant to EndoH. Thus, both EndoD and EndoH were used for deglycosylation of the recombinant RBD. The figure was created in Biorender.com. **B)** Superposition of the RBD^G (purple) and RBD^D (grey) structures done in PyMOL (DeLano, 2002).

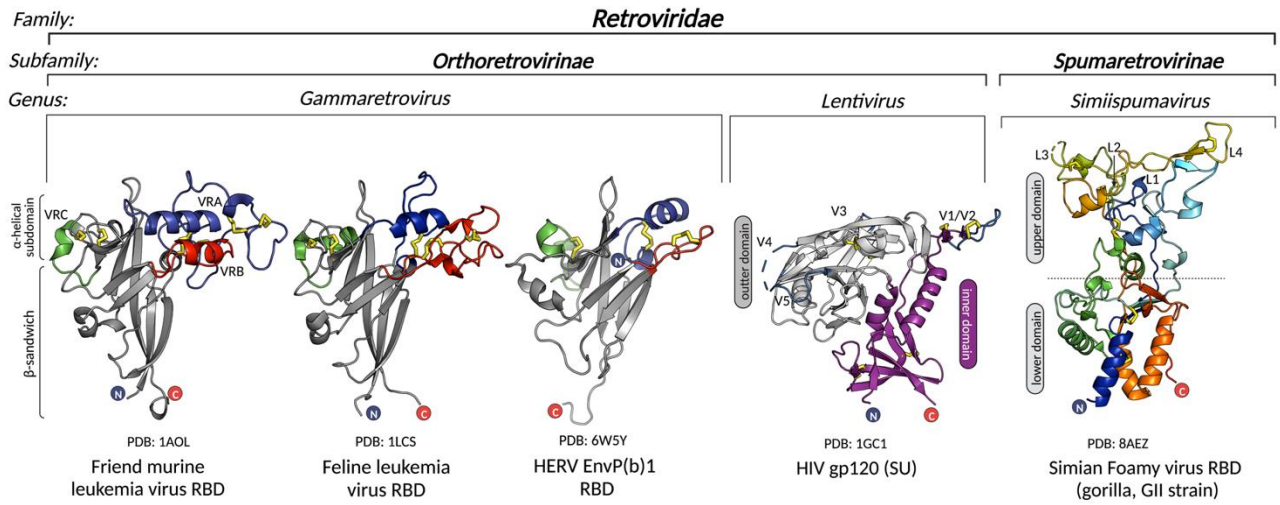
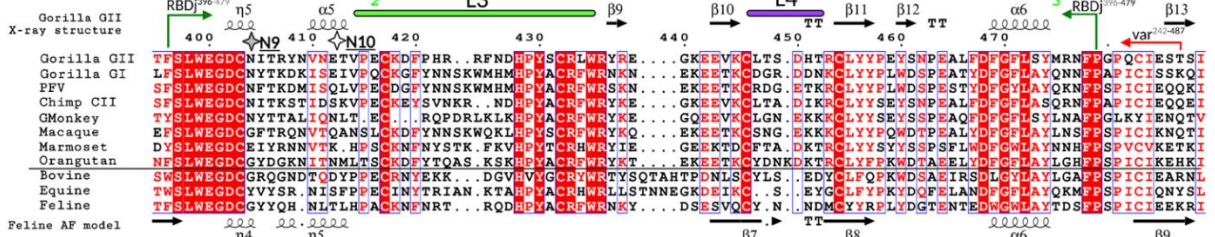
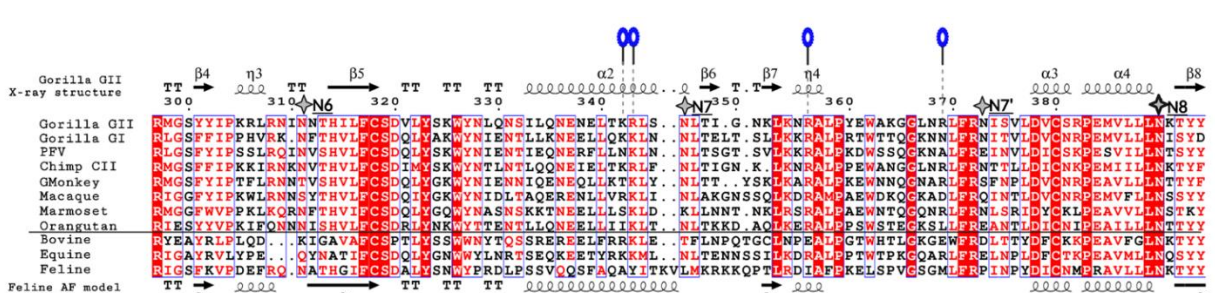
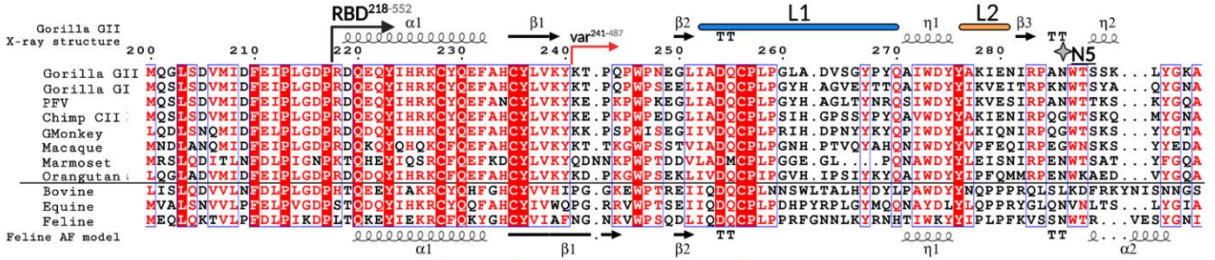
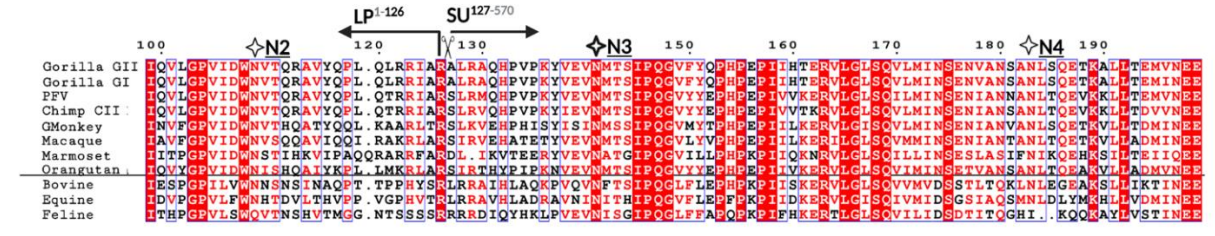
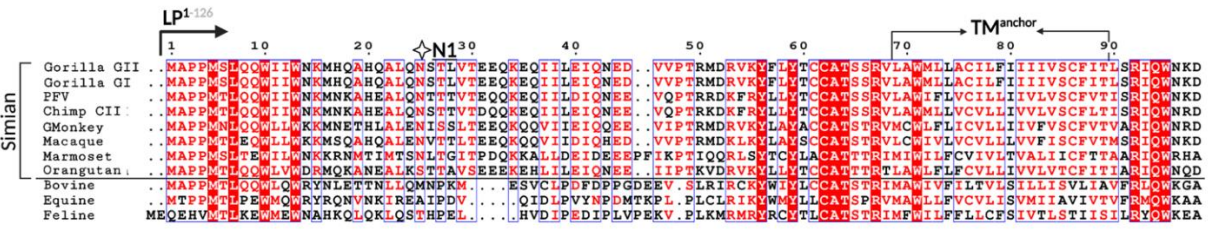


Figure S.IV-4 – Comparison of the SFV RBD fold with that of the RBD of Orthoretroviruses

Structures of RBDs from gammaretroviruses and of SU from HIV are shown to illustrate a lack of structural homology between the RBDs from different genera of retroviruses.

Appendices



Appendices

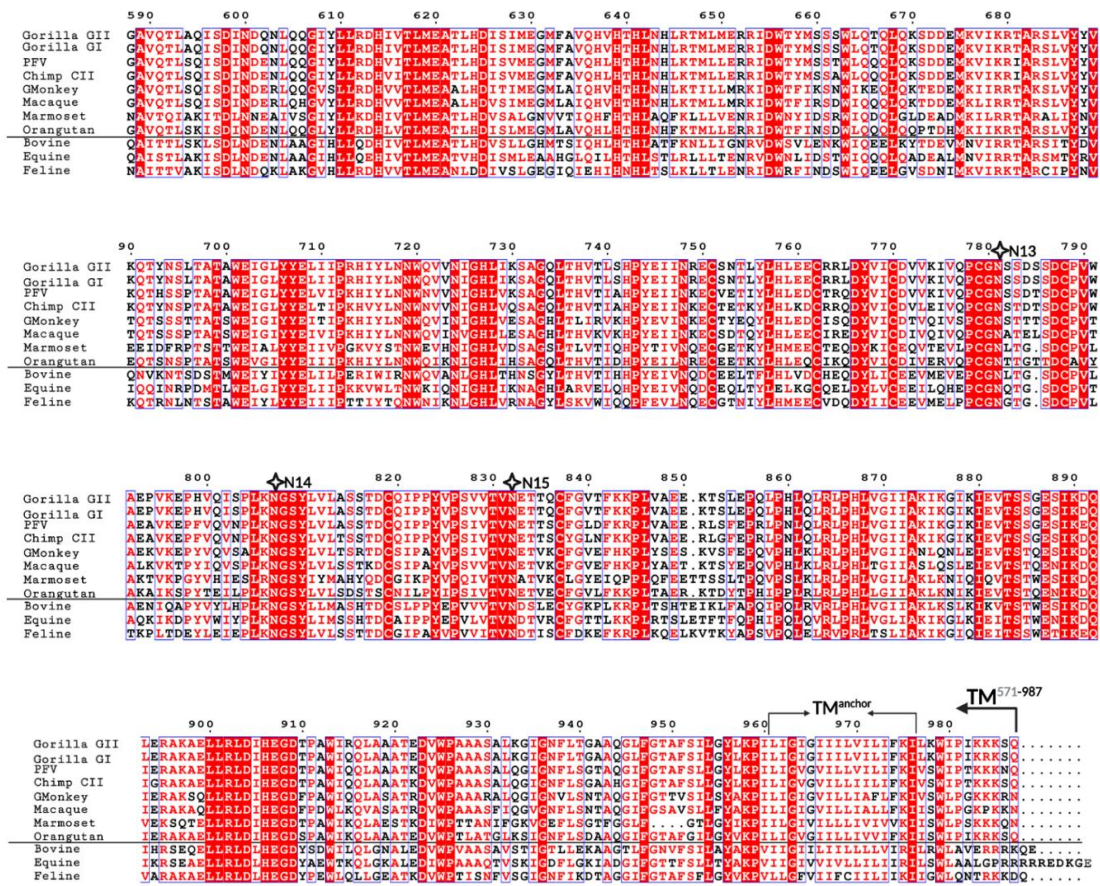


Figure S.IV-5 – Sequence conservation of FV Env

Sequences corresponding to 11 FV Env were aligned in Clustal Omega⁵ and the alignment was plotted using ESPrnt <https://esprnt.ibcp.fr> (Robert and Gouet, 2014), with colors that indicate % identity (white letter, red background 100% identity; red letters, white background >70% identity; black letters, white background, <70% identity). The black, horizontal line separates simian from other FVs. The secondary structure elements corresponding to the SFV RBD X-ray structure and the AF model for the feline FV RBD are plotted above and below the alignment, respectively. The N-linked glycosylation sites are indicated with stars. The already established nomenclature for the N-glycosylation sites (N₁ to N₁₅) is applied. The strictly conserved N-glycosylation sites have a thicker border, and the sites that carried sugars, which could be resolved in our structure, have grey filling. The residues interacting with heparan-sulfate are marked with blue ovals. Loops 1-4 are indicated with bars above the alignment and labeled as L1-L4, using the same color code as in Fig. S2. The boundaries for the LP, SU, RBD, TM subunit are shown, as well as for the RBD variable and RBDjoin regions (the numbering corresponds to that of gorilla SFV Env, GII-K74 genotype). To distinguish the TM subunit from the TM domain, which is the region spanning the membrane, the latter is referred to as the TM^{anchor}. The two furin sites are indicated with the scissors drawing. The Env sequences used in the alignment were obtained from public databases and with following accession numbers: SFVggo_huBAK74 (GII-K74, genotype II gorilla SFV, GenBank: AFX98090.1), SFVggo_huBAD468 (GI-D468, genotype I gorilla SFV; GenBank: AFX98095.1), SFVpsc_huHSRV13 (CI-PFV, known as Prototype Foamy Virus genotype I chimpanzee SFV; GenBank: AQM52259.1), SFVpvePan2 (CII-SFV7, genotype II chimpanzee SFV; UniProtKB/Swiss-Prot: Q87041.1), SFVcae_LK3 (Genotype II African green monkey SFV; NCBI Reference: YP_001956723.2), SFVmcv_FV21 (genotype I macaque SFV; UniProtKB/Swiss-Prot: P23073.3), SFVcja_FXV (Marmoset FV; GenBank: GU356395.1), SFVppy_bella (Orangutan SFV; GenBank: CAD67563.1), BFVbta_BSV11 (Bovine FV; NCBI Reference: NP_044930.1), EFVeca_1 (Equine FV; GenBank: AAF64415.1), and FVfca_FUV7 (Feline FV; UniProtKB/Swiss-Prot: O56861.1). Genotypes I and II have been defined for gorilla, chimpanzee, green monkey and macaque FVs (AIEWSAKUN et al., 2019a; GALVIN et al., 2013; RICHARD et al., 2015).

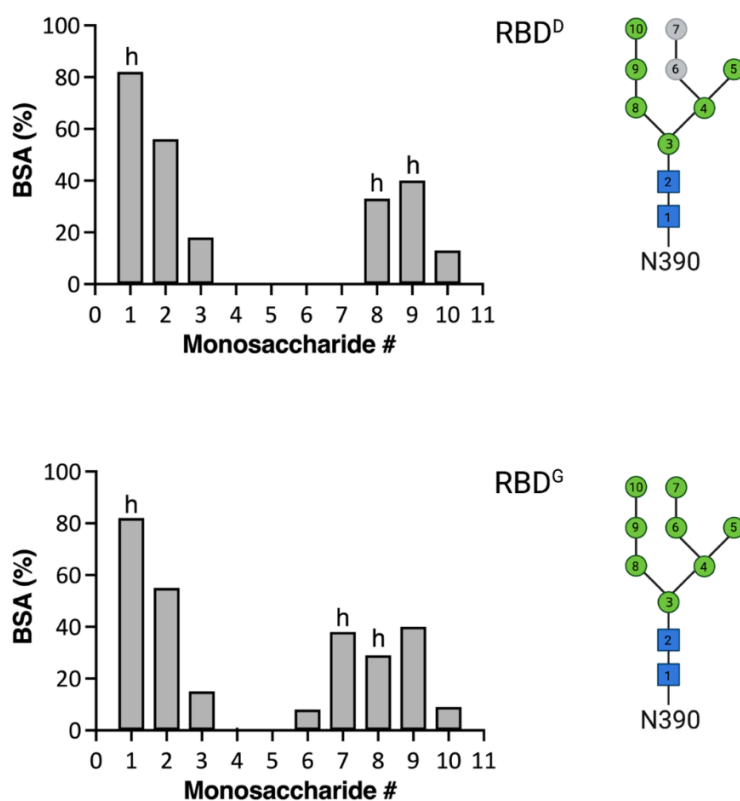


Figure S.IV-6 – Intramolecular contacts between N8 sugar and RBD

The buried surface area (BSA) for each sugar residue was calculated as a percent of the total surface area (\AA^2) in ePISA (Krissinel and Henrick, 2007) and plotted. Sugars that establish hydrogen bonds with the amino acids are indicated with letter 'h'. Sugars 6 and 7 are colored in grey for RBD^D because they were not resolved in the structure.

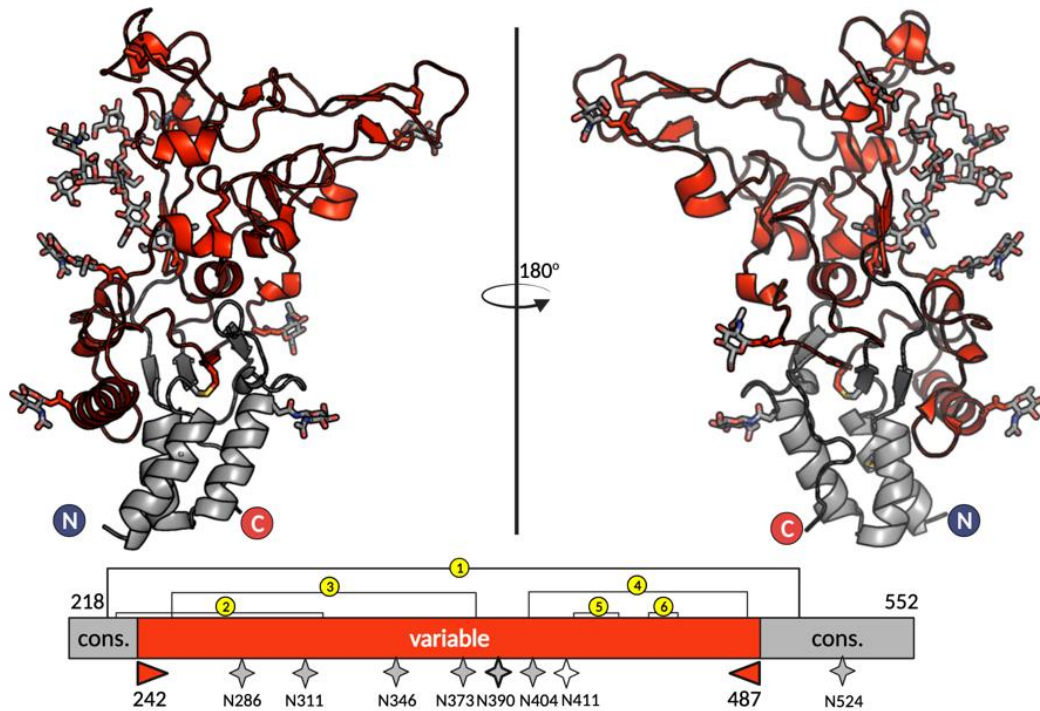


Figure S.IV-7 – Functional features of FV RBD mapped onto the structure

Functional features plotted on the RBD structure. The conserved ‘RBD^{cons}’ (residues 218-241 and 488-552) and variable regions ‘RBD^{var}’ (residues 242-487) are plotted on the X-ray structure of gorilla SFV RBD and colored in light grey and red, respectively. The glycosylation sites are indicated with the stars on the bottom.

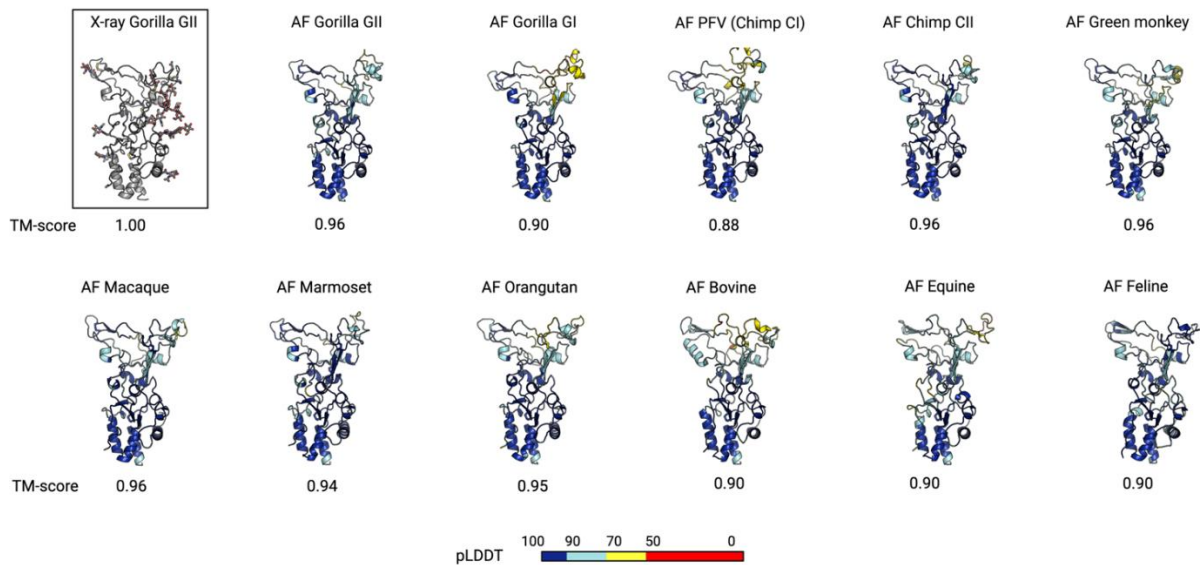


Figure S.IV-8 – AlphaFold models of FV RBDs

Models generated by the AF prediction program (Jumper et al., 2021) colored according to the per-residue confidence metric called ‘predicted local distance difference test’ (pLDDT). The pLDDT can have a value between 0 and 100, with the higher model confidence corresponding to the higher pLDDT number. pLDDT > 90 (rendered in blue on the panels) is the high accuracy cut-off, above which the backbone and rotamers are predicted with

high confidence; values between 70 and 90 (cyan) correspond to the regions where the backbone conformation is correct; values between 50 and 70 (yellow) have low confidence and are not reliably predicted, and regions with pLDDT below 50 (red) should not be interpreted. Structural superpositions of all AF models against each other were carried out using mTM-align server for multiple structural alignments (Dong et al., 2018a; Dong et al., 2018b) available at <https://yanglab.nankai.edu.cn/mTM-align/>. Below each model is a ‘template modelling score’ (TM-score), which is a length-independent scoring function reflecting the similarity of two structures (Zhang and Skolnick, 2004). The TM-scores can take values between 0 and 1, with the higher TM-score indicating higher structural similarity. The indicated TM-scores correspond to the pairwise superimposition of each AF model onto the X-ray Gorilla GII RBD structure.

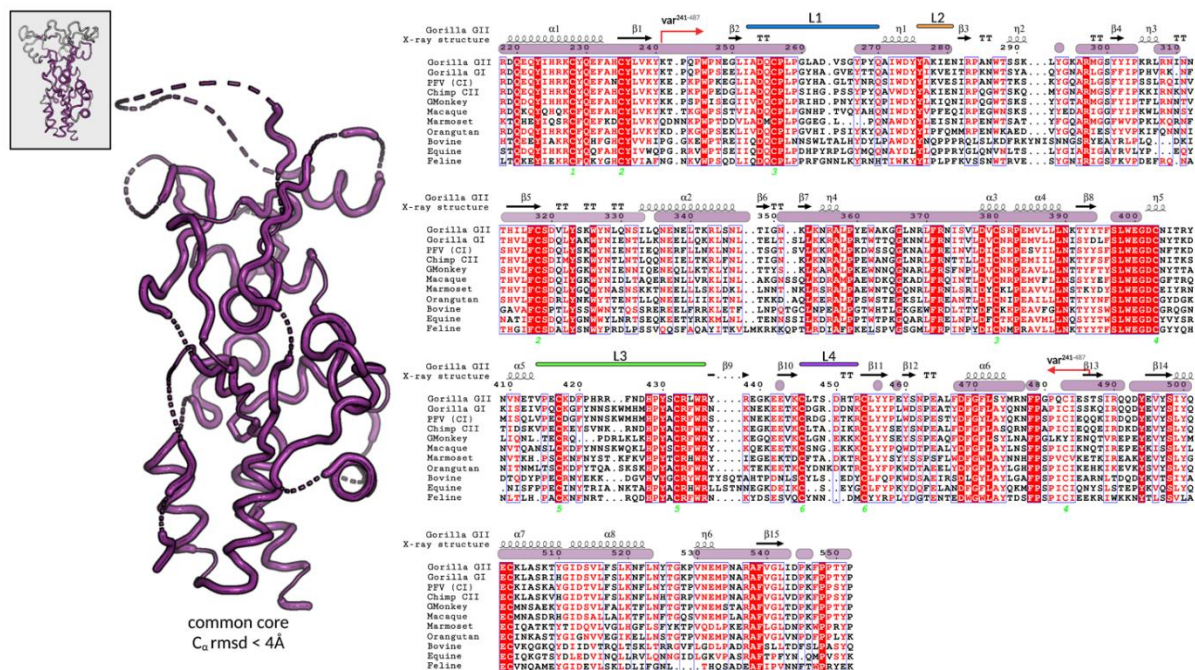


Figure S.IV-9 – FV RBD common core excludes a large portion of the upper subdomain

Superposition of the RBD experimental structure and 11 AF models (Fig. S.IV-8) yielded a ‘common core’, model that includes the residues with $C\alpha$ rmsd $< 4\text{\AA}$ for all pairwise superpositions. Those residues are indicated with purple bars above the sequence alignment, which is colored using the same scheme as in Fig. S.IV-5. The small inlet in the upper left corner represents the entire RBD as a reference for comparison, with the common core colored in purple, and the remaining residues in grey. The structural and sequence alignments were carried out as explained in Figs. S.IV-8 and S.IV-5, respectively.

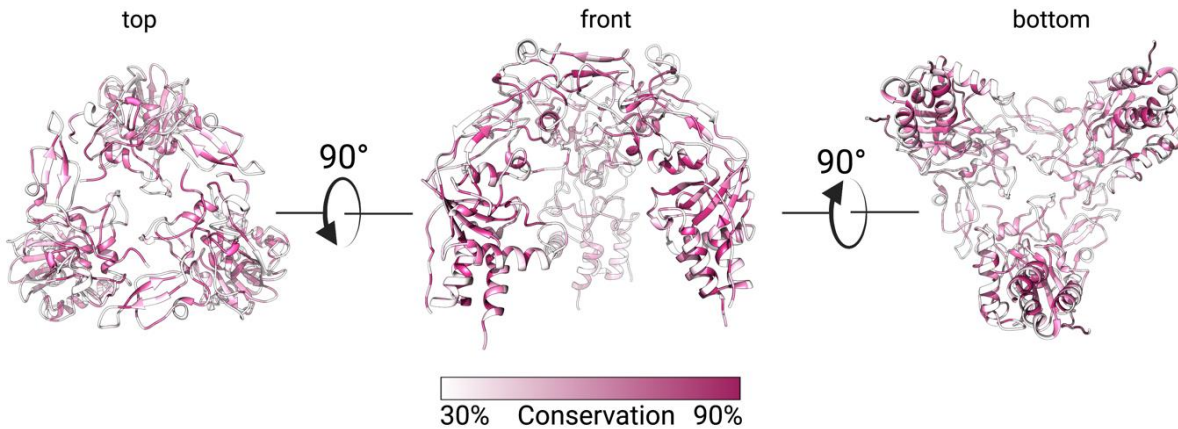


Figure S.IV-10 – The inter-protomer RBD contacts formed by the upper domain loops show poor sequence conservation

Three SFV RBD protomers fitted in the electron density maps obtained for PFV Env (Effantin et al., 2016), as shown in Fig. IV-4 are rendered by residue conservation. The % identity was calculated in Chimera (Pettersen et al., 2004) according to the sequence alignment shown in Fig. S.IV-5, and residues were colored with the white to maroon gradient as indicated with the color key. The residues showing less than 30% and more than 90% sequence identity are colored in solid white and maroon, respectively.

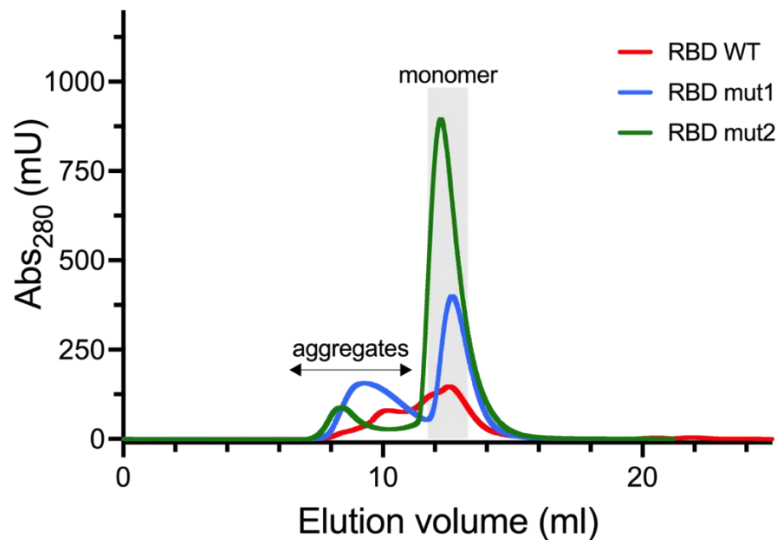


Figure S.IV-11 – Recombinant RBD variants remain monomeric in solution

The size exclusion chromatography (Superdex 200) profiles for the GII RBD expressed in mammalian cells are shown for the WT protein (red line) and the variants (blue and green lines).

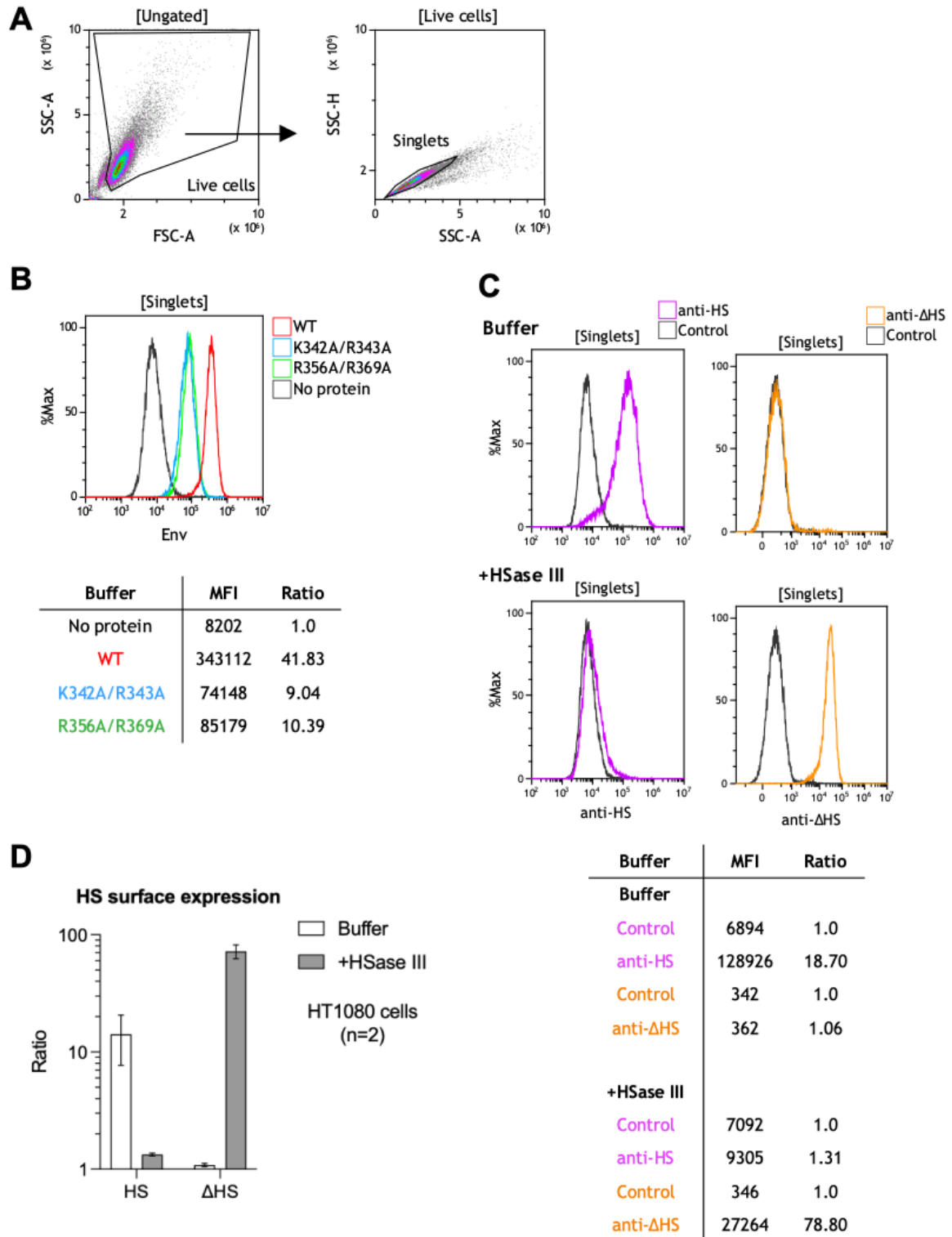


Figure S.IV-12 – Flow cytometry gating strategy

Flow cytometry gating strategy for the detection of Env binding and HS expression on SFV-susceptible cell lines. Cells were treated with trypsin EDTA before labelling with Env proteins or anti-HS antibodies. **A**) Representative example of HT1080 single cell selection: live cells were selected by a gate applied on an FSC-A/SSC-A dot-plot and a single cell gate applied on an SSC-A/SSC-H dot-plot. **B**) Representative example of Env binding analysis. HT1080 cells were labelled with GII-K74 WT, K342A/R343A (mut1) or R356A/R369A (mut2) ectodomain proteins,

anti-StrepMAB-Classic-HRP and anti-HRP-AF488 antibodies. Staining obtained on gated single cells are presented on the histogram overlay: MFI is presented on the x-axis and frequency is expressed as the normalized percentage of gated events on the y-axis (%Max). Cells labelled with secondary antibodies only (“control” condition, black curve) were used as a reference; Env-specific staining was quantified by the ratio of MFI from Env treated to untreated cells. **C)** Representative example of heparan sulfate staining after treatment with heparinase III. HT1080 cells were treated with heparinase III or buffer and stained with the F58-10E4 antibody specific for heparan sulfate (anti-HS) and the F69-3G10 antibody specific for glycans exposed after heparan sulfate removal (anti- Δ HS). Staining obtained on gated single cells are presented on the histogram overlay: MFI is presented on the x-axis and frequency is expressed as the normalized percentage of gated events on the y-axis (%Max). Cells labelled with secondary antibodies only (“control” condition, black curve) were used as a reference; HS and Δ HS-specific staining was quantified by the ratio of MFI from labelled to control cells. **D)** HT1080 cells were treated with heparinase III or buffer and stained with antibodies specific for HS (HS) or glycans exposed after heparan sulfate removal (Δ HS). Expression levels are calculated as the ratio of MFI from labelled to unlabeled cells (Fig. S.IV-12C). Mean and SD from two independent experiments are shown.

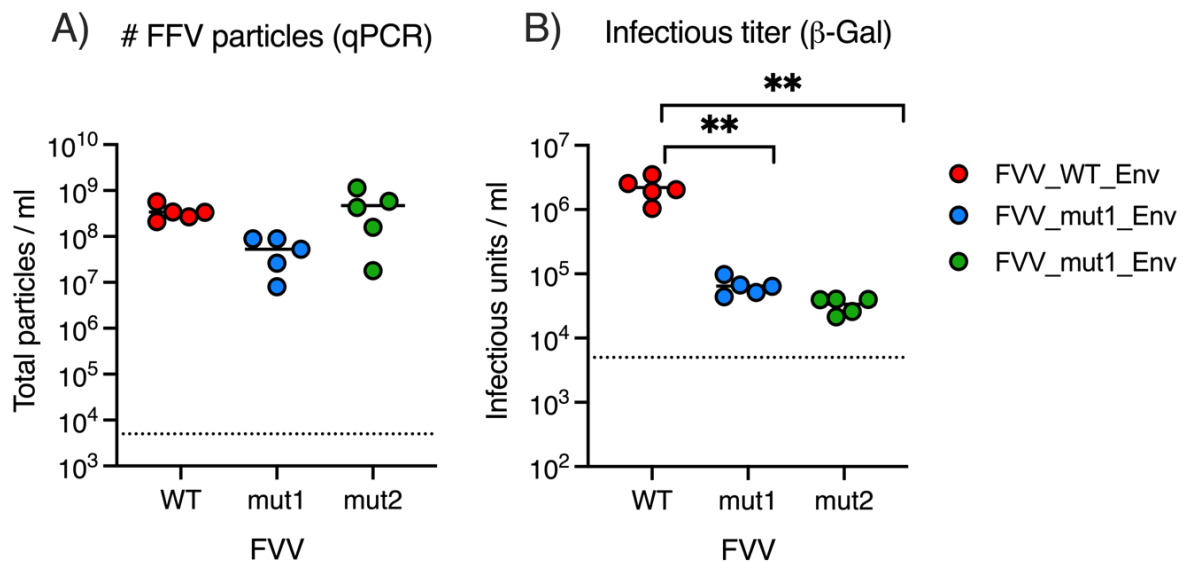


Figure S.IV-13 – Effect of mutations on FVV release and infectious titer

Five batches of FVVs carrying wild-type GII-K74 SU (red), mut1 (blue) and mut2 (green) SU were produced, each represented with a single dot. **A)** The concentration of the vector particles was quantified by RT-qPCR of β -galactosidase transgene. Each batch was titrated twice, and mean titers are presented; lines represent mean values from the five FVV batches. The dotted line represents the quantification threshold. **B)** FVVs infectious titers were quantified on BHK-21 cells. Each batch was titrated twice, and mean titers are presented; lines represent mean values from the five FVV batches. The dotted line represents the quantification threshold. The different FVVs were compared using the paired t-test, * p<0.05, ** p < 0.01.

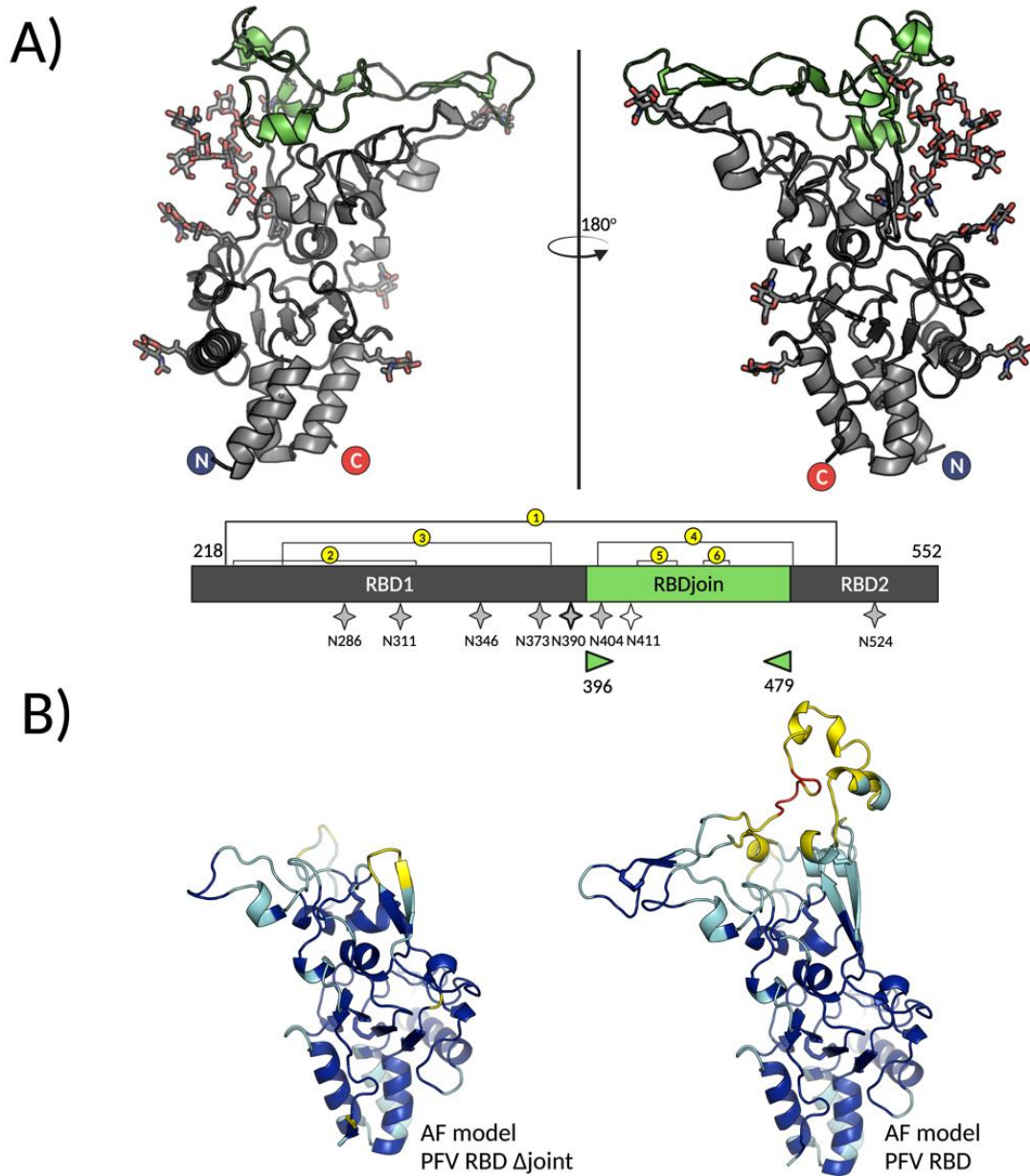


Figure S.IV-14 – Structural basis for RBDjoin region being dispensable for binding to cells

Functional features plotted on the RBD structure. **A)** The regions identified in the bipartite PFV RBD as essential (indicated as RBD1 and RBD2 according to the more recent nomenclature) (Duda et al., 2006) and non-essential (or RBDjoin) (Dynesen et al., 2022, submitted) for SFV entry are colored in dark grey and green, respectively, and plotted on the X-ray structure of gorilla SFV RBD. The numbering corresponds to the gorilla GII RBD. **B)** The AF models of the PFV RBD lacking the non-essential RBDjoin region (left panel) and of the whole PFV RBD (right panel) are colored according to the pLDDT values, using the same palette as in Fig. S.IV-8.

9.3 Supplementary Tables – Manuscript II

Table S.V-1 – Plasma samples used for the ELISA assays

Participant	Ethnicity	SFV infection ^a	Fig. V-2 ^b	Fig. S.V-5 ^b
BAD356	Bantu	Uninfected		X
BAK141	Pygmy	Uninfected		X
BAK183	Pygmy	Uninfected		X
BAK279	Pygmy	Uninfected		X
MEBAK195	Pygmy	GI	X	
BAD448	Bantu	GI	X	X
BAD463	Bantu	GI	X	
BAK132	Pygmy	GI	X	X
BAK56	Pygmy	GI	X	
BAK82	Pygmy	GI	X	
LOBAK2	Pygmy	GI	X	X
BAD551	Bantu	GII	X	X
BAK133	Pygmy	GII		X
BAK232	Pygmy	GII	X	X
MEBAK88	Pygmy	GII		X
BAD348	Bantu	GI+GII	X	
BAD447	Bantu	GI+GII	X	
BAD468	Bantu	GI+GII	X	X
BOBAK153	Pygmy	GI+GII	X	
BAD456	Bantu	GI+GII	X	
BAK177	Pygmy	GI+GII	X	
BAK55	Pygmy	GI+GII	X	
BAK74	Pygmy	GI+GII	X	

^a Participants were infected with a gorilla SFV of which the genotype (GI or GII) was defined by PCR using primers located within SUvar (Lambert et al., 2018). Some participants were coinfecting by strains from both genotypes (GI+GII).

^b The samples used are indicated for each of the two sets of peptides tested and presented in Fig. V-2 and Fig. S.V-5.

Appendices

Table S.V-2 – Synthetic peptides used to search for linear epitopes

Peptide name	Position ^a	Sequence ^b	Length	Prediction ^c
BAD468-247	247-270	RRPSEELIADQCPLPGYHAGVEYTTQ _{RR}	28	Parker
BAD468-267	267-284	RYTTQAIWDYYIKVEITRP	19	Genotype-specific
BAD468-280	280-300	EITRPKNWTSYAQYGNARLGS _R	22	Parker + Lbtope
BAD468-308	308-337	RKNFTHVLFCSQDLYAKWYNIENTLLKNEE _R	31	Ellipro
BAD468-329	329-342	R _{ENTLLKNEELLQKK}	15	Parker
BAD468-340	340-357	LQKKLNNLTELTSLLKKR	18	Genotype-specific
BAD468-350	350-374	TSLLKKRALPRTWTTQGKNNLFRNI	25	Lbtope
BAD468-399	399-418	RWEGDCNYTKDKISEIVPQCKR	22	Parker
BAD468-411	411-432	RSEIVPQCKGFYNN _{SKWMHMHPYR}	24	Parker
BAD468-425	424-444	SKWMHMHPYACRFWRNKNEKE	21	Lbtope
BAD468-435	435-454	RFWRNKNEKEETKCDGRDDN	20	Lbtope
BAD468-441	441-460	RNEKEETKCDGRDDNKCLYYPRR	23	Parker + Lbtope
BAD468-450	450-472	RRGRDDNKCLYYPLWDSPEATYDFGRRR	28	Parker + Lbtope
BAD468-487	487-512	SSKQIRQQDYEVYSIYQECKLASRIH	26	Lbtope
BAK74-247	247-270	RRPNEGLIADQCPLPGLADVSFYQYQRRR	29	Parker
BAK74-267	267-284	RYPYQAIWDYYAKIENIRP	19	Genotype-specific
BAK74-280	280-300	RENIRPANWTSSKLYGKARMGSR	23	Parker + Lbtope
BAK74-308	308-338	RNINNT _{HILFCSVDLYSKWYNLQNSILQENR}	32	Ellipro
BAK74-330	330-348	RQNSILQENELTKRLSNLT	20	Parker
BAK74-339	339-355	ELTKRLSNLTIGNKLKN	17	Genotype-specific
BAK74-350	350-374	GNKLN _{RALPYEWAKGGLNRLFRNI}	25	Lbtope
BAK74-399	399-418	RWEGDCNITRYNVNETVPECKR	22	Parker
BAK74-411	411-430	RNETVPECKDFPHRRFNDHPYR	22	Lbtope
BAK74-425	424-442	RRFNDHPYSCRLWRYREGKE	20	Lbtope
BAK74-435	433-452	RLWRYREGKEEVKCLTSDHTR	21	Lbtope
BAK74-441	439-458	REGKEEVKCLTSDHTRCLYYPRR	23	Parker + Lbtope
BAK74-449	449-470	RRSDHTRCLYYPEYSNPEALFDFGRR	26	Parker + Lbtope
BAK74-485	485-510	RETSIRQQDYEVYSIYQECKLASKTYR	28	Lbtope
PFV-37	251-265	LIADQCPLPGYHAGL	15	Genotype-specific
PFV-41	271-285	SIWDYYIKVESIRPA	15	Genotype-specific
PFV-46	296-310	ARLGSFYIPSSLRQI	15	Genotype-specific
PFV-55	341-355	LNKLNNLTSGTSVLK	15	Genotype-specific
PFV-65	391-405	NTSYYSFSLWEGDCN	15	Genotype-specific
PFV-66	396-410	SFSLWEGDCNFTKDM	15	Genotype-specific
PFV-80	466-470	PESTYDFGYLAYQKN	15	Genotype-specific
PFV-81	471-485	DFGYLAYQKNFSPPI	15	Genotype-specific
PFV-82	476-490	AYQKNFSPICIEQQ	15	Genotype-specific
L1-GI	258-269	R _{LPGYHAGVEYTT} _R	14	RBD structure
L1-GII	258-269	R _{LPGLADVSFYPY} _R	14	RBD structure
L2-GI	279-288	VEITRPKNWT _R	11	RBD structure
L2-GII	279-288	IENIRPANWT _R	11	RBD structure
L3-GI	411-435	SEIVPQCKGFYNN _{SKWMHMHPYACR}	25	RBD structure
L3-GII	410-433	VNETVPECKDFPHRRFNDHPYSCR	24	RBD structure
L4-GI	447-457	R _{KCDGRDDNKCL}	12	RBD structure
L4-GII	445-455	R _{KCLTSDHTRCL}	12	RBD structure

^a Positions refer to each viral sequence.

^b Subscript characters indicate residues added to increase peptide solubility.

Appendices

^c Linear B-cell epitopes were predicted using the software available on the Immune Epitope Data Base (<http://tools.iedb.org/bcell/>): LBtope ((Singh et al., 2013) and Parker hydrophilicity prediction replaced by the Bepipred program (Larsen et al., 2006) and Ellipro (Ponomarenko et al., 2008)). Genotype-specific sequences were manually defined. After resolution of the RBD structure (Fernandez et al., 2022, submitted), eight novel peptides overlapping the four loops were synthesized.

Table S.V-3 – SFV Env proteins produced for the study

Name	Description ^a	Expression level ^b	Coomassie gel shown in Fig. S.V-4	Neutralization experiments presented in	Comment
Immuno-adhesins	(SU fused to murine Fc and Strep-tag				
^{CI} SU	WT immuno-adhesin, CI-PFV strain		Panel A	Fig. V-7	
Kifu ^{CI} SU	WT immuno-adhesin produced in the presence of Kifunensine	Normal	Panel B	Fig. V-7	
Kifu+Endo-H ^{CI} SU	WT immuno-adhesins produced in the presence of Kifunensine and treated with Endo-H	Normal	Panel B	Fig. V-7	
^{CI} ΔN10	N423>A	Normal	Panel E	Fig. V-7	
^{CI} ΔRBDj	ΔF397-S483	Normal	Panel E	Fig. V-7	
^{CI} ΔL2	ΔK278-Y293	Reduced	Panel F	Fig. V-7	
^{CI} ΔL3	ΔI411-R436	Normal	Panel F	Fig. V-7	
^{CI} swapL3	CI-I411-R436 >GII-V410-R433	Normal	Panel F	Fig. V-7	
^{CI} ΔL4	ΔE445-P461	Normal	Panel F	Fig. V-7	
^{CI} 350 _{glyc}	G350N	Normal	Panel F	Fig. V-7	
^{CI} 352 _{glyc}	S352N	Undetectable		Fig. V-7	
^{CI} 463 _{glyc}	W463N	Normal	Panel F	Fig. V-7	
^{GII} SU	WT immuno-adhesin, GII-K74 strain		Panel A	Fig. V-3, V-4, V-5	
Kifu ^{GII} SU	WT immuno-adhesin produced in the presence of Kifunensine	Normal	Panel B	Fig. V-4	
Kifu+Endo-H ^{GII} SU	WT immuno-adhesin produced in the presence of Kifunensine and treated with Endo-H	Normal	Panel B	Fig. V-4	
^{GII} ΔN5	N286>A	Reduced	Panel C	Fig. V-4	
^{GII} ΔN6	N311>A	Normal	Panel C	Fig. V-4	
^{GII} ΔN7	N346>A	Normal	Panel C	Fig. V-4	
^{GII} ΔN7'	N373>A	Reduced	Panel C	Fig. V-4	
^{GII} ΔN9	N404>A	Reduced	Panel C	Fig. V-4	
^{GII} ΔN10	N411>A	Reduced	Panel C	Fig. V-4	

Appendices

GII Δ N9N10	N404>A + N411>A	Insufficient	Panel C	-	Aggregates
GII _{swap} 407	407RYNVNET413 >KDIKSEI	Reduced	Panel D	Fig. V-4	
GII Δ RBDj	Δ F396-G480	Normal	Panel E	Fig. V-5	
GII _{swap} RBDj	GII-F396-G480 >GI-F396-A482	Reduced	Panel E	Fig. V-5	
GII Δ L2	Δ K278-Y293	Reduced	Panel F	Fig. V-5	
GII Δ L3	Δ V410-R433	Reduced	Panel F	Fig. V-5	
GII Δ L4	Δ E442-P458	Normal	Panel F	Fig. V-5	
GII ^{glyc} 263	D263N	Normal	Panel G	Fig. V-6	
GII ^{glyc} 426	H428>T	Normal	Panel I	Fig. V-6	
GII ^{glyc} 450	D450>N	Normal	Panel I	Fig. V-6	
GII ^{glyc} A438-A443	438-REGKKE- 443>AAGAAA	Insufficient			
GII ^{glyc} 459	E459>N	Normal	Panel I	Fig. V-6	
GII ^{glyc} 485	E485>N	Normal	Panel I	Fig. V-6	
GII ^{glyc} 364	K364>N + G366>T	Reduced	Panel I	Fig. V-6	No nAb blocking and no cell binding
GII ^{glyc} 351	L353T	Reduced	Panel H	Fig. V-6, Fig. S.V-6	Aggregates; experiments repeated with SEC purified immunoadhesin
GII ^{glyc} 350	G350>N + K352>S	Reduced	Panel I	Fig. V-6	Aggregates, moderate
GII ^{glyc} 349 _{+E}	E inserted after T348	Reduced	Panel I	Fig. V-6	
GII _{swap} 333	GII-L333-S345 >CI- EQNERFLLNKLN	Reduced	Panel D	Fig. V-6	
GII _{swap} 345	GII-S345-N351 >GI-NNLTELTS	Normal	Panel D	Fig. V-6	
GII Δ T348-L353	Δ T348-L353 + GG	Undetectable			
GII _{swap} 349	GII-I349-N355 >CI-SGTSVLKK	Insufficient			
GII ^{glyc} E502A	E502>A	Reduced	Panel D	Fig. V-6	
GII ^{glyc} L505N	L505>N	Reduced	Panel D	Fig. V-6	
Tagged proteins	Proteins fused to a Strep-tag				
^{MLV} SU	MLV SU, strain FB29	Not applicable	A	Fig. V-3	Three bands are visible in non- reduced conditions that correspond to oligomers formed by the free cysteine thiol group (Gliniak et al., 1991)
GII-K74 SU(m)	WT SU produced in mammalian cells	Not applicable	nd	Fig. S.V-2	Purified by size exclusion chromatography (Fernandez et al., 2022, submitted)
GII-K74 SU (i)	WT SU produced in insect cells	Not applicable	nd	Fig. S.V-2	Purified by size exclusion chromatography (Fernandez et al., 2022, submitted)

Appendices

GII-K74 Ecto(i)	Env 91-907, produced in insect cells	Not applicable	nd	Fig. S.V-2	Purified by size exclusion chromatography (Fernandez et al., 2022, submitted)
^{GII} K342A/R343A	K342>A+R343>A into GII-Ecto(i)	Normal	nd	Fig. V-5	Purified by size exclusion chromatography (Fernandez et al., 2022, submitted)
^{GII} R356A/R369A	R356>A+R369>A into GII-Ecto(i)	Normal	nd	Fig. V-5	Purified by size exclusion chromatography (Fernandez et al., 2022, submitted)

^a aa positions indicated are those of each protein; for GII-K74, some differ from the CI-PFV based numbering (Fig. S.V-1). The symbols > and Δ designate aa substitutions and deletions, respectively.

^b The level of expression was assessed on crude supernatants of transfected cells and categorized as undetected, insufficient to perform the experiments, decreased, or normal relative to the WT counterpart.

Table S.V-4 – Plasma samples used for the neutralization study

Participant	Ethnicity	SFV infection ^a
BAD448	Bantu	GI
BAK132	Pygmy	GI
LOBAK2	Pygmy	GI
BAD551	Bantu	GII
BAK133	Pygmy	GII
BAK228	Pygmy	GII
BAK232	Pygmy	GII
MEBAK88	Pygmy	GII
BAD348	Bantu	GI+GII
BAD447	Bantu	GI+GII
BAD468	Bantu	GI+GII
BAK55	Pygmy	GI+GII

^a Participants were infected with a gorilla SFV of which the genotype was defined by PCR using primers located within SUvar (Lambert et al., 2018). Among the four individuals infected by both genotypes, only one (BAK55) was tested against both genotypes in epitope mapping experiments because his nAb titers were high against both genotypes; the three other samples were tested against a single viral genotype.

Appendices

Table S.V-5 – Methods used to predict epitopic regions and to design the mutant SU proteins

Name	Prediction	Genotype-specific features
GII Δ N5, GII Δ N6, GII Δ N7, GII Δ N9	Functional study (Luftenegger et al., 2005)	
GII Δ N7'	Presence varied according to the viral strain (Richard et al., 2015)	Absent from CI-PFV strain
GII Δ N10, CI Δ N10	Functional study (Luftenegger et al., 2005)	Genotype-specific localization of N10 (Richard et al., 2015)
GII _{swap} 407	Genotype-specific sequence before N10	Genotype-specific localization of N10 (Richard et al., 2015)
GII Δ RBDj, GII _{swap} RBDj, CI Δ RBDj, CI _{swap} RBDj	Functional study (Duda et al., 2006)	GII ^{II} SU with CI ^I RBDj (GII _{swap} RBDj) was expressed; CI ^I SU with GII ^{II} RBDj was not
GII ^K 342A/R343A, GII ^R 356A/R369A	Functional study (Fernandez et al., 2022, submitted)	Mutations introduced in GII-K74 ectodomain; CI-PFV ectodomain is expressed at low levels
GII Δ L2, CI Δ L2	Crystal structure (Fernandez et al., 2022, submitted) + disordered secondary structure ^a	
GII Δ L3, CI Δ L3, CI ^L 3 _{swap} , GII Δ L4, CI Δ L4	Crystal structure (Fernandez et al., 2022, submitted)	
GII ²⁶³ _{glyc} , GII ⁴²⁶ _{glyc} , GII ⁴⁵⁰ _{glyc} , GII ⁴⁵⁹ _{glyc}	Genotype specific + CBtope ^b	
GII ³⁵¹ _{glyc} , GII ³⁶⁴ _{glyc} , GII ⁴⁸⁵ _{glyc}	Genotype specific + CBtope ^b + disordered secondary structure ^a	Loop size around aa351 differs between genotypes
GII ³⁵⁰ _{glyc} , GII ³⁴⁹ _{+E} , GII _{swap} 345, GII _{swap} 333, GII ^E 502A, GII ^L 505N, CI ^G 350 _{glyc}	Designed after testing GII ³⁵¹ _{glyc}	
CI ⁴⁶³ _{glyc}	Designed after testing GII ⁴⁵⁹ _{glyc}	

^a The Protein Homology/analogY Recognition Engine V 2.0 (Phyre2) web portal was used for secondary structure prediction (Kelley et al., 2015). Disordered secondary structures predicted by the software were considered to define epitopic regions to be tested.

^b CBtope software predicts conformational B-cell epitopes on the basis of their primary sequence (<http://crdd.osdd.net/raghava/cbtope/>, (Ansari and Raghava, 2010)). We applied the recommended parameters, i.e. 19 aa-long window, -0.3 threshold, and considered values ≥ 4 as potential epitope.

9.4 Supplementary Figures - Manuscript II

	 LP					
CI-PFV	MAPPMTLQQW	IIWKKMNKAH	EALQNTTTVT	EQQKEQIILD	IQNEEVQPTR	50
GI-D468S....	...N..HQ..	Q.....S.L..	.E.....ED.V...	50
GII-K74S....	...N..HQ..	Q.....S.L..	.E.....ED.I...	50
CI-PFV	RDKFRYLLYT	CCATSSRVLA	WMFLVCILLI	IVLVSCFVTI	SRIQWNKDIQ	100
GI-D468	M.RVK.F...L.A...F.	.II....I.L	100
GII-K74	M.RVK.F...L.A...F.	.II....I.L	100
	 SU					
CI-PFV	VLGPVIDWNV	TQRAVYQPLQ	TRRIARSLRM	QHPVPKYVEV	NMTSIPQGVY	150
GI-D468	L....A..AF	150
GII-K74	L....A..AF	150
CI-PFV	YEPHPEPIVV	KERVGLGSLQI	LMINSENIAN	NANLTQEVKK	LLTEMVNEEM	200
GI-D468	.Q.....IH	T.....VV..	S...S..T.AI....	200
GII-K74	.Q.....IH	T.....VV..	S...S..T.AI....	200
	 RBD1					
	 SUvar					
CI-PFV	QSLSDVMIDF	EIPLGDPRDQ	EQYIHRKCYQ	EFANCYLVKY	KEPKPWPKEG	250
GI-D468H.....	.T.Q...S.E	250
GII-K74	.G.....H.....	.T.Q...N..	250
CI-PFV	LIADQCPLPG	YHAGLTYNRQ	SIWDYYIKVE	SIRPANWTTK	SKYGQARLGS	300
GI-D468VE.TT.	A.....	IT..K...SY	AQ..N.....	300
GII-K74	LADVSF.PY.	A....A.I.	N.....SS	KL..K..M..	300
CI-PFV	FYIPSSLRQI	NVSHVLFCS	QLYSKWYNIE	NTIEQNERFL	LNKLNNLTSG	350
GI-D468	.F..PHV.K-	.FT.....	..A.....	..LLK..EL.	QK.....EL	349
GII-K74	Y...KR..N.	.NT.I.....	V.....LQ	.S.L...NE.	TKR.S...-I	349
	 RBDj					
CI-PFV	TSVLKKRALP	KDWSSQGKNA	LFREINVLDI	CSKPESVILL	NTSYYSFSLW	400
GI-D468	..L.....	RT.TT....N	...N.T...V	.NR..M.L..	.I..DL....	399
GII-K74	GNK..N....	YE.AKG.L.R	...N.S...V	..R..M.L..	.KT..T....	399
CI-PFV	EGDCNFTKDM	ISQLVPECDG	FYNNSKWMHM	HPYACRFWRS	KNEKEETKCR	450
GI-D468Y...K	..EI..Q.K.ND	449
GII-K74I.RYN	VNET....KD	.PHRR--FND	...S..L..Y	REG...V..L	447
	 RBD2					
CI-PFV	DGETKRCLYY	PLWDSPESTY	DFGYLAYQKN	FPSPICIEQQ	KIRDQDYEVY	500
GI-D468	GRDDNK....A..	...F...N.	..A....SSK	Q..Q.....	499
GII-K74	TSDHT.....	.EYSN..ALF	...F.S.MR.	..G.Q...ST	S..Q.....	497
CI-PFV	SLYQERKIAS	KAYGIDTVLF	SLKNFLNYTG	TPVNEMPNA	AFVGLIDPKF	550
GI-D468	.I...C.L..	RIH...S...	K.....	549
GII-K74	.I...C.L..	.T...S...	K.....	547
	 TM					
CI-PFV	PPSYPNVTRE	HYTSCN--NR	KRRSVDNNTYA	KLRSMGYALT	GAVQTLIS	598
GI-D468	..T...I..D	Q.QG..INQ.	RK.E.N...SA...	599
GII-K74	..T...I..D	Q.QG..INQ.	RK.E.N...SA...	597
CI-PFV	DINDENLQQG	IYLLRDHVIT	LMEATLHDIS	VMEGMFAVQH	LHTHLNHLKT	648
GI-D468Q.....IV.	I.....	V.....R.	649
GII-K74Q.....IV.	I.....	V.....R.	647
CI-PFV	MLLERRIDWT	YMSSTWLQQ	QLQKSDDEMKV	IKRIARSLVY	YVKQTHSSPT	698
GI-D468	..M.....S...TT.....YN.L.	699
GII-K74	..M.....S...TT.....YN.L.	697

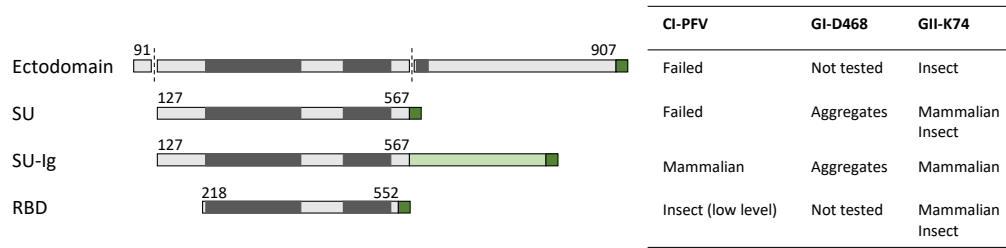
Appendices

CI-PFV	ATAWEIGLYY	ELVIPKHIY	LNNWNVNIGH	LVKSAGQLTH	VTIAHPYEII	748
GI-D468I..R...Q.....	.I.....	..LS.....	749
GII-K74I..R...QI.....	.I.....	..LS.....	747
CI-PFV	NKECVETIYL	HLEDCTRQDY	VICDVVKIVQ	PCGNSSDTS	CPVWAEAVKE	798
GI-D468	.R..SN.L..	...E.R.L..S..P...	799
GII-K74	.R..SN.L..	...E.R.L..S..P...	797
CI-PFV	PFVQVNPLKN	GSYLVLASST	DCQIPPYVPS	IVTVNETTSC	FGLDFKRPLV	848
GI-D468	.H..IS....	V.....Q.	..VT..K...	849
GII-K74	.H..IS....	V.....Q.	..VT..K...	847
CI-PFV	AEERLSFEPR	LPNLQLRLPH	LVGIIAKIKG	IKIEVTSSGE	SIKEQIERAK	898
GI-D468	...KT.L..Q	..H.....D.L....	899
GII-K74	...KT.L..Q	..H.....D.L....	897
CI-PFV	AELLRLDIHE	GDTPAWIQQL	AAATKDVWPA	AASALQGIGN	FLSGTAQGIF	948
GI-D468E.....K....	..T.A...L.	949
GII-K74R..E.....K....	..T.A...L.	947
CI-PFV	GTAFLSLGYL	KPILIGVGI	LLVILIFKIV	SWIPTKKKNQ		988
GI-D468I....I.I.	I.....L	K...I.R.S.		989
GII-K74I....I.I.	I.....L	K...I...S.		987

Figure S.V-1 – CI-PFV, GI-D468, and GII-K74 Env sequence alignment

Env sequences from CI-PFV, GI-D468, and GII-K74 strains were aligned using CLC Mainworkbench software. Identical residues are indicated with dots. Boundaries of the leader peptide (LP), surface protein (SU), transmembrane protein (TM), receptor binding domain (RBD)1, RBDj, and RBD2 are indicated over the sequences. The RBDj domain is highlighted by italic characters and the SUvar domain is highlighted by the grey colored background.

A SFV Env expression constructs and expression in mammalian and insect cells



B

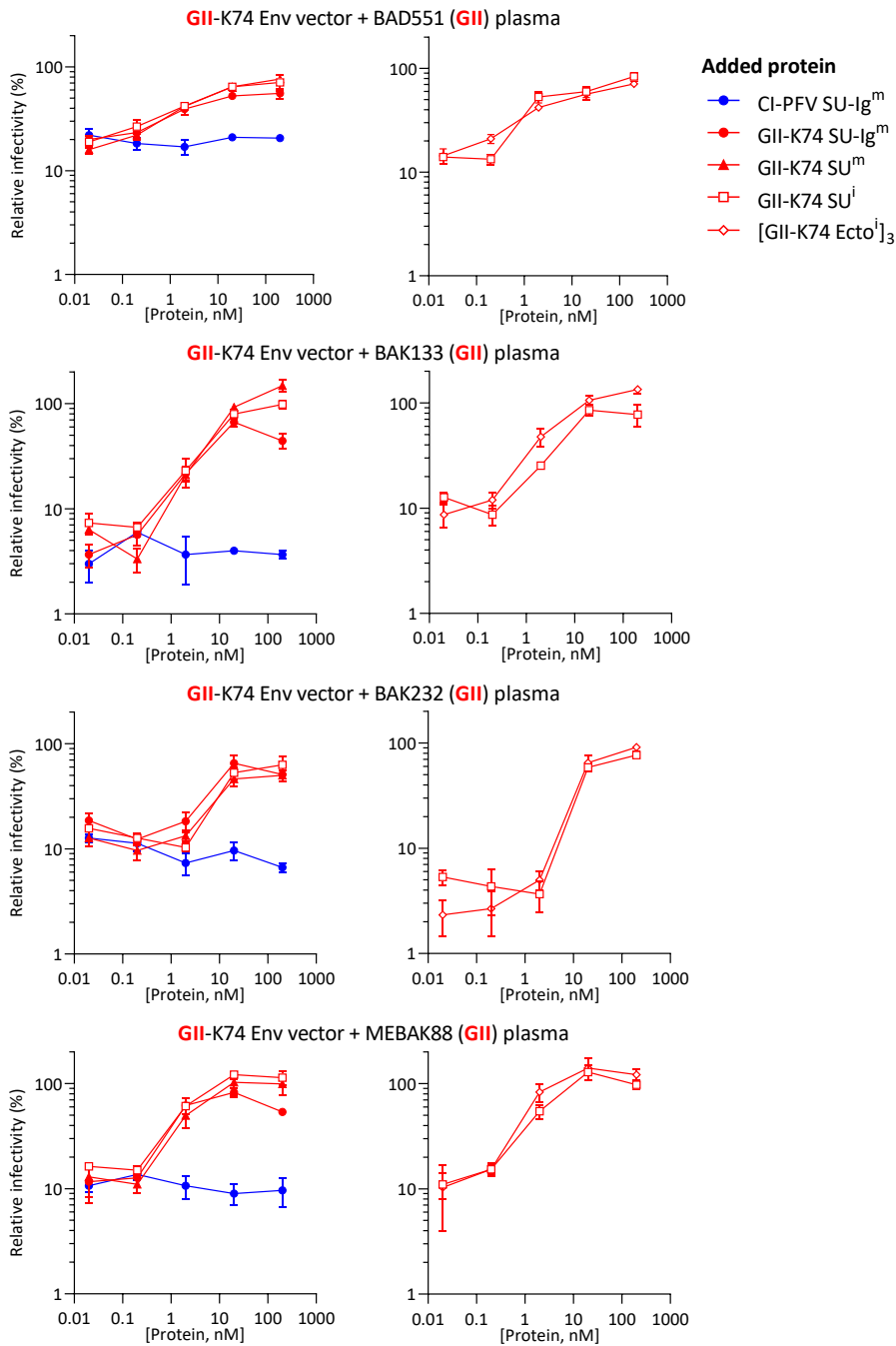


Figure S.V-2 – Recombinant SFV Env oligomerization and mammalian-specific glycosylation do not affect the capacity to inhibit GII-specific nAbs

A. Schematic representation of SFV Env constructs tested for expression in mammalian and/or insect cells. SFV Env is shown in grey; the dark green segment represents the Twin-Strep-tag and the light green segment the murine Fc domain. The outcomes of expression assays for CI-PFV, GI-D468, and GII-K74 Env-derived proteins are summarized in the table. CI-PFV immunoadhesin (^{CI}SU) was the only well-expressed genotype I Env protein and we therefore used immunoadhesins for the project. **B.** GII-specific plasma samples from four individuals were diluted to their \approx IC₉₀ and incubated with Env proteins at concentrations ranging from 200 to 0.02 nM. The mix was then added to FVVs expressing GII-K74 Env before titration. The relative infectivity is presented as a function of the protein concentration. Production in mammalian or insect cells is indicated in the legend with (m) and (i) suffixes, respectively. The abbreviations used to indicate the immunoadhesins in the main text have been replaced by their extended names for the sake of clarity (^{GII}SU in the main text is replaced by GII-K74 SU-Ig^m in the figure). The left and right panels present independent experiments. The inhibition of anti-GII nAb by SU was independent of the nature of the producing cell (GII-K74 SU^m vs. GII-K74 SUⁱ, left panels), dimerization through fusion with the immunoglobulin constant domain (GII-K74 SU^m vs. GII-K74 SU-Ig^m, left panels), and trimerization when expressed as an ectodomain in insect cells (GII-K74 SUⁱ vs. [GII-K7 Ecto]³, right panels). Genotype-mismatched immunoadhesins (CI-PFV SU-Ig^m) failed to inhibit the nAbs (blue curves, left panels).

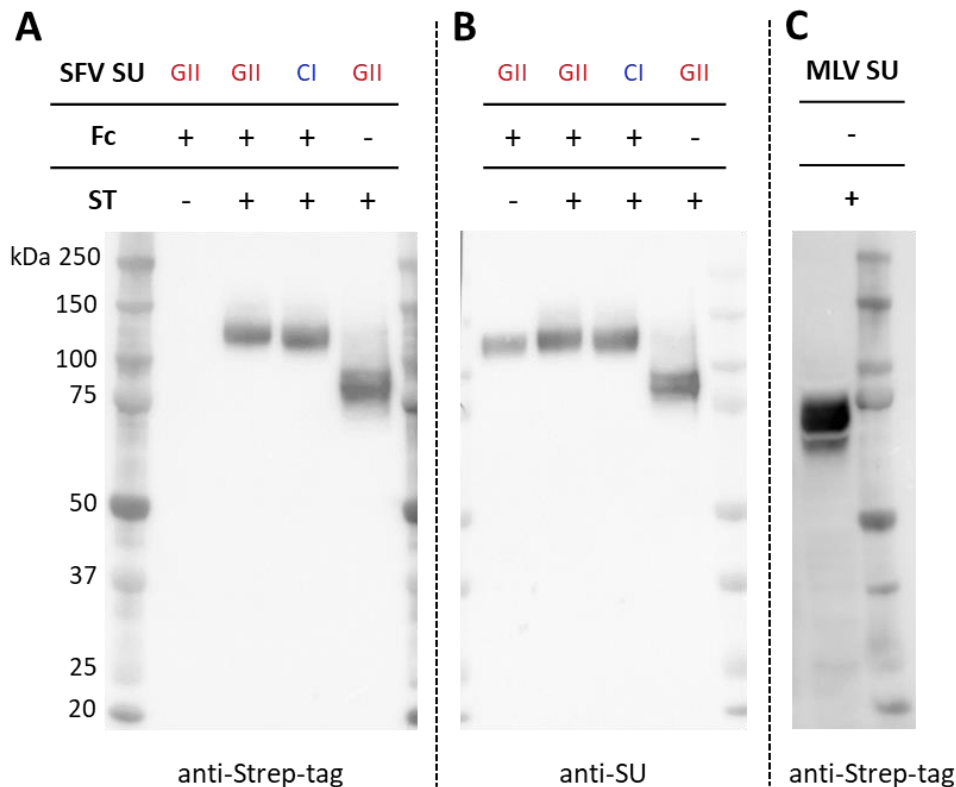


Figure S.V-3 – Western-blot analysis of WT SU proteins used in the study

Western-blotting analysis of WT SU protein and immunoadhesins. Mammalian cell supernatants collected 72 h post-transfection were heat-denatured before immunoblotting with either anti-Strep-tag antibody (**A and C**) or an anti-SU antibody (**B**). SFV SU was expressed as GII-K74 immunoadhesin without a Strep-tag, GII-K74 immunoadhesin with a Strep-tag, GII-K74 SU with a Strep-tag, and as ^{CI}SU with a Strep-tag (**A and B**). ^{MLV}SU was expressed fused to a Strep-tag (**C**). For the CI and GII SUs, two bands are visible, mostly for the SU-ST construct, in accordance with the results of other reports (Herchenroder et al., 1999).

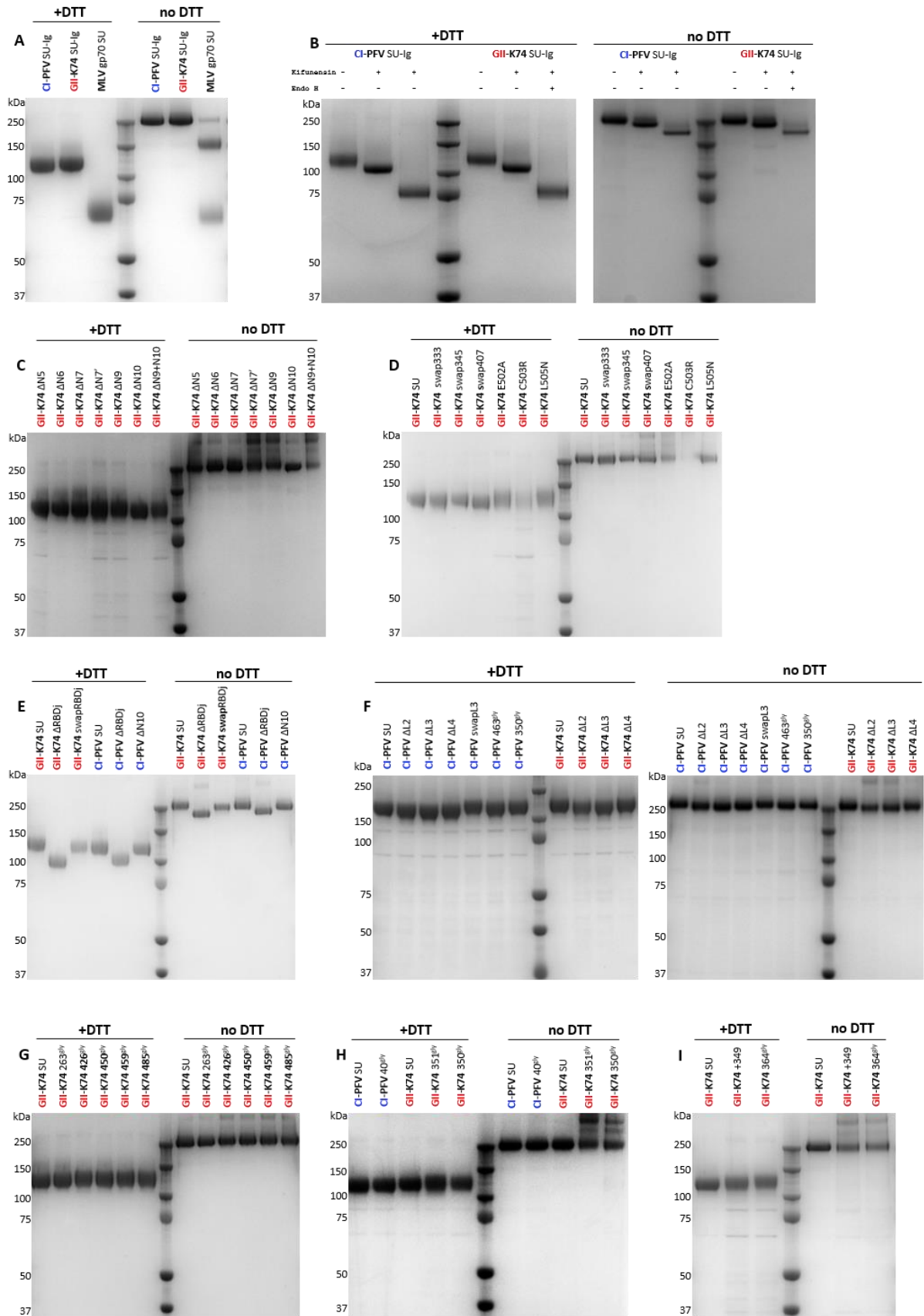


Figure S.V-4 – Purity of immunoadhesins used in the study assessed by Coomassie blue gel staining

To verify immunoadhesin purity and aggregate formation, 1.5 µg of purified immunoadhesins were heat-denatured at 70°C for 10 min, with or without DTT. Samples were loaded onto a precast NuPAGE 4-12% Bis-Tris gel and the proteins separated by electrophoresis. Gels were then stained with Coomassie blue and imaged using a G:BOX (Syngene). A western-blot control was performed for all affinity-purified immunoadhesins. The constructs are listed in Table S.V-3 and their names are indicated over the images.

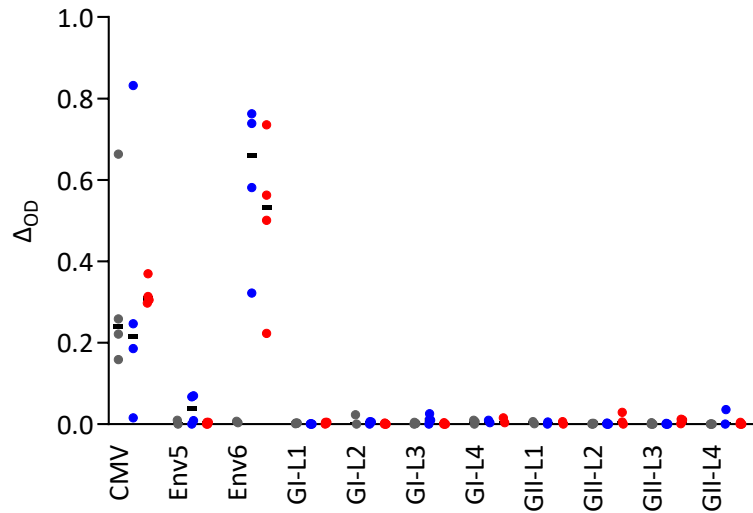


Figure S.V-5 – Plasma antibodies do not bind to peptides covering the loops located at the apex of the RBD and targeted by nAbs

Twelve plasma samples from African hunters (Table S.V-1) were tested for binding to peptides overlapping loops located in the upper subdomain of the RBD (Table S.V-2). Plasma samples from four uninfected (grey symbols), four GI-infected (blue symbols), and four GII-infected (red symbols) individuals were tested. The CMV and SFV Env6 peptides were used as positive controls and the SFV Env5 peptide as a negative control (Lambert et al., 2019). The responses are presented as the net optical density (y-axis) for each peptide (x-axis).

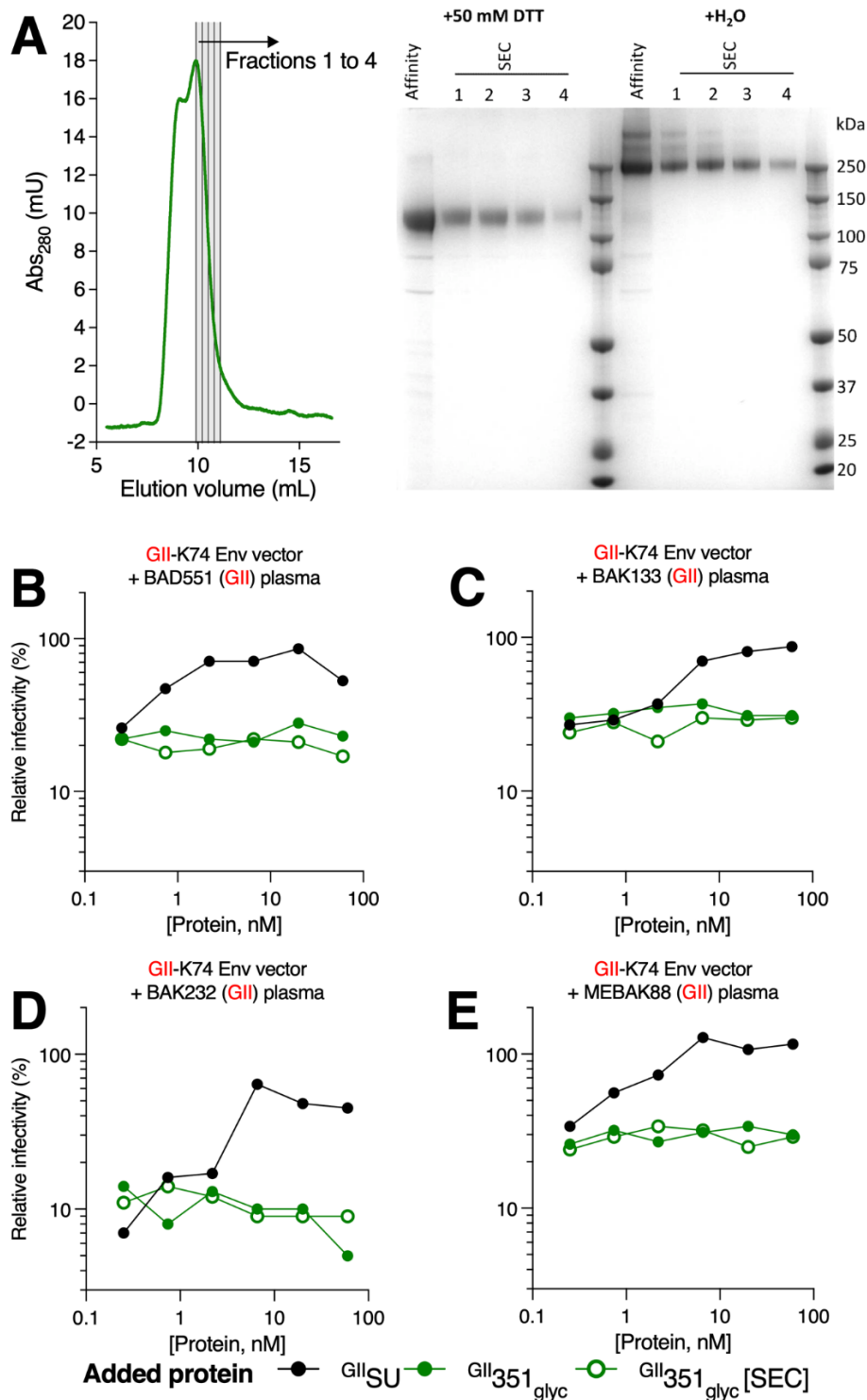


Figure S.V-6 – The GII^{351}_{glyc} immunoadhesin is unable to block nAbs – exclusion of a nonspecific effect of protein aggregation

293-F cells were transfected with the plasmid encoding GII^{351}_{glyc} . The supernatant was collected after 72 h of culture and the immunoadhesin affinity purified using the Strep-Tag fused to the C-terminus. Then, half the volume was purified by size exclusion chromatography. **A**. The affinity-purified and four fractions of chromatography-purified GII^{351}_{glyc} were analyzed on a Coomassie-stained gel, with or without reducing treatment. High molecular weight proteins were present in the affinity purified sample and the first two SEC fractions. **B to E**. The plasma samples from four individuals infected with a GII SFV were diluted to their $\approx IC_{90}$

and incubated with immunoadhesins at concentrations ranging from 60 to 0.02 nM. The mix was then added to FVVs expressing the GII-K74 Env before titrating infectivity. The relative infectivity is presented as a function of immunoadhesin concentration. The addition of ^{GII}SU (black symbols) inhibited the action of the nAbs, whereas affinity-purified ^{GII}351_{glyc} did not (green closed symbols). To exclude that ^{GII}351_{glyc} aggregation led to epitope masking, the chromatography-purified fractions 3 and 4 (^{GII}351_{glyc} [SEC], green open symbols) were pooled, concentrated, and tested in parallel. These contained no aggregates (panel A) but were unable to block nAbs from the four individuals.

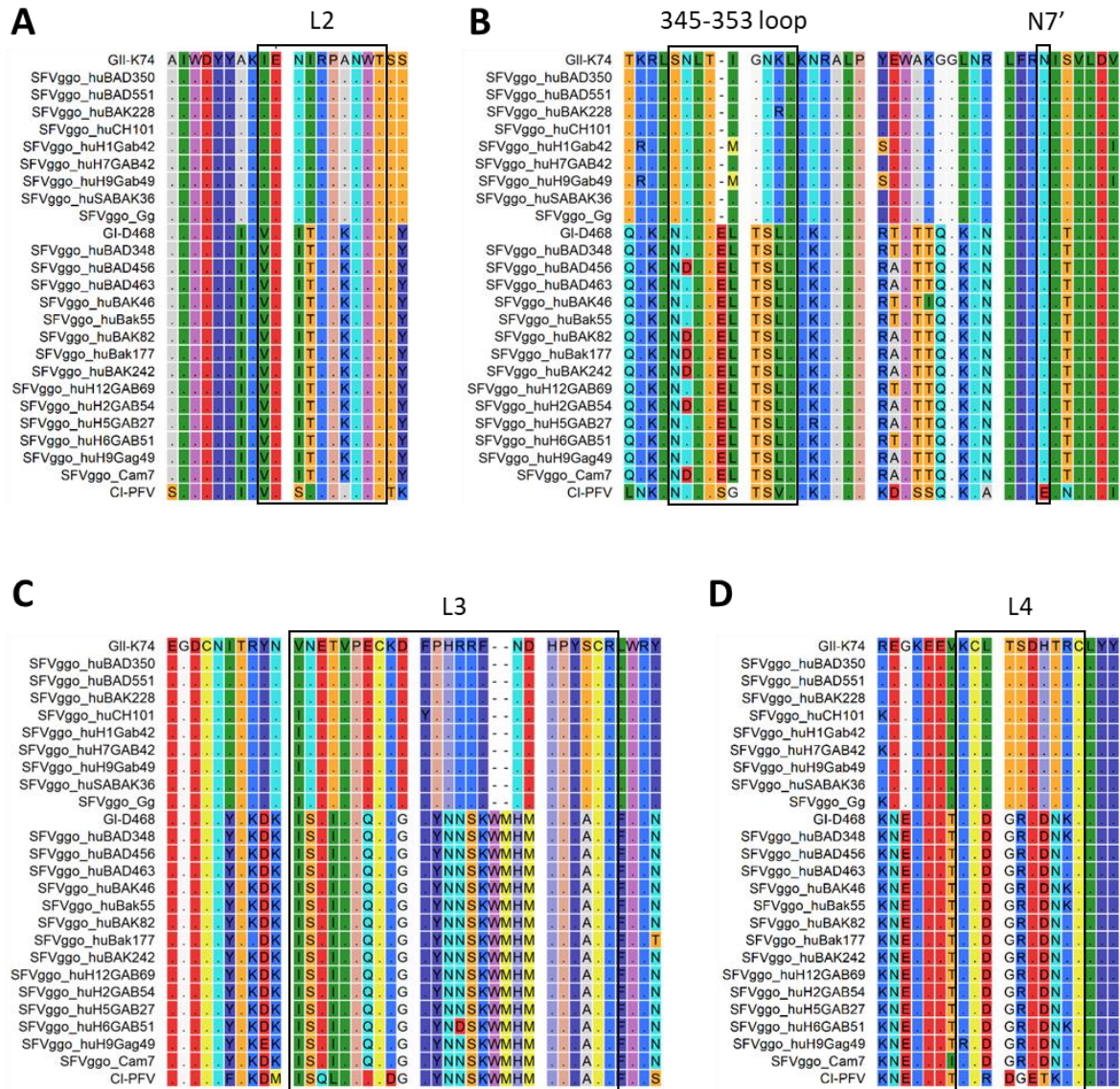


Figure S.V-7 – Sequences from gorilla SFV strains circulating in Central Africa are conserved in the epitopic regions targeted by nAbs

The SUvar protein sequences from the SFVgo strains circulating in Central Africa and CI-PFV were aligned. We included all available sequences: 10 genotype II sequences (nine zoonotic strains and one animal strain (Richard et al., 2015)) and 15 genotype I sequences (14 zoonotic strains and one animal strain (Richard et al., 2015)). Identical residues are indicated by dots, the background colors correspond to the physical properties (rasmol color code). Black squares indicate the identified epitopic regions: L2 (A), 345-353 loop and N7' (B), L3 (C), and L4 (D). Within each genotype, we observed identical sequences or conservative aa changes. The only exception was an N351/D polymorphism in the 345-353 loop from GI that may alter the expression of N7 strain.

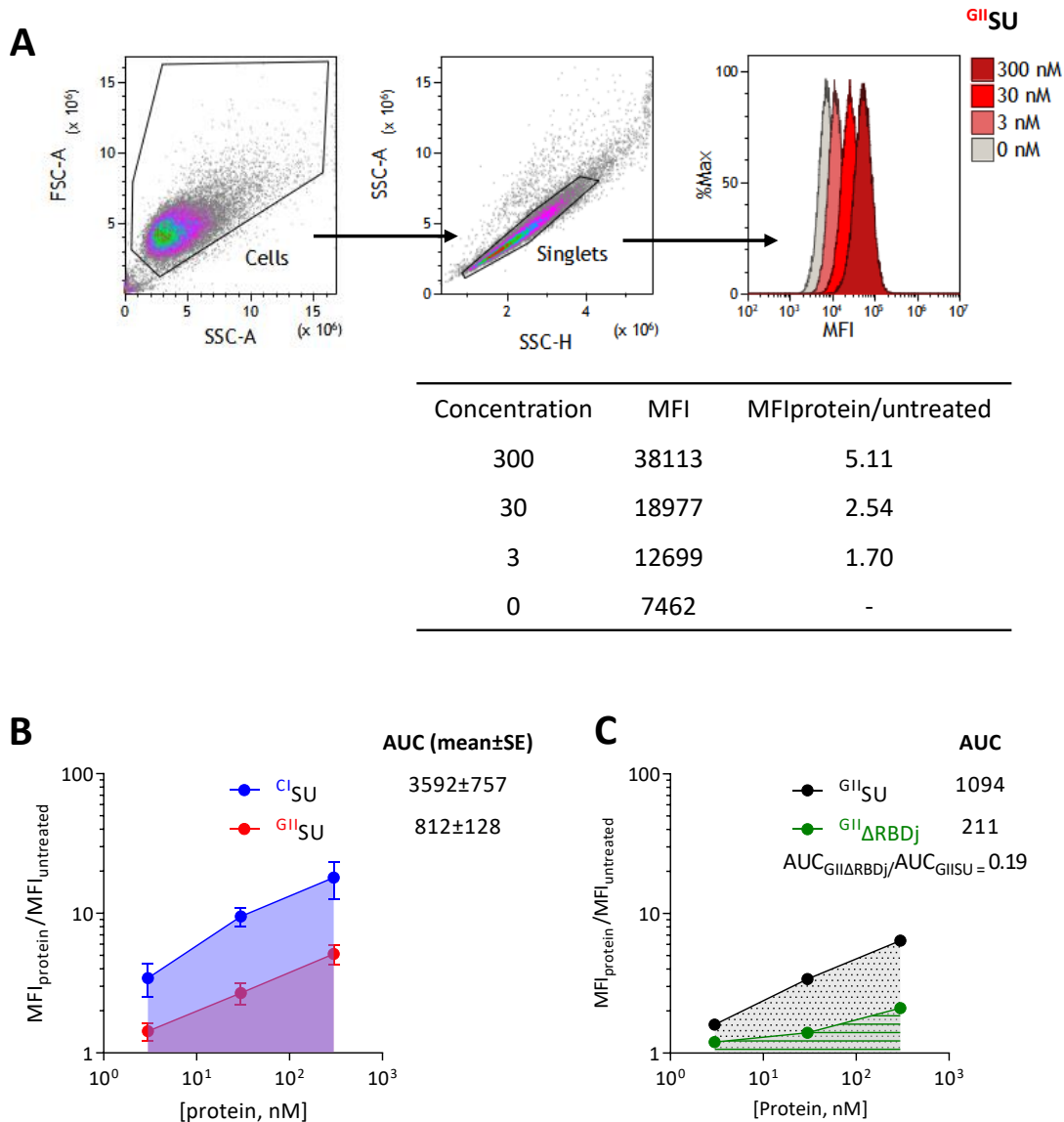


Figure S.V-8 – Recombinant immunoadhesins bind to susceptible cells

HT1080 cells were incubated with immunoadhesins and the bound protein detected by staining with an anti-mouse Fc antibody and flow cytometry analysis. **A**. The gating strategy of viable single cells and staining intensity are shown for ^{GII}SU added at three concentrations. Levels of bound ^{GII}SU are expressed as the ratio of the MFI from immunoadhesin-treated cells to the MFI of untreated cells. **B**. To compare the binding capacity of the immunoadhesins, staining was performed at three doses, the MFI ratios plotted as a function of immunoadhesin concentration, and the area under the curve (AUC) calculated. Shaded regions represent the AUC. Data from five independent experiments performed with WT immunoadhesins are presented as the mean and standard error. ^{Cl}ISU bound at higher levels than ^{GII}SU. **C**. The treated and mutated immunoadhesins were tested for binding to susceptible cells and staining levels were normalized to that of the WT immunoadhesin included in every experiment. The graph shows lower staining by ^{GII}ΔRBDj than ^{GII}SU.

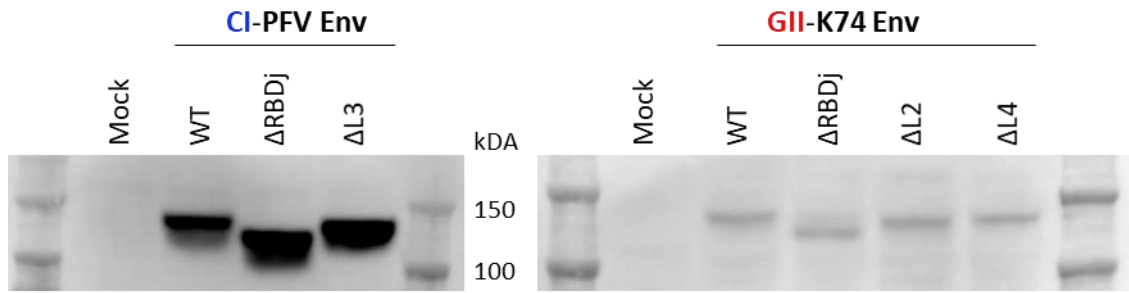


Figure S.V-9 – Env proteins deleted of RBDj, L2, L3 or L4 sequences are expressed in transfected cells

FVVs carrying WT or mutated Env were produced by co-transfection of 293T cells with four plasmids encoding the *env*, *gag*, and *pol* genes and a β -galactosidase transgene. After the collection of supernatants containing the FVV particles, transduced cells were collected and the expression of Env was assessed by Western-blotting. Membranes were stained with a mouse monoclonal antibody that recognizes the LP subunit of Env. The WT gp130 Env precursor was observed, as well as mutant Env with a lower molecular weight, as expected.

ABSTRACT

Simian foamy viruses (SFVs) are ancient and wide-spread complex-type retroviruses that have co-evolved with their non-human primate (NHP) species for millions of years. These viruses can be transmitted to humans, primarily through bites, leading to the establishment of a life-long persistent infection. Despite frequent zoonotic transmission of SFVs from NHPs to humans in Central Africa and Asia, no overt pathology or human-to-human transmission of SFVs have been reported yet. My host laboratory hypothesized that the immune system efficiently controls viral replication in zoonotically infected humans. They demonstrated that neutralizing antibodies (nAbs) are present at high titers in Central African hunters infected with gorilla and chimpanzee SFV strains. My colleagues showed that two viral genotypes are circulating among SFV-infected NHPs and humans. A variant region within the surface domain (SU) of the viral envelope glycoprotein (Env), termed SUvar, forms basis of the two genotypes. The receptor binding domain (RBD) overlaps the SUvar region. The nAbs strictly target the SUvar region on the SFV Env.

I aimed to characterize nAb epitopes located within the SUvar region of SFV Env. To map nAb epitopes within SUvar, I performed neutralization assays in presence of recombinant SU proteins that compete with Env at the surface of viral particles for nAb binding. I used plasma samples from Central African hunters infected with gorilla SFVs and foamy viral vectors expressing SFV Env from each of the two genotypes. I generated mutant SU proteins by systematically deleting glycosylation sites, inserting glycans to disrupt epitopes and by swapping residues between the two genotypes.

I have described that nAb epitopes have a genotype-specific location. Through collaborative work with the laboratory of Prof. Félix Rey who solved the crystal structure of a gorilla SFV RBD, I have discovered that most SFV-specific nAbs target epitopes located at the apex of Env, in particular three mobile loops located at the interface between protomers. Vectors with deleted loops were produced and bound to cells but were non-infectious, suggesting that nAbs target epitopes with functional importance. In addition, we found a second major epitope in the bottom part of the RBD targeted by nAbs from individuals infected by one of the two genotypes. This region is involved in binding to cells. My results suggest that SFV-specific nAbs could block viral entry either by preventing Env binding to the cell surface or by preventing conformational changes of the Env trimer and fusion of viral and cellular membranes. Collectively, my data support the role of nAbs in the control of viral replication and human-to-human transmission.

Key words: Simian foamy virus, Retrovirus, Zoonosis, Neutralizing antibodies, Epitopes